AN ABSTRACT OF THE THESIS OF

Andrew Cody Beedlow for the degree of Master of Science in Geology presented on August 5, 2011

Title: The Use of Surface Energy Balance Models As a Means to Quantify Changes in Glacier Mass Balance: an Application to the Collier Glacier

Abstract approved:

Peter U. Clark

This thesis presents the results of an investigation into the measured and modeled mass balance of the Collier Glacier, a small (0.70 km^2), valley glacier located in the Oregon Cascade Range (44° 10' N, 121° 47' W). Here we present mass-balance measurements conducted for the 2009 and 2010 balance years on the Collier Glacier. The glacier has a unique photo record of retreat throughout the 20^{th} century, thus making it one of the best-recorded glaciers in the Oregon Cascade Range. As part of the study, we installed and maintained automated weather stations (AWS) to collect data needed to apply and validate the OSU surface energy balance model (SEBM). The variations in the mass balance for the Collier Glacier continue previously determined variations where there are years with significant mass loss, and years of mass gain. The general form of the Collier Glacier's net balance did not change appreciably between 1989 and 2010, with high ablation gradients below the ELA and

low gradients above the ELA. However, there was a slight increase in elevation of the location of maximum ablation as well as the terminus, coinciding with the decrease in surface area since completion of the last study in 1994. The net balance curve continues to translate back and forth along the x-axis from year to year depending on the timing and magnitude of winter snow accumulation and summer temperatures. These data suggest that potential negative balance years could result in an ELA that is above the icefall, exposing a significant amount of mass flux to the ablation area, enhancing ablation and subsequent retreat. Model results indicate that the OSU SEBM is capable of capturing the seasonal pattern of mass balance for the Collier Glacier. The model also shows good agreement both spatially and temporally with the mass-balance measurements conducted for the 2009 and 2010 balance years. Model experiments were conducted to compare model performance and investigate the superiority of more complex models with simpler approaches. Model comparisons between the OSU SEBM calculating the turbulent heat fluxes with the bulk method showed similar performances with the SEBM calculating the turbulent heat fluxes with a simpler transfer coefficient method. Furthermore, the OSU SEBM was also compared to a simple positive degree-day (PDD) model. Model simulations indicated that the PDD model explained approximately 82% of the variance in summer ablation, while the SEBM explained approximately 78% of the variance in summer ablation. These results indicate that simpler methods to model glacier mass balance may be just as effective as the more complex methods.

THE USE OF SURFACE ENERGY BALANCE MODELS AS A MEANS TO QUANTIFY CHANGES IN GLACIER MASS BALANCE: AN APPLICATION TO THE COLLIER GLACIER

by
Andrew Cody Beedlow

A THESIS

submitted to

Oregon State University

in partial fulfillment of
the requirements for the
degree of

Master of Science

Presented August 5, 2011
Commencement June 2012

Master of Science thesis of Andrew Cody Beedlow presented on August 5, 2011.

APPROVED:

Major Professor, representing Geology

Chair of the Department of Geosciences

Dean of the Graduate School

I understand that my thesis will become part of the permanent collection of Oregon State University libraries. My signature below authorizes my release of my thesis to any reader upon request.

Andrew Cody Beedlow, Author

ACKNOWLEDGEMENTS

I would like to thank the following people for supporting me on this odyssey. Peter Clark for his inspiration, motivation, and guidance from my undergraduate study to present. It was an undergraduate class taught by Peter that inspired me to become a geologist, and pursue studies in glaciers and climate change. I probably would have still been an engineering major if it were not for that class. It was also Peter who encouraged me to come back to pursue my Masters in Science after my undergraduate studies. I am deeply humbled and honored to have studied under him. Steve Hostetler for supplying the instrumentation, and guiding me through the learning curves associated with meteorological observations and computational modeling. From start to finish, Steve was always available to help me through the various trouble shootings with the OSU SEBM. Steve played a critical role in the development of chapter 3 of this thesis. Ron Waschmann for his help with the calibration and setup of the various sensors used in this thesis. Sam Powell for volunteering all of those days to help me on the Collier Glacier. It takes a special person to volunteer to haul heavy loads in the mountains and dig endlessly deep snow pits. Faron Anslow for his guidance and expertise with the OSU SEBM and his field help on a failed winter balance trip in March 2009. Amy Lange for her support through this entire process, including physical support out in the field and emotional support with the modeling. Finally, I would like to thank my parents. Both mom and dad motivated me to continue my education and they have been a valuable resource for me throughout this experience. My dad also served as another advisor for me with his expertise on field data

collection. His tutelage through the often chaotic realm of fieldwork was truly valuable and will benefit me for years to come.

CONTRIBUTION OF AUTHORS

All of the papers within this thesis benefited from the substantial efforts of several co-authors. Peter Clark provided the motivation, valuable discussions, and insight on all aspects of this thesis. Steve Hostetler provided guidance and motivation with the modeling aspects of this thesis, as well as providing the instrumentation necessary to run the model.

TABLE OF CONTENTS

TABLE OF CONTENTS (Continued)

Page

TABLE OF CONTENTS (Continued)

LIST OF FIGURES

LIST OF FIGURES (Continued)

LIST OF FIGURES (Continued)

LIST OF FIGURES (Continued)

LIST OF TABLES

LIST OF APPENDIX FIGURES

LIST OF APPENDIX TABLES

The Use of Surface Energy Balance Models As a Means to Quantify Changes in Glacier Mass Balance: an Application to the Collier Glacier

Chapter 1

Introduction

1.1 Purpose

Throughout modern history, paintings, photos, and first-hand observations witnessed the ebb and flow of alpine glaciers, raising questions about the mechanisms that control these flowing perennial masses of snow and ice that shape the high mountains and provide important water resources to many. Many of the first connections with glaciers and climate came from the Alps, where local villages relied on the nearby glaciers as natural reservoirs, storing water in the wet winter months, and releasing it in the dry summer months. As early as 1788, Horace-Bénédict de Saussure was one of the first to make high altitude meteorological observations on the Col du Géant (3360 m) on Mount Blanc using a hair hygrometer to record fluctuations in relative humidity. From these data, combined with other observations in Chamonix and Geneva, he was able to study temperature lapse rates and its diurnal fluctuations (Barry, 1992). Nearly a century after de Saussure's meteorological observations above Chamonix, Finsterwalder and Schunk (1887) were the first to assume that glacier melting depends on air temperature from their study of the variations of the Suldenferner in the Eastern Alps. This assumption between air temperature and

glacier melt is the foundation of many melt models still used today. In the early half of the 20th century, Swedish glaciologist Hans Wilhelmsson Ahlmann was one of the pioneers in making glaciology an exact and precise science, laying the foundation for the methodology behind mass-balance measurements. A 1934 Swedish-Norwegian Spitsbergen Expedition, led by H.W. Ahlmann and H.U. Sverdrup, carried out detailed glaciological measurements as well as the study of the heat balance between the atmosphere and the snow surface (Ahlmann, 1935). Here, Sverdrup carried out detailed meteorological measurements investigating the dependence of ablation on solar radiation and convection in the atmospheric boundary layer above a melting glacier, pioneering the relationship between ablation and energy balance. His results indicated that the majority of ablation was attributed to solar radiation, followed by convection (Ahlmann, 1946). Furthermore, Sverdrup noted that the importance of convection decreases with altitude and increases over the course of the ablation season (Ahlmann, 1946). These observations developed through the years into complex numerical models that quantify the behavior of glaciers in response to changes in climate. The development of these melt models, combined with a larger network of glacier monitoring programs, led to a better understanding of the different meteorological parameters that govern the response of mountain glaciers, thus furthering our understanding of these critical linkages between glaciers and climate change (Meier, 1965).

The quantitative relationship between glaciers and climate change lies in a glacier's mass balance. A glacier's mass balance documents the amount of mass a

glacier accumulates and ablates over a given year. A positive mass balance reflects a mass gain and subsequent advance for a glacier, while a negative mass balance reflects a mass loss for a given year resulting in a subsequent retreat. Furthermore, mass-balance studies have also provided insights on the socioeconomic ramifications of glacier fluctuations, both locally and globally. It was not until the 1980's that it became apparent that glaciers and ice caps are significant contributors to sea level rise (Meier, 1984). Recent studies compiling the present understanding of glacier fluctuations indicate that small glaciers and ice caps (GICs) are significant contributors to 21st century sea level rise, due to their larger mass turnover and resultant faster response times than the large ice sheets of Greenland and Antarctica (Meehl et al., 2007; Meier et al., 2007; Pfeffer et al., 2008).

Alpine glaciers are highly influenced by local meteorological conditions, which varies significantly both spatially and temporally. However, glacier-monitoring programs worldwide are concentrated in a few locations. Furthermore, only approximately 70 of the 340 glacier mass-balance programs worldwide have uninterrupted annual mass-balance observations spanning longer than 20 years (Dyurgerov, 2010). Furthermore, logistical and economic difficulties of working in mountainous environments have prevented continuous mass-balance measurements, as in the case with the Collier Glacier monitoring program conducted by Oregon State University from 1989-1994.

In North America, the United States Geological Survey (USGS) has long-term monitoring programs on two glaciers in Alaska (Gaulkana and Wolverine Glaciers)

and one in Washington (South Cascade Glacier). Although such programs provide critical long-term records of these three glaciers, these data are mostly representative of their respective geographic location. Furthermore, recent mass balance compilation projects stress that very small glaciers (areas less than 1 km^2) are poorly represented in the world inventory of monitored glaciers (Dyurgerov, 2010). In addition, their mass-balance regime may be quite different from that of larger glaciers, where the majority of glacier monitoring programs resides (Kuhn, 1995). These benchmark glaciers are the foundation for the calibration of statistical models, estimating the contribution of small glaciers to global sea level rise (Meier, 1984). However, these long-term records constitute a biased sample of the world's small glaciers (Meier, 1984). Thus, as our understanding of the linkages between glaciers and climate change grow, the demand for more robust models and more efficient monitoring programs also grow, stressing the importance of setting up efficient monitoring programs in more remote localities to alleviate any potential biases associated with the benchmark glacier system. Glacier mass-balance data are also important for climate change policy where much of the focus is centered on detecting global climate change and explaining sea level rise (Meier, 1984; Oerlemans and Fortuin, 1992; Meehl et al., 2007; Meier et al., 2007).

One strategy to assess a glacier's response to climate is to measure directly the glacier's mass balance over a long (decadal) time period. Mass-balance measurements typically consist of measuring the amount of accumulation by snow density profiles from pits dug in representative locations, and depth-sounding profiles up the glacier's

centerline. Summer ablation can be measured with reference stakes drilled in the ice to measure surface lowering. The water equivalent ablation is determined by multiplying the measured ice surface lowering by a constant density of ice, often 0.917 g cm^{-3}. Measuring mass balance on an alpine glacier, however, requires an extensive investment in time and equipment. Moreover, because glaciers are often located in remote areas, it is difficult to carry out mass-balance measurements. An alternative strategy is to use numerical melt models to simulate ablation and help quantify the sensitivity of glaciers, providing a means to evaluate the response of ecosystems and water resources of glaciated regions of the world (Anslow et al., 2008). Such models, however, require validation with field measurements of mass balance.

The purpose of this research is to calibrate the OSU surface energy balance model (SEBM) developed by Anslow et al. (2008) with mass-balance measurements from the Collier Glacier in the Oregon Cascade Range (44° 10' N, 121° 47' W). Previous studies, combined with new mass-balance measurements made as part of this thesis, helped further validate the OSU SEBM and adjust the parameters to fit different glaciers. Monitoring the energy balance, and the associated mass balance, of the Collier Glacier provides additional insight on the temperature and precipitation effects that govern the Collier Glacier's mass balance. Furthermore, the OSU SEBM was compared to other models using simpler calculations to validate and determine the practicality of using more physically comprehensive models to simulate glacier mass balance on remote glaciers.

1.2 Summary of Chapters

Chapter 2 presents the mass-balance measurements conducted on the Collier Glacier from 2008-2010. The field methods for both the winter accumulation and summer ablation are described. These measurements were compared to previous measurements on the Collier Glacier from 1989-1994, providing an update on the status of the Collier Glacier with regards to its mass balance. Such measurements, however, are not typically conducted in the Oregon Cascade Range due to logistical constraints.

Chapter 3 presents the calibration of a distributed surface energy balance model (SEBM), originally developed on the South Cascade Glacier, Washington (Anslow et al., 2008). The field methods used for this model are described. This chapter presents simulations of the 2009 and 2010 ablation seasons on the Collier Glacier. Model comparisons were also conducted to validate and compare the practicality of the OSU SEBM with simpler modeling methods. Finally, a sensitivity analysis was performed for all melt models considered in this study for the 2010 ablation season to determine the various meteorological inputs and parameters that govern the Collier Glacier's mass balance.

1.3 References

Ahlmann, H.W. (1935), Contribution to the Physics of Glaciers, *The Geographical Journal*, 86, 97-107.

Ahlmann, H.W. (1946), Researches on Snow and Ice, 1918-40, *The Geographical Journal*, 107, 1, 11-25.

Anslow, F.S. (2008), Modeling and Dating Glacier Fluctuations and Their Relation to Pacific Ocean Climate, *Unpublished PhD*. Thesis, Oregon State University, 159 pp.

Anslow, F. S., S. Hostetler, W. R. Bidlake, and P. U. Clark (2008), Distributed energy balance modeling of South Cascade Glacier, Washington and assessment of model uncertainty, *Journal of Geophysical Research*, 113, F02019.

Barry, R.G. (1992), *Mountain weather and climate*, Routledge, Chapman, and Hall, Inc., New York, NY, 402 pp.

Dyurgerov, M.B. (2010), *Reanalysis of Glacier Changes: From the IGY to the IPY, 1960-2008*, Data of Glaciological Studies, Publication 108, Moscow, 116 pp., ISSN 0130–3686.

Finsterwalder, S. and H. Schunk (1887), Der Suldenferner. Zeitschrift des Deutschen und Oesterreichischen.

Kuhn, M (1995), The mass balance of very small glaciers, Zeitschrift für Gletscherkunde und Glazialgeologie, 31, 171-179.

Meehl, G.A., T.F. Stocker, W.D. Collins, P. Friedlingstein, A.T. Gaye, J.M. Gregory, A. Kitoh, R. Knutti, J.M. Murphy, A. Noda, S.C.B. Raper, I.G. Watterson, A.J. Weaver and Z.-C. Zhao (2007), *2007: Global Climate Projections. In: Climate Change 2007: The Physical Science Basis. Contribution of Working Group I to the Fourth Assessment Report of the Intergovernmental Panel on Climate Change* [Solomon, S., D. Qin, M. Manning, Z. Chen, M. Marquis, K.B. Averyt, M. Tignor and H.L. Miller (eds.)]. Cambridge University Press, Cambridge, United Kingdom and New York, NY, USA.

Meier, M.F. (1965). Glaciers and climate. *In* Wright, H.E. and D.G. Frey (eds.), *The Quaternary of the United States*, Princeton University Press, Princeton New Jersey, 795-805.

Meier, M.F. (1984), Contribution of Small Glaciers to Global Sea Level, *Science*, 226, 4681, 1418-1421.

Meier, M.F, M.B. Dyurgerov, U.K. Rick, S. O'Neel, T. Pfeffer, R.S. Anderson, S.P. Anderson, and A.F. Glazovsky. (2007), Glaciers Dominate Eustatic Sea-Level Rise in the 21st Century, *Science*, 317, 1064-1066.

Oerlemans, J., and J.P.F Fortuin (1992), Sensitivity of Glaciers and Small Ice Caps to Greenhouse Warming, *Science*, 258, 5079, 115-117.

Pheffer, W.T., J.T. Harper, and S. O'Neel (2008), Kinematic constraints on glacier contributions to 21st century sea-level rise, *Science*, 321, 1340-1343.

Chapter 2

Collier Glacier Mass Balance 1989-2010

A. Cody Beedlow[*1], Peter U. Clark[1], and Steven W. Hostetler[2]

[1]Department of Geosciences, Oregon State University
Corvallis, Oregon 97331

[2]United States Geological Survey, Oregon State University
Corvallis, Oregon 97331

2.1 Abstract

Mass-balance measurements have been conducted on the Collier Glacier for the 2009 and 2010 balance years, adding to similar measurements that were conducted on the glacier from 1989-1994. Results indicate that although the variations in the Collier Glacier's mass balance are characterized by years with significant mass loss and years of mass gain, the general form of the Collier Glacier's net balance did not change appreciably between the 1989 and 2010, with high ablation gradients below the ELA and low gradients above the ELA. Nevertheless, there was a slight increase in elevation of the location of maximum ablation as well as the terminus, coinciding with the decrease in surface area from 0.85-0.9 km^2 to 0.6-0.7 km^2 since completion of the last study in 1994. These data suggest that the net balance curve continues to translate back and forth along the x-axis from year to year, depending on the timing and magnitude of winter snow accumulation and summer temperatures. The present glacier hypsometry and position of the ELA suggests that potential negative balance years could result in an ELA that is above the icefall, exposing a significant amount of mass to the ablation area, enhancing ablation and subsequent retreat.

2.2 Introduction

Changes in glacier size and volume reflect the integrated response of a glacier to fluctuations in precipitation and surface energy balance that result from climatic fluctuations. Alpine glaciers are particularly sensitive to such changes in climate with response times measured from decadal to centennial time scales, depending on the glacier size and its mass balance. Thus, a glacier's mass balance provides a critical linkage between changes in climate and advances and retreats of glaciers (Figure 2.1). Glaciers adjust according to periods of positive or negative mass balance by thickening and advancing, or thinning and retreating. Thus, glacier mass balance quantifies the amount of water a glacier gains or loses annually. As a result, mass-balance data are valuable indicators of changes in climate, because it is a consequence of the combination of conventional climate parameters, temperature and precipitation. Extended mass-balance measurements help quantify the contribution of glaciers to local hydrology, and assess the possible impacts of present glacial fluctuations. Nevertheless, the complexity and expense of working in an alpine environment makes these measurements difficult and limited, thus restricting our full understanding of the spectrum of variability each glacier possesses. Most mass-balance measurements are conducted on a handful of benchmark glaciers worldwide. As a result of these limited measurements, our understanding of the response of these alpine glaciers to climate change and their contribution to 21st century sea level rise is not fully understood.

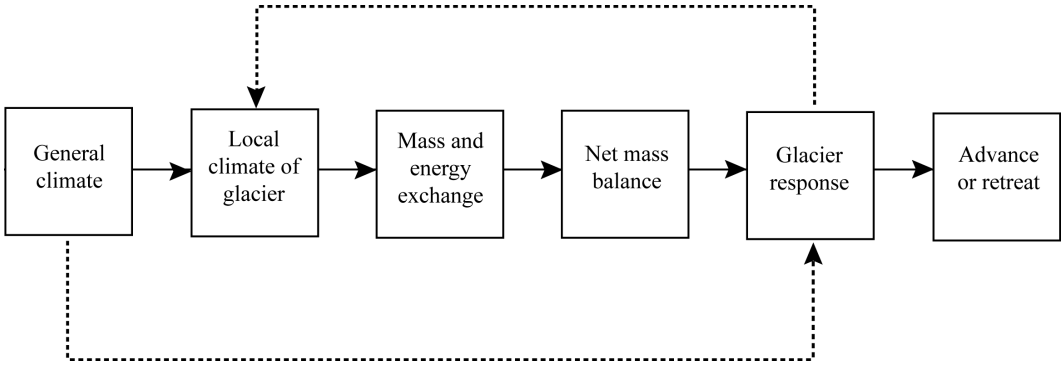

Figure 2.1: Generalized linkage between general climate and the advances or retreat of glaciers. *Figure from Meier (1965)*

Although the amount of ice stored in alpine glaciers is only a fraction of that stored in the Greenland and Antarctic Ice Sheets, alpine glaciers are an important component of the 21st century sea-level budget, since their response time is shorter than that of large ice sheets due to their larger mass turnover (Oerlemans and Fortuin, 1992). Global sea level rise is a matter of international concern since it threatens low-lying coastal areas, many of which are highly populated. Meier et al. (2007) suggested that glaciers and ice caps (GIC), which comprise all land ice excluding Greenland and Antarctic ice sheets, contribute about 0.1 to 0.25 m of the eustatic component of 21st-century sea-level rise. The Intergovernmental Panel on Climate Change (IPCC) Assessment Report 4 (AR4) (2007) predicted a total sea level rise by the end of the century of approximately 0.2 to 0.5 m with 0.14 to 0.17 m from GIC, with a large fraction of the present global GIC mass disappearing as a result (Meehl et al., 2007). Pfeffer et al. (2008) determined that a minimum contribution from all sources, including the Greenland and Antarctic ice sheets, over the next 100 years would most likely be around 0.8 m. Nevertheless, these relationships between climate and sea level rise are convoluted by the ablation of snow and ice, which is difficult to measure in remote mountain settings (e.g. Ahlmann, 1935; Østrem and Brugman, 1991; McDonald, 1995). These uncertainties associated with 21st century sea level rise can be minimized with better constraints, both spatially and temporally, on the mass balance of small glaciers and ice caps.

For some regions of the world, the retreat of alpine glaciers would have additional socioeconomic impacts since glaciers act as natural reservoirs, storing water

in the winter and releasing it in the dry summer months, making them an important water resource. A reduction in glacier mass could jeopardize water resources for large populations living near mountainous regions such as Europe, India, China, and the Pacific Northwest of the United States and Canada. Such reductions could strongly impact sanitation, agriculture, hydroelectricity, and even recreation, thus jeopardizing the socioeconomic structure in many of these regions. Most glaciers in these regions have minimal mass-balance records, so little is known about their sensitivities to climate change as well as their contributions to regional hydrology.

2.2.1 Field Site

The Collier glacier is a small temperate valley glacier, covering approximately 0.6-0.7 km^2. Located in the Three Sisters Wilderness in the Oregon Cascade Range (44° 10' N, 121° 47' W), this north-northwest facing glacier originates on the northern flanks of Middle Sister (3062 m) at an elevation of 2720 m, and crosses below the western face of North Sister (3074 m), where it terminates at an elevation of 2295 m (Figure 2.2). Its maximum areal extent during the Little Ice Age (locally circa 1300-1850) was approximately 2.4 km^2 (O'Connor et al., 2001; McDonald, 1995). Previous studies on the Collier Glacier from 1989-1994 determined the area of the glacier to be approximately 0.85-0.9 km^2 (O'Connor et al., 2001; McDonald, 1995). Photographs

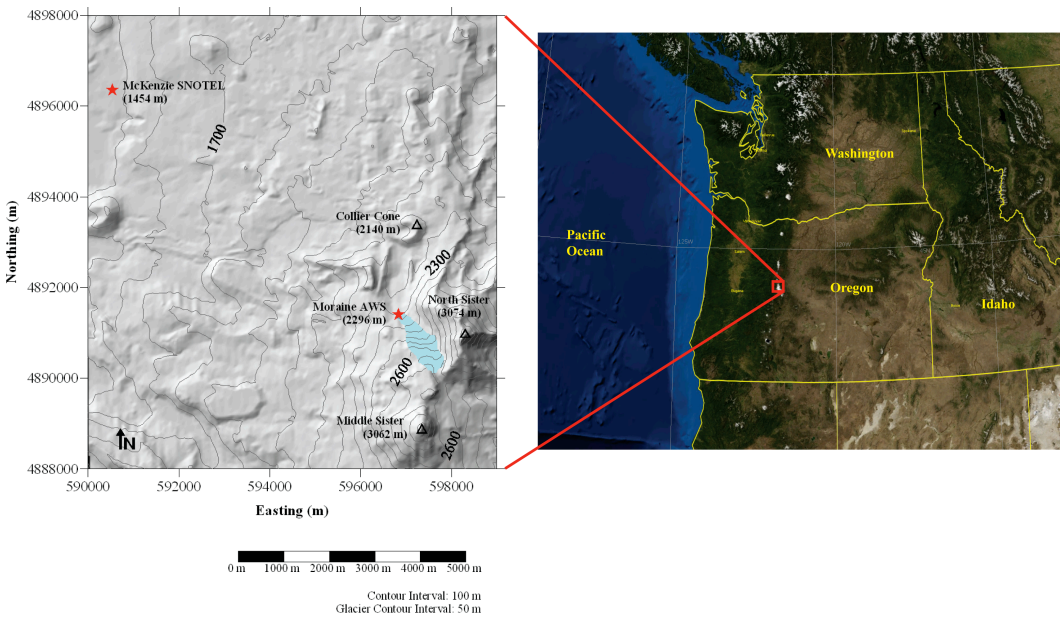

Figure 2.2: The location of the Collier Glacier. The glacier originates from an elevation of approximately 2720 m and terminates at an elevation of approximately 2300 m. The icefall lies between 2450 and 2600 m.

taken throughout the 20th Century of the Collier Glacier provide one of the most complete records of historic glacier retreat in Oregon (Figure 2.3) (Hopson, 1960; O'Connor et al., 2001). Nevertheless, glacier monitoring and records of glacier change are elusive in the Oregon Cascades, with studies centralized to the Elliot Glacier on Mt. Hood (e.g. Jackson and Fountain, 2007; Lundstrom et al., 1993) and the Collier Glacier on North and Middle Sister (e.g. Hopson, 1960; Mountain, 1977; Mountain, 1990; McDonald, 1995). This unique photo record, however, documents the Collier Glacier's retreat from its Little Ice Age maximum extent to its present position, approximately 1.6 km up valley. These records, coupled with areal photography and digital elevation models (DEMs), provide areal data necessary for 20th century reconstructions (McDonald, 1995). These data suggest that there was a substantial reduction in glacier mass during the period between the late Little Ice Age maximum extent (approximately 1850) and 1910, which was accompanied by glacier thinning (McDonald, 1995; O'Connor et al., 2001). However, the terminus position did not retreat substantially from its Little Ice Age moraines until the early 20th century (McDonald, 1995; O'Connor et al., 2001). This lagged response was most likely due to the large volume of ice stored behind the tall terminal and lateral moraines associated with the presence of Collier Cone, which blocked the advance of the glacier, resulting in over thickening of ice (McDonald, 1995; O'Connor et al., 2001). Between 1910 and 1950, there was a rapid retreat of the Collier Glacier's terminus, which resulted in a significant reduction of glacial area and ice volume

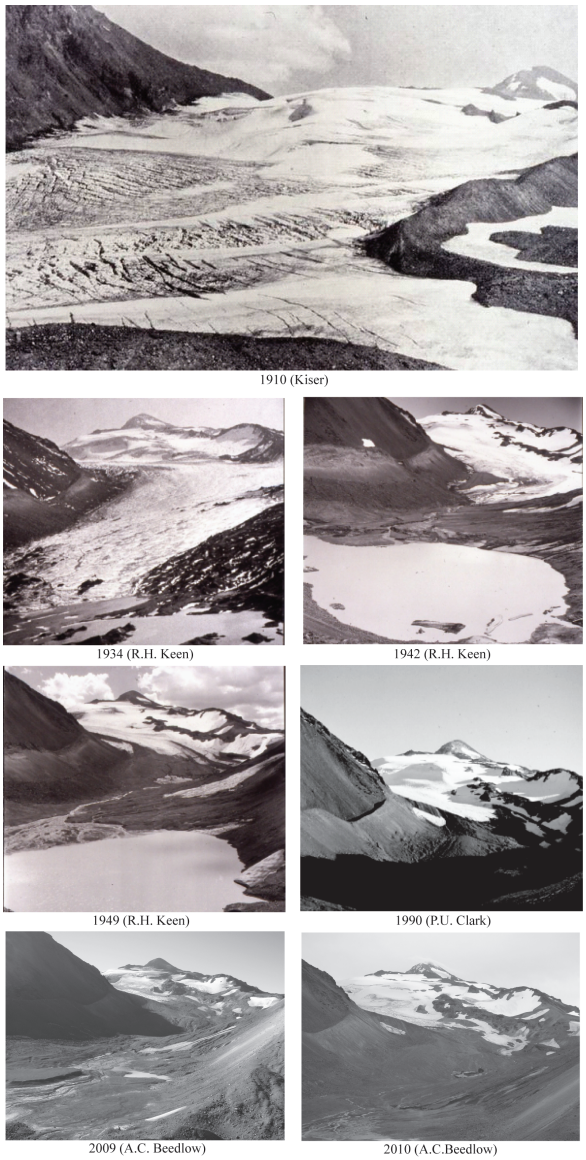

Figure 2.3: A sequence of photographs displaying the retreat of the Collier Glacier from 1910 to 2010. The lower six photographs were taken, looking south from the Collier Glacier viewpoint on Collier Cone. Note, North Sister's western spur is visible on the upper left corner, as well as Middle Sister on the upper right of each photograph for reference.

(Hopson, 1960; McDonald, 1995). Studies in the Three Sisters Wilderness indicated that since the early 1980's and through the mid 1990's, there has been continued retreat of glaciers in the Cascade Range (McDonald, 1995; O'Connor et al., 2001). These observations coincide with the Collier Glacier's rise in terminus elevation from 1990's to 2010, as also seen in the mass balance data.

Ice thickness surveys conducted by Drieger and Kennard (1986) used ground-penetrating radar to estimate an ice volume of 1.98×10^7 m^3, with a maximum thickness of 91.44 m. Total ice volume in the Three Sisters Wilderness was approximately 1.59×10^8 m^3 (Drieger and Kennard, 1986). However, there are have been no recent surveys in the Three Sisters Wilderness for accurate volumetric changes since 1986.

2.2.2 Regional Climatology

The Three Sisters Wilderness includes a cluster of composite volcanoes exceeding 3000 m, creating large vertical relief for the region. This dramatic vertical relief, in conjunction with moist, mid-latitude winter cyclonic storms, provides winter snowfall that is conducive to glaciation. Most of the precipitation in this region is derived from the North Pacific. The regional climate of the Collier Glacier and the Three Sisters Wilderness is highly dependent upon the dominant direction of storm tracks moving across the Pacific Northwest (PNW) as determined by regional

circulation patterns. In the PNW, annual circulation patterns are controlled by two semi-permanent high and low pressure systems situated near the Aleutian Islands in the Northeast Pacific (Phillips, 1960). In the winter months, a low-pressure cell (Aleutian Low) dominates this region of the Pacific, bringing in westerly and southwesterly flows to the PNW. In the summer months, a high-pressure cell (Pacific High) moves into the North Pacific Ocean, bringing westerly and northwesterly flows to the PNW. Other air masses can also influence the PNW climate. For example, sometimes during the winter months, polar continental air masses located east of the Rocky Mountains can encroach on the Pacific Coast regions, causing anomalously cold and dry winter weather (Mountain, 1978).

As a result of these shifts in these high and low pressure systems of the North Pacific, the PNW is considered a temperate maritime climate, dominated by winter Pacific frontal systems moving eastward over the continental United States. The Cascade Mountains are a major orographic barrier that intercepts much of the eastward-flowing moisture from the Pacific, and as a result, these frontal systems bring ample snowfall to the higher regions in the Cascades. For example, the Collier Glacier's average net winter balances for 2008-2009 and 2009-2010 were 1.6 m.w.e and 3.06 m.w.e respectively. In the summer months, the northward expansion of the Pacific High and diversion of the prevailing westerlies to the north result in warm, dry summers in the PNW (O'Connor et al., 2001). As a result, precipitation generally occurs largely during the winter months and is at the greatest magnitude at the higher elevations of the High Cascades, while the summer months receive little precipitation.

Since the climate in this region is highly influenced by the North Pacific, natural modes of variability from large climatic oscillations in the Pacific Ocean, such as the Pacific Decadal Oscillation (PDO) and the El Niño-Southern Oscillation (ENSO), can influence both regional temperature and precipitation, thus influencing the glacier mass balance in this region (Josberger et al., 2007). Mote et al. (2005) determined that only a small fraction of the variance of precipitation is explained by any Pacific climate indices. In addition, the fairly monotonic increase in temperature exceeds what can be explained by Pacific climate variability and is consistent with the global pattern of temperature increases, suggesting the importance of temperatures on snowpack in the Cascade Range.

The observed 19th and 20th century glacier retreat in the Oregon Cascades is likely the result of regional and worldwide warming since the 19th Century following the end of the Little Ice Age (Hopson, 1960; Meier, 1984; McDonald, 1995; O'Connor et al., 2001). Photo records and long term mass balance measurements (primarily from USGS benchmark glaciers) in this region demonstrate the sensitivity of these temperate alpine glaciers to changes in climate (Hopson, 1960, Meier and Tangborn, 1965; Tangborn, 1980; Josberger et al., 2007). These changes in climate are often reflected in the mass budget of these glaciers. Tangborn (1980) demonstrated that a decrease in summer air temperature of just over 0.5 degrees Celsius or an increase in winter accumulation of slightly more than 10% (350 mm w.e) from average would result in glacier growth and subsequent advance. For Cascade Range glaciers, where the mass turnover is high, the changes in temperature or precipitation required to cause

a terminus response is quite small (O'Connor et al., 2001). Furthermore, the response times of these glaciers to perturbations in regional climate are quite small, likely decadal timescales or less (Hubley, 1956; Burbank, 1982; McDonald, 1995). Thus, the Cascade Range glaciers respond to the combined influence of winter snowfall accumulation and summer ablation, as observed from long-term mass balance programs such as the one on the South Cascade Glacier, Washington (Meier and Tangborn, 1965; Tangborn, 1980).

2.3 Methods

2.3.1 Mass-Balance Measurements

A glacier's mass balance is the algebraic sum of the amount of accumulation and ablation a glacier undergoes annually. Accumulation consists of all processes by which snow and ice is added to a glacier, which includes precipitation as snow, refreezing of liquid water, condensation of ice from vapor and transport of snow from wind and avalanches. Ablation consists of all processes by which snow and ice are lost from the glacier, which includes melting, evaporation, wind erosion, removing of ice and snow from avalanching, and calving. Therefore, a glacier's net budget, or mass balance, is the algebraic difference between accumulation and ablation, making the glacier's net budget a vital link between the climatic environment and the

dynamical adjustments of the glacier (Figure 2.1) (Meier, 1965). There can be surface, englacial, and/or subglacial accumulation and ablation, however, englacial and subglacial accumulation and ablation are generally negligible compared with surface accumulation and ablation, except in the case of ice shelves and floating glacier tongues (Meier, 1962). In the case of mass-balance measurements conducted on the Collier Glacier, the primary focus was on surface ablation and accumulation. Making similar assumptions as Meier (1962), mass-balance quantities were measured vertically so they can be related to locations and then projected on a horizontal surface to represent an area.

For any point on a particular glacier's surface, the winter mass balance (b_w) will be positive, and the summer mass balance (b_s) will be negative. Thus, the net balance (b_n) at any point on the glacier's surface is the algebraic sum of accumulation and ablation, where b_w is positive and b_s is negative (Paterson, 1994).

$$b_n = b_w + b_s \tag{1}$$

Over the course of one balance year, typically October to October, all points that have a $b_n \geq 0$ m.w.e fall within the accumulation area, while all points that have a $b_n \leq 0$ m.w.e fall within the ablation area on the glacier's surface. The location of the elevation that divides these two primary zones of net annual mass gain and net annual mass loss is known as the equilibrium line altitude (ELA).

Mass balance quantities can be expressed volumetrically by integrating the net mass balance quantities over the entire area of the glacier (S) so that they have dimensions of volume. These unites are denoted B_w, B_s, and B_n for the area-weighted

values of b_w, b_s, and b_n respectively. Thus, the net balance, B_n, can be determined from the relation (Paterson, 1994):

$$B_n = \int_{S_c} b_n ds + \int_{S_a} b_n ds \quad (2)$$

Where S_c is the area of the accumulation area and S_a is the area of the ablation area.

In all studies of the Collier Glacier's mass balance, attention was directed towards the specific net budget which is the gain or loss of mass at a specific point on the glacier, and the mean specific net budget which is the area average of specific net budgets of the whole glacier (Meier, 1962). The mean specific budget ($\overline{b_n}$) for the whole glacier can be determined from (Paterson, 1994):

$$\overline{b_n} = B_n / S \quad (3)$$

Where S is the area of the glacier. This is one of the most useful parameters for summarizing the change in a glacier over a given year (Paterson, 1994).

According to Paterson (1994), the balance year is defined by two instantaneous points in time where mass attains a maximum in early spring and a minimum in later summer. To record the mass budget at these two instants in time, a field team would need to occupy and perform measurements for some duration of time to determine the precise timing of these points in mass extreme for a particular glacier, which varies from year to year. This method is known as the time-stratigraphic method, which was the method used in the 2008-2010 studies, where routine trips to the glacier from April to October helped constrain the maximum accumulation and ablation on the Collier Glacier. For the 1989-1994 studies, logistical constraints of working on the Collier

Glacier prevented the use of the time-stratigraphic method to measure net mass balance. Instead, data were collected at points in time that defined a floating date measurement year, in which the end and beginning of each balance year were estimated to be early October. This method is referred to as the fixed date (Andrews, 1975), or annual system (Meier et al., 1971).

For both the 1989-1994 and the 2008-2010 studies, measurements were conducted in a similar fashion. Snow-covered areas of the glacier were measured with probes and crevasses to measure snow depth with respect to the previous year's surface, or summer surface (SS). Snow pits were dug in representative locations to measure snow thickness and density. These two quantities combined were used to estimate the water equivalent amount of snow on the glacier. Snow density was measured with a Taylor-LaChapelle snow density kit. Snow-free areas of the glacier were measured with PVC ablation stakes drilled into the ice and were measured routinely over the course of the ablation season.

2.3.2 1989-1994 Mass-Balance Measurements

2.3.2.1 Winter Balance

Due to the logistical difficulties associated with winter road closures and fickle weather, the only previous winter measurements conducted on the Collier Glacier was

in April of 1993. These accumulation measurements, however, were only conducted in the ablation area of the glacier, thus providing incomplete knowledge of winter accumulation in the upper reaches of the glacier. Other attempts were unable to approach the glacier, let alone collect accumulation measurements.

2.3.2.2 Net Balance

Ablation measurements were conducted on the Collier Glacier in early October from 1989-1994 with two parallel transects of ablation stakes along the presumed primary flowline that runs down the longitudinal axis in the ablation area. The lowest elevation stake was planted close to the terminus with each subsequent upglacier stake being planted at 100 m intervals (McDonald, 1995). The second transect of ablation stakes were deployed 30 m normal to this primary transect. The ablation stakes were constructed out of 1.25 inch PVC, cut into 1-meter segments, and planted into holes in the ice surface using a Kovacs drill system (McDonald, 1995). For the accumulation area, multiple snow pits and probe soundings were conducted in the accumulation area to estimate the net balance for the glacier (McDonald, 1995).

2.3.3 2008-2010 Measurements

2.3.3.1 Winter Balance

The 2008-2009 winter balance was measured on 10 May 2009. This date was assumed to be the time of maximum accumulation due to late spring snowstorms that prevented field measurements on 1 April 2009, in conjunction with the aid of local United States Department of Agriculture (USDA) Natural Resources Conservation Service (NRCS) SNOTEL stations, which provided a qualitative proxy for snow accumulation near Collier Glacier. The 2009-2010 winter balance measurements however, were conducted on 15 April 2010, 15 May 2010, and 26 June 2010, and these data, along with nearby SNOTEL stations, determined that the 15 May measurements represented the maximum accumulation for the glacier.

Both the 2008-2009 and 2009-2010 winter balance measurements were conducted by a transect of depth soundings every 100 meters up the glacier's centerline and a snow pit dug at 2600 meters to get a snow density profile (Figure 2.4). This pit was situated in a location above the icefall, near the glacier's centerline, which was thought to be the most representative location for the glacier. To better constrain the snow density differences between the accumulation area and ablation area, the 2009-2010 winter balance measurements had an additional pit dug near the terminus of the glacier at 2300 m. Snow density measurements were collected by

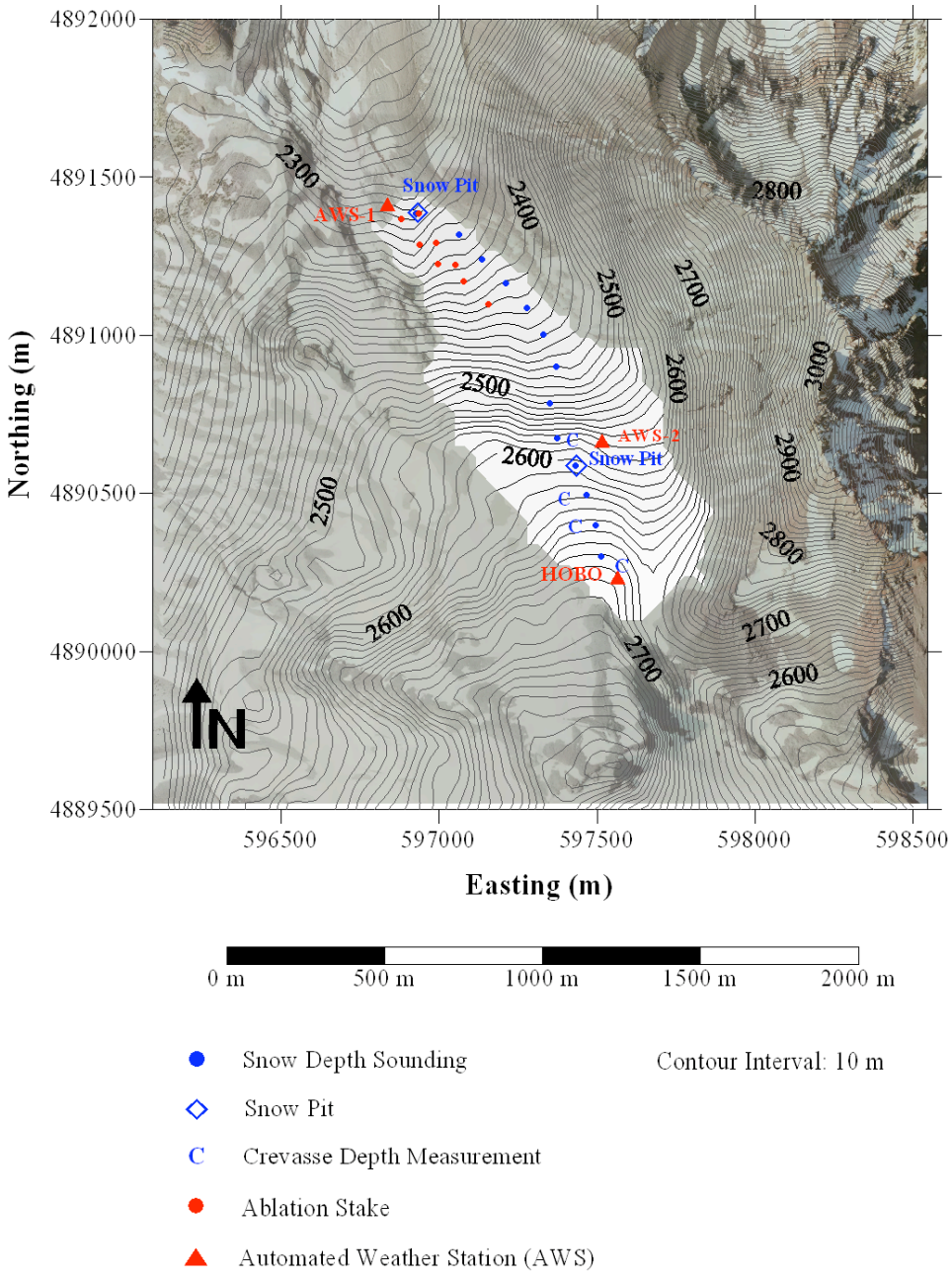

Figure 2.4: Orthotopo map displaying the measurement (red and blue circles) and AWS locations (red triangles) for the 2008-2010 studies. Blue circles are snow depth soundings, blue "C's" are crevasse snow depth measurements, red circles represent ablation stake locations, and blue diamonds represent snow pits for density measurements. North Sister is to the right of the glacier.

weighing approximately 100 cm^3 of snow every 3 cm for the depth of pit. The pit depth for the 2008-2009-balance year was approximately 4.5 m deep, and the pit depth for the 2009-2010-balance year was approximately 4 m deep at 2600 m and 2 m deep at 2300 m. Time constraints and fickle weather prevented the field teams from reaching the summer surface for the pits dug at 2600 m. Probe soundings at the deepest points in the pit revealed that the summer surface (SS) was less than 1 m below the deepest part of the snow pit. Thus, as a result of the difficulties of sampling deep snow packs, these measurements are likely to be minimum values. Nevertheless, we feel that the depths of these pits still provide adequate representation of the snowpack's average density. The pit dug at 2300 m reached the ice, providing a complete representation of the winter snowpack in the ablation area. In addition to the snow pits, both the 2008-2009 and 2009-2010 winter balance measurements also consisted of 13 probe soundings along the glacier's presumed flowline. These probe locations were made from the same coordinates along the presumed flowline for both the 2008-2009 and 2009-2010 winter balances for better comparison between the two balance years. The probes used for the depth soundings were made from solid aluminum, minimizing the uncertainties associated with probe deflections through ice lenses and dense snow layers.

2.3.3.2 Net Balance

Both the 2008-2009 and 2009-2010 net balance measurements were conducted by setting two parallel transects, approximately 50 meters apart, of ablation stakes in the lower reaches of the ablation area. The upper two stakes were set in a single transect near the center flowline to avoid crevasses and rock fall from North Sister. The stakes were set at 100-meter distances from each other, similar to the 1989-1994 mass-balance measurements (McDonald, 1995). The easternmost transect was set earlier in the summer of 2009, when the snow depth became less than 0.5 m. The westernmost transect was set later in the summer of 2009 when the snow depth became less than 0.5 m. Due to the constraints of working in a protected wilderness area, all ablation stakes were hand drilled using a Kovacs drill system, thus limiting the spatial coverage of stakes in the ablation area. Like McDonald (1995), each ablation stake consisted of three 1-meter long, 1.25-inch diameter white PVC pipe. These segments were allowed to melt out of the ice, minimizing any uncertainty associated with long ablation stakes leaning over due to its own weight. Each segment was marked to indicate the stake locality and depth.

Measurements were conducted every month during the ablation season and stakes were re-drilled when necessary to avoid lost data. For the ablation area, data recorded at individual locations were multiplied against their respective defined areas, and using a constant density for glacier ice of 0.917 gm cm^{-3} to determine the mass loss in meters of water equivalent (m.w.e). For the accumulation area, individual

measurement points were also area-weighted and used the average density from the snow pits to determine the mass gain in m.w.e. For the mean specific net balances, volumetric mass balance values (B_n) were calculated by taking the net balance at individual measurement locations and multiplying those values by the representative areas between each measurement location. Similar to McDonald (1995), the representative areas for the individual measurement points were defined by a boundary 50 m up glacier, a lower boundary 50 m down glacier, and lateral boundaries defined by local glacial margins. For the ablation area, the upper-most boundary for the highest ablation stake was defined by the ELA, while the terminus defined the lower boundary for the lowest ablation stakes. For the accumulation area, the upper-most boundary for the highest measurement point was defined by the local glacial margin, while the lower-most boundary was defined by the ELA. These data were converted into meters of water equivalent (m.w.e) to determine the mean specific net budget for the glacier.

Due to inclement weather during the fall of 2009, a net balance at the end of the ablation season was not conducted until the following summer of 2010. The summer balance measurements, in the accumulation area, were measured by snow pits and identifying the previous year's summer surface from the 2009-2010-winter accumulation. Crevasses also provided a stratigraphic estimation of the summer accumulation with distinct debris layers separating each balance year. Changes in snow density from the end of the ablation season were thought to be minimal, however, measurements were conducted below the SS to estimate snow density. For

the 2009-2010-balance year, monthly mass-balance measurements were conducted up the glacier to provide an evolution of the net balance of the glacier through the 2009-2010-ablation season (Figure 2.5). These data also helped with the calibration of the Oregon State University Surface Energy Balance Model (OSU SEBM), which was developed on the South Cascade Glacier (Anslow et al., 2008). Furthermore, these monthly measurements constrained the beginning and end of the ablation season, and provided an assessment of the temporal changes in the net balance over the course of the ablation season.

2.4 Results and Discussion

2.4.1 1989-2010 Mass Balance

When comparing the net balance (b_n) curves from the 2009-2010 balance year with the 1989-1994 mass-balance measurements, the Collier Glacier has characteristic mass-balance curve exhibiting a relatively steep gradient of b_n verses elevation in the ablation area below the ELA, and a relatively gentle gradient in the accumulation are above the ELA (Figure 2.6). Additionally, the net balance in the accumulation area from all studies indicates less variability when compared to the ablation area in terms of amount of ablation with elevation. Table 2.1 summarizes the Collier Glacier's mass

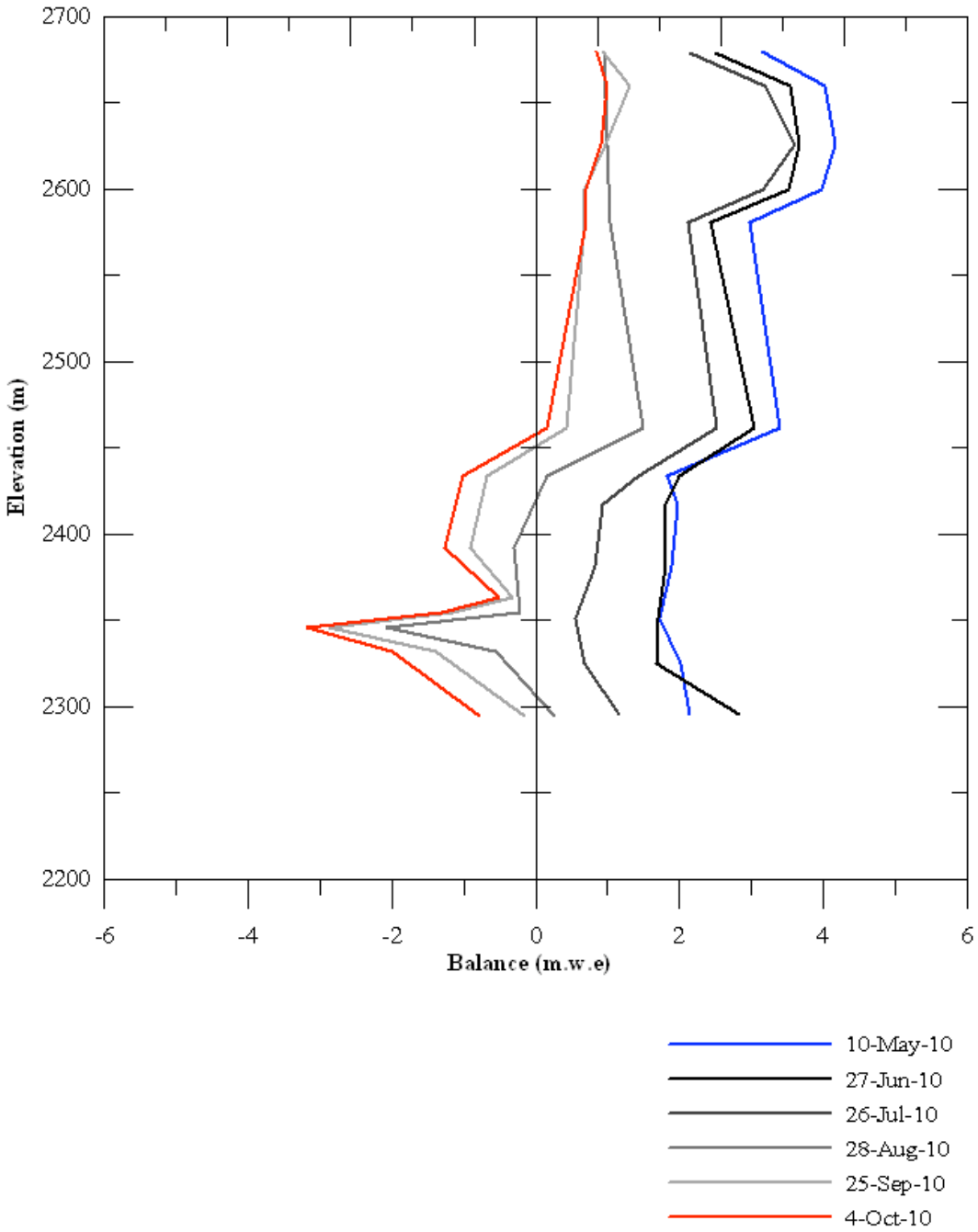

Figure 2.5: Collier Glacier monthly net balance (b_n) measurements from maximum accumulation to maximum ablation.

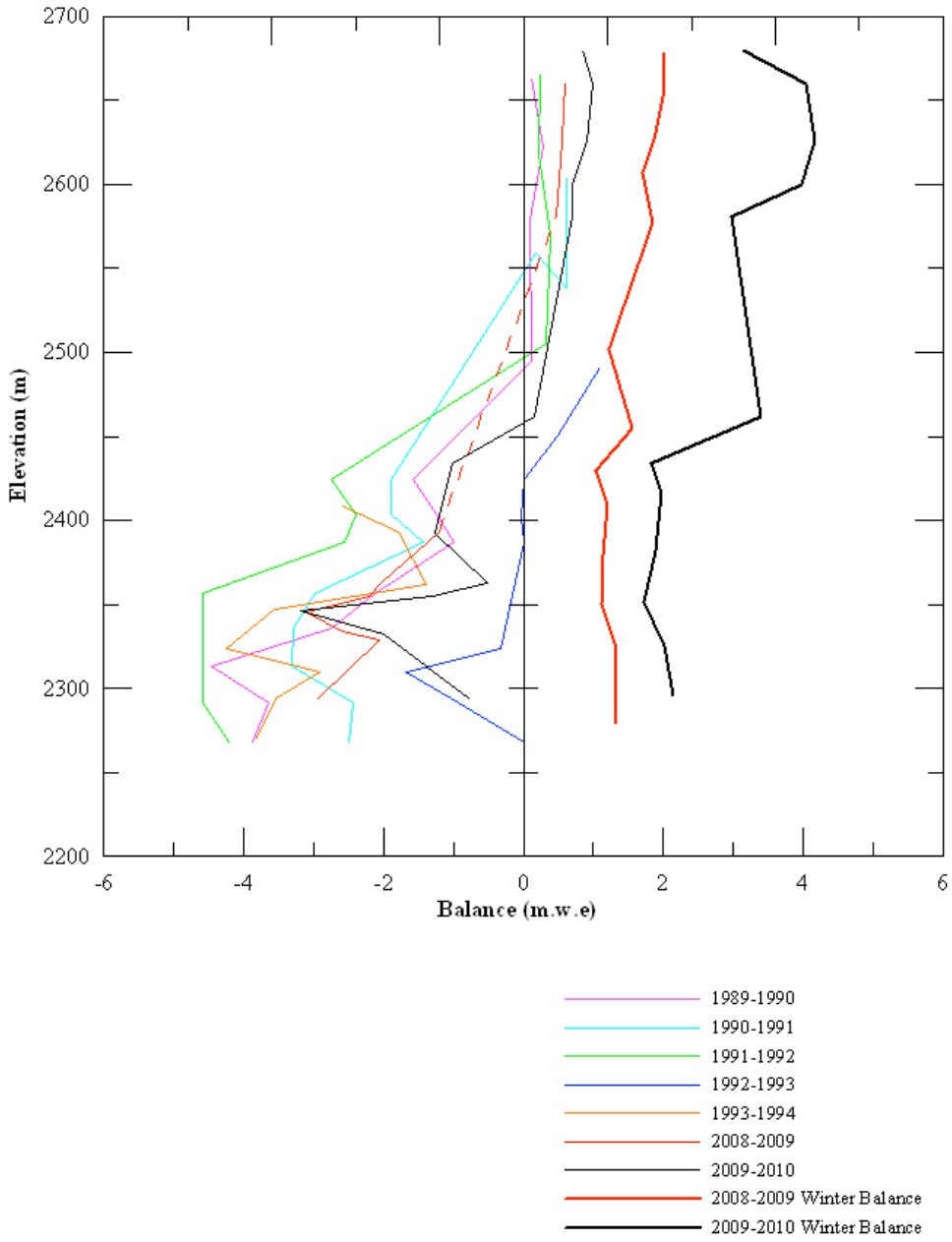

Figure 2.6: Net balance (b_n) verses elevation for all studies on the Collier Glacier (1989-1990), including winter balance measurements for 2008-2009 and 2009-2010 balance years (bold lines). *1989-1994 mass-balance measurements from McDonald (1995).*

Table 2.1: 1989-2010 mass balance results displaying the mean specific net balance (Ave. bn), ELA, AAR, and AI for all studies on the Collier Glacier.

Balance Year	Ave b_n (m H_2O)	ELA	AAR	AI
1989-1990	-0.62	2464.308 m (±15.24 m)	0.67	10-15 mm/m
1990-1991	-0.58	2472.538 m (±50.292 m)	0.67	20 mm/m
1991-1992	-1.5	2468.88 m (±24.384 m)	0.5	22 mm/m
1992-1993	1	2407.92 m (±4.572 m)	0.81	3 mm/m
1993-1994	NA	2529.84 m (±30.48 m)	0.35	NA
2009-2010	0.19	2458.8 m (±7.3 m)	0.75	23.8 mm/m

balance from field studies conducted between 1989 and 2010. The b_n curve for the 1990-1991-balance year shows a similar form and trend with the 1989-1990-balnce year, with a relatively steep gradient in the ablation area below the ELA, a relatively gentle gradient in the accumulation area above the ELA, and corresponding secondary fluctuations in the ablation area. The mean specific net balance for the 1989-1990-balance year was -0.62 m.w.e, while the 1990-1991-balance year resulted in a mean specific balance of -0.58 m.w.e. The 1991-1992-balance year represented a mass loss minimum as the result of a number of ablation stakes planted the previous year completely melted out. Thus, the corresponding B_n and mean specific net balance for this balance year represent minimal loss values. The mean specific net balance for the 1991-1992-balance year was -1.5 m.w.e. Nevertheless, the b_n curve for the 1991-1992 balance year shows similar form and trend with the previous balance years, with a relatively steep gradient in the ablation area below the ELA, a relatively gentle gradient in the accumulation area above the ELA, and secondary fluctuations in the ablation area. The 1992-1993-balance year was one of robust accumulation, which resulted in deep snowpack throughout the accumulation area. As a result of the difficulty in sampling the deep snowpack in the accumulation area, it is likely that the accumulation data derived from the upper reaches of the glacier represent a minimum, implying that the estimate for total accumulation, and the resultant positive net mass balance of 1.0 m.w.e represented a minimum value. In contrast to other measurement years, the 1992-1993-balance year's b_n curve exhibits a uniformly gentle gradient both above and below the ELA. However, due to the limitation in accumulation area

measurements and the resultant minimum values, it is plausible that the gradient of the curve above the ELA is steeper than represented. Nevertheless, the b_n curve shows a form and trend below the ELA similar to other measurement years, with similar secondary fluctuations. In contrast to the previous balance year, the 1993-1994-balance year was one of robust ablation, and as a result, many of the ablation stakes completely melted out. Thus, several of the b_n values calculated from stake data represent a mass loss minimum. Also, the development of the icefall prevented measurements in the accumulation area, thus a mean specific balance for the entire glacier could not be calculated. However, the mean specific balance for the ablation area was -2.67 m.w.e.

The 2008-2009-balance year experienced early fall storms that prevented measurements around the icefall. As a result, there were not enough data to estimate an ELA and net balance for the glacier. Nevertheless, the ablation area measurements showed a very similar shape and trend with the 1993-1994 and 1989-1990 balance years, and the mean specific balance for the ablation area was -2.10 m.w.e.. The b_n curve displays a relatively steep gradient in the ablation area with secondary fluctuations in the ablation area. When comparing the elevation of these secondary fluctuations with the 1989-1994 balance years, these fluctuations had risen to a higher elevation, along with the terminus elevation. Approximations of the ELA, when linearly interpolating between measurement locations below and above the icefall show a similar ELA with the 1989-1994 mass-balance measurements, falling somewhere between 2500 and 2550 m. These data suggest that this could be a

negative balance year, but there is no conclusive evidence due to the lack of measurements above and below the icefall to constrain the ELA.

The 2009-2010-balance year had late spring snowfall that resulted in a positive mass balance, with a mean specific net balance of 0.19 m.w.e and an ELA of approximately 2459 m ±7 m. This ELA was only second lowest to the 1992-1993-balance year's ELA of 2407 m ±4 m, both of these balance years resulted in a positive mass balance for the glacier, however, the ablation gradients below the ELA are much steeper, signifying greater mass loss in the ablation area compared to the 1992-1993-balance year. The b_n curve had a similar shape and trend as previous mass balance years with a steep gradient in the ablation area with secondary fluctuations leading to a gentler gradient in the accumulation area. Nevertheless, as also seen in the 2008-2009-balance year, some of the secondary fluctuations in the ablation area as well as the terminus had risen to a higher elevation, where the terminus elevation rose from approximately 2272 m to 2296 m. Even though the 2009-2010-balance year resulted in a positive mass balance, there was still considerable ablation, with a mean specific net summer balance of -3.07 m.w.e. As with the 2008-2009-balance year, maximum ablation occurred between the elevations of 2332 m and 2550 m, where there was a net balance of approximately -2.0 m.w.e and -2.25 m.w.e respectively, which is the locality of maximum ablation that characterizes the Collier Glacier's b_n curve.

2.4.2 Discussion

The variations in the b_n for the Collier Glacier during the 2008-2009 and 2009-2010 balance years are consistent with previous year's values in showing interannual variability, with significant mass loss, such as the 1991-1992 and 1993-1994 balance years, and years of mass gain, such as the 1992-1993 and 2009-2010 balance years. Such rapid changes in b_n have been observed on many other temperate alpine glaciers (Meier and Tangborn, 1965; Meier et al., 1971; Josberger et al., 2007). The Collier Glacier has maintained its distinctive b_n curve with steep ablation gradients below the ELA with secondary fluctuations, and shallow ablation gradients above the ELA. These secondary fluctuations reflect the elevations of maximum ablation. It is likely that these secondary fluctuations area a result of the local surface energy exchange in relation to slope, aspect, and surrounding topography. Ablation season observations noticed significant changes in the surface roughness due to crevasse development, ablation hollows, and surface melt runoff creating surface channels in the ablation area, all of which varied in size and shape over the course of the ablation season. Surface energy balance studies on temperate glaciers indicate that changes in the aerodynamic surface roughness length can greatly influence the surface energy balance of the glacier by affecting turbulent exchanges as well as the absorption of shortwave radiation (Brock et al., 2006; Anslow et al., 2008). This can be a significant amount of energy, considering the present katabatic flow on the Collier Glacier. Also influencing ablation in these lower regions is the presence of debris

derived from rock fall off of North Sister's west face, which lowers the surface albedo, thus increasing the contribution of net radiation to the glacier's energy balance. Wind transport and deposition also causes some variability in how snow accumulates on the glacier, as seen in the winter balance curves (Figure 2.6). This differential snow deposition influences the timing at which bare ice is exposed during the ablation season. These characteristics could also be a function of the glacier's slope and aspect. These observations, combined with ablation stake data, demonstrate an east-west variability in ablation across the ablation area.

The general form of the b_n curve did not change appreciably between 1989 and 2010, with a slight increase in elevation of the location of maximum ablation as well as the terminus elevation. The b_n curve continues to translate back and forth from a negative to positive mass balance year as a function of summer temperatures and winter precipitation. Meier and Tangborn (1965) described similar relationships in the b_n curve from mass balance studies on the South Cascade Glacier, Washington. This could be the result of the natural modes of variability associated with the Eastern Pacific. In addition, Folland et al. (1990) determined that there was a 0.45 ± 0.15 °C increase in global (combined land and ocean) air temperature since the late 19th century, which could explain the significant mass loss experienced by glaciers in the Cascade Range. However, on decadal timescales, temperature change has not been monotonic, but irregular, with periods of increasing temperature separated by periods of declining temperatures, explaining some of the variability in mass balance data over the 20th century in the Cascade Range (Meier and Tangborn, 1965; Meier, 1984;

McDonald, 1995; Josberger et al., 2007). These natural modes of variability could amplify the magnitude of the net balance by enhancing precipitation and/or temperature, but there is not a long enough mass-balance record to support this hypothesis for the Collier Glacier.

Mass balance data from 1989-1994 and 2008-2010 suggest relatively small changes in the ELA, ranging from 2450 m to 2550 m (Table 2.1), supporting the notion that the glacier is approximately in steady state with its mass budget. Nevertheless, areal calculations using from the most recent digital elevation models (DEMs) on Golden Software's SURFER suggest there has been significant areal loss. The 1989-1994 studies estimated the Collier Glacier to be around 0.85-0.9 km^2, whereas the 2008-2010 studies estimated the Collier Glacier to presently be around 0.6-0.7 km^2, suggesting an areal loss of greater than 20 percent with respect to the 1989-1994 calculations. These minimal changes in the ELA suggest that the relatively flat topography of this region of the glaciers allows significant areal and associated mass loss with minimal changes in the ELA (Figure 2.6).

The 2009-2010-balance year had an average b_n of around 0.19 m.w.e and an ELA of 2458 m located just below the icefall. The 1989-1990, 1990-1991, and 1991-1992 balance years had an ELA that ranged between 2464 m and 2473 m. The 1992-1993-balance year was a positive mass balance year so as a result, the ELA dropped to an elevation of 2408 m, the lowest of all measurement years. The 1993-1994-balance year saw robust ablation and as a result, the ELA climbed to an elevation of 2530 m. This range in the ELA describes the Collier Glacier's continued variable nature in

mass balance. These data also suggest that potential negative balance years could have an ELA that is above the icefall (2500 m), exposing a significant amount of mass to the ablation area, affecting the glacier's mass budget negatively and possibly enhance retreat. This was observed in the 1993-1994 balance years where the ELA climbed to an elevation of 2530 m.

A glacier's hypsometry plays an important role in the response of a glacier's terminus position with a changing climate (Furbish and Andrews, 1984). The relatively narrow tongue, fed by a relatively large accumulation area, must respond strongly to small changes in the glacier's mass balance (Furbish and Andrews, 1984). As a result of the hypsometry of Collier Glacier, the ablation area substantially increases as the ELA rises. Since the ELA is presently situated below the icefall, there is significant ablation occurring in the elevations below the icefall, further steepening the icefall. This steepening of the icefall creates a topographic barrier, where the slope of the glacier is gentle below the icefall, allowing significant mass loss and associated areal reduction without a significant rise in the ELA. Since the 2009-2010 average b_n was positive (0.19 m.w.e) and an ELA of 2460 m (second lowest out of the study years), situated just below the icefall, suggests that the current mass balance equilibrium is still below the icefall (2500 m). Reconstructions with an AAR of 0.65 put the ELA approximately at 2498 m, suggesting that if the ELA were to rise with possible negative balance years, it could rise to an elevation above the icefall, exposing this significant topographic feature to the ablation area, enhancing retreat. The hypsometry of the Collier Glacier is also conductive to retreat since surface area

increases with elevation (Figure 2.7). Thus, as the ELA rises in elevation due to potential negative balance years, more area will be exposed to the ablation area, further enhancing retreat (Furbish and Andrews, 1984). These two topographic features can have a pronounced influence on the Collier Glacier's future net budget, as 21st century temperatures are expected to rise (Meehl et al., 2007).

Andrews (1972) suggested that the accumulation area ratio (AAR) for temperate glaciers in steady-state equilibrium typically have a range of 0.6 to 0.7. The AAR is a useful general indication of the condition of the glacier's budget total (Meier, 1963). These values vary according to differences in glacier shapes and mass balance profiles (Furbish and Andrews, 1984; Bahr et al., 2009). Typical e-folding response times for glacier flow range from 10's to 1000's of years (decadal to millennial timescales) depending on the glacier's size (Bahr et al., 1998; Pfeffer et al., 2008). However, a glacier's climate can change from year to year, thus as the climate changes, the current AAR will not represent an equilibrium value (Bahr et al., 2009). As a result, a glacier must respond by changing its size until it reaches equilibrium with its local climate. AAR values for the Collier Glacier varied from 1989-1994 depending on the net balance of the glacier for that particular balance year (Table 1). Positive balance years (1992-1993 and 2009-2010) had AAR values that exceeded 0.7 suggesting a healthy balance year for the glacier, while negative balance years had AAR values as low as 0.35 as estimated in the 1993-1994-balance year. These values further support the high variability in mass balance associated with temperate glaciers.

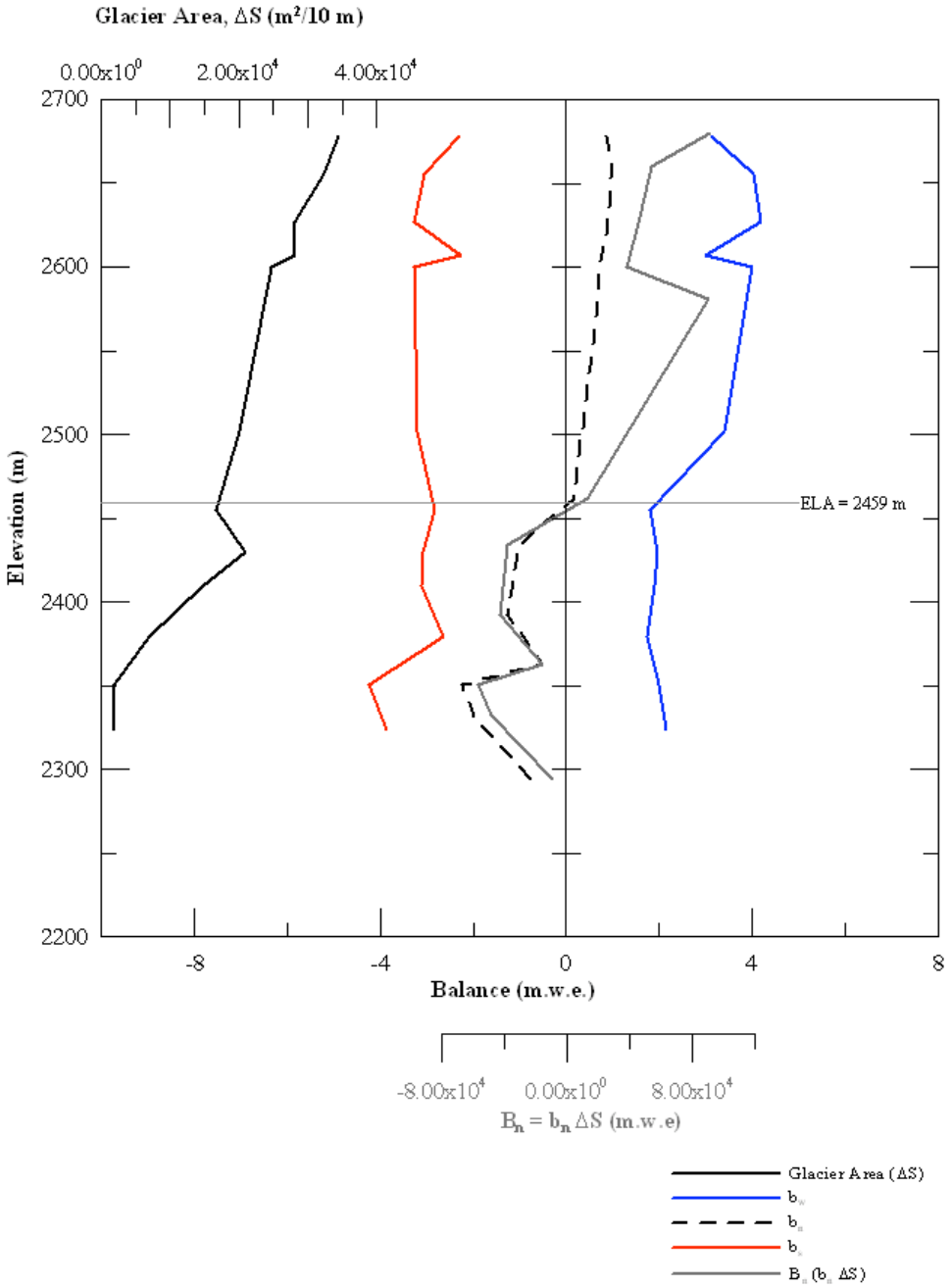

Figure 2.7: 2009-2010 Collier Glacier mass balance and hypsometry. The dashed curve represents the net balance (b_n), and the solid grey line represents the volumetric mass net balance (B_n). Summer (b_s) and winter (b_w) balances are the red and blue curves, respectively. The Collier Glacier's hypsometry is shown with the bold line to the far left.

A useful way to compare the Collier Glacier with other glaciers is to look at the activity index (AI) of that particular glacier. The AI is the gradient of the b_n curve through the ELA, and represents the mass flux through the ELA. Variations in the AI on the Collier Glacier were a direct reflection of the balance year (Table 1). Typical AI values for temperate glaciers near the Collier Glacier include: 5 mm/m (1700 m ELA) for the Blue Glacier, Washington; 17 mm/m (1900 m ELA) for the South Cascade Glacier, Washington; 20 mm/m for the Nisqually Glacier, Washington; and 23 mm/m (3600 m ELA) for the Maclure Glacier, California (Meier et al., 1971). The AI of the Collier Glacier ranged 3 mm/m to 22 mm/m during the 1989-1994 balance years. The 2009-2010-balance year had an AI of around 24 mm/m, still within typical range for temperate glaciers.

2.4.3 Uncertainties

The evaluation of potential error associated with mass-balance measurements as discussed in this section is difficult to quantify due to the inherent difficulty of measuring large masses of moving snow and ice. Observations on the Collier Glacier were concentrated towards the center flowline of the glacier to avoid crevasses and rock fall. Thus to determine the mean specific net balance for the entire glacier, measurements were extrapolated over the entire glacier, resulting in a generally

unknown error. Since these data are extrapolated over relatively large areas, a conservative estimate of error may be as high as ±0.12 m.w.e, following Meier et al. (1971), where the error of an indirectly measured quantity is equal to the square root of the sum of the squares of the errors of the directly measured quantities. Glacier mass-balance measurements obtained from point measurements contain errors associated with determining layer thickness and firn density. These errors may be accentuated with adverse weather and environmental conditions. The installation of ablation stakes, measuring snow density from pits, and probing deep and dense snow will inherently produce measurement errors (Østrem and Brugman, 1991). For instance, according to Østrem and Brugman (1991), the error in stake measurements is primarily due to stake sinking. Error in stake measurements is greater if placed in firn as opposed to ice due to the differences in density (Østrem and Brugman, 1991). In response to these uncertainties, ablation stakes were not placed in the accumulation area; instead depth measurements in the accumulation area were conducted with solid aluminum probes and northern walls of crevasses.

2.4.4 Future Work

To gain a better knowledge of the sensitivity of Collier Glacier's mass balance, longer and more complete measurement records are necessary. These longer records are necessary when analyzing the governing controls over Collier Glacier's mass

balance, as well as evaluating the role natural modes of variability from the North Pacific have on the Collier Glacier's mass balance. These records could be supplemented with melt models, such as the OSUSEBM (Anslow et al., 2008). Such distributed energy balance models have shown to simulate glacier mass balance with relatively high accuracy (Anslow et al., 2008; Andreassen et al., 2008). However, motivation to conduct routine mass balance measurements in a protected wilderness area is rather difficult, and experienced help is limited. This is especially true for the winter balance measurements, where the access to the glacier is limited due to road closures.

Ice volume data are necessary for estimating the contribution to future sea level rise. Mountain glaciers and ice caps (GICs), such as the Collier Glacier, are quite sensitive to changes in climate, which is reflected in their mass balance. This sensitivity makes them major contributors to 21st century sea level rise, since their response time is of decadal timescales. Thus understanding mass changes in GICs are critical for early-detection strategies of global climate-related observations, such as 21st century sea level rise. Ice volume estimations of GICs are key factors in their contribution to sea level rise; however, ice volume data are sparse for alpine glaciers. The last ice volume measurements in the Three Sisters Wilderness was conducted by the USGS in 1986 (Driedger et al., 1986). These data can be obtained with field surveys with ground penetrating radar.

2.5 Conclusions

Mass-balance measurements on the Collier Glacier indicate a high degree of variability associated with the local climate regime, mainly from regional temperature and precipitation patterns. However, it appears that this variability that results in positive and negative mass balances has resulted in significant areal reduction since the 1989-1994 studies. The relatively flat topography of the upper ablation area has allowed significant areal and associated mass loss without a significant change in the ELA. Local climatological influences could be enhanced and/or dampened by the surrounding topography, which can have a control on shading, debris, slope, and aspect, all of which can greatly influence the surface energy exchange, and resulting energy available for melt for the glacier. The b_n curves from 1989-2010 all indicate high mass loss in the lower portions of the glacier relative to the upper reaches of the glacier. Of particular interest is the region between 2300 and 2400 m, where there is a high degree of mass loss relative to the elevations adjacent to this elevation band. However, these secondary fluctuations in the b_n curve seem to have risen to a higher elevation relative to the 1989-1994 measurements, supporting the continued areal loss since the 1989-1994 measurements, as well as the increasing proximity of the ELA to the icefall.

The 1989-2010 measurements demonstrate that the mass balance of the Collier Glacier is still a variable governed by timing and magnitude of summer temperatures and precipitation that falls as snow on the glacier. Both of these variables strongly

dictate the net balance of a glacier by influencing its surface energy exchange, and the associated energy available for melt. In the case of the 2009-2010 balance year, the moist cyclonic storms that came through in April and May delivered a significant amount of fresh snow, enough to keep the glacier entirely snow covered past July, thus maintaining a high albedo and lowering the net solar radiation contribution to the energy budget. As a result, this late season snow accumulation minimized ice ablation through peak insolation in July and August. This suggests that the Collier Glacier, and possibly other glaciers of the region, are under the influence of large modes of variability from the eastern Pacific, such as ENSO and PDO, which could have a pronounced influence on the timing and magnitude of both the winter accumulation and summer temperatures. Nevertheless, the lack of mass balance data for the Collier Glacier prevents further exploration of the influence of these natural modes of variability on the accumulation and/or ablation of mass, such as principle component analysis. These observations, however, stress the influence of summer temperatures as well as the energy balance on the ablation process for the Collier Glacier. Glacier modeling by means of surface energy balance models (SEBMs) and enhanced temperature index models could provide insights on the parameters that govern ablation and their influence on the Collier Glacier's mass balance. Distributed SEBMs such as the OSU SEBM (Anslow et al., 2008) can also take into account the influence of surrounding topography, slope and aspect on the glacier's surface energy balance, and the associated energy available for melt, providing insights on their role in glacier mass balance.

Glacier mass-balance measurements are subject to many uncertainties, due to estimating large quantities of moving ice and snow. Many of these uncertainties are associated with the transportation and deposition of snow by wind. Greater spatial coverage of measurements could minimize these uncertainties, however, time constraints due to mountain weather and lack of field help makes these measurements difficult to accomplish. Also, uncertainties associated with snow density measurements could be minimized with greater spatial coverage of snow pits, although digging these pits is time and energy consuming. There are also uncertainties associated with the representation of the measurement locations along the glacier. For the 2008-2010 studies, the locations were thought to be the best representation due to their close proximity to the glacier's center flowline, however, these uncertainties could be minimized with greater spatial coverage, but this would increase the risks associated with working around crevasses, avalanches, rock fall, as well as other hazards with working in an alpine environment.

The 1989-2010 mass-balance measurements show a similar trend indicating a continuing retreat since its Little Ice Age maximum in a step-like fashion, where there are periods of significant mass loss, accompanied by steady-state conditions. The cause of this step-like retreat is most likely due to changes in the regional climate of the Three Sisters Wilderness coupled with the unique topographic setting encompassing the Collier Glacier. These mass-balance measurements conducted from 1989-2010 suggest Collier Glacier's mass balance is highly variable, where there are years of positive and negative mass balance depending on the timing and magnitude of

winter accumulation as well as the magnitude of summer temperatures. Observations, however, indicate a continued terminus and areal reduction, as well as continued development of the icefall. The 2009-2010 balance year suggests that even with a large amount of late spring snow accumulation, surpassing the previous year's winter balance by 1.46 m.w.e (3.06 m.w.e in 2009-2010 and 1.60 m.w.e in 2008-2009), there was still a significant amount of ablation through the summer to result in a summer balance of -3.07 m.w.e. These data suggest that any future climatic perturbation resulting in anomalously warm summers or dry winters could influence the Collier Glacier's mass budget negatively. Such perturbations could arise from natural modes of variability such as an El Niño event, which has been known to negatively influence snow accumulation in the Cascade Range, as recorded by local SNOTEL stations. Limited mass balance data for the Collier Glacier, however, limits the understanding of the role these natural modes of variability have on glacier mass balance. The current location of the ELA just below the icefall, small rises in the ELA due to potential negative balance years would expose large volumes of ice to the ablation area with very little change in the ELA, greatly altering the Collier Glacier's mass budget indicative to large, rapid retreat.

2.6 References

Andreassen, L. M., M. R. Van Den Broeke, R. H. Giesen, and J. Oerlemans (2008), A 5 year record of surface energy and mass balance from the ablation zone of Storbreen, Norway, *Journal of Glaciology*, 54, 185.

Andrews, J.T. (1972), Glacier power, mass balances, velocities and erosion potential, *Zeitschrift für Geomorphologie Suppl. Bd.*, 13, 1-17.

Andrews, J.T. (1975), *Glacial Systems: An Approach to Glaciers and their Environments*. Duxbury Press, North Scituate, Mass.

Anslow, F.S. (2008), Modeling and Dating Glacier Fluctuations and Their Relation to Pacific Ocean Climate, Unpublished PhD. Thesis, Oregon State University, 159 pp.

Anslow, F. S., S. Hostetler, W. R. Bidlake, and P. U. Clark (2008), Distributed energy balance modeling of South Cascade Glacier, Washington and assessment of model uncertainty, *Journal of Geophysical Research*, 113, F02019.

Bahr, D.B., W.T. Pfeffer, C. Sassolas, and M.F. Meier (1998), Response time of glaciers as a function of size and mass balance: 1 Theory, *Journal of Geophysical Research*, 103, B5, 9777-9782.

Bahr, D.B., M. Dyurgerov, and M.F. Meier (2009), Sea-level rise from glaciers and ice caps: A lower bound, *Geophysical Resarch Letters*, 36, L03501.

Barry, R.G. (1992), *Mountain weather and climate*, Routledge, Chapman, and Hall, Inc., New York, NY, 402 pp.

Bitz, C.M., and D.S. Battisti (1999), Interannual to Decadal variability in Climate and the Mass Balance in Washington, Western Canada, and Alaska, *Journal of Climate*, 12, 3181-3196.

Braithwaite, R.J. (1985), Calculation of degree-days for glacier-climate research, *Z. Gletscherkd. Glazialgeol.*, 20, 1-8.

Braithwaite, R.J., and Y. Zhang (2000), Sensitivity of mass balance of five Swiss glaciers to temperature changes assessed by tuning a degree-day model, *Journal of Glaciology*, 46, 152.

Brock, B. W., I. C. Willis, and M. J. Sharp (2000), Measurement and parameterization of albedo variations at Haut Glacier d'Arolla, Switzerland, *Journal of Glaciology*, 46, 155.

Brock, B.W., I.C. Willis, and M.J. Sharp (2006), Measurement and parameterization of aerodynamic roughness length variations at Haut Glacier d'Arolla, Switzerland, *Journal of Glaciology*, 52, 281-297.

Brun, E, E. Martin, V. Simon, C. Gendre, and C. Coleou (1989), An energy and mass model of snow cover suitable for operational avalanche forecasting, *Journal of Glaciology*, 35, 121.

Burbank, D.W. (1982), Correlations of climate, mass balance, and glacial fluctuations at Mount Rainier, Washington, USA, since 1980, *Arctic and Alpine Res.*, 14, 2, 137-148.

Driedger, C.L., and P.M. Kennard (1986), Ice Volumes on Cascade Volcanoes: Mount Rainier, Mount Hood, Three Sisters, and Mount Shasta: U.S. Geological Survey Professional Paper 1365, 28 pp.

Fountain, A.G., M.J. Hoffman, F. Granshaw, and J. Riedel (2009), The 'benchmark glacier' concept – does it work? Lessons from the North Cascade Range, USA, *Annals of Glaciology*, 50(50), 163-168.

Furbish, D.J, and J.T. Andrews (1984), The use of hypsometry to indicate long-term stability and response of valley glaciers to changes in mass transfer, *Journal of Glaciology*, 30, 105, 199-211.

Hock, R (2003), Temperature index melt modeling in mountain areas, *Journal of Hydrology*, 282, 104-115.

Hostetler, S., and P. U. Clark (1997), Climatic controls of western U.S. glaciers at the last glacial maximum, *Quaternary Science Reviews*, 16, 505-511.

Hostetler, S., and P. U. Clark (2000), Tropical Climate at the Last Glacial Maximum Inferred from Glacier Mass-Balance Modeling, *Science*, 290, 1747-1750.

Hubley, R.C. (1956), Glaciers of the Washington Cascade and Olympic Mountains; their present activity and its relation to local climatic trends, *Journal of Glaciology*, 2, 19, 669-674.

Jackson, K.M., and A.G. Fountain (2007), Spatial and morphological change on Eliot Glacier, Mount Hood, Oregon, USA, *Annals of Glaciology*, 46.

Josberger, E.G., W.R. Bidlake, R.S. March, and B.W. Kennedy (2007), Glacier mass-balance fluctuations in the Pacific Northwest and Alaska, USA, *Annals of Glaciology*, 46, 291-296.

Klok, E. J., and J. Oerlemans (2003), Deriving historical equilibrium-line altitudes from a glacier length record by linear inverse modeling, *The Holocene*, 13,3, 343-351.

Kuhn, M. (2003), Redistribution of snow and glacier mass balance from a hydrometeorological model, *Journal of Hydrology*, 282, 95-103.

Lundstrom, S.C., A.E. McCafferty, and J.A. Coe (1993), Photogrammetric analysis of 1984-89 surface altitude change of the partially debris-covered Eliot Glacier, Mount Hood, Oregon, USA, *Annals of Glaciology*, 17, 167-170.

Marks, D., and J. Dozier (1992), Climate and energy exchange at the snow surface in the Alpine Region of the Sierra Nevada: 1. Meteorological measurements and monitoring, *Water Resources Research*, 28, 3029-3042.

Marks, D., and J. Dozier (1992), Climate and energy exchange at the snow surface in the Alpine Region of the Sierra Nevada: 2. Snow cover energy balance, *Water Resources Research*, 28, 3043-3054.

Marks, D., J. Kimball, D. Tingey, and T. Link (1998), The sensitivity of snowmelt processes to climate conditions and forest cover during rain-on- snow: A case study of the 1996 Pacific Northwest flood, *Hydrological Processes*, 12, 1569-1587.

McDonald, G.D. (1995), Changes in mass of Collier Glacier, Oreon, 1910-1004, Unpublished Master's Thesis, Oregon State University.

Meehl, G.A., T.F. Stocker, W.D. Collins, P. Friedlingstein, A.T. Gaye, J.M. Gregory, A. Kitoh, R. Knutti, J.M. Murphy, A. Noda, S.C.B. Raper, I.G. Watterson, A.J. Weaver and Z.-C. Zhao (2007), *2007: Global Climate Projections. In: Climate Change 2007: The Physical Science Basis. Contribution of Working Group I to the Fourth Assessment Report of the Intergovernmental Panel on Climate Change* [Solomon, S., D. Qin, M. Manning, Z. Chen, M. Marquis, K.B. Averyt, M. Tignor and H.L. Miller (eds.)]. Cambridge University Press, Cambridge, United Kingdom and New York, NY, USA.

Meier, M.F. (1962), Proposed definitions for glacier mass budget terms, *Journal of Glaciology*, 4, 33, 252-263.

Meier, M.F. (1965). Glaciers and climate. *In* Wright, H.E. and D.G. Frey (eds.), *The Quaternary of the United States*, Princeton University Press, Princeton New Jersey, 795-805.

Meier, M.F. and W. Tangborn (1965), Net budget and flow of South Cascade Glacier, Washington, *Journal of Glaciology*, 5, 547.

Meier, M.F. (1984), Contribution of Small Glaciers to Global Sea Level, *Science*, 226, 4681, 1418-1421.

Meier, M.F, M.B. Dyurgerov, U.K. Rick, S. O'Neel, T. Pfeffer, R.S. Anderson, S.P. Anderson, and A.F. Glazovsky. (2007), Glaciers Dominate Eustatic Sea-Level Rise in the 21st Century, *Science*, 317, 1064-1066.

Mote, P.W., A.F. Hamlet, M.P. Clark, and D.P. Lettenmaier (2005), Declining mountain snowpack in Western North America, *Bulletin of the American Meteorological Society*, 86, 39-49.

Mountain, K.R. (1978), The Chronology, Geomorphology, and Climate of Collier Glacier with Special Reference to the Ablation Process, *Unpublished M.A. Thesis*, University of Oregon, 197 pp.

Mountain, K.R. (1990), A clear sky net radiation model for the high elevation glacial environment, *Unpublished PhD. Thesis*, The Ohio State University, Dept. of Geography, 290 pp.

O'Connor, J.E., J.H. Hardison III, and J.E. Costa (2001), Debris Flow from Failures of Neoglacial-Age Moraine Dams in the Three Sisters and Mount Jefferson Wilderness Areas, Oregon: U.S. Geological Survey Professional Paper 1606, 93 pp.

Oerlemans, J., and J.P.F Fortuin (1992), Sensitivity of Glaciers and Small Ice Caps to Greenhouse Warming, *Science*, 258, 5079, 115-117.

Oerlemans, J., and B.K. Reichert (2000), Relating glacier mass balance to meteorological data by using a seasonal sensitivity characteristic, *Journal of Glaciology*, 46, 152, 1-6.

Oerlemans, J. (2001), *Glaciers and Climate Change*. A.A. Balkema Publishers, Lisse, 148 pp.

Østrem, G., and M. Brugman (1991), Glacier Mass-Balance Measurements: A manual for field and office work. *National Hydrology Research Institute Scientific Report*, 4 Environment Canada, N.H.R.I., Saskatoon and Norges Vassdrags-og Elektrisitetsvesen, Oslo.

Paterson, W. S. B. (1994), *The Physics of Glaciers*. Pergamon Press, Oxford, 480 pp.

Pheffer, W.T., J.T. Harper, and S. O'Neel (2008), Kinematic constraints on glacier contributions to 21st century sea-level rise, *Science*, 321, 1340-1343.

Ropelwski, C.F., and M.S. Halpert (1986), North American precipitation and temperature patterns associated with El Niño/southern oscillation (ENSO), *Monthly Weather Reviews*, 114, 2352-2362.

Tangborn, W. (1980), Two models for estimating climate-glacier relationships in the North Cascades, Washington, USA, *Journal of Glaciology*, 25, 91, 3-21.

Chapter 3

Modeling The Collier Glacier's Mass Balance

A. Cody Beedlow[*1], Steven W. Hostetler[2], and Peter U. Clark[1]

[1]Department of Geosciences, Oregon State University
Corvallis, Oregon 97331

[2]United States Geological Survey, Oregon State University
Corvallis, Oregon 97331

3.1 Abstract

A physically based, spatially distributed surface energy balance model, developed on South Cascade Glacier, WA, has been calibrated to the Collier Glacier, OR. As part of this study, we have installed and maintained an automated weather station to collect meteorological data needed to apply and validate the surface energy balance model. Model results indicate that the surface energy balance model is capable of capturing the seasonal pattern of mass balance for the Collier Glacier. The model also shows good agreement, both spatially and temporally, with the mass-balance measurements conducted for the 2009 and 2010 balance years. Model comparisons were conducted with the surface energy balance model to compare model performance and investigate the superiority of more complex models with simpler approaches. Model simulations for the 2010 balance year indicated that the positive degree-day model explained approximately 82% of the variance in summer ablation, while the surface energy balance model, calculating the turbulent heat fluxes with both the bulk and transfer coefficient method, explained approximately 78% of the variance in summer ablation. These results indicate that simpler methods to model the Collier Glacier's mass balance are just as effective as the more complex methods.

3.2 Introduction

A glacier's mass balance is controlled by accumulation and ablation, which are governed by a combination of local meteorological inputs of precipitation and energy. These inputs can be recorded with automated weather stations (AWS) and used as inputs for ablation models, such as temperature degree-day, or positive degree-day (PDD) models, and the more physically comprehensive surface energy balance models (SEBMs). Because each glacier has its own unique climate, however, modeling glacier mass balance requires detailed monitoring of the surface climate in remote mountainous regions, which limits application of models. Most continuous or long-term mass balance and meteorological observations are available only on select, representative glaciers, often referred as benchmark glaciers. In most cases, meteorological data must be obtained from distant weather stations, raising the question about the robustness of applying models on remote glaciers where routine measurements are not regularly conducted. Due to the lack of meteorological observations taken at high altitude sites, meteorological observations necessary to drive mass balance models are often from lower elevation sites that are in non-alpine locations; interpolating data to higher elevations and add to the uncertainties associated with these models.

Modeling the surface mass balance by using climatic forcing from observations and climate models can provide an opportunity to model past and future responses of glaciers to climate change, as well as simulating mass balance on remote

glaciers. Here we present surface energy balance measurements and the related modeled mass balance for the Collier Glacier, Three Sisters Wilderness, Oregon, a small (0.60-0.70 km^2), temperate valley glacier located in the Oregon Cascade Range (44° 10' N, 121° 47' W). Glacier monitoring and records are limited in the Oregon Cascade Range, with studies focused on to the Eliot Glacier on Mt. Hood (e.g. Lundstrom et al., 1993; Jackson and Fountain, 2007) and the Collier Glacier on North and Middle Sisters (e.g. Mountain, 1978; Mountain, 1990; McDonald, 1995). The Collier glacier has a unique photo record that spans the 20th Century and documents its retreat from its Little Ice Age maximum extent, making it one of the best-recorded glaciers in the Oregon Cascades (Hopson, 1960).

As part of this study, we have installed and maintained automated weather stations (AWS) to collect data necessary to apply and validate the OSU Surface Energy Balance Model (OSU SEBM). Model validation and calibration are compared to mass-balance measurements conducted for the 2008-2009 and 2009-2010 balance years. The main goals of this study are 1) to implement and test the robustness of a SEBM developed on South Cascade Glacier, and 2) to determine if the model is capable of capturing the seasonal pattern of mass balance on the Collier Glacier.

3.2.1 Setting

The Central Oregon Cascade Range is the result of Quaternary volcanism related to the subduction of the Juan de Fuca plate under North America and active rifting within the arc. Within the Three Sisters Wilderness in the Central Oregon Cascades, three of the five composite volcanoes exceed 3000 m, comprising the Three Sisters (North, Middle, and South Sister). This dramatic vertical relief, in conjunction with moist, mid-latitude winter cyclonic storms, provides winter snowfall and mild summers that are conducive to glaciation. Most of the precipitation in this region is derived from the North Pacific. The regional climate of the Collier Glacier and the Three Sisters Wilderness is highly dependent upon the dominant direction of storm tracks moving across the Pacific Northwest as determined by Northern Hemisphere atmospheric circulation patterns. In the Pacific Northwest (PNW), annual circulation patterns are controlled by two surface-level semi-permanent high and low pressure systems situated near the Aleutian Islands in the Northeast Pacific (Phillips, 1960). In the winter months, a low-pressure cell dominates this region of the Pacific, bringing in westerly and southwesterly flows to the PNW. In the summer months, the North Pacific high-pressure cell migrates into this region in the North Pacific Ocean, resulting in mild summers with minimal precipitation. Other normally unimportant air masses, however, can influence the PNW climate. Occasionally in the winter months, polar continental air masses originating east of the Rocky Mountains encroach on the

Pacific Coast regions, causing anomalously cold and dry winter weather (Mountain, 1978).

As a result of shifts in the Aleutian low, the majority of the annual precipitation in the PNW is dominated by winter Pacific frontal systems that move eastward off the Pacific. The Cascade are a major orographic barrier that intercepts much of the eastward-flowing moisture from the Pacific, bringing ample snowfall to the higher elevations in the Oregon Cascade Range. In the summer months, the northward expansion of the eastern Pacific high-pressure system and diversion of the prevailing westerlies to the north result in warm, dry summers in the PNW (O'Connor et al., 2001).

The Collier glacier is a small temperate valley glacier, covering approximately 0.6-0.7 km^2. Located in the Three Sisters Wilderness in the Oregon Cascade Range (44° 10' N, 121° 47' W), this north-northwest facing glacier originates at the northern flanks of Middle Sister (3062 m) at an elevation of 2720 m, and cuts the western face of North Sister (3074 m) where it terminates at an elevation of 2295 m (Figure 3.1). Its maximum areal extent during the Little Ice Age (locally circa 1300-1850) was approximately 2.4 km^2 (McDonald, 1995; O'Connor et al., 2001). Previous studies on the Collier Glacier from 1989-1994 determined the area of the glacier to be approximately 0.85-0.9 km^2, indicating a continued decline is areal extent since these previous studies (McDonald, 1995; O'Connor et al., 2001).

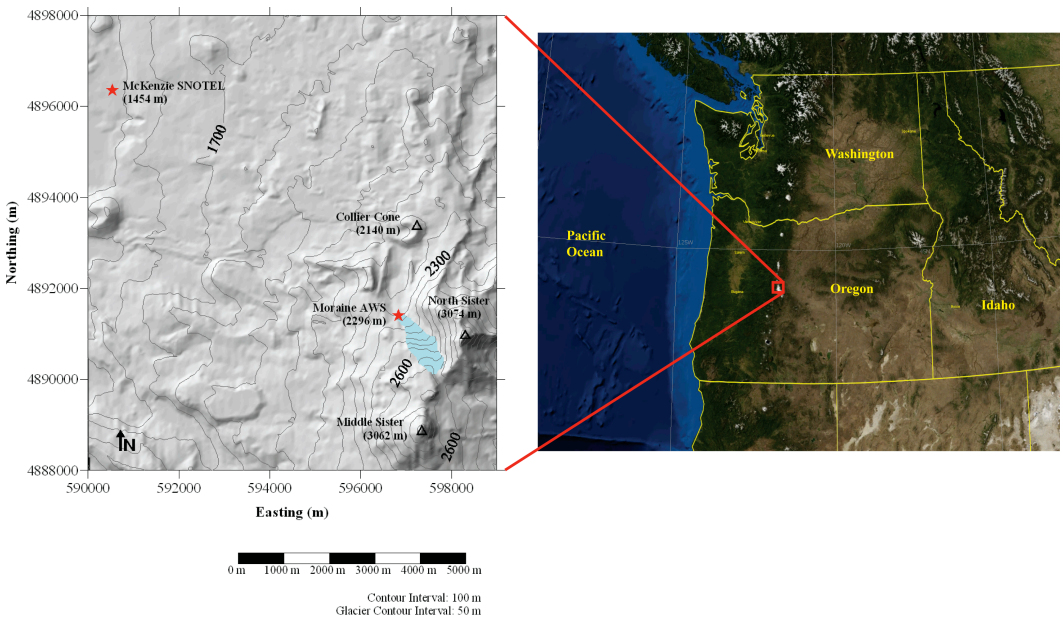

Figure 3.1: (**right**) Collier Glacier Study area relative to the Pacific Northwest (PNW) (*image: NASA World Wind*). (**left**) Collier Glacier (blue) relative to North and Middle Sister. The red stars identify locations of the Moraine AWS and McKenzie SNOTEL station.

The observed 19th and 20th Century glacier activity in the Oregon Cascades is likely the result of regional and hemispheric warming since the 19th Century, which is often considered the end of the Little Ice Age (Hopson, 1960; McDonald, 1995; O'Connor et al., 2001). Photo records and long-term mass balance measurements, such as the United States Geological Survey's (USGS) South Cascade Glacier monitoring program demonstrate the sensitivity of these temperate alpine glaciers to changes in climate. However, questions arise at the representation of these benchmark glaciers over larger areas, where differences between glaciers largely result from differences in local topographic effects that control snow accumulation and ablation (Fountain et al., 2009). Such changes in climate can often be reflected in the mass balance of these glaciers. Tangborn (1980) demonstrated that a decrease in summer air temperature of just over 0.5 °C or an increase in winter accumulation of slightly more than 10% (350 mm w.e) from average would result in glacier growth and subsequent advance. Studies from these benchmark glaciers indicate that Cascade glaciers respond to the combined influence of winter snowfall accumulation and summer ablation, as observed from long-term mass balance programs such as the one on the South Cascade Glacier, Washington (Meier et al., 1971; Tangborn, 1980; Josberger et al., 2007).

3.2.2 Temperature

It is well documented from meteorological observations and long-term mass-balance measurements that temperature and precipitation have the greatest influence in the glacier's mass balance (Oerlemans and Fortuin, 1992; Josberger et al., 2009). Finsterwalder and Schunk (1887) were among the first to assume a relationship between ablation and air temperature from their study of the variations of the Suldenferner in the Eastern Alps. Oerlemans (1992, 2001) concluded that the net balance of maritime glaciers in Southern Norway is much more sensitive to temperatures than the net balance of continental glacier. His studies of these glaciers in Norway found that to compensate for a 1 K-temperature increase, precipitation would need to increase by 20 to 40% (Oerlemans, 1992; Oerlemans, 2001). On Collier Glacier, air temperatures are often above freezing during the ablation season and as a result, the surface of the glacier is often near freezing point, thus less energy is required to induce melt. Temperature contrasts with the surrounding terrain can influence the interaction of the glacier surface with the atmospheric boundary layer above. Such temperature contrasts can influence the turbulent exchange of energy by inducing local circulation patterns. In the winter months, when temperatures are low, there is little temperature contrast with the glacier, atmospheric boundary layer, and its surrounding terrain due to the presence of snow, thus making these local circulations less influential (Oerlemans, 2001). During the summer months, air temperatures are higher, and the temperature contrast with the glacier, atmospheric boundary layer, and

the surrounding topography increases, driving local circulation patterns and influencing the sensible heat flux, helping drive energy available for melt (Oerlemans, 2001).

3.2.3 Wind

Like many valley glaciers, the Collier Glacier has two dominant modes of wind direction: up- and down-glacier. Most of the observed wind direction from field observations during the ablation season indicated either an up- or down-glacier flow, depending on the time of day, indicating a presence of a valley and slope wind. On the Collier Glacier, this down-glacier flow consistently occurs around dusk, when the sun angle drops below the western moraine and the air temperature rapidly cools. This slope wind brings cold air down from the upper reaches of the glacier. The initiation of a slope wind is determined by the temperature deficit in the near-surface layer (Oerlemans, 2010). This deficit is defined by the difference between the actual air temperature and the temperature of the ambient atmosphere (Oerlemans, 2010). Such situations occur when the surface of the glacier is melting and the air temperature is above the melting point, generating a temperature deficit. A temperature deficit, in conjunction with the slope of the glacier initiates down-glacier flow of dense, cold air, acting as a heat pump for melting glaciers. Thus, the heat flux towards the glacier's surface cools the air, forcing this slope, or katabatic flow (Oerlemans, 2010).

The interaction of the flow with the irregular glacier surface generates turbulence, which then enhances the sensible heat flux to the surface of the glacier, further sustaining this heat pump (Oerlemans, 2010). This is especially the case with the heavily crevassed regions around icefalls, where the sharp changes in the surface topography enhances this turbulent exchange of heat. The Collier Glacier's north facing icefall creates a sharp break in slope which tends to separate airflow from the ground, causing vertical bolster eddies to form at the base of the icefall, enhancing the turbulent exchange of in the glacier's energy budget (Mountain 1978, 1990; McDonald, 1995). This wind regime can greatly influence the snow surface morphology, creating channels, which can entrain debris, further altering the surface energy exchange by influencing both the net radiation and turbulent heat fluxes.

Mountain (1978) observed that wind conditions present on the Collier Glacier had some of the greatest effects on the microclimate of the Collier Glacier. Mountain (1978) identified two major patterns regarding the Collier Glacier's wind regime: (1) under conditions of high wind, North Sister deflects the westerlies eastward across the ablation zone, while (2) pushing winds via a strong north to northwesterly component up-glacier across the firn zone. As a result of this deflection from North Sister, air passing over the glacier surface tends to be warmer on the eastern margin, and cools as it passes over the ice surface (Mountain, 1978). This deflection also introduces debris from North Sister's west face. Furthermore, North Sister's west face heats up with incident solar radiation, while the opposite facing walls of the western margin of the glacier do not. As a result, this differential heating of the valley walls of the glacier

can induce a cross-valley circulation. This circulation brings warm air mixed with debris from North Sister's unstable west face across the ablation area of the glacier. Such circulations were commonly observed throughout the daytime. Distribution of debris associated with North Sister influences the observed albedo across the ablation area of the glacier, where throughout the ablation season the eastern margin had a lower albedo than the western margin due to the distribution of debris from North Sister, helping generate this east-west variability in ablation. The presence of mass wasting from North Sister is persistent from the start to the end of the ablation season (May to October). Such events, in conjunction with local wind circulation distribute debris across the Collier Glacier, lowering the surface albedo and contributing towards melt energy by the absorption of solar radiation.

3.2.4 Precipitation

The locality of the Collier Glacier with respect to the prevailing storms from the Pacific Ocean, results in high winter snowfall. During the summer months, the shifts in the Aleutian Low Pressure System reduce the amount of precipitation throughout the PNW. Sporadic rainstorms, however, do occur throughout the Cascade Range in the summer months. Field observations noted their duration was usually small and it is assumed that the total amount of precipitation is very small, making its

contribution to the glacier's mass and energy budget minimal in comparison to the other fluxes exchanged at the glacier's surface.

Throughout the ablation season, the local temperature lapse rates can cause more precipitation to fall in the form of rain in the ablation area relative to the accumulation area, thus creating a situation where there is potential accumulation above the ELA while ablation occurs below. However, during the accumulation season, the temperatures in the ablation area are below freezing, so precipitation typically falls as snow, and the distribution becomes more uniform as the entire surface of the glacier is accumulating mass. Local wind patterns, however, can influence the spatial variability of snow cover on the glacier with wind drifting and scouring. Thus the spatial variability of precipitation that falls as snow can become more dependent on local wind speed, turbulence, and predominant wind direction characteristics.

Winter balance measurements from 2008-2009 and 2009-2010 balance years provide some insight in the distribution of snow accumulation with elevation, indicating different seasonal accumulation patterns for these individual balance years (Figure 3.2). These measurements also indicated elevation bands that receive more snow accumulation, especially in the regions adjacent to the icefall (2500 m to 2600 m), indicating a non-uniform accumulation of snow with elevation.

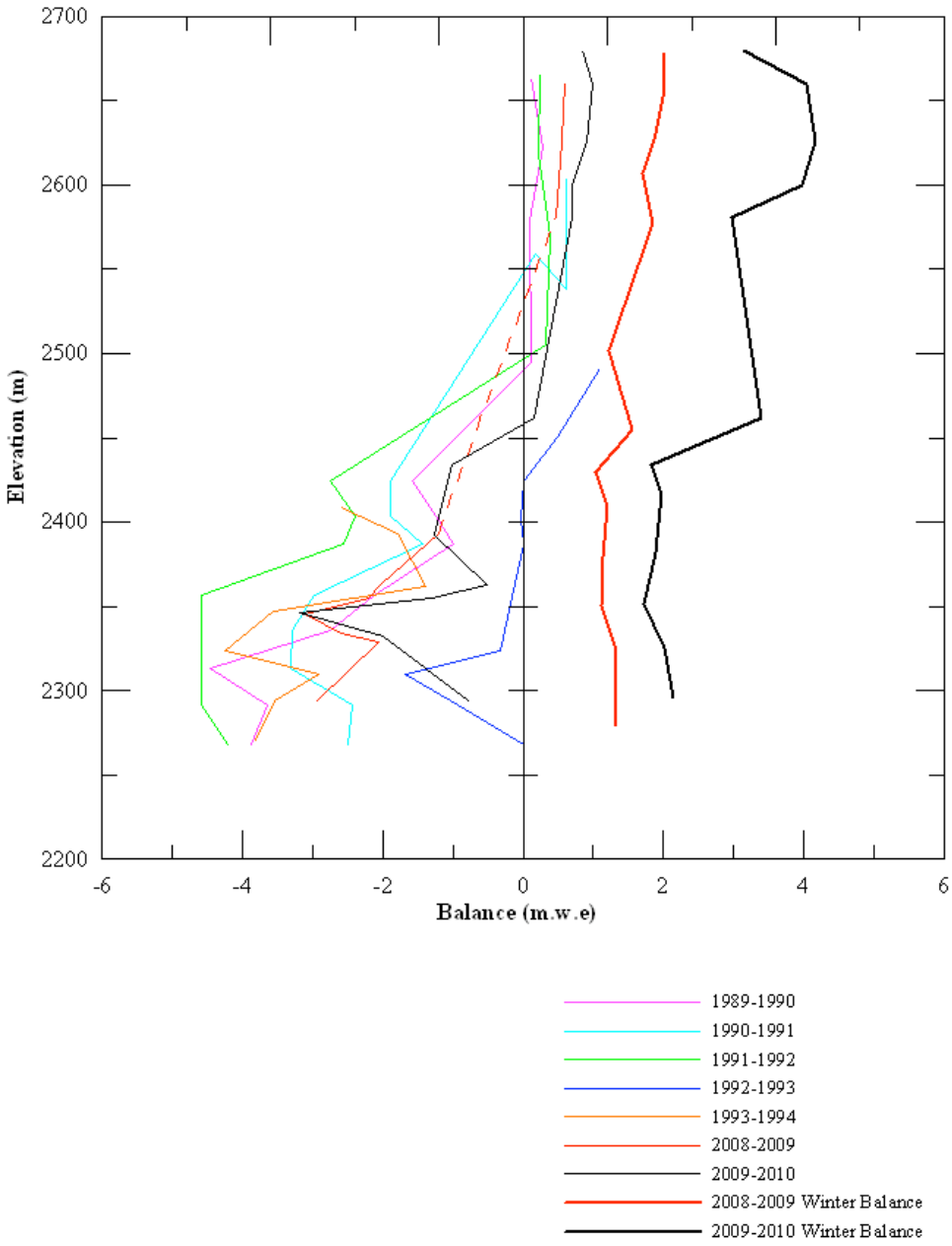

Figure 3.2: Collier Glacier net balance curves from 1990 to 1994 (McDonald, 1995) and 2009 to 2010. In bold are the 2008-2009 and 2009-2010 winter balance measurements. These data display distribution of mass with elevation on the Collier Glacier.

3.3 Methods

3.3.1 Meteorological Measurements

Most glacier energy balance studies are conducted in locations where helicopter or snowmobile access is permitted, thus allowing easy access to instrumentation. The Collier Glacier, however, is located in a protected wilderness area, where mechanized vehicles are prohibited, thus all instrumentation and towers needed to be as light as possible so a field team could haul in all the necessary equipment by foot. Most AWS available towers are heavy and cannot easily be carried in a backpack. The AWS towers used in this study were constructed to be light and portable, utilizing lighter materials and manufacturing to save both overall weight and packable volume (Figure 3.3). Table 3.1 lists the meteorological instrumentation and precision of each sensor used in this study.

An AWS was erected on 12 July 2009 on the terminal moraine (2296 m) to collect the meteorological data necessary to run the OSU SEBM. Figure 3.4 displays the location of each AWS used in this study. The moraine AWS (AWS-1) consists of a center mast that holds the instrumentation and three guy-out cables supporting the mast. The center mast was constructed out of 1.5-inch exhaust pipe cut into

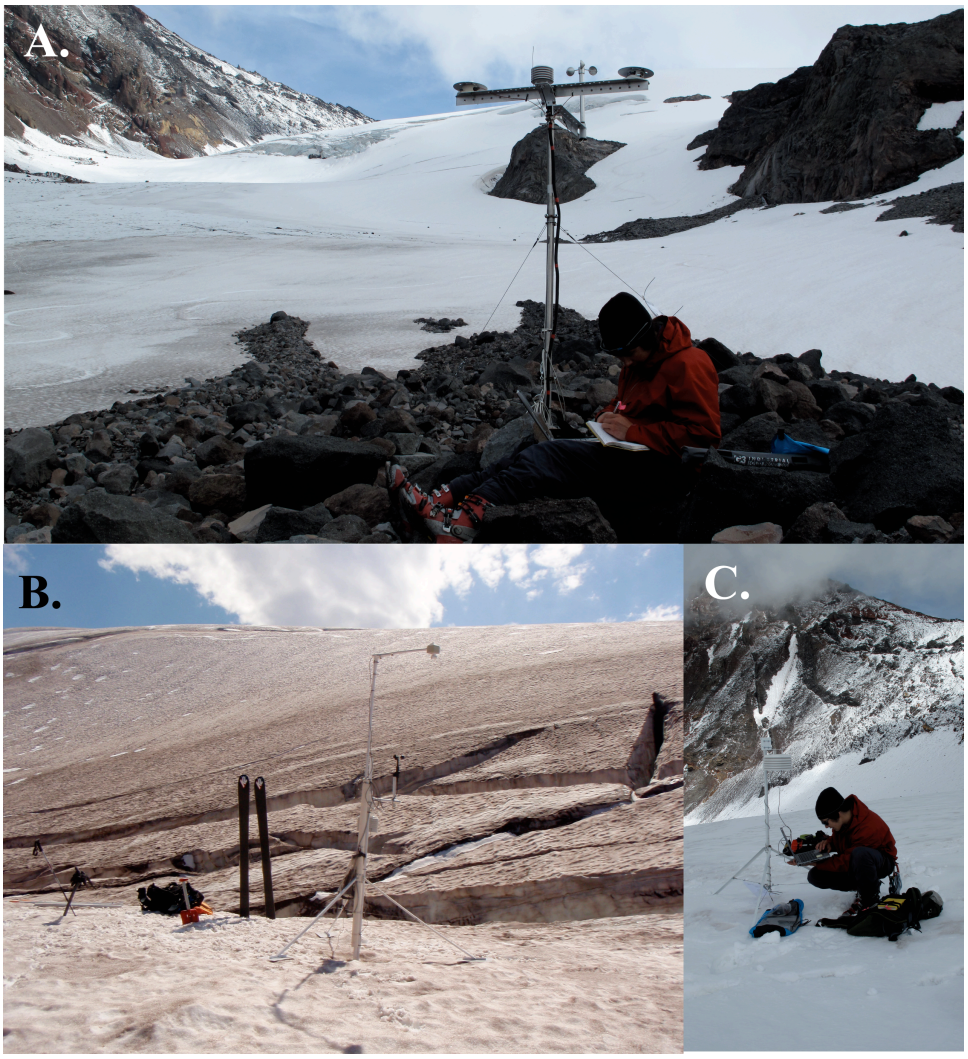

Figure 3.3: Automated weather stations used for this study. (**A.**) The moraine AWS located at 2296 m, recording incoming shortwave and longwave radiation, temperature, relative humidity, and wind speed. (**B.**) The on snow AWS located at 2577 m, recording air temperature, wind speed, and snow surface lowering. (**C.**) The HOBO temperature sensor located at 2700 m, recording air temperature.

Table 3.1: Instrumentation used in this study and its measurement precision.

Variable	Instrument	Precision	Station
Temperature	Vaisala HMP60-L Temperature/RH Probe	± 0.6 °C	Moraine AWS
Relative Humidity	Vaisala HMP60-L Temperature/RH Probe	± 4%	Moraine AWS
Wind	Met One 014A Anemometer	± 0.11 m/s	Moraine AWS
Wind	Campbell Scientific 03101-L Anemometer	± 0.5 m/s	On Snow AWS
Broadband Solar Radiation	Eppley Precision Spectral Pyranometer	± 2%	Moraine AWS
Downwelling Longwave Radiation	Eppley Precision Infrared Radiometer	± 2%	Moraine AWS
Temperature	Onset HOBO Pro	± 0.2 °C	On Snow AWS
Temperature	Onset HOBO Pro	± 0.2 °C	HOBO 2700 m
Surface Height Lowering	Judd Communication Ultrasonic Depth Sensor	± 0.4%	On Snow AWS

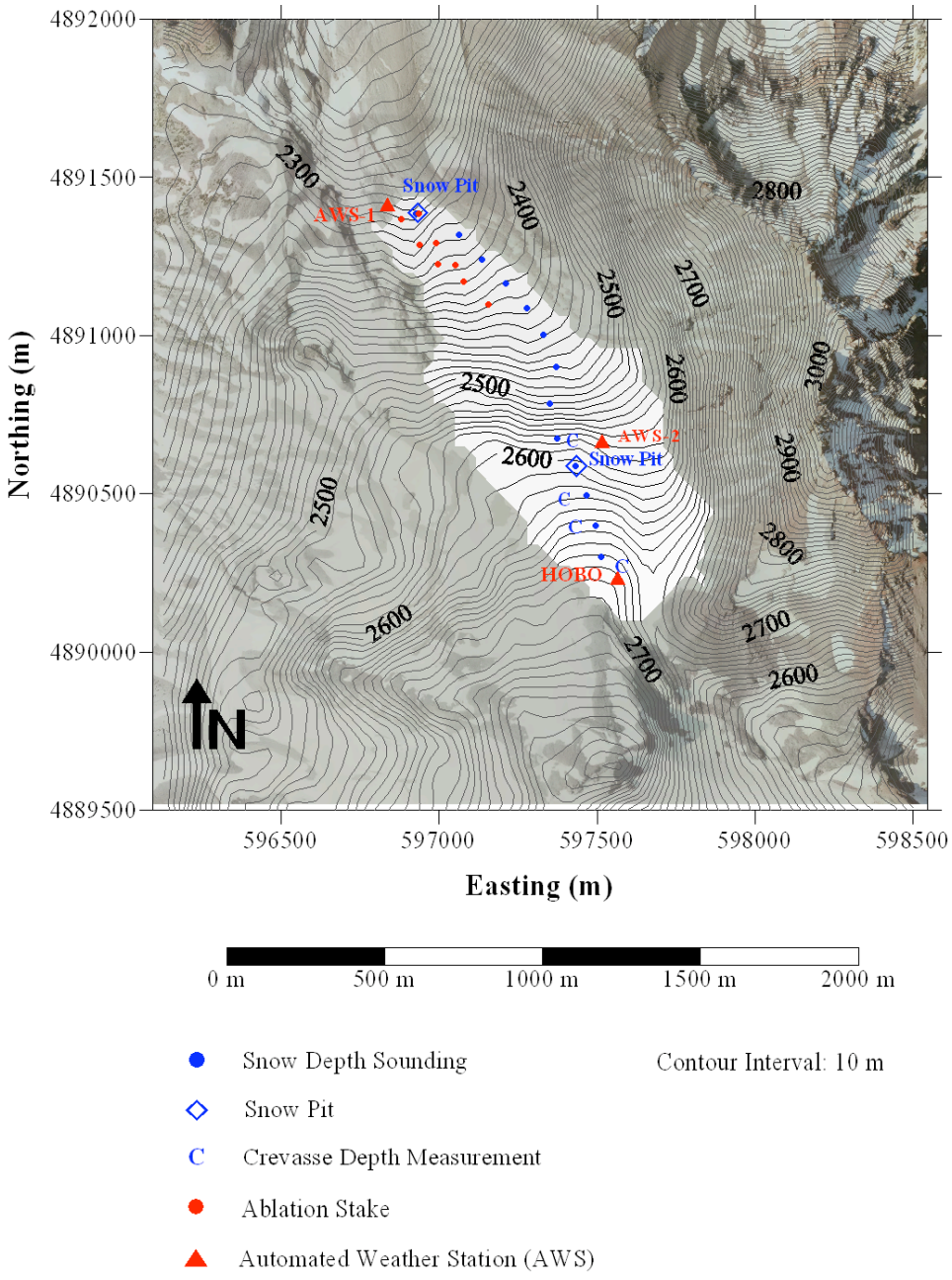

Figure 3.4: Orthotopo map of the Collier Glacier and surrounding topography, showing the measurement and AWS locations for this particular study.

three sections that could easily fit in a backpack for transport to the glacier. The instrument panels were constructed out of aluminum and machined to reduce weight and wind drag. Figure 3.3 (A.) shows the Moraine AWS. The AWS was placed as close to the ice as possible, to avoid ice-cored moraines that could alter the position of the AWS over time. The fixed arrangement of this AWS allowed the radiometers to remain level throughout the experiment, minimizing any uncertainties associated with the tilt of the instrumentation. Meteorological data were recorded every 5 minutes on a Campbell Scientific CR10-XPB datalogger to resolve the diurnal cycle of energy balance fluxes. These values were aggregated to hourly averages for input into the OSU SEBM.

For the 2008-2009-balance year, an additional AWS (AWS-2) was deployed above the icefall, at an elevation of 2577 m to record air temperature, wind speed, and snow surface lowering (Figure 3.4). Both air temperature sensor and anemometer remained at a constant height of 1.8 meters above the ablating surface over the course of the ablation season. The ultrasonic depth sensor was attached to a mast that was drilled into the snow; the mast remained fixed in order to record the lowering snow surface. This setup required the center mast to be reset every couple of weeks to avoid complete melt out and loss of data. These data were recorded on a Campbell Scientific CR800 datalogger every 5 minutes from 28 August to 26 September 2009. As with the Moraine AWS, these data were aggregated to hourly averages for the 2009 model simulations. The Onset HOBO temperature sensor on this station helped

establish temperature contrasts above and below the icefall. The tower was also designed to be light and portable, allowing a small field team to carry and deploy the AWS anywhere on the glacier (Figure 3.3 B.). Unfortunately, due to inclement weather at the end of the ablation season this station remained on the surface of the glacier through the accumulation season and was buried. Because the AWS was located above the ELA, it remained buried in the snow throughout the 2009-2010-balance year and it remains missing.

In response to the loss of the on snow AWS, an additional HOBO temperature sensor was deployed at the top of the glacier at an elevation of 2700 m, continuously recording air temperature from 26 June to 5 October 2010 (Figure 3.4). These data were recorded every 10 minutes and then aggregated to hourly averages for model simulations. The tower for this temperature sensor stood at a constant 1.6-meter height above the glacier surface and was allowed to lower with the ablating snow (Figure 3.3 C.). The tower was constructed entirely out of aluminum to minimize weight. This temperature sensor established temperature lapse rates up the glacier, thus documenting temperature changes at the top of the glacier. The location at the top of the glacier, in conjunction with the moraine AWS, better constrained the temperature lapse rates up the glacier, since temperature was recorded at both the top and bottom of the glacier.

3.3.2 Glacier Mass-Balance Measurements

The OSU SEBM was calibrated to the Collier Glacier with mass-balance measurements conducted for the 2008-2009 and 2009-2010 balance years. Accumulation measurements were conducted in early May (10 May 2009 and 16 May 2010) with probe depth soundings approximately every 100 meters up the glacier centerline (Figure 3.4). Local SNOTEL stations also served as qualitative indicators for the timing of maximum accumulation. For the 10 May 2009 measurements, one snow pit was dug above the icefall near the centerline at an elevation of around 2600 m. For the 16 May 2010 measurements, reference pits were dug at two locations, one near the terminus of the glacier (2300 m) to represent snow density in the ablation area, and another at 2600 m above the icefall to represent density changes in the accumulation area. Probe depth soundings were conducted in the same locations for both the May 2009 and 2010 accumulation measurements.

Ablation measurements were conducted with a stake network in the ablation area to serve as a reference for ice surface lowering. Ablation, in meters of water equivalent (m.w.e) was estimated by using ice surface lowering measurements from the ablation stakes and a value of 0.917 g cm^{-3} for the constant density of ice. Accumulation, also in m.w.e, was estimated by using probe depth soundings in the accumulation area in conjunction with snow density measurements from the representative snow pit at 2600 m (Figure 3.4). For the 2009-2010-balance year, mass-balance measurements were conducted every month from 16 May to 5 October

in conjunction with the meteorological data recorded from the various AWS locations to run and validate the OSU SEBM.

3.3.3 Model Descriptions

Typical glacier mass balance models consist either of temperature index models or surface energy balance models (SEBMs). Temperature index, or positive degree-day (PDD) models (e.g. Braithwaite, 1977; Braithwaite 1985; Hock, 1999; Braithwaite and Zhang, 2000; Hock, 2005) parameterize ablation in terms of air temperature, where total summer ablation is assumed to be proportional to the sum of positive temperatures, or temperature index. Constants for proportionality, or melt factors, are chosen for snow and ice surfaces to account for the differences in albedo. Due to their limited parameterization, the validity of PDD models should be questionable for mass-balance studies on alpine glaciers since it is assumed in the models that solar radiation and temperature change proportionally. Another approach to glacier mass-balance modeling is to use a physically based surface energy balance model (SEBM). Such models focus on the physical parameters of surface melt, which include radiative and turbulent fluxes. SEBMs however, require more detailed meteorological input. Due to their complexity, there are a number of potential uncertainties associated with the calculation of the energy balance terms, in particular the methods used to calculate the turbulent heat fluxes and albedo.

3.3.4 Positive Degree-Day Model

A simple Positive Degree-Day (PDD) model was implemented to compare the validity and practicality of the more complex distributed SEBM. Following Braithwaite (1977, 1985), the modeled balance b^*_j at j^{th} altitude is given by:

$$b^*_j = c^*_j - a^*_j \tag{1}$$

where c^*_j and a^*_j are the annual accumulation and ablation at the j^{th} altitude, respectively.

For the PDD model, the annual ablation, a^*, consists of the sum of ice ablation a^*_i and snow ablation a^*_s. Thus, annual ablation at the j^{th} altitude is given by:

$$a^*_j = k_i PDD_i + k_s PDD_s \tag{2}$$

where PDD_i and PDD_s are the positive degree-day sums for ice and snow, respectively. The parameters k_i and k_s are the degree-day factors for ice melt and snow melt, respectively. The positive degree-day sums are the sum of positive air temperatures measured at screen height (1-2 m) above the glacier. For this study, air temperature was recorded at two AWS locations, one at the terminus (2296 m) and another near the top of the glacier (2700 m). The modeled mass balance is given by:

$$b^*_j = c^*_j - k_i PDD_i - k_s PDD_s \tag{3}$$

The model computes ablation for each grid cell based on the snow depth. Thus, if the snow depth at a particular grid cell is greater than 0.0 meters, then the model computes ablation using the degree-day factor for snow (k_s). If the snow depth is less than or equal to 0.0 meters, then ice is exposed at that grid cell and the model computes ablation using the degree-day factor for ice (k_i).

Snow accumulation c^*_j, is initialized from accumulation measurements recorded in May and was distributed across the glacier's surface in one of two ways: through a polynomial fit of the measured accumulation with elevation from multiple years worth of accumulation measurements, or using a piecewise linear interpolation between each accumulation measurement taken for that particular balance year along the glacier's centerline. These two methods are described in greater detail in the following section.

3.3.5 Distributed Surface Energy Balance Model

The melt model used in this study was the OSU SEBM, initially developed to test the sensitivity of former glaciers to changes in temperature and precipitation. The model originally simulated mass balance from the 1990 ablation season at Haut Glacier d'Arolla, Valais, Switzerland, in addition to simulations for the 5 Pleistocene glaciers reconstructed on San Francisco Mountain, Arizona, using output from a regional climate model (Poellot, 2000). The model was expanded to simulate mass

balance and test model uncertainty on South Cascade Glacier, Washington (Anslow et al., 2008). The SEBM is a distributed surface energy balance for alpine glaciers and it accounts for the surrounding topography, slope, and aspect. Terrain slope, aspect, and topographic shading are derived from a 30-meter digital elevation model (DEM) of the glacier and the surrounding topography using a terrain computation technique based on the work by Dozier and Frew (1990) and Arnold et al. (1996). The OSU SEBM is governed by the energy balance equation:

$$\rho C_i \delta h \frac{dT_s}{dt} = S_{net} + L_{net} + H_s + H_l + K + C + M - E \quad (4)$$

where S_{net} is the net solar radiation flux, L_{net} is the net longwave radiation flux, H_s is sensible heat flux, H_l is latent heat flux, K is the geothermal heat flux, C is conduction into the snowpack, M is heat contributed by falling rain at temperatures greater than 0.0 °C, E is energy for melting or refreezing, ρ is the density of ice in kg m^{-3}, C_i is the specific heat capacity of ice in J K^{-1} kg^{-1}, δh is a small element of thickness in m, T_s is surface temperature in °C, and t is time in s. All fluxes are in units of W m^{-2} and positive values represent fluxes towards the surface (Figure 3.5). Snow and ice melt is initiated when the surface receives more energy than it loses over a period of time and after sufficient energy is utilized to increase the surface temperature to the melting temperature (0.0 °C). Once this threshold has been achieved, any additional input of energy will result in snow or ice melt (Marks et al., 1992). Thus melting and runoff occurs when the surface energy flux is positive. This modeling assumption also implies that the surface temperature of the glacier is at melting point and refreezing does not occur. Due to the high mass turn over associated with high accumulation and

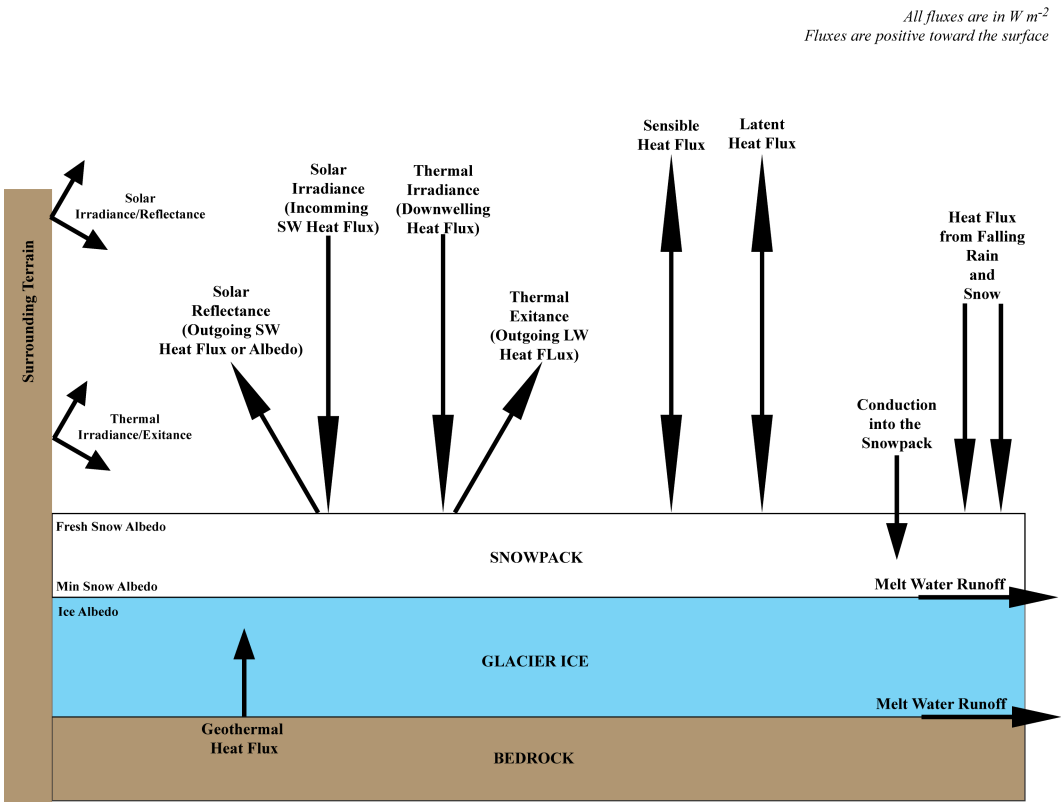

Figure 3.5: Schematic displaying the energy exchange on a glacier's surface, as well as the contributions from surrounding terrain. Note that fluxes are positive towards the surface, indicating energy for melt.

ablation, characteristic of temperate glaciers, an assumption of perpetual melting at the glacier's surface is valid, however in drier and colder climates, typical for polar and continental glaciers, refreezing is an important process that must be incorporated in the model (Greuell and Oerlemans, 1986).

3.3.5.1 Shortwave Radiation Flux

At higher elevations, there is a greater intensity of solar radiation in the 0.285-2.8 μm range that results in high absolute surface temperatures. This meteorological phenomenon is the result of the thinner atmosphere at high elevation. The OSU SEBM separates the diffuse and direct fractions of shortwave radiation. In the complex topography of mountainous terrain, diffuse radiation originates from two sources, the sky and from reflection off of the surrounding topography. The partitioning of measured incoming solar radiation into direct and diffuse components is accomplished through the ratio of potential to measured radiation values following Hock and Holmgren (2005).

$$G_{pot} = S_0 \cdot (1-\iota)^2 \frac{P}{\psi^{P_s \cdot \sin(\theta_0)}} \tag{5}$$

Where G_{pot} is potential radiation, calculated using the relationship expressed by Iqbal (1983), which is described in Equation (5). The potential radiation is a function of the solar constant S_0, which is adjusted for the distance between the sun and the earth (ι),

the atmospheric transmissivity (ψ), which is adjusted for pressure (P), and the solar elevation angle (θ_0). Calculated potential radiation is compared to measured solar radiation, G_m, to determine the diffuse fraction, f.

$$f = \begin{cases} 0.2 & \frac{G_m}{G_{pot}} \geq 0.8 \\ -2 \cdot \frac{G_m}{G_{pot}} + 1.8 & 0.4 \leq \frac{G_m}{G_{pot}} < 0.8 \\ 1 & \frac{G_m}{G_{pot}} < 0.4 \end{cases} \quad (6)$$

Following the work of Anslow et al. (2008), the end-member for completely cloudy conditions is a ratio of G_m to G_{pot} equal to 0.4. Ratios greater than or equal to 0.8 are assumed to represent clear skies with diffuse component equal to 20% of the measured incoming radiation (Anslow et al., 2008). A linear relationship is used between the two end-members Equation (6). This approach follows a relationship derived by Collares-Pereira and Rabl (1979) that was applied to alpine glaciers near Storglaciären, Sweden by Hock and Holmgren (2005). The diffuse component and direct component are calculated utilizing f from Equation (6).

$$G_{dif} = \frac{G_m}{\sin(\theta_0)} f \quad (7)$$

$$G_{dir} = \frac{G_m}{\sin(\theta_0)} (1 - f) \quad (8)$$

The $\sin(\theta_0)$ terms adjust measured radiation for the elevation angle of the sun at the time of measurement and the resulting G_{diff} and G_{dir} represent the diffuse and direct shortwave radiation components, respectively. Diffuse radiation is received from

surrounding terrain by considering the hemispheric fraction of terrain viewable at a given grid cell and, conversely, the fraction of viewable sky which is calculated using the algorithm of Dozier and Frew (1990).

$$G = \left[G_{dif} + G_{dir} \cdot \cos(\Theta)\right] \cdot (\Phi) + G_{dir} \cdot \alpha_{terrain}(1 - \Phi) \tag{9}$$

The radiative contribution from surrounding terrain is the product of direct shortwave radiation, the albedo of surrounding terrain, and the skyview fraction of the terrain, which ranges from 5% to 65%. In Equation (9), Φ is the skyview fraction, and Θ is the angle between the solar beam and the vector normal to the grid cell in question. This angle is calculated as the dot product of the unit vectors representing the direction of the solar beam and the normal direction of the grid cell in question.

$$\cos(\Theta) = \cos(\theta_0) \cdot \sin(\theta) + \sin(\theta_0) \cdot \cos(\theta) \cdot \cos(\phi_0 - \phi) \tag{10}$$

This dot product is expressed in Equation (10), in which θ represents the solar elevation angle, $\boldsymbol{\phi}$ is the solar azimuth angle, θ_0 is the slope angle, and $\boldsymbol{\phi}_0$ is the aspect. Absorbed shortwave radiation is computed from G by adjusting for surface albedo.

$$S_{net} = (1 - \alpha) \cdot G \tag{11}$$

Where S_{net} is the net solar radiation, and α is albedo.

3.3.5.2 Albedo

It is evident from looking at a glacier surface during the ablation season that there is a large degree of variability in albedo. As the snow melts over the course of the ablation season, the albedo decreases, which increases the absorption of incoming shortwave radiation. This process is enhanced when glacier ice, which typically has a lower albedo, becomes exposed further increasing the absorption of incoming shortwave radiation. The reflection of shortwave radiation by the glacier's surface is the outcome of complicated scattering processes in the upper snow/ice surface that depends on the snow/ice grain size as well as the concentration of contaminants and the spacing/size of air bubbles (Armstrong and Brun, 2008).

Various energy balance studies over ablating glaciers have determined that the net radiation flux was one of the most dominant fluxes contributing towards melt energy (Oerlemans, 1992; Anslow et al., 2008; Andreassen, 2008). Variability in net radiation flux can in part be attributed to the changes in albedo, which varies strongly both spatially and temporally, and is therefore unique for each glacier (Brock et al., 2006). Brock et al. (2006) determined that short-term variations in albedo on the surface of a melting glacier are related to fluctuations in cloud cover, while solar elevation and changes in the concentration of debris on the glacier surface is of secondary importance. Thus, the performance of an energy-balance model in simulating glacier mass balance depends on a large extent on the way albedo is treated. Many studies (e.g. Oerlemans, 1992; Andreassen et al., 2008) directly

measure albedo from radiometers located over the melting glacier. Other studies (e.g. Brock et al., 2000; Anslow et al., 2008) implement an albedo submodel to parameterize the albedo changes over the glacier's surface.

Following Anslow et al. (2008), the albedo submodel used in the OSU SEBM is empirically based and is similar to Brock et al. (2000). The model calculates the broadband albedo of snow, corresponding to solar radiation measurements, as it decreases from a prescribed maximum albedo value for fresh snow as a function of cumulative positive degree-days (PDDs).

$$\alpha_{snow} = \alpha_{decay} \cdot \ln\left(\sum PDD\right) + \alpha_{fresh} \tag{12}$$

Unrealistically high albedo calculated for fractional PDDs are reset to the albedo for fresh snow (α_{fresh}). In this approach, temperatures that are higher than the melting point act as surrogates for the increase in grain size and liquid water content responsible for lowering the surface albedo (Wiscombe and Warren, 1980).

In the OSU SEBM it is assumed that the subfreezing changes in snow structure occur at a rate that is insignificant relative to the effects of summer melt water production and changes in snow grain morphology on a particular glacier. More detailed grain evolution albedo models also introduce more free parameters into the model, thus limiting the robustness of the model. These models also require some sort of quantification of the debris content of the snowpack, which was not measured in this study.

As snow melts over the course of the ablation season, a base or minimum albedo value is set for the ice/firn surface and is used when all snow has ablated off that surface (Oerlemans, 1992).

$$\alpha_{ice} = a_1 \cdot \tan^{-1}\left(\frac{z - z_{ELA}}{a_2}\right) + a_3 \tag{13}$$

Equation (13) represents a bimodal function with an abrupt increase near the value of z_{ELA}, which was set to 2498 m (AAR=0.65) for all studies on the Collier Glacier. In this function, a_1-a_4 are parameters that affect the shape of the transition from low albedo below the ELA to high albedo above the ELA, z is elevation, z_{ELA} is the ELA, and α_{ice} is the calculated background albedo. The albedo submodel keeps track of multiple snowfall layers such that new layers are added when a threshold of 10 or more PDDs have passed between successive snowfalls. Anslow et al. (2008) determined that the model proved to be insensitive to a range of degree-day thresholds from 1 to 10 and sensitivity simulations of these thresholds for the Collier Glacier support the finding of Anslow et al. (2008). A value of 10 was chosen to limit the total number of snowfall layers to expedite the simulations. The translucence of snow is incorporated to allow surfaces with a lower albedo, situated below the topmost surface to affect energy absorption at the surface.

$$\alpha = \alpha_1 + \exp\left(\frac{-d_{snow}}{d_0}\right)(\alpha_2 - \alpha_1) \tag{14}$$

In Equation (14), α_1 is the top layer albedo, α_2 is the underlying surface's albedo, d_{snow} is the snow depth, d_0 is a reference snow water equivalent depth. A value of 0.025 m.w.e was chosen for consistency with the ranges of other studies (Oerlemans and

Knap, 1998; Brock et al., 2000; Denby et al., 2002; Willis et al., 2002; Anslow et al., 2008). For ice, a background albedo was applied, and no temporal variation in ice albedo was incorporated.

3.3.5.3 Longwave Radiation Flux

In the thermal spectrum (5-40 μm), snow behaves almost as a perfect blackbody (Dozier and Warren, 1982; Warren, 1982; Armstrong and Brun, 2008). As a result, it absorbs nearly all the long-wave radiation emitted by the atmosphere or by surrounding terrain and, in turn, reemits the maximum thermal radiation allowed by its surface temperature, as computed from the Stephan-Boltzmann equation. Longwave radiation is completely absorbed in the first millimeter of snow due to the high emissivity of ice (Hobbs, 1974). As a result, the longwave radiation reflected at the surface is negligible. Under normal conditions, the amount of longwave radiation emitted from the snow or ice surface slightly exceeds the down-welling longwave radiation, thus resulting in a net negative longwave radiation balance. However, in certain situations such as when air temperatures are warm, humidity is high, and clouds are present, the longwave balance can be positive.

Longwave radiation at each grid point is the sum of measured incoming and computed outgoing fluxes that are determined by air temperature, humidity, and topographic features.

$$L_{net} = L_{\downarrow} - L_{\uparrow} \tag{15}$$

Where $L_{\downarrow}$ is downwelling longwave radiation, $L_{\uparrow}$ is upwelling longwave radiation, and L_{net} is the net longwave radiation. The downwelling longwave radiation is adjusted by the ratio of that calculated for the moraine AWS to that calculated for the grid cell in question using the relationship between relative humidity and emissivity (Figure 3.6). The adjustment incorporates changes in downwelling longwave radiation associated with changes in temperature with elevation. Downwelling radiation at a particular cell is a combination of the measured value adjusted for elevation and that emitted by surrounding terrain. Longwave radiation emitted by terrain is calculated using the Stephan-Boltzmann relationship with a prescribed rock emissivity (ε_r) of 0.95.

$$L_{terrain} = \varepsilon_r \cdot \sigma \cdot T_a^4 \tag{16}$$

This calculation of emission from surrounding terrain, $L_{Terrain}$, relies on near-surface air temperature despite the likelihood that the air temperature at the average emission level of surrounding topography is probably colder. Plüss and Ohmura (1997) demonstrated that the majority of longwave radiation emitted by a surface is attenuated by the atmosphere within a radius of one half kilometer, suggesting that longwave radiation emitted from valley walls 500 meters above the glacier will largely combine with the emission from air between the emitting wall and the glacier. This finding supports the notion that the application of air temperature in this calculation is a reasonable approximation (Greuell and Knap, 1997). Thus, net incoming longwave radiation is determined with the following equation.

$$L_{\downarrow} = L_{inmeas}(\Phi) + L_{Terrain}(1 - \Phi) \tag{17}$$

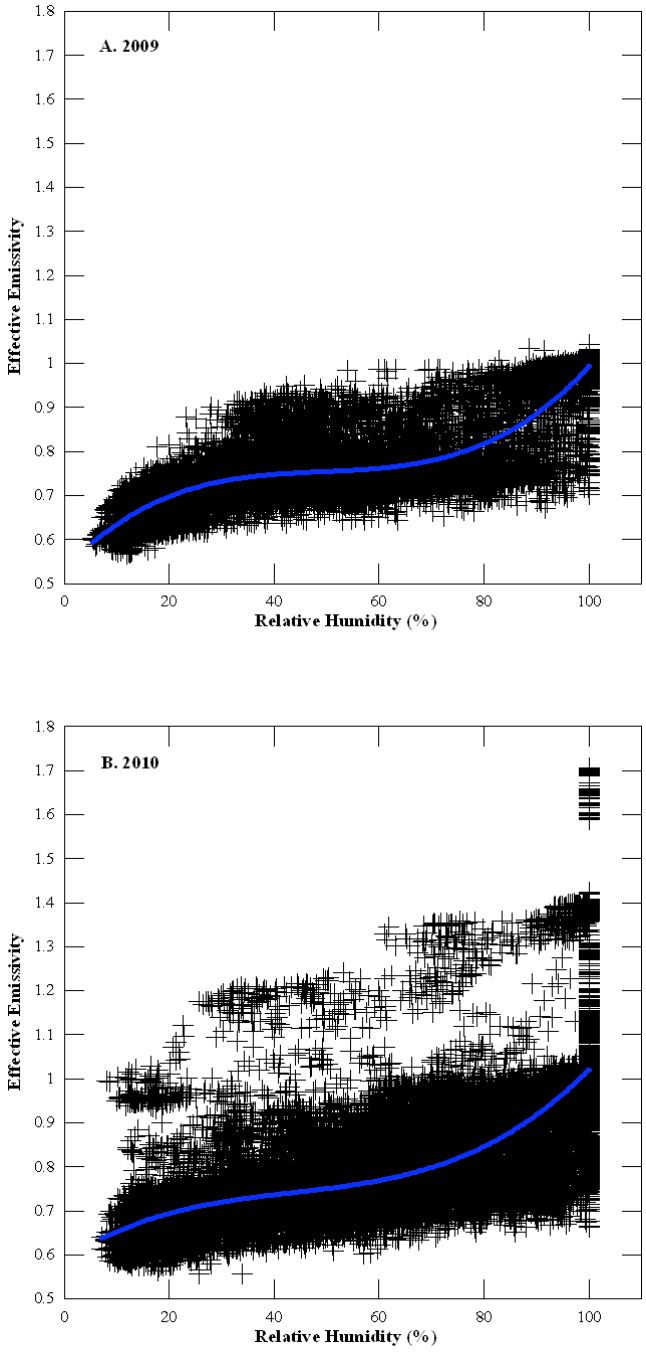

Figure 3.6: The relationship between effective atmospheric emissivity and relative humidity at the moraine AWS for the 2009 (**A.**) and 2010 (**B.**) simulations. The solid blue line represents the 3rd order polynomial covering the transition from cloud-free to cloud-covered conditions where the emissivity reaches 1.

The terrain and the sky longwave radiation components, L_{inmeas}, are combined using the skyview factor Φ of Equation (17). Ice nearly behaves as a blackbody in the longwave radiation spectrum; so outgoing longwave radiation from the glacier surface is calculated from the surface temperature using the Stephan-Boltzmann relationship for a blackbody with emissivity of ice (ε_i) of 0.98:

$$L_{\uparrow} = \varepsilon_i \cdot \sigma \cdot T_s^4 \tag{18}$$

In the model, surface temperature is specified to be at the melting point (273.16 K) when air temperature is above freezing and equal to air temperature when below the melting point.

3.3.5.4 Clouds

Cloud cover plays an important role in the variability in the net radiation budget. Similar to Anslow et al. (2008), the Collier Glacier 2008-2010 study lacked an independent, continuous estimate of cloud cover, thus the model incorporates the influence on cloud cover through an empirical relationship between effective emissivity of the atmosphere and relative humidity. The relationship was parameterized with a third-order polynomial using the 2010 meteorological data collected from the moraine AWS (Figure 3.6). The effective emissivity is determined from the ratio of measured to the calculated potential incoming longwave radiation using measured air temperature and the Stephan-Boltzmann law. Clouds can be

highly influential on albedo because they can alter the spectral distribution of solar radiation. The effect of clouds on the radiation portion of the energy budget is opposite for the shortwave and longwave fluxes. Thus, cloudy periods on a glacier leads to less shortwave and more longwave radiation. Nevertheless, the net effect on the energy budget depends on the surface albedo and on cloud transmissivity (Brock et al., 2000). When the albedo is high, such as when fresh snow is present along the glacier surface, the net change in the longwave flux for a given increase in cloudiness is larger than the net change in the shortwave flux, and as a result, the net radiation balance increases (Oerlemans, 2010). As the albedo decreases over the course of the ablation season and bare ice becomes exposed, the shortwave flux dominates the net radiation budget and decreases with cloudiness. Remote sensing techniques have benefitted our basic understanding of cloud properties, but there is still limited data over highly reflective surfaces, thus limiting their usefulness on applications on remote glaciers. Progress has been made, however, over ice sheets and ice caps, but little data is available for small valley glaciers (Oerlemans, 2010).

3.3.5.5 Turbulent Heat Fluxes

There are a number of ways to calculate the turbulent heat fluxes over glaciers (Munro, 1989; Paterson, 1994; Oerlemans, 2001; Brock et al., 2006; Oerlemans, 2010). The turbulent exchange of heat and moisture can be a significant contributor to

melt energy, especially on temperate glaciers where the surface temperatures are near freezing during the ablation season. Furthermore, such fluxes are persistent throughout both the accumulation and ablation season. In the winter months, turbulent fluxes can be significant when the sun angle is low, or in the summer months when air temperatures are high. When air temperatures are above freezing, the sensible flux is towards the surface (positive), contributing towards melt energy, while the latent flux can go in both directions, depending on the relative humidity (RH) of the air (Oerlemans, 2010). In the case of latent heat flux, at a lower RH, evaporation cools the surface, however at a higher RH, condensation heats the surface.

3.3.5.6 The Bulk Method

Sensible and latent heat fluxes at the glacier surface are computed through the OSU SEBM from the so-called bulk method, wherein the turbulent fluxes are expressed in terms of differences between surface meteorological variables and the values of those meteorological variables at some reference height. The variables include surface and air temperatures, relative humidity, and wind speed. In the bulk method, it is assumed that airflow in the surface-atmospheric boundary layer (SABL) is turbulent and fully adjusted to the underlying terrain (Brock, 2006). Provided the influence of atmospheric stability is taken into account, this method is the most appropriate on sloping glacier surfaces where wind-speed maxima are within a few

meters of the surface (Denby and Gruell, 2000). The main advantage with this method is that measurements of horizontal wind speed, temperature, and humidity need only to be taken at one height (1 to 2 m) above the surface. However, the accuracy of this method is dependent on the accuracy with which the aerodynamic surface roughness, z_0, can be specified.

Following a similar approach as Anslow et al. (2008) for a stable boundary layer, like the layer over a melting glacier, we apply the Monin-Obukhov (MO) similarity theory. We note that the Collier Glacier has a persistent slope, or katabatic flow that according to Oerlemans (2001, 2010) can invalidate the MO similarity theory. The calculation of the latent (H_l) and sensible (H_s) heat fluxes are as follows:

$$H_l = \rho_{air} L_{vap} u A \left(\frac{R}{R^*} \right) \left(\frac{e_a - e_s}{P} \right) \tag{19}$$

$$H_s = \rho_{air} u A (T_a - T_s) \tag{20}$$

For Equations (19) and (20), ρ_{air} is dry air density, u is the measured wind speed, L_{vap} is the latent heat of vaporization for water, R is the dry air gas constant, R^* is the gas constant for water vapor, e_a is the vapor pressure at measurement height, e_s is the surface vapor pressure (taken as the saturation vapor pressure), and P is air pressure. For Equation (20), T_a and T_s are the air and surface temperatures, respectively. The bulk transfer coefficient, A, is calculated as:

$$A = \left[\frac{k}{\ln\left(\frac{z_i}{z_0} \right) + \Psi(z_i, \lambda) \left(\frac{z_i}{\lambda} \right)} \right]^2 \tag{21}$$

Where k is the unitless von Kármán constant (k=0.4), z_i is the measurement height for wind speed and temperature, z_0 is the surface roughness length, Ψ is a unitless stability function, and λ is the Monin-Obukhov length. Brock et al. (2006) defined the surface roughness length as the height above a surface at which the logarithmic horizontal wind-speed profile reaches zero. This is an important control on the turbulent exchange between the glacier surface and the air above it. In energy balance studies, z_0 is rarely measured, so published values from other studies, which may or may not be appropriate for the glacier of study, must be used instead. The Monin-Obukhov length, λ, is calculated as:

$$\lambda = \frac{\rho_{air} C_p u^{*3} \frac{(T_a + T_s)}{2}}{kgH_s} \tag{22}$$

Where C_p is the heat capacity of dry air at constant pressure, u^* is the frictional velocity, and g is the gravitational acceleration. The frictional velocity, u^*, is calculated as:

$$u^* = \frac{ku}{\ln\left(\frac{z_i}{z_0}\right) + \Psi(z_i, \lambda)\left(\frac{z_i}{\lambda}\right)} \tag{23}$$

One consequence of this treatment of surface temperature is that sensible heat flux goes to zero when air temperatures are below the melting point, resulting in an infinite Monin-Obukhov length so that z_i/λ goes to zero, yielding a neutrally stable log profile. The unit-less stability function, Ψ, is determined as:

$$\Psi(z_i,\lambda) = \begin{cases} \Psi = 5 & \frac{z_i}{\lambda} > 0 \\ \Psi = 0 & \frac{z_i}{\lambda} \leq 0 \end{cases} \quad (24)$$

The stability function described in Equation (24) is used to adjust the log profile used in the transfer coefficient (A) and frictional velocity (u^*) Equations (21 and 23).

The equations 19-24 are solved by numerical iteration using the bulk method. For typical meteorological conditions, the solution converges as determined by a less than 5% change in λ between successive steps. For low wind speeds (e.g. $u < 2$ m s^{-1}), convergence can be unattainable and so, in low wind speed situations, wind speed is gradually increased until convergence is achieved. Artificially increasing wind speed to achieve convergence might lead to a small overestimation of heat flux, but because the lowest converging wind speeds are associated with low fluxes of sensible and latent heat, the errors associated with this simplification minimal (Anslow et al., 2008).

3.3.5.7 Flux Calculations Using Transfer Coefficients

For comparison with the bulk method, OSU SEBM was also setup to calculate turbulent heat fluxes using a simpler approach to calculate the sensible and latent heat fluxes from air temperature, wind speed, atmospheric pressure, and vapor pressure (Paterson, 1994). These relationships incorporate dimensionless, specified parameters

K_{hs} and K_{hi} for the transfer coefficient for snow and ice respectively. When a grid cell is snow covered, the model calculates the turbulent fluxes using the transfer coefficient for snow and when a grid cell snow-free, the turbulent fluxes are calculated using the transfer coefficient for ice. The sensible heat flux is calculated as:

$$H_s = \begin{Bmatrix} \left(1.29 \times 10^{-2}\right) K_{hs} P u \left(T_a - T_s\right) & \text{Snow Depth} > 0 \\ \left(1.29 \times 10^{-2}\right) K_{hi} P u \left(T_a - T_s\right) & \text{Snow Depth} < 0 \end{Bmatrix} \quad (25)$$

where P is the atmospheric pressure, u is the wind speed, T_a is the air temperature measured at screen height (1-2 m), and T_s is the surface temperature. In most cases, during the ablation season T_s is usually 0 °C.

The latent heat flux calculations also incorporate:

$$H_l = \begin{Bmatrix} 22.2 K_{hs} u \left(e_a - e_s\right) & \text{Snow Depth} > 0 \\ 22.2 K_{hi} u \left(e_a - e_s\right) & \text{Snow Depth} < 0 \end{Bmatrix} \quad (26)$$

where e_a is the vapor pressure at screen height and e_s is the vapor pressure at the surface. For a melting surface, e_s is assumed to be 611 Pa. Table 3.2 lists the values of the parameters used in this study.

3.3.5.8 Modeled Precipitation

Precipitation increases with elevation in the model by applying a multiplication factor calculated as a function of vertical distance from the measurement elevation:

$$\text{Pre(z)} = \text{Pre}_{\text{meas}} \left[\Gamma_p \cdot \left(z - z_{pre} \right) + 1 \right] \quad (27)$$

Equation (27) is analogous to a dimensionless precipitation lapse rate, but scales the enhancement or depletion by the measurement such that precipitation enhancement or reduction factor is calculated. The method follows that used to distribute precipitation in the PRISM data sets described by Daly et al. (1994). Precipitation was not recorded by any AWS during the field studies on the Collier Glacier due to the difficulty of installing and maintaining precipitation gauges on the glacier. Nearby McKenzie SNOTEL station (44° 13' N, 121° 52' W, 1454 m), which has a similar aspect and geographic location as the Collier Glacier, served as the precipitation input for the model (Figure 3.1). Following Arnold et al. (2006), a snowfall threshold temperature of 1 °C was specified so that precipitation falling at or below 1 °C is assumed to be snow.

The snowpack initialization for the OSU SEBM can be handled in two ways, depending on type and quantity of accumulation measurements. The snowpack can be initialized at the beginning of the simulations using coefficients from a second order-polynomial fit between winter accumulation and elevation determined from the May accumulation measurements from 2009-2011, as indicated in Figure 3.7 (Anslow et al., 2008). Limited accumulation measurements in conjunction with the use of polynomial fits to initialize the snowpack can lead to uncertainties and potential biases with this approach. An alternative snowpack initialization method was developed

Table 3.2: PDD and SEBM Parameters

Symbol	Parameter Description	Value and Units
Γ_p	Precipitation Lapse Rate	Var[a] m^{-1}
α_{fresh}	Fresh Snow Albedo,	0.81
α_{decay}	Albedo Decay Coef.,	Var[a]
$\alpha_{terrain}$	Albedo of Surrounding Terrain,	Var[a]
a_1	Background Albedo Parameters	0.12
a_2	Background Albedo Parameters	40 m
a_3	Background Albedo Parameters	0.3
C_p	Specific Heat Capacity of Dry Air	1004 J K^{-1} kg^{-1}
C_i	Specific Heat Capacity of Ice	2097 J K^{-1} kg^{-1}
ψ	Atmospheric Transmissivity, ψ	Var[a]
d_0	Scale Length for Snow Transmissivity	0.025 m.w.e
g	Gravitational Acceleration	9.807 m s^{-2}
k	Vonkarman Constant	0.4
P_0	Sea Level Pressure	101,325 Pa
R	Dry Air Gas Constant	287.05 J K^{-1} kg^{-1}
R^*	Water Vapor Gas Constant	461.5 J K^{-1} kg^{-1}
S_0	Solar Constant	1365 W m^{-2}
z_1	Instrument Height	1.85 m
$z_{0\ Ice}$	Ice Surface Roughness	Var[a] m
$z_{0\ Snow}$	Snow Surface Roughness	Var[a] m
K_{hi}	Ice Transfer Coef., K_{hi}	Var[a]
K_{hs}	Snow Transfer Coef.,	Var[a]
ki	DDF Ice	Var[a] m d^{-1} °C^{-1}
ks	DDF Snow	Var[a] m d^{-1} °C^{-1}
β_0	Humidity-Emissivity Relationship Coefficient	0.53[b], 0.59[c]
β_1	Humidity-Emissivity Relationship Coefficient	1.2 x 10^{-2} [b], 7.8 x 10^{-3} [c] $\%^{-1}$
β_2	Humidity-Emissivity Relationship Coefficient	-2.4 x 10^{-4} [b], -1.5 x 10^{-4} [c] $\%^{-2}$
β_3	Humidity-Emissivity Relationship Coefficient	1.6 x 10^{-6} [b], 1.1 x 10^{-6} [c] $\%^{-3}$
ε_i	Ice Emissivity	0.98
ε_r	Rock Emissivity	0.95
ρ	Density of Ice	900 kg m^3
σ	Stefan-Boltzmann Constant	5.67 x 10^{-8} W m^{-2} K^{-4}

[a] *Indicates that the parameter varied in this study*

[b] *Indicates parameter value used for the 2009 simulations*

[c] *Indicates paraneter value used for the 2010 simulations*

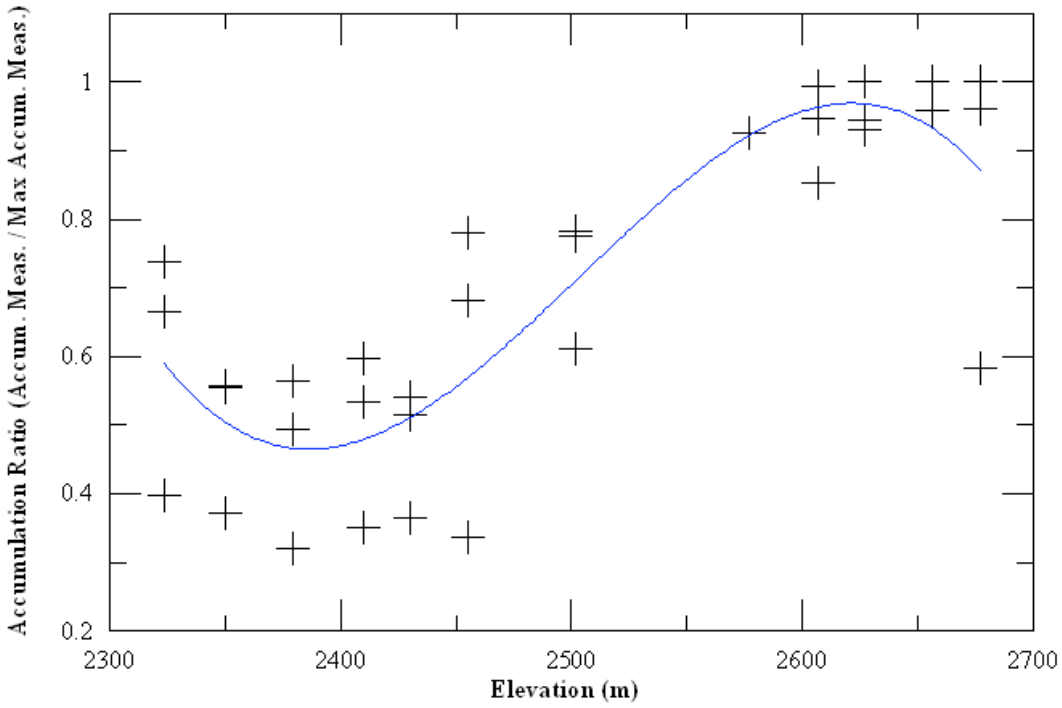

Figure 3.7: Collier Glacier 2009-2011 accumulation ratio and elevation. Accumulation ratio was determined by making the deepest measurement equal to 1 and all other measurements a factor of the deepest measurement. The solid blue line represent the 2nd order polynomial fit used to distribute snow accumulation with elevation across the grid.

utilizing a piecewise linear interpolation of snow accumulation with elevation between each accumulation measurement point. For the 2009-2011 accumulation measurements at least 12 measurement points (probe soundings and snow pits) were collected up the glacier centerline, and those measurements serve to initialize the snowpack in the model (Figure 3.4). Due to the relatively small areal extent and elevation difference of the Collier Glacier, these measurements provided adequate representation of the changes in snowpack with elevation.

3.3.6 Model Assumptions

For the Collier Glacier, we made similar assumptions to Anslow et al. (2008), that the glacier is at steady state and isothermal, thereby eliminating the energy storage term on the left hand side of the energy balance equation (Equation 4). This assumption leads to the total melt (E) being set equal to the sum of the energy input terms, and thus simplifies the energy balance equation (Equation 4) by eliminating the geothermal heat flux term (K) and simplifying the conduction term (C) when air temperature is above the melting point. Refreezing of melt water in the snowpack in late spring/early summer are assumed to be insignificant on the Collier Glacier due to its large mass turnover.

Mountain (1990) found that at no position on the Collier Glacier had englacial temperatures of less than 0 ºC at the 50 cm level over the ablation season. Mountain

(1990) concluded that the entire surface of the Collier Glacier is very close to or at 0 ºC over the ablation season, resulting in diurnal stability in the longwave emission over the glacier, which supports the above assumptions.

3.3.7 Model Calibration

Coarse calibration of the OSU SEBM begins with secularly adjusting each input parameter independently within their respected literature ranges, while holding all other input parameters constant. This process was carried out for each parameter to achieve a best fit between the time series of modeled and measured average net balance, and net balance for each individual stake measurement (Figures 3.8 and 3.9). Table 3.3 lists the final values for the parameters for the OSU SEBM compared with the representative literature ranges. The stake comparisons aided in adjusting the parameters so that modeled ablation rates approached the measured ablation rates for both the ablation and accumulation zones. The value of the coefficient of determination was used as an indicator of the quality of fit between the measured and modeled net balances for each stake location. The coefficient of determination, or R^2, is calculated as:

$$R^2 = 1 - \frac{\sum (y_i - \hat{y})^2}{\sum (y_i - \bar{y})^2} \tag{28}$$

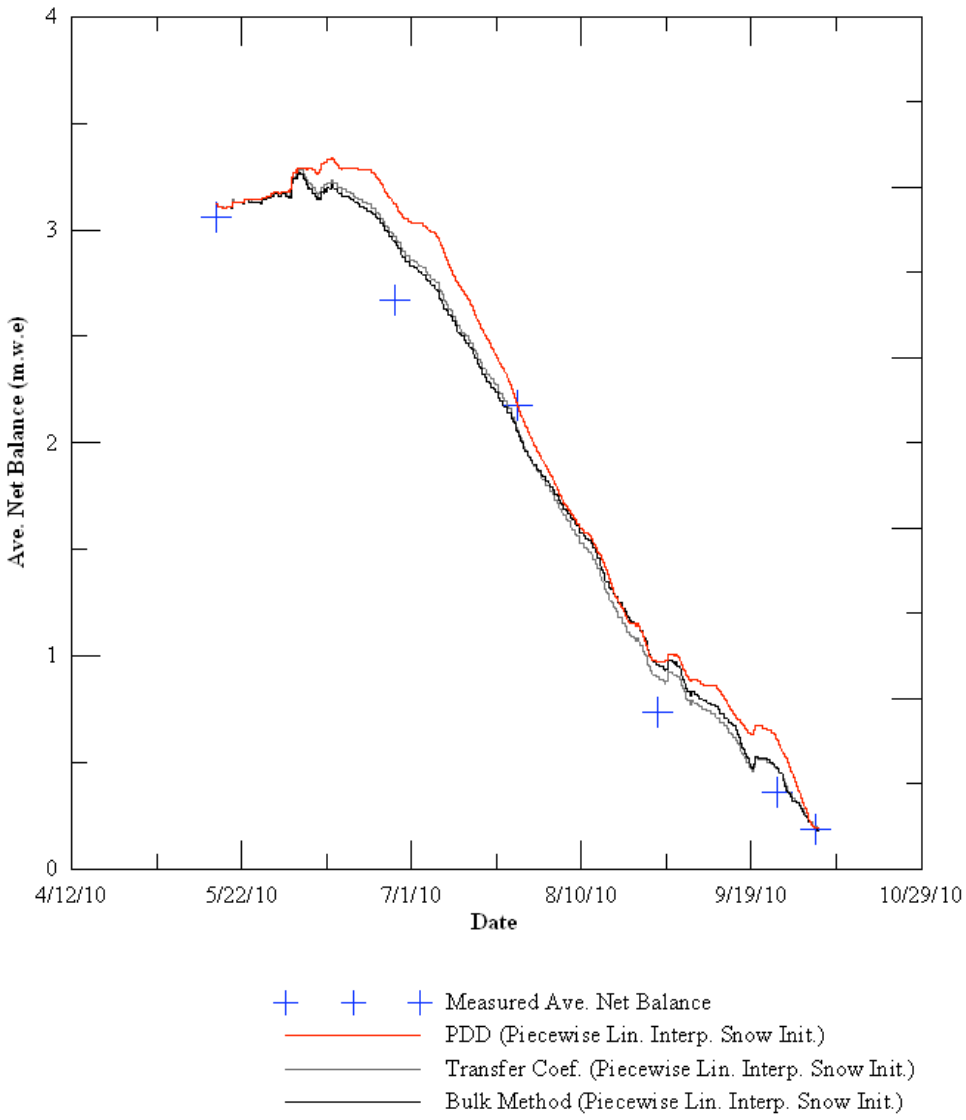

Figure 3.8: Time series of measured versus modeled average net balance for the 2010 simulation period.

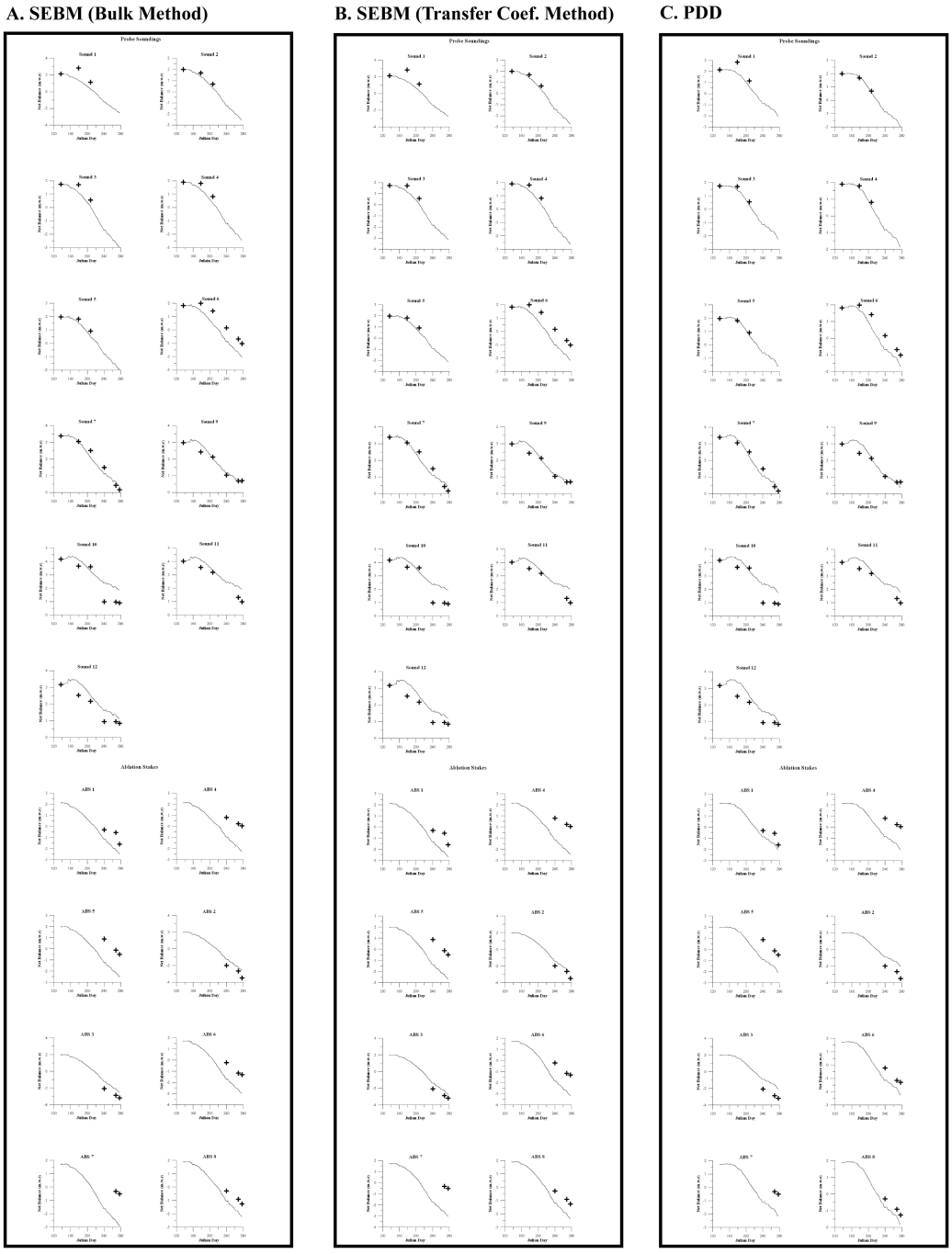

Figure 3.9: Time series of measured versus modeled net balance for each stake/probe measurement location for the 2010 simulation period.

Table 3.3: Optimized parameter values used for each model, as well as their comparisons with the representative literature ranges and the values used for the OSU SEBM on South Cascade Glacier (Anslow et al., 2008).

Parameter	2009 Collier Glacier Value	2010 Collier Glacier Value	2004 South Cascade Glacier Value[k]	2005 South Cascade Glacier Value[k]	Representative Literature Ranges	2010 Sensitivity Range	2010 Sensitivity (PDD), m.w.e $\%^{-1}$	2010 Sensitivity (SEBM, Bulk Method), m.w.e $\%^{-1}$	2010 Sensitivity (SEBM, Transfer Coef.), m.w.e $\%^{-1}$	2004 South Cascade Glacier Sensitivity[k], m.w.e $\%^{-1}$
Precipitation Lapse Rate (SEBM), Γ_p (m^{-1})	0.0025	0.0018	0.0028	0.0035	0.001-0.003[b]	0.0016-0.0020	-	0.005	0.006	0.011
Precipitation Lapse Rate (PDD), Γ_p (m^{-1})	0.0025	0.0011	-	-	-	0.00099-0.00121	0.002	-	-	-
Fresh Snow Albedo, α_{fresh}	0.81	0.81	0.81	0.81	0.8-0.97[i,j]	0.73-0.89	-	0.06	0.06	-
Albedo Decay Coef., α_{decay}	-0.04	-0.04	-0.042	-0.038	-0.067 to -0.049[g,h]	-0.036 to -0.044	-	-0.01	-0.01	-0.023
Albedo of Surrounding Terrain, $\alpha_{terrain}$	0.2	0.2	0.2	0.26	0.1 (variable)[e,f]	0.18-0.22	-	-0.0004	-0.0004	-0.001
Atmospheric Transmissivity, ψ	0.62	0.62	0.62	0.67	0.69-0.76[d]	0.56-0.68	-	-0.0006	-0.0006	-0.002
Ice Surface Roughness, z_o Ice (m)	0.0006	0.0004	0.044	0.0096	0.0001-0.08[c]	0.00034-0.00048	-	-0.0005	-	-0.005
Snow Surface Roughness, z_o Snow (m)	0.001	0.0008	0.004	0.0017	0.0002-0.03[c]	0.00072-0.00088	-	-0.003	-	-0.005
Ice Transfer Coef., K_{hi}	0.0016	0.0017	-	-	0.0015-0.002[i]	0.0015-0.0019	-	-	-0.003	-
Snow Transfer Coef., K_{hs}	0.0014	0.0016	-	-	0.0015-0.002[i]	0.0014-0.0018	-	-	-0.015	-
DDF Ice, k_i (m d^{-1} $°C^{-1}$)	0.0045	0.0046	0.008	0.008	0.005-0.0117[k]	0.0041-0.0051	-0.005	-	-	-
DDF Snow, k_s (m d^{-1} $°C^{-1}$)	0.003	0.004	0.003	0.003	0.0027-0.0055[k]	0.0036-0.0044	-0.03	-	-	-

[a] *Anslow et al.* (2008)
[b] *Daly et al.* (1994)
[c] *Brock et al.* (2006)
[d] *Greuell and Knap* (1997)
[e] *Hock and Holmgren* (2005)
[f] *Tsvetsinkaya et al.* (2000)
[g] *Brock et al.* (2000)
[h] *Pellicciotti* (2004)
[i] *Paterson* (1994)
[j] *Armstrong and Brun* (2008)
[k] *Hock* (2003)

where y_i is an ablation measurement at a known data point, $\hat{y}_i$ is the value of y predicted by the least squares fit at the known data point i, and $\bar{y}$ is the mean ablation for all measurements. The order in which parameter were calibrated depended on the model's sensitivity, thus parameters that were most sensitive were adjusted first. For finer tuning, the model's various parameters were adjusted independently around a control value determined through the course calibration process to achieve an optimal least squares fit with the model and measured ablation.

An optimal value was chosen as a balance between the highest R^2 value from the least squares fit of the modeled verses measured ablation and achieving a least squares slope that approached the 1:1 line between the measured and modeled ablation for each individual stake. The slope of this fit was also compared to this 1:1 line as a gauge for model under/overestimation (Figure 3.10). Slopes less than 1.0 indicate the model overestimates ablation. Plots were made for each parameter, to display the changes in the R^2 value from the least squares fit of the modeled verses measured ablation and the net balance to investigate how secular changes in each parameter within the respected literature range influenced the agreement between measured and modeled ablation and net balance (tables and plots are displayed Appendix C). Optimal parameters were chosen from these model runs to achieve the highest possible agreement between the measured and modeled ablation (Table 3.3).

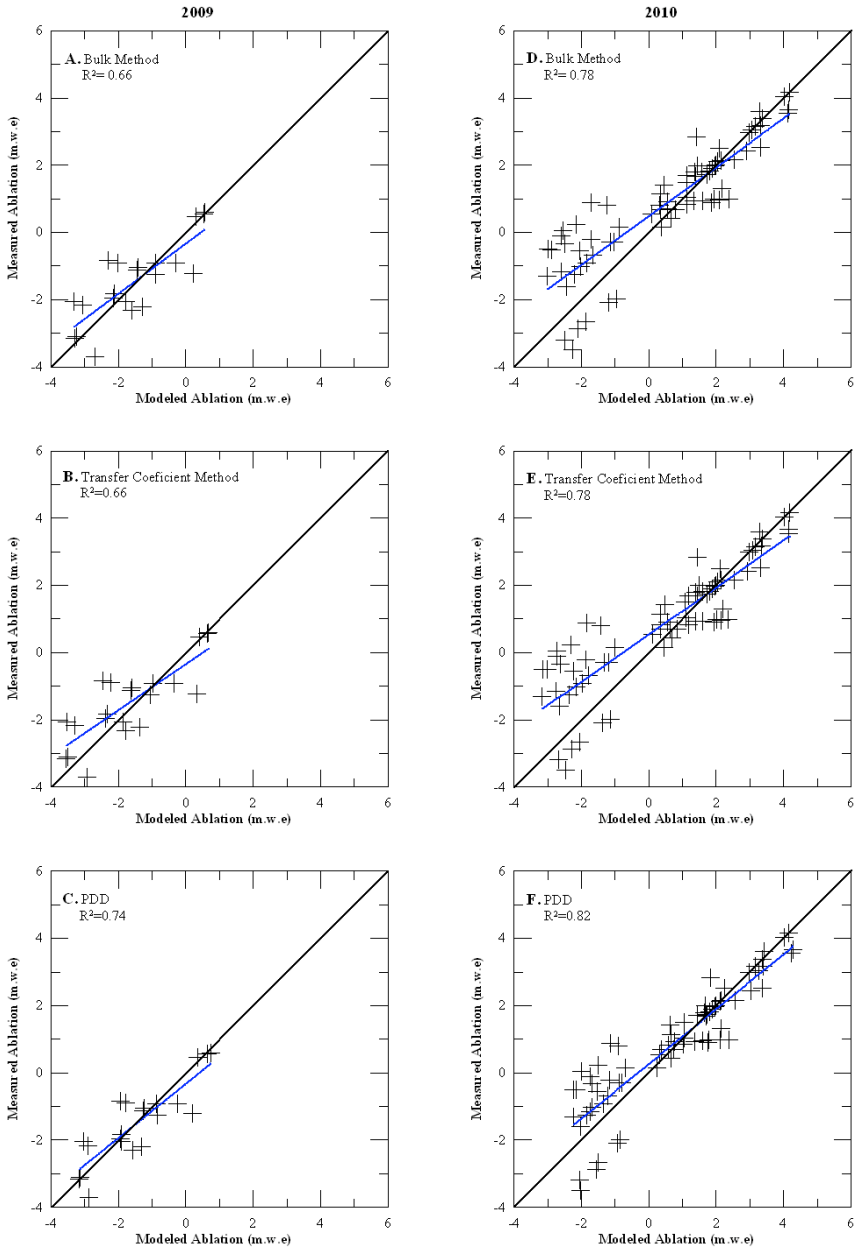

Figure 3.10: Scatter plots for each model displaying the measured verses modeled net balance for each measurement location over the 2009 (**A**, **B**, and **C**) and 2010 simulation periods (**D**, **E**, and **F**). The heavy black line is the 1:1 line between the measured and modeled net balance. The least squares fit of the data is shown with a blue line. Slopes less than 1 indicate the model's overestimation of ablation.

The OSU SEBM was calibrated to the 2010 mass balance and meteorological data. The long, continuous AWS records, spanning from 16 May to 5 October, in conjunction with monthly mass-balance measurements for the 2010 ablation season provided the most comprehensive data set for calibration. To test the validity of the OSU SEBM, model comparisons were made between the distributed SEBM and PDD model. Model comparisons were also conducted within the SEBM to compare two different methods of calculating the turbulent fluxes (the bulk method and the transfer coefficient method). The intent of these comparisons was both to validate the output from the OSU SEBM and to determine whether more computationally complex models are superior to simpler approaches.

Inclement weather at the end of the 2009 ablation season prevented making mass-balance measurements for the entire glacier, however, ablation stake measurements were recorded bi-monthly from August to September 2009, providing ablation measurements necessary to implement the OSU SEBM and assess its performance in the ablation area. Because no measurements were conducted in the accumulation area during the 2009 ablation season, the 2009 simulations are representative for the ablation area only. Some accumulation measurements were conducted on 10 May 2009, but the moraine AWS was not erected until 12 July 2009, resulting in a significant gap in the datasets.

To fill this gap, the winter balance measurements recorded on 10 May 2009 were adjusted to 12 July 2009 by estimating the snowpack with a linear snowpack model from the 1982-2009 average snow water equivalent (SWE) recorded at the

McKenzie SNOTEL station. SWE from 10 May until 12 July determined that the ablation rate of snow at the McKenzie SNOTEL station were consistent, and the intra and inter-annual variability was represented by changes in the y-intercept. Thus, higher amounts of snow accumulation resulted in a higher y-intercept of SWE verses time. The average of those data were plotted against time and a least squares fit of those data was used as a means to determine a linear SWE change over time. The slope of this fit represents the rate of snow ablation as determined from the SNOTEL station and the changes in the y-intercept represented the difference in the measured SWE on the glacier and SWE recorded at McKenzie SNOTEL.

$$SWE_{Collier}(t) = C_1 t + \left(C_2 + \left(b_{w,z} - SWE_{McKenzie}\right)\right) \tag{29}$$

Where $SWE_{Collier}$ is the meters of water equivalent depth at time t, C_1 is the snow ablation rate (m.w.e d^{-1}) determined by the slope of the least squares fit of the 1982-2009 McKenzie SNOTEL average SWE from 10 May through 12 July, C_2 is the y-intercept of the least squares fit of the 1982-2009 McKenzie SNOTEL average SWE from 10 May until 12 July, $b_{w,z}$ is the May winter net balance at an elevation z, and $SWE_{McKenzie}$ is the snow water equivalent depth (m.w.e) at McKenzie SNOTEL for the May winter-balance measurements.

A correction, C_3, was added to the snowpack model's output to account for the initial difference between the snowpack model and the winter-balance measurements b_w at time t_1. This correction is computed as:

$$C_3 = b_w(t_1) - SWE_{Collier}(t_1) \tag{30}$$

The C_3 value was approximately 0.1 for both the 2009 and 2010 snowpack simulations. The snowpack initialization for the model, SWE_{mod}, was determined as:

$$SWE_{\text{mod}} = SWE_{Collier} + C_3 \quad (31)$$

For finer tuning, the precipitation for the model was adjusted within a range of ±5% to account for the yearly variability at the SNOTEL station until an optimum agreement between measured and modeled ablation was achieved.

To test the validity of the model, the 2010 winter-balance measurements were implemented into this simple linear model, and the model was run through 27 June 2010, to compare the mass-balance measurements conducted on the glacier during this time. Differences between the measured and modeled SWE ranged from 0.13 to 1.45 m.w.e. The average difference between the measured and modeled snowpack was 0.38 m.w.e with a standard deviation of 0.55 m.w.e, suggesting a reasonable approach to estimating snowpack on the glacier from winter balance measurements and SWE recorded at the nearest SNOTEL station. The snowpack model output served as the snow initialization for the 2009 SEBM and PDD simulations, since the meteorological record did not start until 13 July 2009.

To aid in the calibration of the 2009 simulations, some 2009 accumulation measurements were conducted during the 2010 ablation season by using crevasses as a means of estimating snow depth. The north-facing walls of the upper crevasses had distinct debris layers separating the current year's accumulation from the previous year's accumulation, allowing one to measure the 2009 snowpack. Snow density was obtained by collecting density measurements below the 2009 summer surface at the

snow pit located at approximately 2600 m. These crevasse measurements, in conjunction with the snow density measurements, provided an approximate estimate of the snow accumulation for the 2009 balance year in the Collier Glacier's accumulation area. It is assumed that these measurements represent minimum values for snow accumulation above the ELA.

3.3.8 Sensitivity Tests

One key element in the linkages between glaciers and climate is the sensitivity of a glacier's mass balance to perturbations in its local climate (Figure 3.11). Oerlemans and Reichert (2000) estimated glacier mass-balance sensitivity to temperature, based on the modeling study of 12 individual glaciers located in different climate regimes. They found that glacier sensitivity depends on the rate of mass turnover (Orelemans and Reichert, 2000). Maritime glaciers experience a larger mass turnover, higher melt rates at the tongue, and small annual temperature range in comparison to continental glaciers (Oerlemans and Reichert, 2000). Furthermore, maritime glaciers may also receive precipitation that falls as rain in the ablation area and snow in the accumulation area in the spring and fall, resulting in a higher sensitivity to changes in spring and fall temperatures. However, in drier, continental climates, where all precipitation virtually falls as snow, the sensitivity becomes restricted to summer temperatures (Oerlemans and Reichert, 2000).

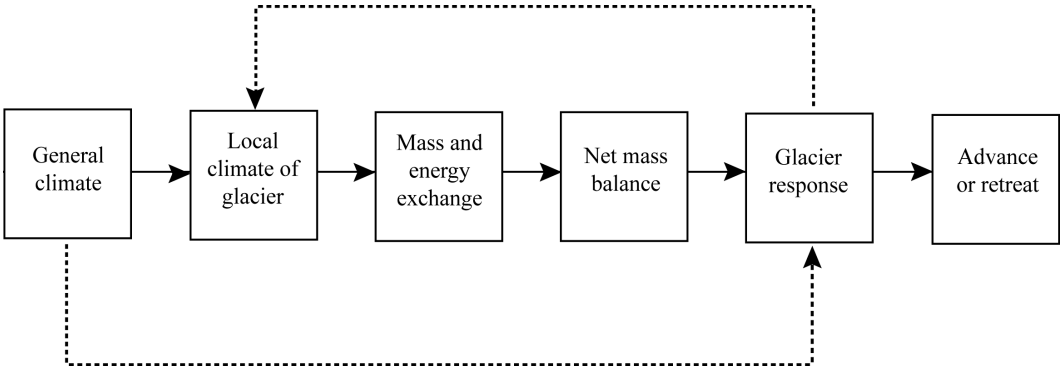

Figure 3.11: The linkages between glacier response and climate change. *From Meier (1965).*

To investigate the influence each input parameter has on the Collier Glacier's mass balance, sensitivity tests were conducted for each model by varying the input parameters individually around optimum values determined through the calibration process. These parameters varied around the optimal values at 5% intervals, over a range of ±10%. Additional, sensitivity tests were conducted with the input meteorological data by varying the input parameters individually around optimum values. Except for temperature, all of the input meteorological data varied by factors of 0.1 over the range of 0.5 to 1.5 times the measured values. In the case of temperature, the measured values were varied in 0.5 °C increments from -2.0 °C to 2.0 °C to determine the glacier's sensitivity to changes in temperature changes. The sensitivity to changes in nighttime and daytime temperatures were determined by changing the temperature in 0.5 °C increments from -2.0 °C to 2.0 °C between the hours of 20:00 to 8:00 for nighttime simulations and 8:00 to 20:00 for daytime simulations. Following Anslow et al. (2008), the model sensitivity was computed by fitting second order polynomials to the results for a given variable or parameters and the slope was determined about the origin.

3.4 Results and Discussion

Parameter values were chosen based on the optimal R^2 between the measured and modeled net balances for each stake/probe measurement, the slope of the least squares fit between the measured and modeled ablation, as well as the agreement between the measured and modeled mean specific mass balance (average net balance for the entire glacier). Like Anslow et al. (2008), we did not simulate time-varying parameters although surface roughness, albedo of surrounding topography, and atmospheric transmissivity are all time dependent. Recent studies have better constraints on the time-dependencies of these parameters (Brock et al., 2000; Hock and Holmgren, 2005; Brock et al., 2006). However, further implementation of the OSU SEBM using the bulk method would stress the importance for further investigations into the temporal variations in aerodynamic surface roughness for snow and ice.

3.4.1 Mass Balance

Depending on the chosen melt model, the optimized model runs simulated ablation that explained 66%-74% and 78%-82% of the variance in the measured ablation for the 2008-2009 and 2009-2010 balance years, respectively (Figure 3.10). The optimized parameter values are summarized in Table 3.3 where they are

compared with the representative literature values and the values used from the OSU SEBM simulations on South Cascade Glacier (Anslow et al., 2008). The optimized parameter values fall within the literature ranges and are broadly similar to those used by Anslow et al. (2008). However, differences do exist in the regional climates of each glacier, stressing the uniqueness of each glacier's microclimate and their governing role on a particular glacier's mass balance, which is reflected by these different parameter values. Differences in the optimized parameter values between South Cascade Glacier and Collier Glacier may also be attributed to the fact that the calibration year for the Collier Glacier was a positive balance year (0.19 m.w.e), while the South Cascade Glacier study calibrated their model to a negative balance years (-1.65 m.w.e and -2.45 m.w.e for the 2004 and 2005 balance years, respectively). Differences in snow cover could result in differences in how the parameters that govern snow and ice melt are calibrated as well as their subsequent sensitivities.

The differences in the microclimates of the South Cascade and Collier Glaciers is attributed to geographic location, surrounding topography, as well as altitudinal differences between the two different glaciers, resulting in slightly different climate regimes. South Cascade Glacier is situated at approximately 48º N in latitude, while the Collier glacier is at 44º N in latitude, such differences in latitude can influence the microclimates of these two glaciers since net radiation and temperature decrease with increasing latitudes, explaining the higher altitude of the Collier Glacier (Barry, 1992). Relative humidity also decreases with altitude, decreasing the latent heat flux due to evaporation (Barry, 1992). This was observed on the Collier Glacier, where the latent

heat flux was negative throughout the ablation season. Such latitudinal differences could also influence the seasonal and diurnal climatic rhythms as determined by the seasonal trend in the daily sun path at different latitudes (Barry, 1992). Both of these factors can greatly influence the surface energy exchange through the ablation season for each glacier, reflecting in the glacier's mass balance. These latitudinal differences may also influence the winter accumulation on each glacier from differences in atmospheric circulation patterns, primarily from mid-latitude cyclonic storms from the Pacific Ocean. Surrounding topography, both locally and regionally, can influence how temperature and precipitation get distributed around a particular glacier. They also influence local glacier features such as shading slope, aspect, and local wind circulations.

One area where there are discrepancies between the measured and modeled mass balance lies in the timing of the maximum accumulation, as indicated in Figure 3.8. Monthly field measurements conducted from April to June 2010 indicated that maximum accumulation occurred around the 16 May 2010 field measurements. Model simulations indicate, however, that the maximum accumulation occurred in early June 2010 just after major storm fronts brought snow to the upper reaches of the glacier (Figure 3.8). The lack of field measurements in the early part of June 2010 prevents any conclusions towards the validity of these simulations are correct, stressing the need for higher temporal resolution field measurements from April to June to better constrain the timing of maximum accumulation. Nevertheless, the 16 May 2010 measurements served as the initialization for the model, since that was the

observed maximum accumulation. Model simulations demonstrated good agreement between the modeled and measured net balances. There was also good agreement in the location and orientation of the ELA, as well as the general shape of the net balance curves between the melt models and the mass-balance measurements (Figure 3.12). All three models used in this particular study showed similar discrepancies between the measured and modeled net balance at the individual stake resolution. Such discrepancies were most prevalent in the ablation area where processes not captured by the models further enhanced the variability in ablation throughout the lower reaches of the glacier below the ELA. Discrepancies between the measured and modeled ablation could be attributed to processes such as snow drift in the early part of the ablation season, and the transport of fine-grained debris North Sister, influencing the surface energy exchange and resulting in a east-west variability in ablation across the lower reaches of the Collier Glacier. These discrepancies are reflected in the secondary fluctuations in the net balance curve for the Collier Glacier's ablation area (Figure 3.12). All melt models considered in this study displayed similar fluctuations in the net balance curves, however they all underestimate the magnitude of the observed mass-balance measurements, suggesting processes not captured by the models are influencing amplitude of these secondary fluctuations.

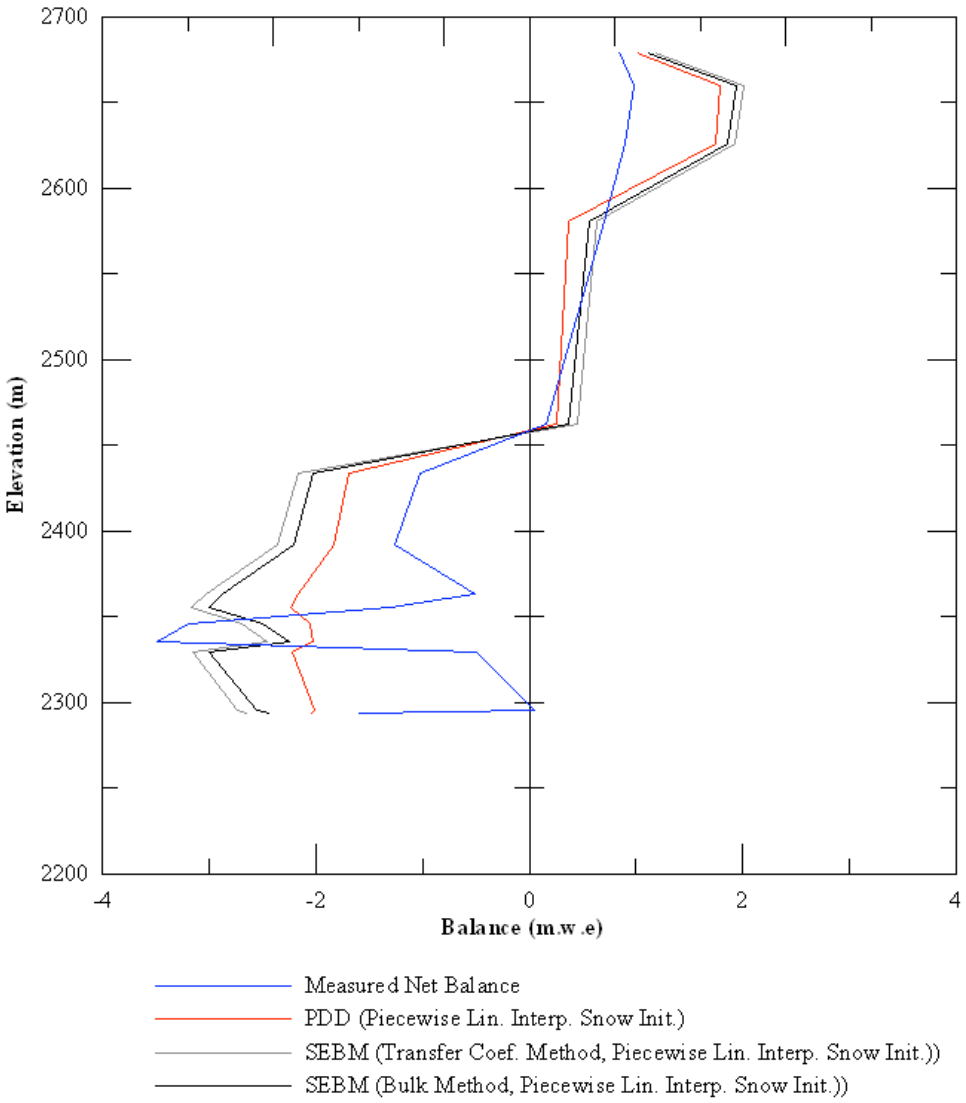

Figure 3.12: Measured and modeled net balance curves for the 2010 simulations, displaying the altitudinal changes in mass balance for the Collier Glacier. The solid blue line represents the 4 October 2010 net balance. The gray, black and red lines represent the various models used in this particular study.

The linear snowpack model developed to initialize the 2009 simulations is useful in determining the snowpack on the glacier at some time in the ablation season after winter balance measurements were collected. This becomes an issue if the meteorological records, which serve as inputs for the melt models, start after the date the winter balance measurements were collected. It is important to note, however, that there are many uncertainties with these 2009 simulations primarily due to the limited field measurements collected for the 2008-2009-balance year. Furthermore, the lack of mass-balance measurements collected at the onset of the meteorological records exposes the OSU SEBM and the PDD model to the uncertainties associated with the linear snowpack model used to initialize the 2009 simulations. When comparing the results from the linear snowpack model with the 2010 mass-balance measurements, the mean difference between the measured and modeled glacier snowpack was 0.38 m.w.e with a standard deviation of 0.55 m.w.e.

Model calibration for the 2009 simulations were based on measured ablation stake measurements, recorded bi-monthly from July to September 2009, providing reasonable temporal resolution in ablation measurements necessary to calibrate the OSU SEBM. The optimized model runs for the 2008-2009-balance year explained approximately 66% to 74% of the variability in ablation for the Collier Glacier (Figure 3.10 and Table 3.4). The lack of accumulation measurements limits the validity of these results to just the ablation area of the glacier, thus creating a bias towards the ablation area in the calibration process. Nevertheless, mass-balance measurements conducted from 1989 to 1994 (McDonald, 1995) and 2010 suggest that the majority of

the variability in the Collier Glacier's mass balance was concentrated in the ablation area (Figure 3.10). Early storms in the fall of 2009 prevented measurements in the accumulation area, thus a 2009 net balance for the Collier Glacier was not determined. Accumulation measurements, however, were conducted the following summer using the north-facing walls of crevasses. The 2009 firn layer was deciphered from the 2010 snow pack by distinct debris layers separating each individual year's accumulation. Snow density measurements were conducted for these 2009 accumulation measurements at the 2600 m snow pit. These density measurements were sampled below the 2010 summer surface to achieve a water equivalent depth of accumulation above the ELA. It is important to note that there are many uncertainties associated with such measurements, many of which are associated with the changes in snow density and depth over the course of one balance year. Furthermore, these minimal measurements in the accumulation area limits the precision of the model, thus stressing the need for accumulation area measurements with regards to any future modeling the Collier Glacier's mass balance or any future implementation of the OSU SEBM. Nevertheless, many of the optimal parameter values used for the 2009

Table 3.4: Model performances, listing the simulated average net balance (m.w.e) and the coefficient of determination (R^2) for a least squares fit of the modeled verses measured ablation for all measurements in this particular study.

		Piecewise Linear Interp. Snow Init.			Polynomial Snow Init.		
Glacier	**Simulation Year**	**Model Type**	**Simulated Ave. Net Balance (m.w.e)**	**Measured vs. Modeled Stake Coef. Of Det. (R^2)**	**Model Type**	**Simulated Ave. Net Balance (m.w.e)**	**Measured vs. Modeled Stake Coef. Of Det. (R^2)**
Collier	2010	PDD	0.19	0.82	PDD	0.21	0.81
Collier	2010	Bulk Method	0.18	0.78	Bulk Method	0.18	0.80
Collier	2010	Trans. Coef.	0.19	0.78	Trans. Coef.	0.21	0.80
Collier	2009	PDD	-1.07	0.74	PDD	-1.09	0.85
Collier	2009	Bulk Method	-1.03	0.66	Bulk Method	-1.15	0.79
Collier	2009	Trans. Coef.	-1.05	0.66	Trans. Coef.	-1.17	0.82
South Cascade	2005	-	-	-	Bulk Method	-1.69[a]	0.91[a]
South Cascade	2004	-	-	-	Bulk Method	-2.09[a]	0.97[a]

[a]*Anslow et al.* (2008)

simulations were similar to the 2010 simulations and are summarized in Table 3.3, along with their comparisons with the 2010 simulations and representative literature ranges. One parameter in particular that was different from the 2010 simulations was the precipitation lapse rate, which was set higher for the 2009 simulations since the snowpack model used to initialize the OSU SEBM and PDD model had a tendency to underestimate the snowpack for the start of the meteorological record. The parameters that govern snow and ice were also different to account for the difference in snow and ice coverage between the 2009 and 2010 simulations, since the 2010 balance year resulted in a positive net balance.

3.4.2 Model Comparisons

For the 2010 simulations, model comparisons between the OSU SEBM and a simple PDD model both explained around 78% and 82% of the variance in the Collier Glacier's ablation, respectively, using the piecewise linear interpolation snow initialization scheme (Figure 3.8). When comparing measured verses modeled ablation, the PDD model had a tendency to underestimate ablation in comparison to the SEBM, as indicated by the higher least squares slope between the measured and modeled stake net balances (Figure 3.10). The SEBM, using both the bulk method and the transfer coefficient method to calculate the turbulent heat fluxes, had a

tendency to overestimate ablation, as indicated by the lower least squares slope between the measured and modeled stake net balances (Figure 3.10). These differences are likely attributed to the temporal resolution of the SEBM over the PDD model, since the degree-day factors are assumed to be constant for the simulation period. Furthermore, the spatial variability of the melt rates are not modeled as accurately with the PDD model, since the SEBM takes into account the small-scale variations over the glacier, as a result of the effects of surrounding topography, slope aspects, and slope angles. Such small-scale variations in ablation are apparent in the simulated mass-balance maps (Figure 3.13).

The meteorological inputs from the Moraine AWS and the optimal SEBM outputs are summarized in Figures 3.14 and 3.15. Both figures highlight the relatively small contribution the energy flux associated with falling rain, in comparison to the fluxes associated with radiation and turbulence. As mentioned earlier, there are a number of approaches in the treatment of the turbulent flux calculations (Paterson, 1994; Oerlemans, 2001; Oerlemans, 2010). Typically for mass-balance modeling, turbulent fluxes are calculated using the bulk method (e.g. Anslow et al., 2008; Andreassen et al., 2008). However, Oerlemans (2010) indicates that assumptions made with the MO similarity theory, on which the bulk method is based, are not valid in the prescience of wind speed maximum. Furthermore, the MO similarity theory was developed for homogeneous conditions above a horizontal surface, and many glaciers have sloping surfaces where horizontal homogeneity is rarely probable

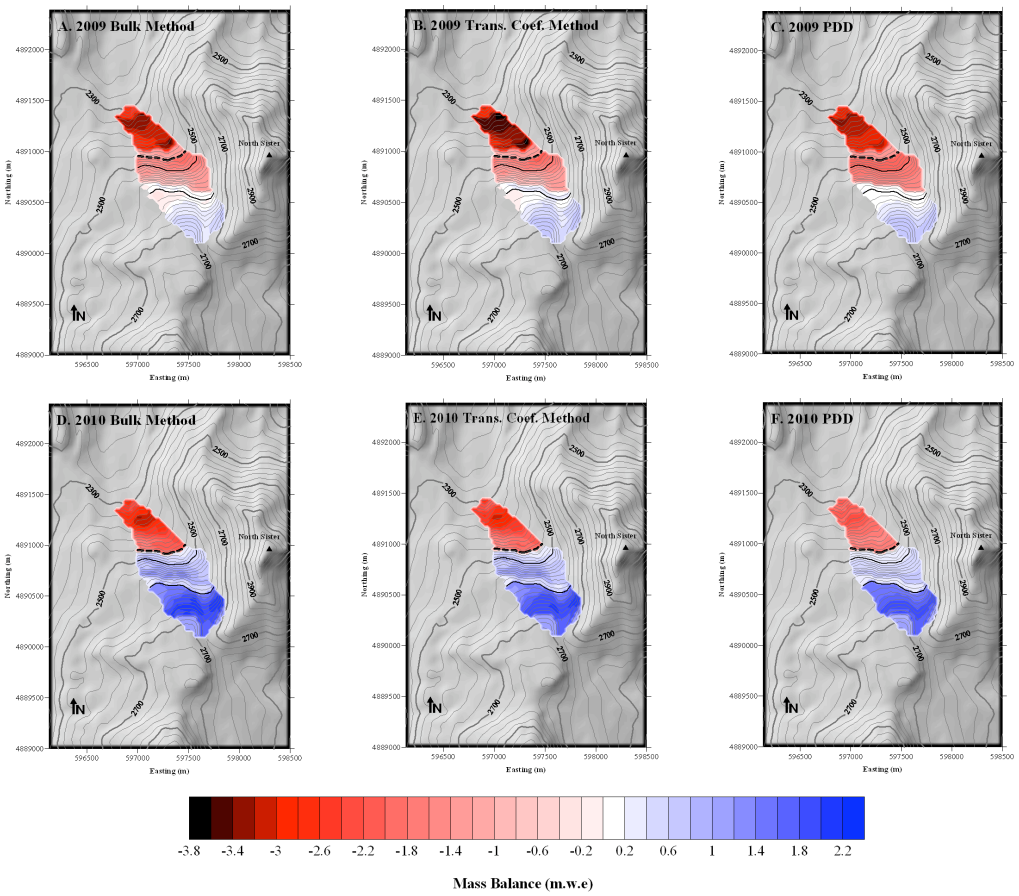

Figure 3.13: Distributed mass balance maps from the 2009 (**A**, **B**, and **C**) and 2010 simulations (**D**, **E**, and **F**). The thick, black dashed line marks the 2010 ELA as determined from mass-balance measurements. The thick, black solid line represents the upper and lower elevations of the icefall.

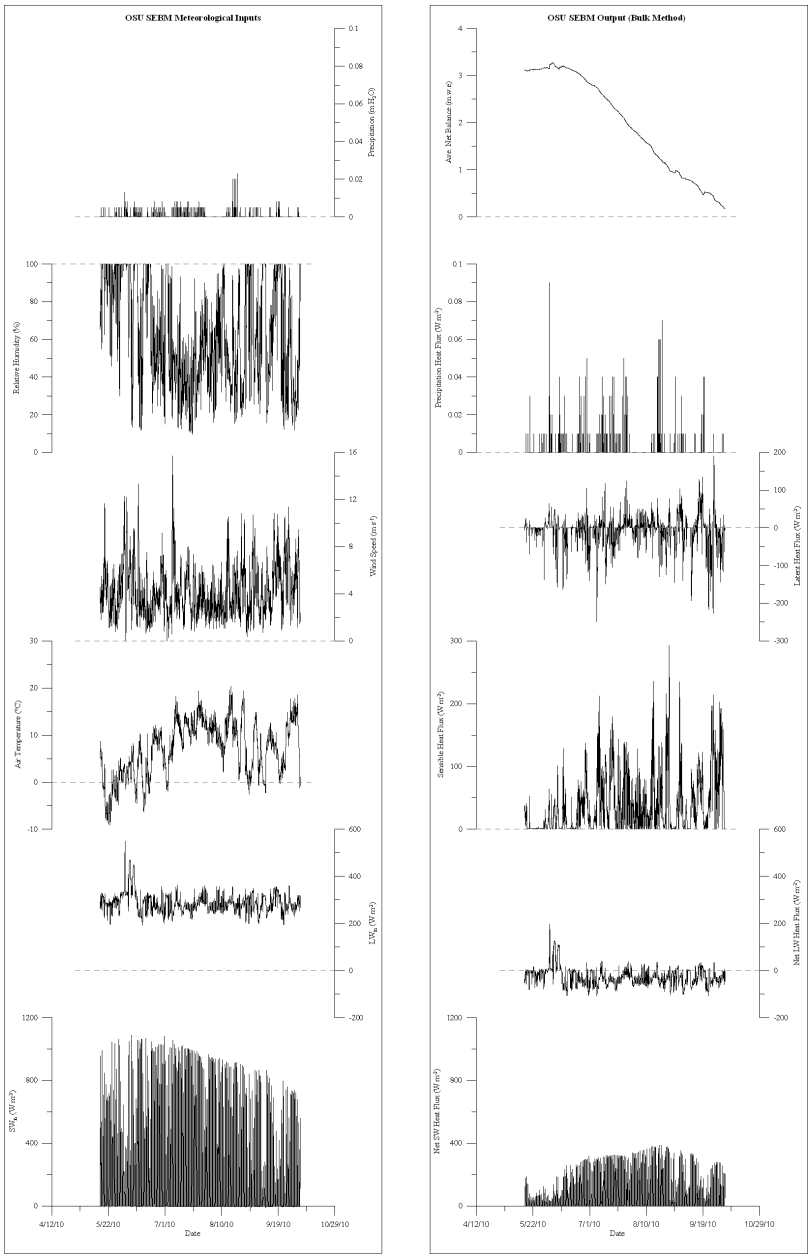

Figure 3.14: (**left**) OSU SEBM meteorological inputs recorded from the moraine AWS for the 2010 simulations. *From top to bottom*: precipitation, relative humidity, wind speed, air temperature, incoming longwave radiation, and incoming shortwave radiation. (**right**) OSU SEBM outputs. *From top to bottom*: simulated average net balance, heat flux associated with precipitation that falls as rain, latent heat flux, sensible heat flux, net longwave radiation flux, and net shortwave radiation flux.

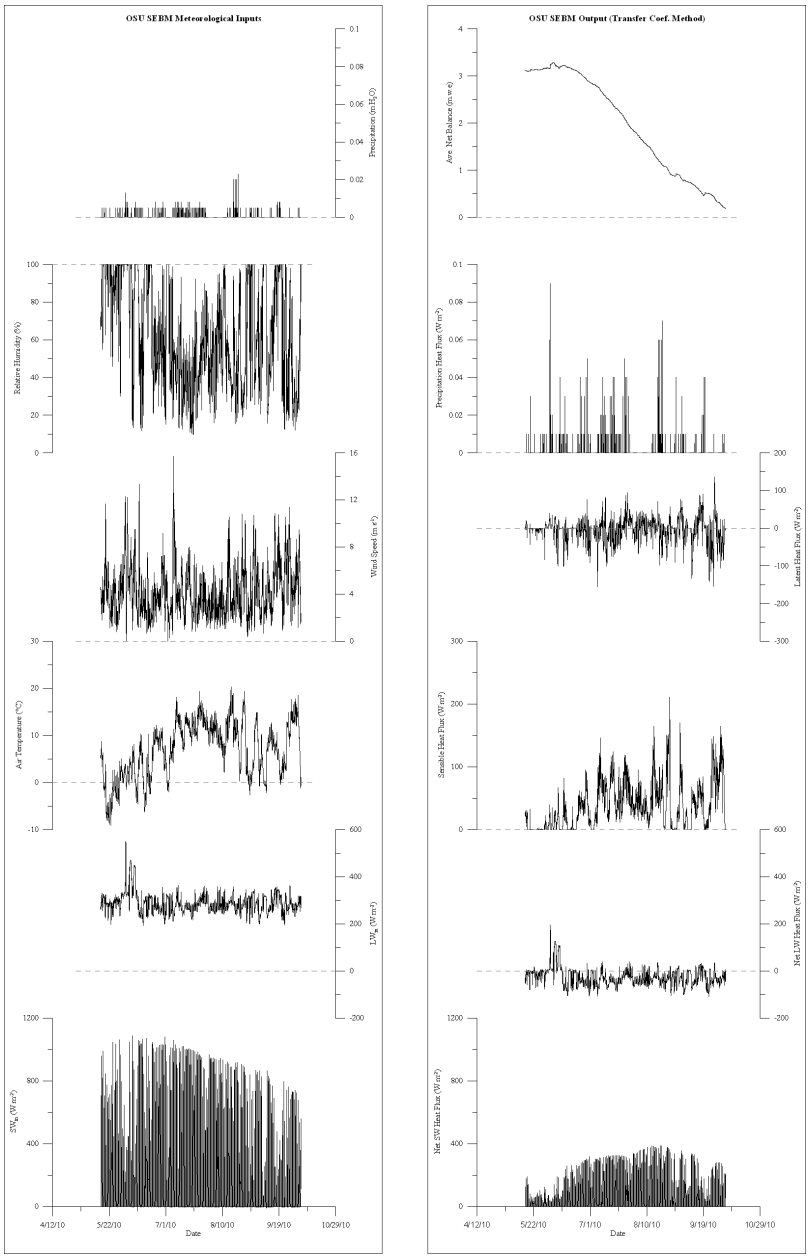

Figure 3.15: (**left**) OSU SEBM meteorological inputs recorded from the moraine AWS for the 2010 simulations. *From top to bottom*: precipitation, relative humidity, wind speed, air temperature, incoming longwave radiation, and incoming shortwave radiation. (**right**) OSU SEBM outputs. *From top to bottom*: simulated average net balance, heat flux associated with precipitation that falls as rain, latent heat flux, sensible heat flux, net longwave radiation flux, and net shortwave radiation flux.

(Monin and Obukhov, 1954; Paterson, 1994; Oerlemans, 2001; Oerlemans, 2010). Denby and Greuell (2000), however, found that the bulk method gave good results when the measurement level is below the wind speed maximum. Locating this wind speed maximum can be an issue with glaciological studies on remote glaciers, where a wind profile is often not directly measured in the field and instrumentation are typically installed at screen height (1-2 m). The bulk method also stresses the parameterization of the aerodynamic surface roughness of snow and ice, a medium that has been known to vary significantly both spatially and temporally (Brock et al., 2006). These parameters greatly increase the complexity of the model, as well as potentially exposing the model to a greater number of uncertainties associated with these parameterizations. The differences in the treatment of the turbulent flux calculations are apparent in Figures 3.14 and 3.15 with the time series of sensible and latent heat fluxes. It is apparent that the bulk method's turbulent heat fluxes are represented by slightly larger energy flux amplitudes through the simulations, thus translating to slightly more ablation than the transfer coefficient method. Nevertheless, model comparisons between the bulk approach and a simpler method utilizing transfer coefficients to calculate the turbulent heat fluxes, indicated no superiority when modeling the Collier Glacier's mass balance (Figures 3.8 and 3.12). Both approaches explained approximately 78% of the variability in the Collier Glacier's 2010 mass balance, suggesting that the more complex approaches do not explain the variability in the Collier Glacier's mass balance any better than the simpler approaches. However, despite the potential downfall of the bulk method with regards

to wind speed measurements being conducted near the wind speed maximum, reasonable simulations of turbulent fluxes were obtained in this study, as indicated by the similar performances of the SEBM using the bulk method and the transfer coefficient method. These results are summarized in Table 3.4.

Average monthly energy balance components were calculated from both the SEBM using the bulk method and the transfer coefficient method and are summarized in Table 3.5. Both the bulk method and the transfer coefficient method displayed similar mean turbulent heat fluxes through the ablation season, indicating model consistencies. Furthermore, both models indicated a predominately negative latent heat flux throughout the simulation periods, suggesting that evaporation was the dominant control of the latent heat flux throughout the ablation season. Relatively high sensible heat fluxes from both models indicate that the turbulent exchange of heat, associated with the Collier Glacier's wind regime plays an important role in the energy balance. Net longwave averages were negative throughout the simulation periods, with the lowest negative values occurring at the beginning of the ablation season, where late spring and early summer storms brought cloud sporadic cloud coverage to the Collier Glacier. These negative values indicate that the majority of the net longwave radiation contribution to the energy budget was through outgoing longwave radiation from the glacier's surface. The lower net shortwave values could be attributed to the high degree of snow-coverage throughout the early half of the ablation season, as well as the shading aspects associated with the surrounding topography. Nevertheless, these model simulations indicate that the net shortwave

flux was one of the major controls of the energy balance through the ablation season, supporting the findings from other glacier surface energy balance experiments (Brock et al., 2000; Oerlemans, 2001; Anslow et al., 2009). The net shortwave energy flux was at a minimum at the beginning of the ablation season, where snow covered the entire glacier, maintaining a high albedo through the first few months of the ablation season. Table 3.5 indicates that peak energy fluxes contributing to melt energy occurred in July and August, with the largest of these contributions coming from the net shortwave radiation flux. Coinciding with the net energy flux for the glacier, the net shortwave flux also reached a maximum in July and August, however these averages decreased in September and October as the sun angle decreased. These results are supported by the mass-balance measurements conducted during this period, as indicated in Figure 3.8. It is apparent from Figure 3.16 that the net radiation had a dominant control over the energy balance from May through August. However towards September and October, the turbulent fluxes began to dominate the Collier Glacier's energy balance. Thus, late in the ablation season, the turbulent heat fluxes, primarily from the sensible heat flux, still contribute to melt energy. These simulations suggest that the turbulent fluxes, primarily through the sensible heat flux associated with the Collier Glacier's wind regime, contribute to melt well into the later portions of the ablation season and possibly into the beginning of the accumulation season, stressing the variability associated with the seasonality around the Three Sisters Wilderness as well as the timing of maximum ablation on the Collier Glacier.

Table 3.5: Monthly averaged energy balance components for the 2009 and 2010 simulations.

	Bulk Method										Transfer Coeficient Method									
	SW_{net}		LW_{net}		H_s		H_l		Σ		SW_{net}		LW_{net}		H_s		H_l		Σ	
Averaging Period	2009	2010	2009	2010	2009	2010	2009	2010	2009	2010	2009	2010	2009	2010	2009	2010	2009	2010	2009	2010
May	-	*25*	-	*-14*	-	*5*	-	*-4*	-	*12*	-	*25*	-	*-14*	-	*3*	-	*-2*	-	*12*
June	-	60	-	-14	-	24	-	-11	-	59	-	60	-	-14	-	19	-	-8	-	58
July	*104*	100	*-31*	-35	*53*	51	*-1*	-9	*126*	107	*106*	100	*-31*	-35	*56*	54	*2*	-5	*133*	114
August	95	97	-37	-35	38	44	-5	-6	90	101	95	98	-37	-35	37	47	0	-3	94	108
September	*82*	60	*-36*	-31	*60*	53	*-22*	-4	*85*	77	*82*	59	*-36*	-31	*53*	47	*-15*	-2	*83*	73
October	-	*61*	-	*-27*	-	*97*	-	*-33*	-	*99*	-	*61*	-	*-27*	-	*83*	-	*-26*	-	*92*
JJA Means	**-**	**86**	**-**	**-28**	**-**	**39**	**-**	**-9**	**-**	**89**	**-**	**86**	**-**	**-28**	**-**	**40**	**-**	**-5**	**-**	**93**

[a]The italicized entries indicate less than a month's worth of data for the 2009 and 2010 simulation periods.

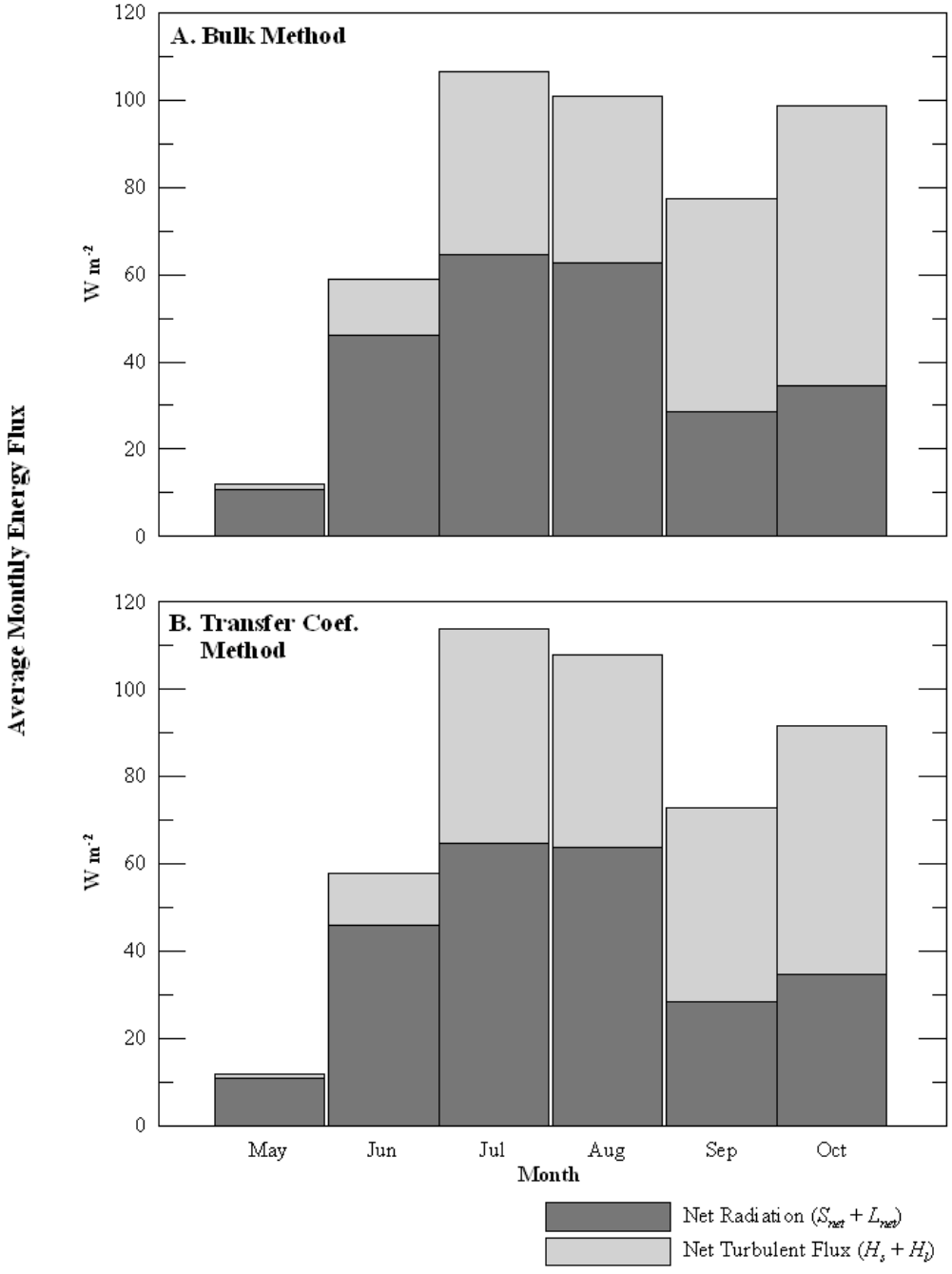

Figure 3.16: Monthly net radiation and turbulent flux averages for the 2010 simulation, indicating their contribution towards the Collier Glacier's energy budget over the course of the ablation season.

The multiple model comparisons conducted for the 2010 balance year, suggest that the more complex approaches did not explain the variability in the Collier Glacier's mass balance any better than the simplest methods. All three methods explained approximately 78% to 82% of the variance in the Collier Glacier's 2010 ablation. As mentioned earlier, the area of the greatest discrepancy between the model and measured mass balance occurred in the ablation area, where all models had a tendency to over estimate ablation along the western margin of the ablation area and underestimate the ablation along the eastern margin of the glacier. Thus, the models did not fully capture the secondary fluctuations in the net balance curve that are characteristic for the Collier Glacier (Figure 3.12). As mentioned earlier, these comparisons suggest that factors not captured by the models, such as wind loading of snow and distribution of debris across the ablation area, are not fully resolved in the model. However, further parameterization of these factors could compromise model robustness, thus compromising the model's ability to accurately simulate mass-balance on other remote glaciers. Nevertheless, the simplest method, the PDD model, simulated mass balance with highest agreement between the measured and modeled ablation, with a R^2 of 0.82 (Table 3.4). These findings support other model comparisons, where temperature-index models often match the performance of energy-balance models on a catchment scale (Rango and Martinec, 1995; Hock, 1999; Hock 2005). Thus, the performance of the PDD model was generally attributed to the high correlation of temperature with the various components of the surface energy balance equation (Equation 4), primarily from the net longwave and turbulent heat

fluxes. Furthermore, the degree-day factors for snow and ice where the only parameters necessary to calibrate the model, further simplifying the complexity of model calibration. The robustness and performance of the PDD model, as highlighted in this particular study, suggests this modeling approach is best suited for modeling mass balance on remote glaciers. Furthermore, modeling mass balance with a simple PDD model requires less instrumentation to simulate mass balance, thus simplifying field logistics and significantly reducing the overall research budget since temperature sensors are much less expensive than instrumentation necessary to implement SEBMs.

3.4.3 Model Sensitivity

Sensitivity tests were conducted on the 2010 calibrated models to investigate which parameters were most influential to the simulated mass balance. As mentioned earlier, the lack of continuous winter balance measurements stressed the use of the piecewise linear interpolation snow initialization scheme since it captured the seasonal variability in snow accumulation in comparison to the polynomial snow initialization scheme, thus being more representative of the 2010 snowpack at the start of the model simulations. Comparisons between these two snow initialization schemes will be discussed later. The sensitivity of the SEBM to secular changes in input metrological data is presented in Table 3.6. All three models displayed similar internal sensitivities

Table 3.6: 2010 model sensitivity to secular changes in the input meteorological variables.

Meteorological Variable	2010 Sensitivity (PDD)	2010 Sensitivity (SEBM, Bulk Method)	2010 Sensitivity (SEBM, Transfer Coef.)	2004 Sensitivity (SCG, Bulk Method)
Air Temperature (m.w.e $\%^{-1}$)	-0.04	-0.03	-0.04	-2.15
Air Temperature (m.w.e $°C^{-1}$)	-0.59	-0.61	-0.63	-0.86
Day Air Temperature (m.w.e $°C^{-1}$)	-0.33	-0.36	-0.39	-1.15
Night Air Temperature (m.w.e $°C^{-1}$)	-0.30	-0.29	-0.27	0.60
SW_{in} (m.w.e $\%^{-1}$)	-	-0.03	-0.03	-0.06
LW_{in} (m.w.e $\%^{-1}$)	-	-0.07	-0.07	-0.16
RH (m.w.e $\%^{-1}$)	-	-0.02	-0.02	-0.04
Wind (m.w.e $\%^{-1}$)	-	-0.024	-0.015	-0.05
Wind Above ELA (m.w.e $\%^{-1}$)	-	-0.013	-0.007	-
Wind Below ELA (m.w.e $\%^{-1}$)	-	-0.011	-0.007	-
Precipitation (m.w.e $\%^{-1}$)	0.03	0.04	0.04	0.02

to secular changes in the meteorological input data. All modeling approaches utilized in this study displayed similar sensitivities to changes in both temperature and precipitation. The SEBM using the transfer coefficient method to calculate turbulent fluxes, showed a slightly higher sensitivity to changes in temperature, when compared to the other modeling approaches. For all three melt models, there was a slightly higher sensitivity to changes in daytime temperatures, since daytime temperatures were typically above the melting point in comparison to nighttime temperatures, resulting in a less energy necessary to melt snow and ice. Nevertheless, these discrepancies between the three models were minimal, further demonstrating the internal consistencies in how mass balance was simulated regardless of the chosen melt model. Furthermore, these internal consistencies between each model demonstrated the validity of each method in simulating glacier mass balance, supporting each other with similar results.

The OSU SEBM displayed the highest sensitivity to incoming longwave radiation (-0.07 m.w.e $\%^{-1}$) as opposed to a sensitivity of -0.03 m.w.e $\%^{-1}$ for incoming shortwave radiation. These results support the notion that the glacier should be more sensitive to variations in the net longwave radiation flux due to the fact that energy exchange associated with the longwave energy flux occurs at all hours of the day, while the net shortwave radiation flux has a diurnal fluctuation due to the position of the sun, as well as the shading from surrounding topography. Nevertheless, the 2010 sensitivity simulations indicated that the Collier Glacier's mass balance displayed a slightly higher sensitivity to the meteorological inputs that influence the

net radiation budget when compared to the inputs that govern the turbulent fluxes. These sensitivity simulations also displayed internal consistencies between the SEBM using the bulk method and the transfer coefficient method, however, these simulations suggest that the bulk method is slightly more sensitive to changes in the wind speed, thus stressing the importance of the location and height at which wind speed is recorded. This higher sensitivity to wind speed could be the result of the bulk method's dependency on the wind speed profile and the parameterization of the aerodynamic surface roughness for snow and ice.

Sensitivity experiments were also conducted for each calibration parameter for each modeling method, as displayed in Table 3.3. The parameters governing the elevation gradient of precipitation, or precipitation lapse rate, the decay in albedo over time, as well as the parameters that govern melt over snow covered surfaces, including the degree-day factor for snow, snow transfer coefficient, and snow surface roughness, displayed the highest sensitivity over the modeled mass balance. The initialization for fresh snow albedo also had a significant control over the modeled mass balance for both SEBM methods used in this particular study. However, the parameters that govern the reflectivity, or albedo of surrounding terrain, and the atmospheric transmissivity were the least influential in the simulated mass balance. Again, these results were consistent with all melt models used in this particular study, displaying the internal consistencies between each modeling method.

As mentioned earlier, since the 2010 sensitivity experiments were conducted on a positive mass balance year for the Collier Glacier, resulting in a higher degree of

sensitivity to the parameters that govern energy exchange over snow-covered surfaces as opposed to ice-covered surfaces. This could be due to the fact that this particular balance year had an AAR of 0.75, meaning that the majority of the glacier was snow covered during the 2010 ablation season. These differences are reflected in all three modeling approaches with degree-day factors (DDF) for ice and snow, transfer coefficients for ice and snow, and the aerodynamic surface roughness for ice and snow. Differences in balance years could also explain the differences in parameter sensitivities between the Collier Glacier study and the South Cascade Glacier studies of 2004 and 2005 that were both negative balance years (Anslow et al., 2008). Furthermore, the glacier's geometry and hypsometry could also account for some of these differences in glacier sensitivity between the Collier and South Cascade Glaciers, thus influencing how these simulated fluxes and the resulting ablation gets distributed across the glacier, influencing the resulting average net balance for the glacier. This could possibly explain why both the meteorological and parameter sensitivities are lower for the Collier Glacier when compared to South Cascade Glacier. Thus, questioning the representations of these benchmark glaciers on the mass balance of remote glaciers, since topographic features that surround and encompass the glacier, as well as the microclimates of each glacier are unique and will influence the resulting glacier's mass balance differently. Furthermore, supporting the findings of Oerlemans and Reichert (2000) where the glacier sensitivity depends on the rate of mass turnover, was the fact that the 2010 sensitivity experiments were conducted during a positive mass balance year, where the mass turnover is likely to be

much lower, resulting in the overall lower sensitivity of the Collier Glacier to changes in both the meteorological and parameter inputs in comparison to South Cascade Glacier, where the 2004 sensitivity tests were conducted on a negative balance year (Anslow et al., 2008) (Tables 3.3 and 3.6). The same could also be true if the sensitivity simulations were conducted on a negative balance year for the Collier Glacier.

In addition, the resulting net balances from the sensitivity simulations were plotted against elevation to examine how the model's sensitivity variations in parameter and meteorological inputs influence the net balance curves, similar to the methods used by Oerlemans and Hoogendoorn (1995) (Figures 3.17-3.22). The Collier Glacier's sensitivity to each parameter or variable was reflected by the degree of spread between the control and each secular change. Thus, parameters or meteorological input variables with the highest sensitivity were reflected by larger changes in the net balance curve, and vice versa for parameters or meteorological variables that were least influential in the modeled mass balance, reflecting in a close spread between the control and the secular changes in the parameter or variable. These mass balance gradients for both model parameters and meteorological inputs also reflect their influence on the balance gradients above and below the ELA. Furthermore, these model simulations not only display the influence these parameters

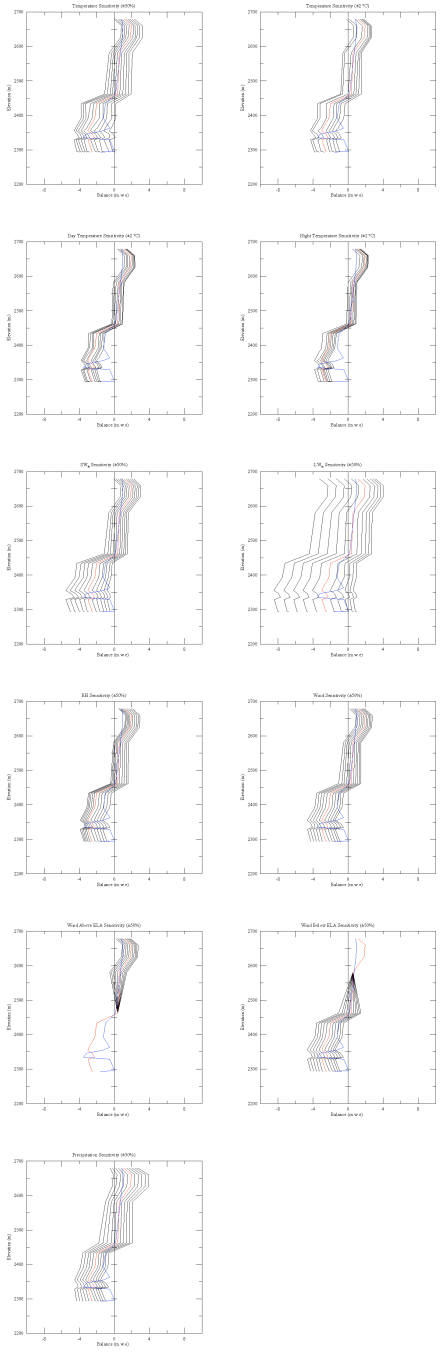

Figure 3.17: 2010 sensitivity as displayed by the mass balance gradients to secular changes in the meteorological inputs for the SEBM using the bulk method.

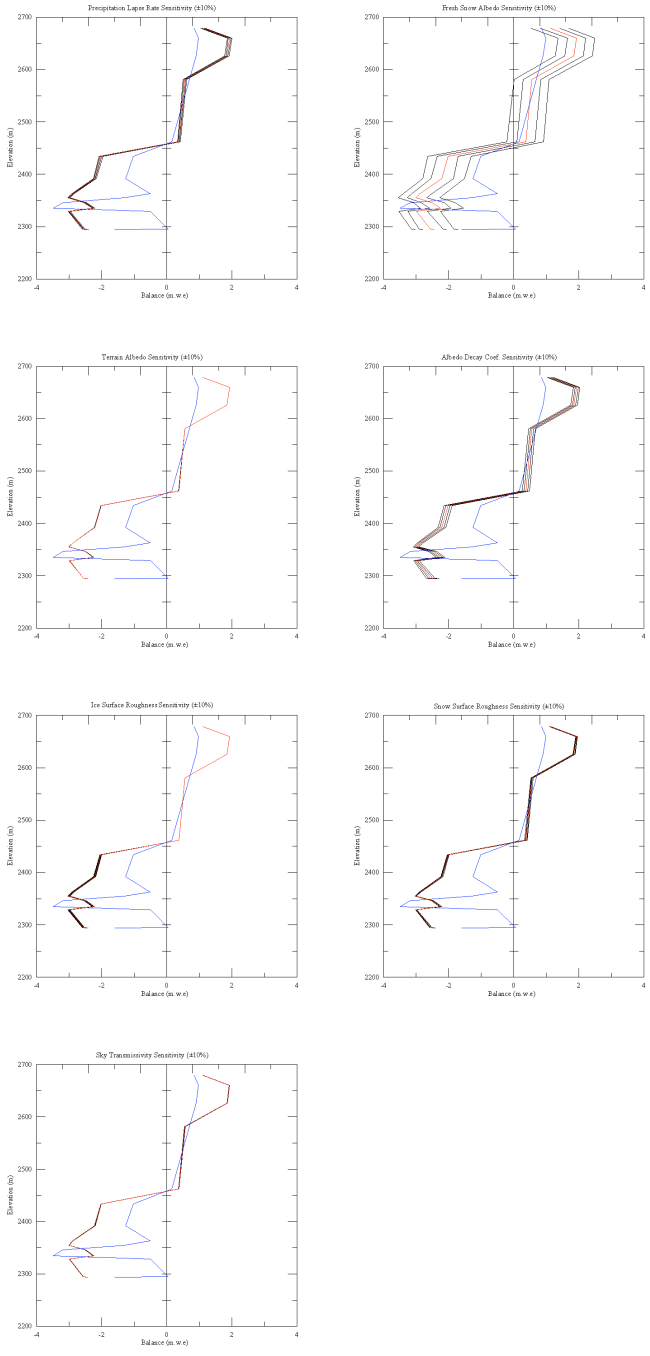

Figure 3.18: 2010 sensitivity as displayed by the mass balance gradients to secular changes in the parameters for the SEBM using the bulk method.

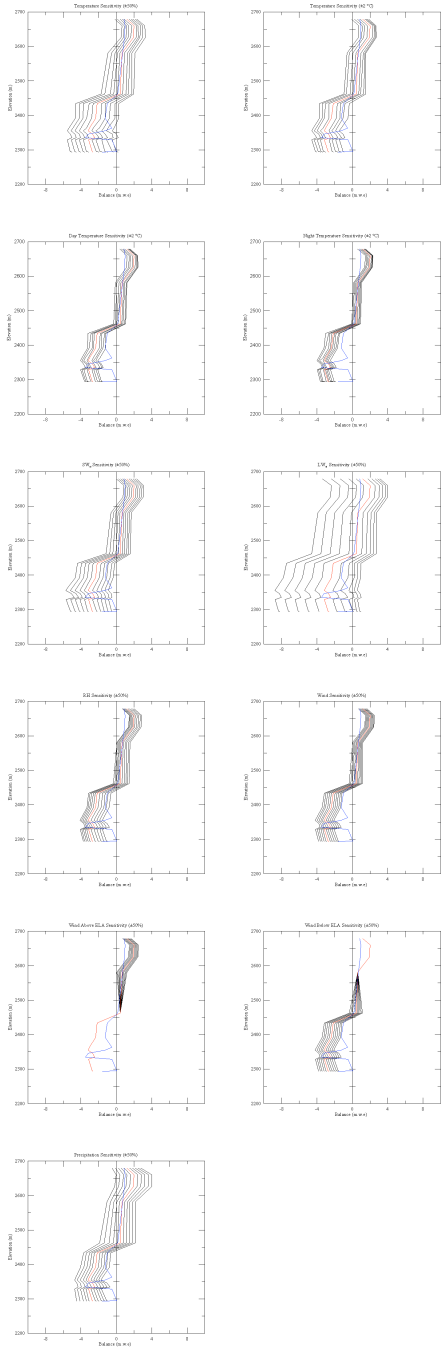

Figure 3.19: 2010 sensitivity as displayed by the mass balance gradients to secular changes in the meteorological inputs for the SEBM using the transfer coefficient method.

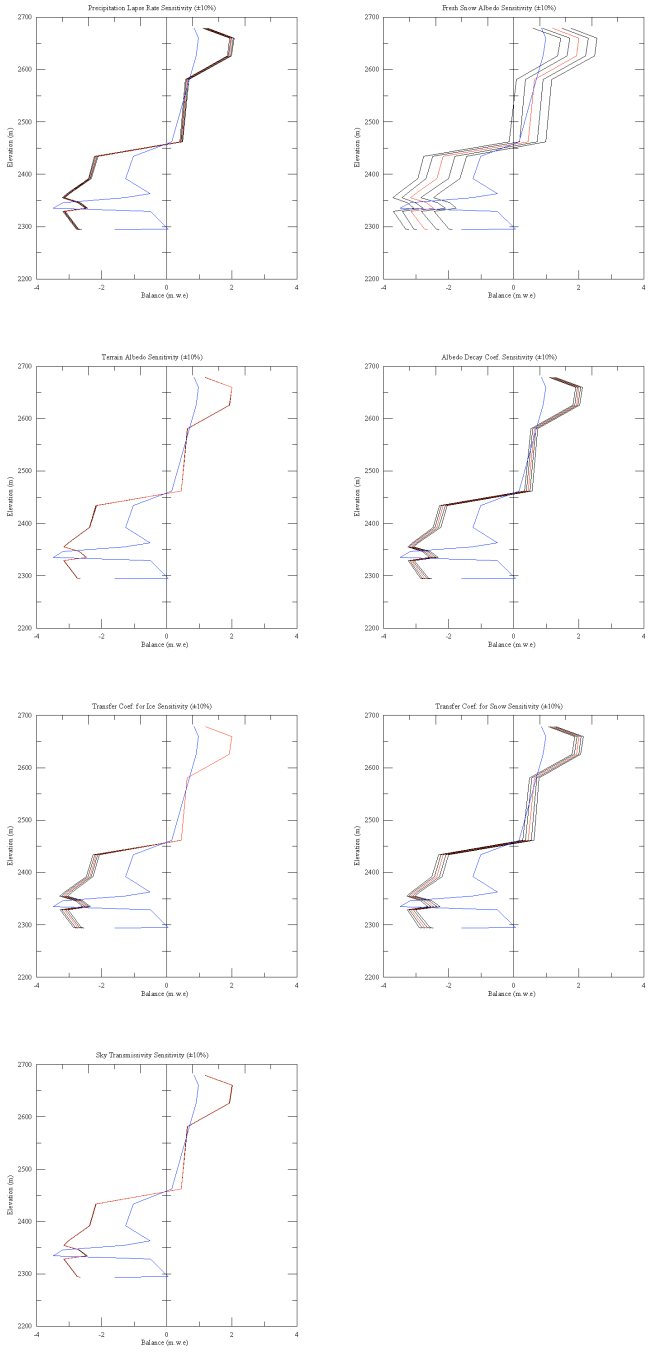

Figure 3.20: 2010 sensitivity as displayed by the mass balance gradients to secular changes in the parameters for the SEBM using the transfer coefficient method.

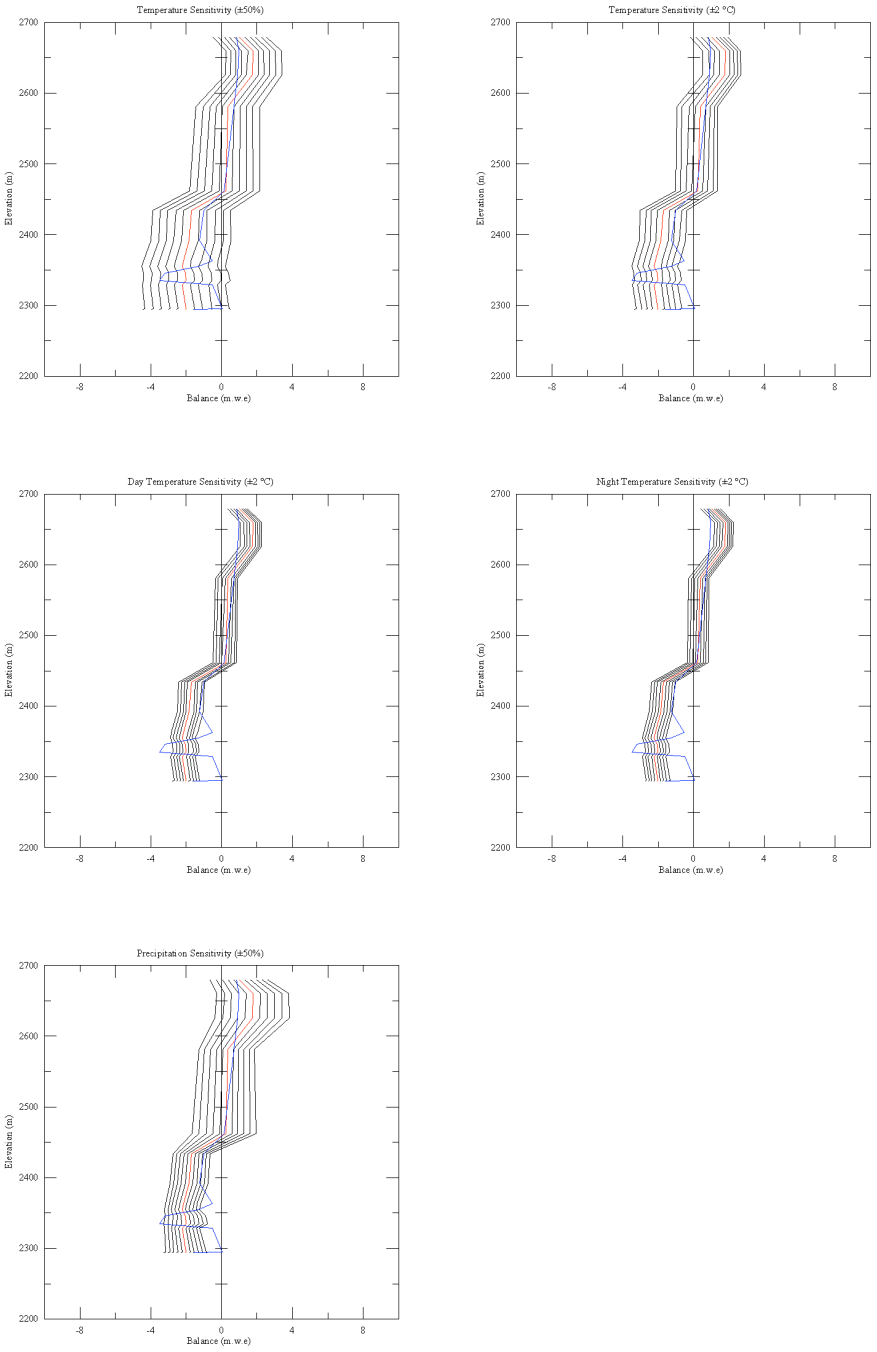

Figure 3.21: 2010 sensitivity as displayed by the mass balance gradients to secular changes in the meteorological inputs for the PDD model.

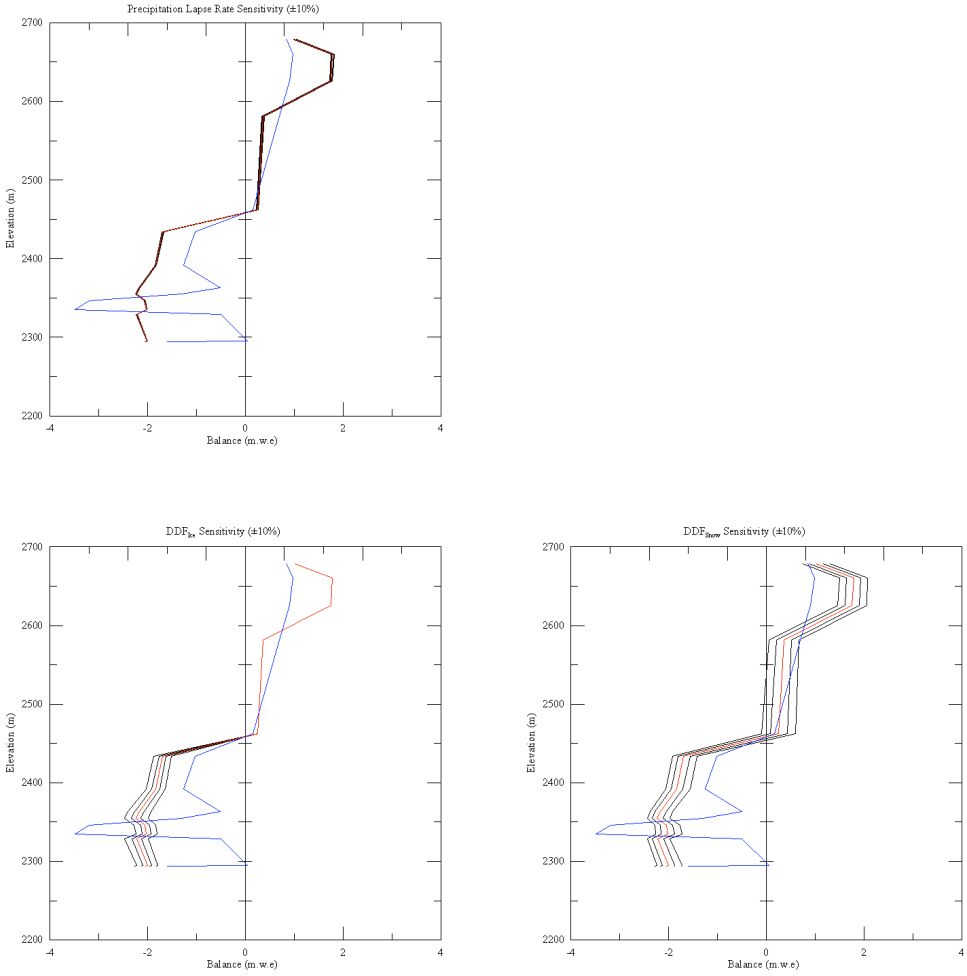

Figure 3.22: 2010 sensitivity as displayed by the mass balance gradients to secular changes in the parameters for the PDD model.

and meteorological variables have on the net balance curve and the balance gradients, but also display the changes in elevation of the ELA. For all model simulations, an increase of 2 °C results in a rise in the ELA to an elevation of around 2600 m, an elevation above the icefall, suggesting that the Collier Glacier's hypsometry and the increased mass flux into the ablation area could result in a rapid response by the glacier, due to the significant mass loss. Coupling these melt models with a glacier flow model may provide further insight into the dynamic response of the Collier Glacier to these sensitivity tests. Such coupling of models would be useful in predicting the glacier's dynamic response to future climate change scenarios. Furthermore, sensitivity simulations from all models suggest that a reduction of precipitation of approximately 40% from the 2010 value would also raise the ELA to an elevation of approximately 2600 m. The temperature sensitivity simulations for all models show similar results, suggesting a 40% increase in temperature from the 2010 values would result in a rise in the ELA to an elevation of approximately 2600 m, which is again located at an elevation above the icefall. Tables 3.3 and 3.6 summarize these sensitivity simulations. These sensitivity experiments from all 2010 model simulations suggest that the Collier Glacier is equally sensitive to changes in both temperature and precipitation. However, as mentioned before, the sensitivity of a particular glacier depends on its mass turnover (Oerlemans and Reichart, 2000). Thus, since 2010 was a positive balance year, the sensitivity of the Collier Glacier to changes in parameter or meteorological input values, may be lower in comparison to other glaciers, or even other balance years on the Collier Glacier due to the positive

mass balance in 2010, thus stressing the importance for continued glacier mass-balance monitoring to compare these sensitivity simulations to negative balance years.

3.4.4 Measured verses Modeled Ablation

Similar to Anslow et al. (2008), the models had a slight tendency to underestimate ablation in the region where there were higher ablation measurements, as evidenced by the least squares fit with a slope less than one, as well a larger degree of variability between the measured and modeled stake balances in the higher ablation regions of the glacier, as indicated in Figure 3.10. Thus, the largest discrepancies between the measured and modeled ablation were all situated in the ablation area. As mentioned earlier, this was primarily a function of the models inability to capture the east-west ablation variability in the ablation across the lower reaches of the glacier. However, the optimized model runs for the 2010-balance year showed good agreement between the measured and modeled ablation for the accumulation area of the glacier, as evidenced by a close agreement with respect to the 1:1 line in Figure 3.10. These results suggest that the processes that govern the ablation of snow in the accumulation area are well represented in the models. However, processes not captured in the model, such as the distribution of snow and debris by wind, avalanches, and mass wasting events across the glacier's ablation area not captured by the models, result in some discrepancies between the measured and modeled ablation,

as mentioned earlier. Observations from field measurements indicated that bare ice became exposed earlier along the eastern margin of the glacier. This transition zone between snow and ice migrated westward over the course of the ablation season, as captured by the ablation stake measurements (Figure 3.23). These photographs in Figure 3.23 suggest that the eastern margin of the glacier experienced a quicker decline in albedo due to its close proximity to North Sister's west face. One explanation could be from fine debris carried by wind deflected off North Sister and distributed toward the western margin of the ablation area, increasing the debris content along the glacier's surface altering the albedo. The model, however, does capture some this east-west variability, due to a net radiation contributions from North Sister as well as shading and slope characteristics throughout the ablation area, as indicated in Figures 3.13 and 3.24, but not to the magnitude recorded by the ablation stakes. Figure 3.24 shows the daily net energy flux as well as the net shortwave flux across the Collier Glacier on a clear day, demonstrating that much of the characteristics in the variability of the daily energy flux across the ablation area are the result of the net shortwave flux contribution to the glacier, thus suggesting that the primary mode for the east west variability in ablation across the lower reaches of the Collier Glacier can be attributed to the net shortwave energy flux. Such variability in the daily net shortwave flux on a clear day could likely be attributed to terrain shielding from surrounding topography as well as slope and aspect characteristics.

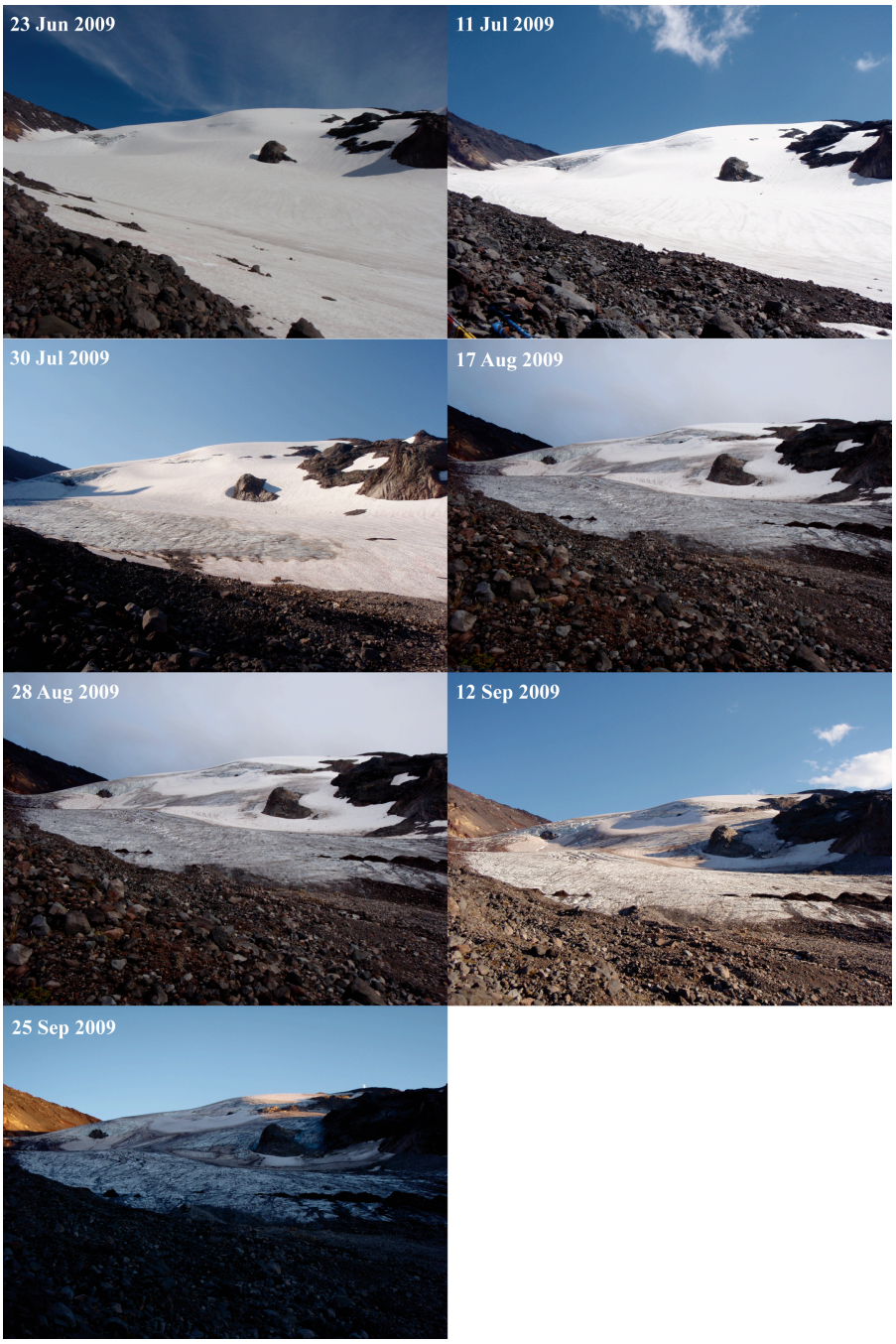

Figure 3.23: 2009 field photographs looking south towards the glacier, documenting the surface changes in the ablation area from June through September.

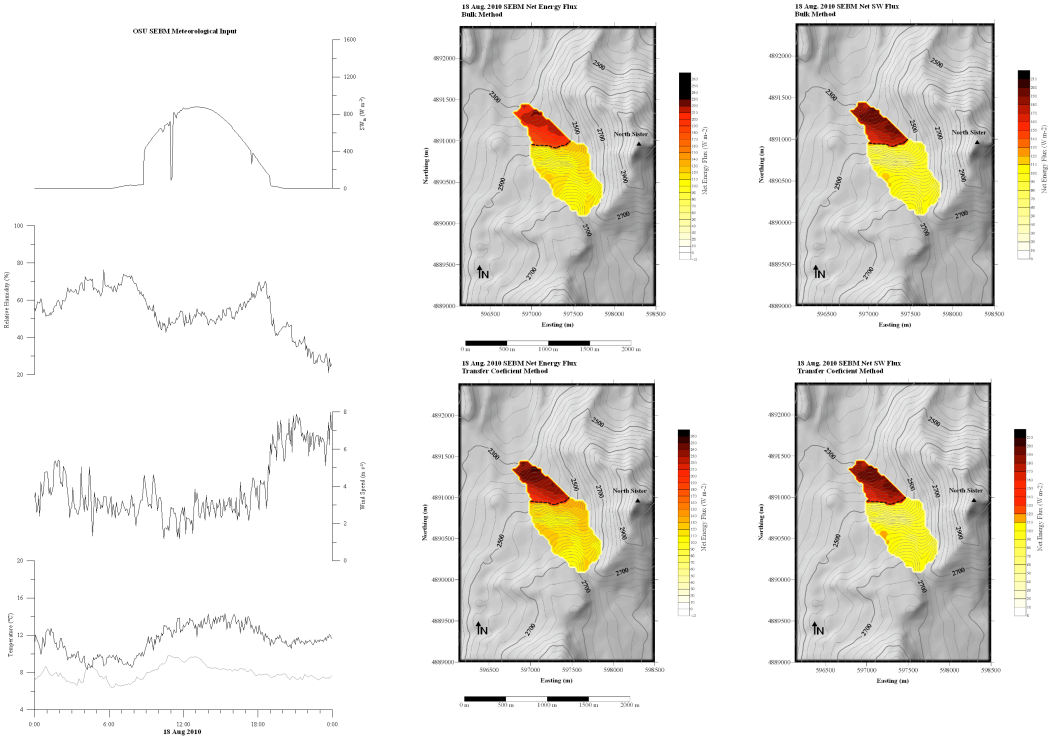

Figure 3.24: Clear day meteorological inputs recorded by the moraine AWS and output maps showing the net energy flux and net shortwave flux for 18 August 2010. These results were supported by field observations taken on that same day.

These results suggest that multiple processes may be involved to create this east-west variability across the Collier Glacier's ablation area. Furthermore, these simulations suggest that this east-west variability could likely be the consequence of surrounding terrain influencing the net radiation budget, and being further amplified by entrained debris being distributed across the glacier, lowering the albedo, with a maximum concentrated along the eastern margin of the glacier. Local wind patterns may also play a role in this east-west variability, where wind gets deflected off North Sister's west face, where it is warmed due to the thermal emission from North Sister's west face, as well as collecting debris, and gets redirected across the ablation area of the glacier. These observations were also noted in Mountain (1978, 1990), where the distribution of debris influenced the eastern margin of the glacier, with low albedo magnitudes situated along this margin. Furthermore, Mountain (1990) found that the ablation zone and the eastern flank emerged as a continuous zone of maximum net radiation these observations are supported by the OSU SEBM as seen in Figure 3.24. The highest shortwave radiation values from Mountain (1990) were estimated for the central portion of the ablation zone where the effects of terrain shielding are minimized, and the surface roughness increases with the adjacent crevasses. These observations are supported from mass-balance measurements in the ablation zone from 1989-2010, where the secondary fluctuations in the net balance curve indicate a maximum near the central portion of the ablation area (Figure 3.2). Furthermore, these observations are also supported by the OSU SEBM output, where maximum ablation were concentrated in the regions along the eastern margin of the glacier, with

the highest net energy values being estimated for the central portion of the ablation area (Figure 3.24). Incoming shortwave radiation measurements collected by the moraine AWS also demonstrated the influence of terrain shielding by North Sister, where it influences the timing of the incoming shortwave radiation during the morning hours, as indicated in Figure 3.24.

Some discrepancies did occur, however, in the accumulation area where there was a period between July and August where significant mass loss were indicated by the mass-balance measurements. Figure 3.8 displays these discrepancies between simulated and observed mass balance, where all models considered in this study consistently underestimated ablation during this period. Temporal changes snow albedo and aerodynamic surface roughness above the ELA, not considered in the models, could explain these discrepancies. Also not captured by any of the models in these simulations was the development of ablation hollows over the course of the ablation season. The development of these ablation hollows could have implications on both the net radiation and turbulent fluxes, influencing albedo and the aerodynamic surface roughness. Such micro topographical changes were observed in the field; however, measurements of these features were not conducted in this study. One possibility to provide better constraints on the development of these ablation hollows could be from direct measurements of the crests and valleys of these features over the course of the ablation season, and integrate those data across the glacier's area to investigate the areal contribution of these micro-topographical features. Another possibility to put better constraints on the timing and magnitude of these

morphological features could be from the implementation of LIDAR on the glacier's surface over the course of the ablation season to attempt to capture these micro topographical changes across the glacier's surface. Such observations, however, were beyond the scope of this particular study. Observations over the 2010 ablation season indicated maximum ablation hollow development from late July until early August, while storms towards the end of August significantly reduced these ablation hollows due to fresh snowfall accumulating in each hollow. These ablation hollows might also form due to debris accumulating on the surface (Rhodes et al., 1987). The processes that develop these ablation hollows may act as a positive feedback mechanism for snow ablation by influencing both the net radiation and turbulent fluxes (Rhodes et al., 1987). Considering the temporal variability of the snow and ice surface could increase model precision and better constrain the processes that govern snow ablation, however these additions could sacrifice model robustness and portability.

The observed variability in the upper reaches of the glacier could also be the result of wind transport of snow. Winter balance measurements of the upper reaches of the Collier Glacier's accumulation area suggest a relatively high degree of variability in how snow accumulates, as indicated in Figure 3.2. One possible explanation could be from high winds in the upper accumulation area blowing snow eastward during the early part of the ablation season. Such wind transport not only reduces the snow depth in these regions, but also changes the snow's grain size, changing the snow's reflective properties and thus altering its albedo, and increasing the net radiation's contribution toward melt energy. Furthermore, this region of the

glacier experienced the least amount of topographic shading throughout the day, also increasing the net radiation's contribution toward energy available for melt, as indicated by Figure 3.24. Such variability in the snow pack in the upper reaches of the Collier Glacier's accumulation area stresses the continuation of winter balance measurements to capture this variability over longer timescales. Furthermore, the 2009-2011 winter balance measurements provide some representation on how snow accumulates on the Collier Glacier. However, these data may not be representative outside of their respective balance year.

Another possible explanation for this variability in the accumulation area could be from englacial melting and refreezing processes not captured by the model. This process consists of surface melt water percolating into the snow, where at a certain depth; the temperature is still below freezing and this melt water refreezes to form layers of superimposed ice (Paterson, 1994). Furthermore, this process of refreezing of melt water into the snow raises the latent heat flux, where one gram of water produces enough latent heat to raise the temperature of 160 grams of snow by one degree (Paterson, 1994). Snow pit studies conducted in the accumulation area throughout the 2010 ablation season observed the development of large ice lenses (~30 mm) at various depths within the snowpack. These ice lenses make the snowpack heterogeneous, making it difficult to make representative density measurements. Observations from snow pits and crevasses indicate that the larger ice lenses were evenly distributed throughout the accumulation area. However, the OSU SEBM does not consider englacial processes. In addition to influencing the

snowpack's energy budget, it is plausible that as the snow ablates over the course of the summer, many of these larger ice lenses become exposed at the surface, altering radiative properties, mainly albedo, of the surface skin of the ablation area, enhancing melt. Compaction of the snowpack may also have an impact on this temporal variability in snow ablation observed in the upper accumulation area. Thus, snow compaction over the course of the ablation season may have had an impact on the accumulation measurements due to the small changes in density of the deepest layers. Such density measurements over the course of the ablation season, especially in July and August where ablation was at a maximum, were not recorded in this particular study.

3.4.5 Snow Initialization Schemes

As mentioned earlier, the OSU SEBM had two ways to initialize the snowpack at the beginning of model runs. The piecewise linear interpolation snow initialization scheme was used for calibration, and sensitivity runs for the 2010 balance year due to the limited amount of winter balance measurements for the Collier Glacier. Furthermore, this initialization scheme captured the seasonal variability of snow distribution across the glacier, since the winter balance measurements, and not a polynomial fit, that initialized the model. For this particular study, at least 12

measurements were conducted up the glacier's centerline providing a good spatial coverage of winter snow accumulation with elevation.

The other initialization scheme utilized a second order polynomial in elevation with coefficients determined through accumulation measurements taken from 2009-2011 winter balance measurements. As mentioned earlier, these accumulation measurements were made into a ratio of the maximum snow accumulation, thus the deepest measurement on the glacier had a value of 1.0 and all other regions are a fraction of this maximum snow depth. These measurements were plotted with elevation and a second-order polynomial in elevation was fit to the accumulation measurements. The coefficients from this polynomial fit determined each individual year's accumulation measurements, as shown in Figure 3.7. This snow initialization was adjusted so the model initialization fit the mass-balance measurements at the beginning of the meteorological record. This method was adequate, providing enough winter accumulation measurements to capture the seasonal variability in snow accumulation across the Collier Glacier.

Comparisons between these two initialization schemes display similar results with regards to the simulated mass balance, where the polynomial snow initialization scheme had a tendency to underestimate ablation for the 2010 simulations and overestimate ablation for the 2009 simulations as summarized in Table 3.4. It is important to note, however, that the lack of mass-balance measurements for the 2009 balance year prevented an average net balance for the glacier, thus comparisons between these two initialization schemes was focused on the 2010 simulations.

Figure 3.25 displays the mass balance maps taken at the end of the model simulations, comparing the distributed mass balance from the 2010 multiple model simulations. These figures display a smoothed distributed mass balance for the polynomial snow initialization scheme in comparison to the piecewise linear interpolation snow initialization scheme. Furthermore, these maps also indicate a slight underestimation of ablation for the polynomial fit. When comparing the net balance time series between the two different initialization schemes, the two methods performed comparably for all the different models, however the polynomial initialization scheme overestimated ablation for the first half of the ablation season. Around September the polynomial initialization scheme started to underestimate ablation in comparison to the piecewise linear interpolation scheme, resulting in an underestimation of average net balance for the ablation season as indicated in Figure 3.26. It is apparent, however, that the polynomial fit smoothed the resulting net balance for the Collier Glacier, where the net balance curves for the various models indicated an underestimation in ablation below the ELA, virtually eliminating the secondary fluctuations in the net balance curves that are characteristic of the Collier Glacier, as indicated in Figure 3.27. These comparisons suggest that that both methods adequately simulate the Collier Glacier's mass balance, however the polynomial fit smoothed the distribution of the snowpack at the beginning of the simulations, eliminating any sort of annual variability associated with snow distribution across the glacier. Thus, for analysis for individual years or if there are a limited amount of

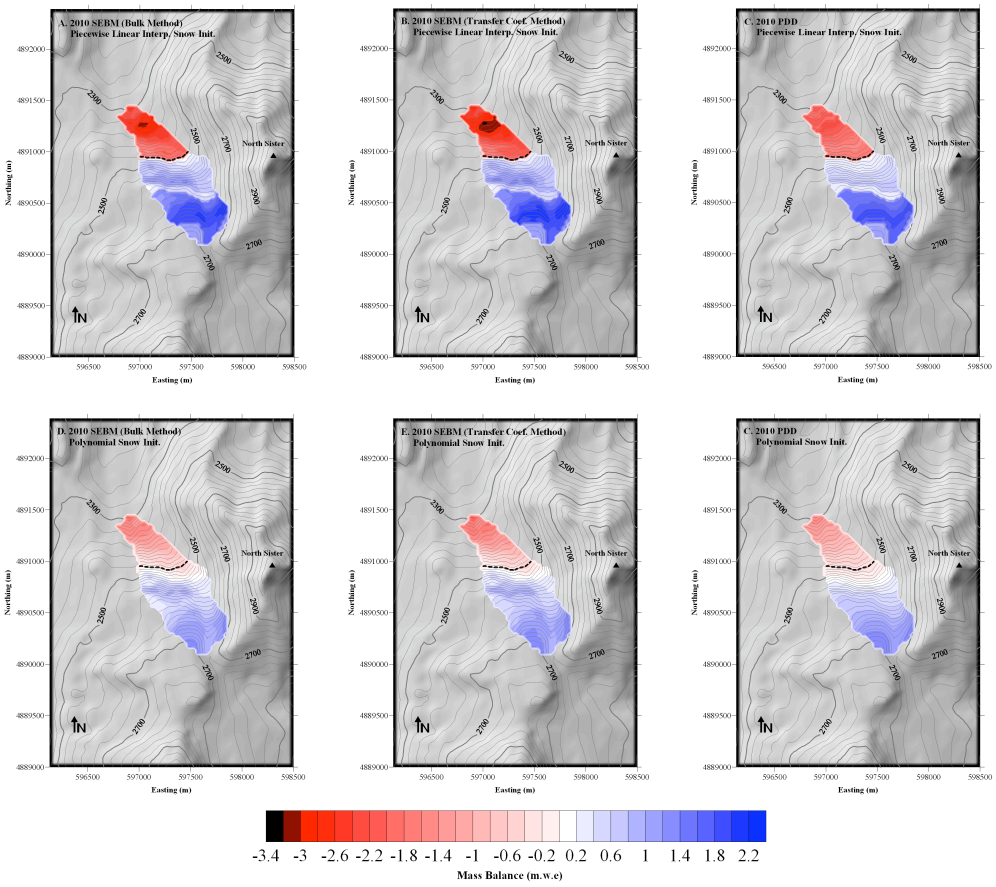

Figure 3.25: 2010 simulated mass balance maps for the Collier Glacier comparing the different snow initialization schemes for all models used in this study. (**A**, **B**, and **C**) Model simulations using the Piecewise-linear interpolation snow initialization scheme. (**D**, **E**, and **F**) Model simulations using the 2nd order polynomial fit of the 2009-2011 May winter-balance measurements.

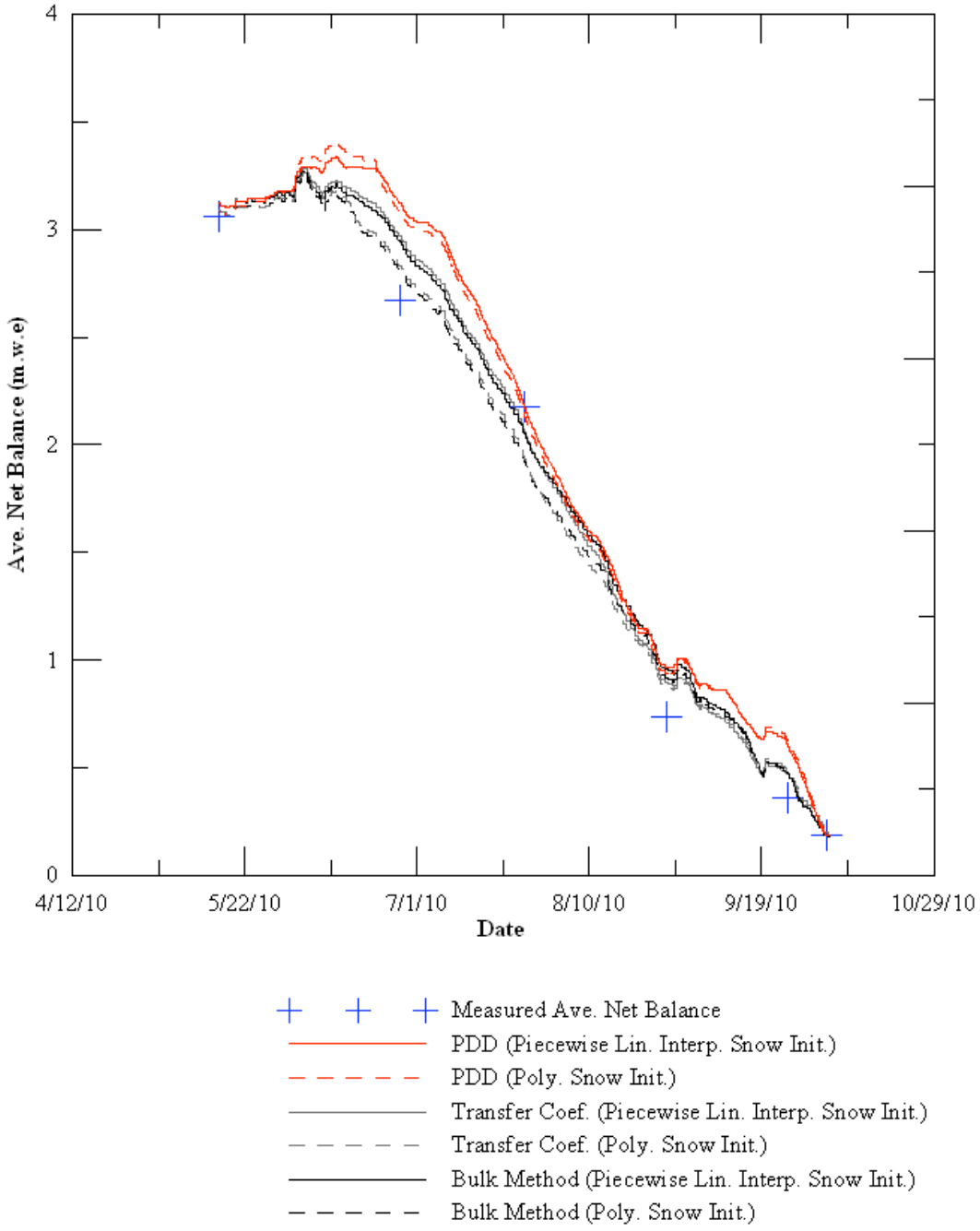

Figure 3.26: 2010 average net balance time series for all models and snow initialization schemes. The solid lines represent the piecewise linear interpolation snow initialization scheme. The dashed lines represent the polynomial snow initialization scheme.

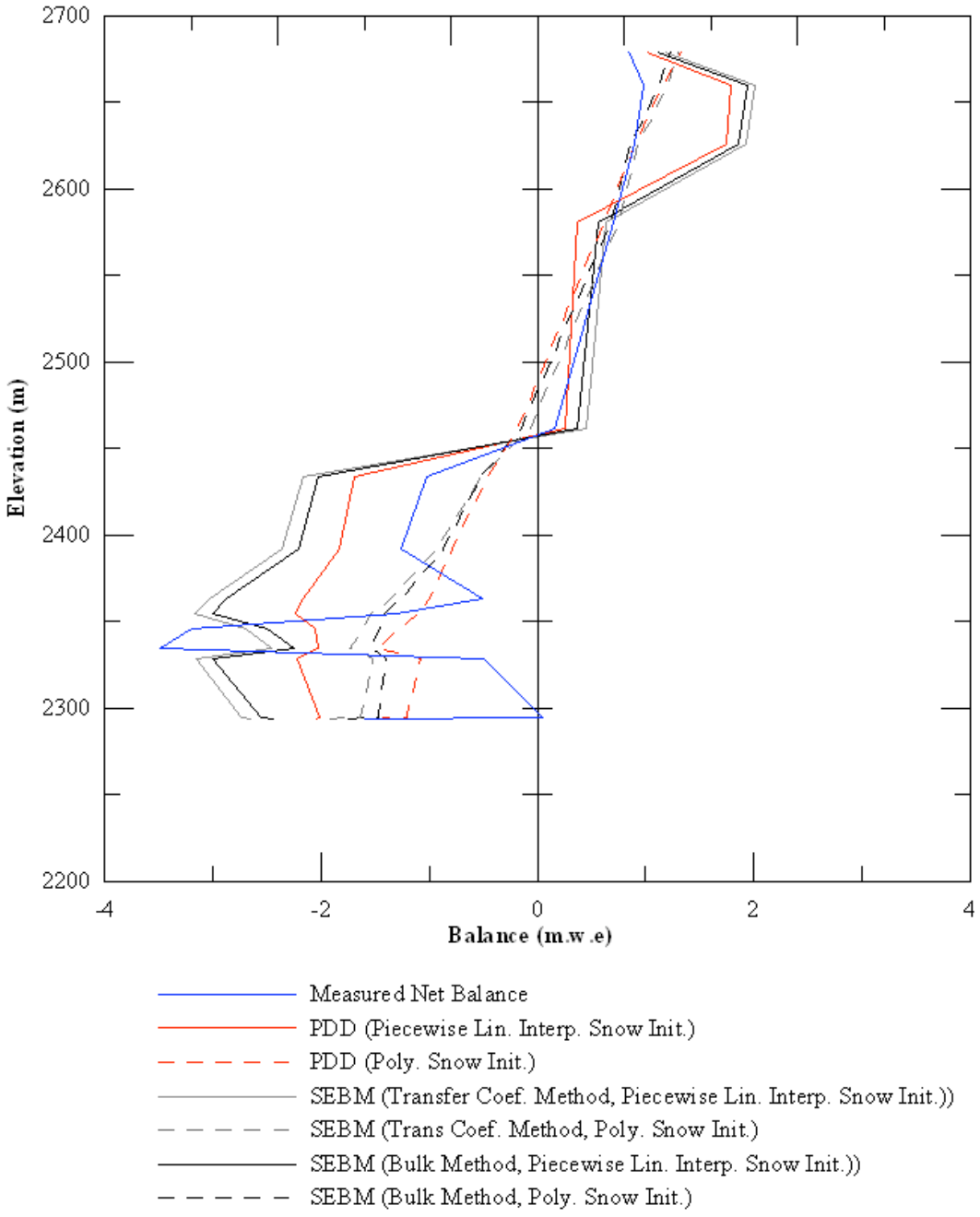

Figure 3.27: 2010 average net balance time series for all models and snow initialization schemes. The solid lines represent the piecewise linear interpolation snow initialization scheme. The dashed lines represent the polynomial snow initialization scheme.

winter balance measurements, the piecewise linear interpolation snow initialization scheme would be a stronger choice since it is able to better capture the seasonal variability in snowpack across the glacier, which reflects in the resulting average net balance at the end of the ablation season.

3.4.6 McKenzie SNOTEL

The ability of the PDD model to simulate the Collier Glacier's mass balance opens the possibility to simulate mass balance from distant weather stations, since temperature is the only required meteorological input. Near the Collier Glacier is the McKenzie SNOTEL station (Figure 3.1), which shares a similar aspect and geographic location with respect to the Collier Glacier. Comparisons between hourly temperature data from the Moraine AWS (2296 m) and McKenzie SNOTEL (1454 m) indicates some agreement with the two stations however a large degree of variability does exists between the two stations as indicated in Figure 3.28. Temperature lapse rates between the Moraine AWS and McKenzie SNOTEL suggest frequent temperature inversions during clear sky days between the two stations, displayed in Figure 3.29 with lapse rates that exceed 0 ºC m^{-1}. Furthermore, the periods of highest ablation occurred during these inversions between the two stations, where temperatures were higher up on the glacier than down at McKenzie SNOTEL station. These frequent temperature

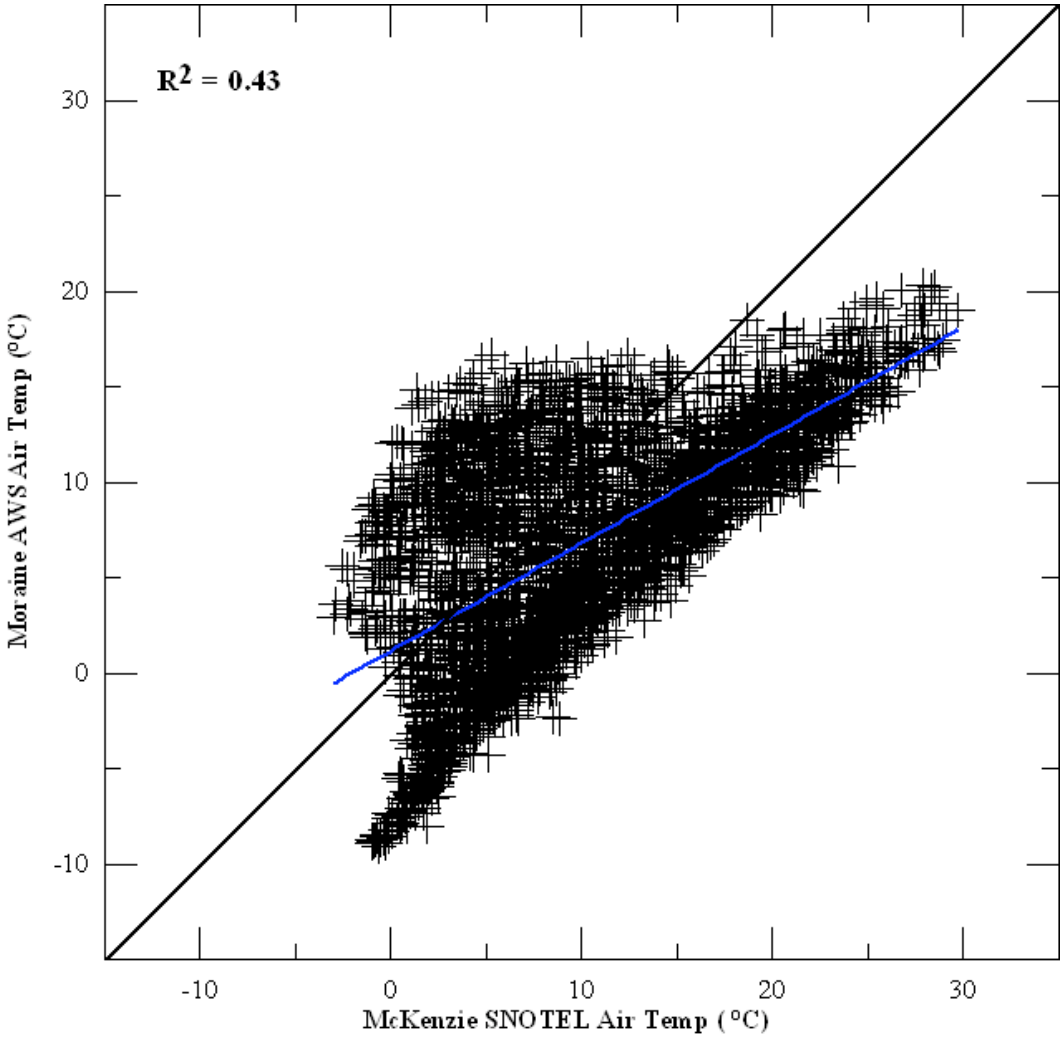

Figure 3.28: Linear regression between the Moraine AWS and McKenzie SNOTEL air temperature. The blue line indicates the least squares fit between the two stations, and the coefficient of determination (R^2) is indicated in the upper left corner. The thick black line is the 1:1 line.

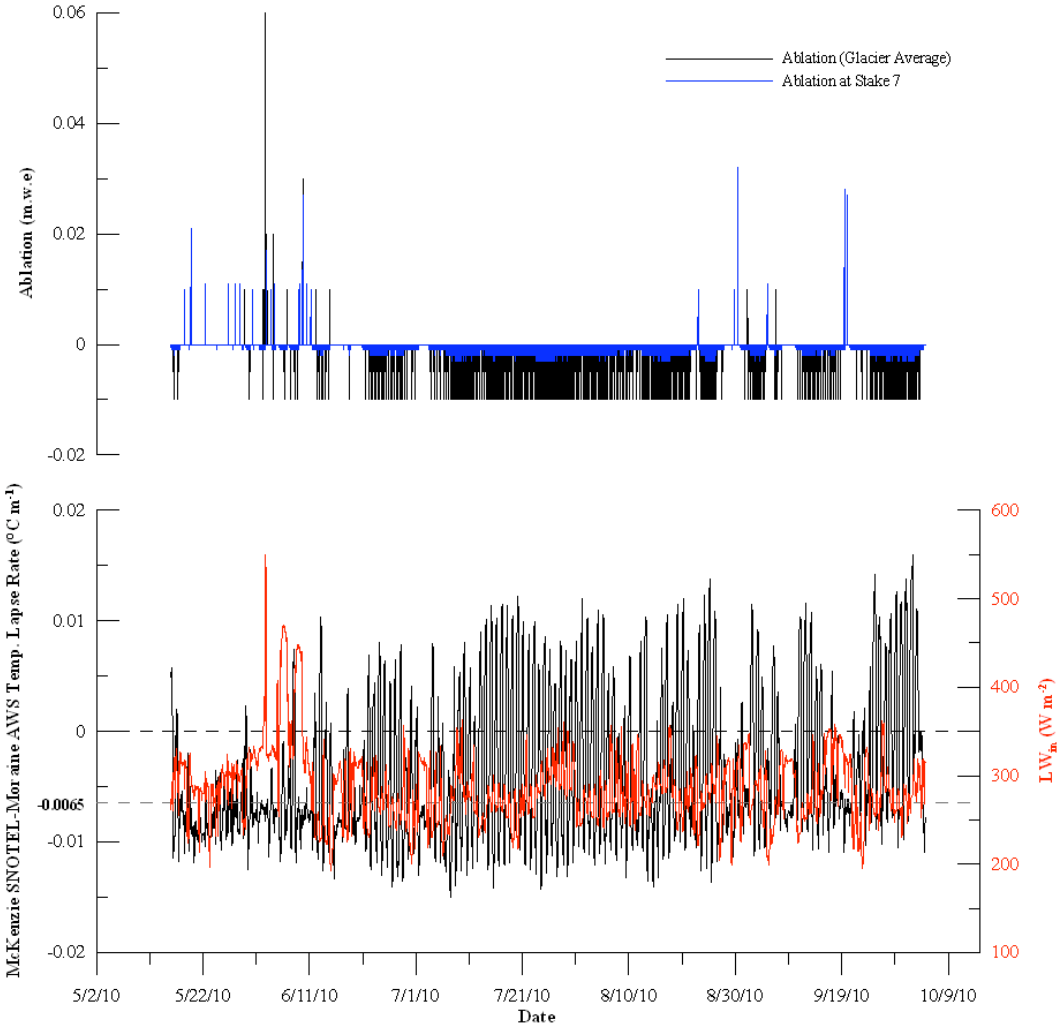

Figure 3.29: Temperature lapse rate variations between the Moraine AWS and McKenzie SNOTEL. The upper plot displays glacier averaged ablation (black) as well as ablation at a representative stake location (blue). The lower plot displays temperature lapse rate (black) and incoming longwave radiation (red) as a means to determine clear sky conditions.

inversions between the two stations indicate a potential problem with using distant weather stations, such as McKenzie SNOTEL station, to drive the PDD model due to the difficulty of determining an appropriate temperature lapse rate between the station and the glacier. Further investigating these changes in temperature lapse rate between the two stations, indicates a diurnal cycle to these inversions (Figure 3.30). One simple approach would be to average the temperature lapse rates between the Moraine AWS and the McKenzie SNOTEL station, and use a fixed temperature lapse rate to determine positive degree-days up on the glacier. Using a fixed temperature lapse rate of -0.004 ºC m^{-1}, temperature data from the McKenzie SNOTEL was able to simulate the Collier Glacier's mass balance, as indicated in Figures 3.31 and 3.32. Table 3.7 summarizes the results from this experiment and compares them with the various PDD simulations driven by the Moraine AWS. When comparing this experiment with the optimized PDD simulations from the Moraine AWS, it is evident that the McKenzie SNOTEL air temperature has a tendency to overestimate the 2010 average net balance. Nevertheless, these simulations display similar results since the main driver in the PDD model is the accumulation of positive degree days, in which the primary forcing is coming from the daytime hours, when these temperature inversions are less frequent and air temperatures on the glacier during the 2010 ablation season rarely dropped below freezing, as indicated in Figure 3.30. Nevertheless, these results are limited to just the 2010 ablation season where an average lapse rate between the Moraine AWS and the McKenzie SNOTEL station can be established. These frequent inversions

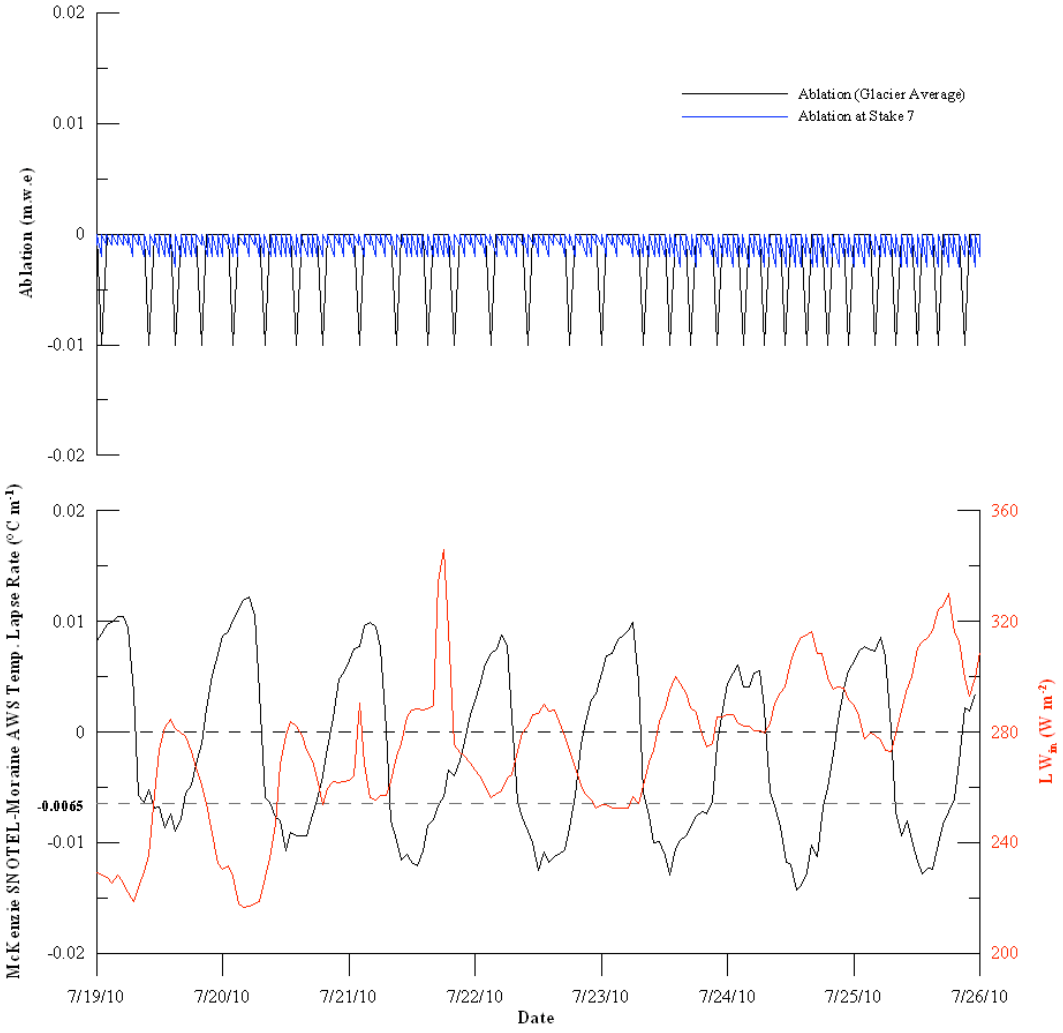

Figure 3.30: Temperature lapse rate variations between the Moraine AWS and McKenzie SNOTEL from 19 July to 26 July 2010.

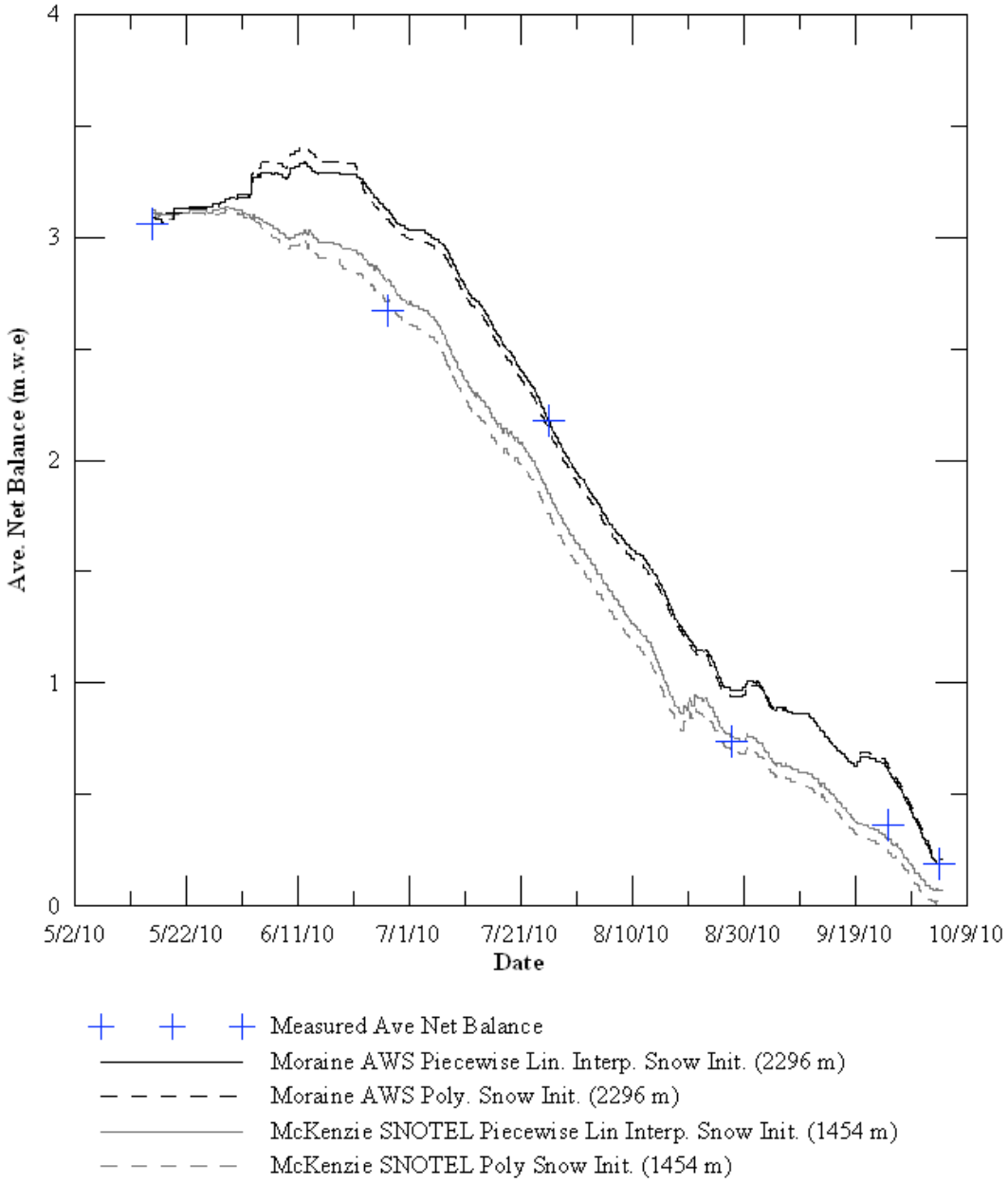

Figure 3.31: Collier Glacier average net balance time series comparisons with the PDD model using air temperature from the Moraine AWS and McKenzie SNOTEL using a fixed temperature lapse rate.

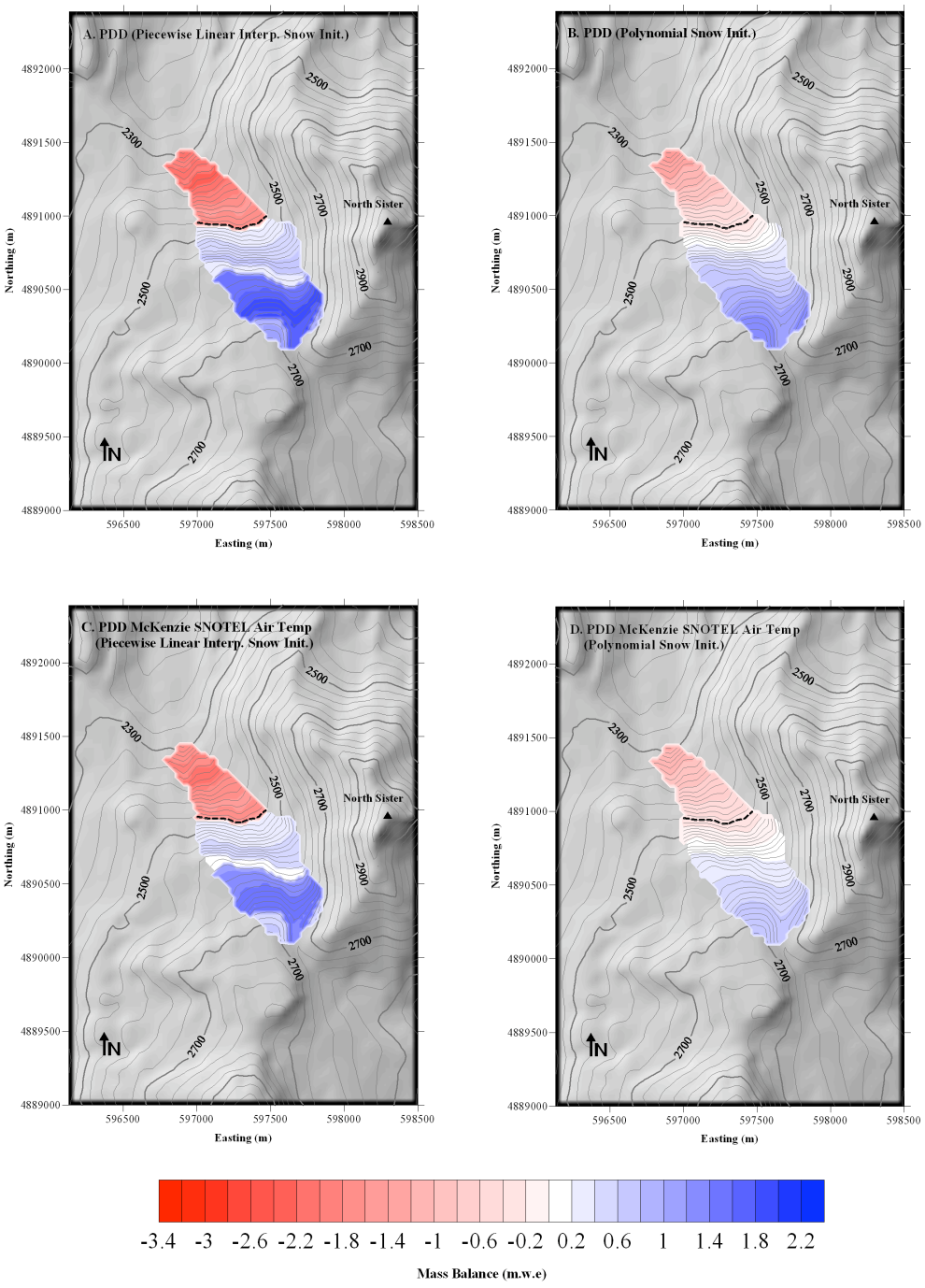

Figure 3.32: Mass balance maps at the end of the 2010 simulations comparing simulated mass balance from temperature data from the Moraine AWS and McKenzie SNOTEL using a fixed temperature lapse rate.

Table 3.7: PDD model performance comparisons between temperature data from the Moraine AWS and McKenzie SNOTEL.

2009				2010			
Station	**Model Type**	**Simulated Ave. Net Balance (m.w.e)**	**Measured vs. Modeled Stake Coef. Of Det. (R2)**	**Station**	**Model Type**	**Simulated Ave. Net Balance (m.w.e)**	**Measured vs. Modeled Stake Coef. Of Det. (R2)**
Moraine AWS (2296 m)	PDD (Piecewise Linear Interp. Snow Init.)	-1.07	0.82	Moraine AWS (2296 m)	PDD (Piecewise Linear Interp. Snow Init.)	0.19	0.82
Moraine AWS (2296 m)	PDD (Polynomial Snow Init.)	-1.09	0.81	Moraine AWS (2296 m)	PDD (Polynomial Snow Init.)	0.21	0.81
McKenzie SNOTEL (1454 m)	PDD (Piecewise Linear Interp. Snow Init.)	-	0.82	McKenzie SNOTEL (1454 m)	PDD (Piecewise Linear Interp. Snow Init.)	0.07	0.82
McKenzie SNOTEL (1454 m)	PDD (Polynomial Snow Init.)	-1.05	0.79	McKenzie SNOTEL (1454 m)	PDD (Polynomial Snow Init.)	0.01	0.79

during the ablation season prevents any sort of time varying temperature lapse rate relationships between the McKenzie SNOTEL and the Collier Glacier, limiting any sort of use of this station to simulate past mass balance of the Collier Glacier, since these temperature relationships are not documented beyond the 2009 and 2010 simulations. Longer, and more continuous temperature records from the Moraine AWS may provide further insights into the diurnal and seasonal temperature lapse rate changes between these two stations, however, this localized phenomena limits the representation of this station and its ability to simulate mass balance over larger areas.

3.4.7 Uncertainties

As with Anslow et al. (2008) the difference between simulated and observed ablation may likely be attributed to the limitations of modeled wind speed and/or humidity, resulting in uncertainties in the calculation of the turbulent heat fluxes. Wind speeds are not adjusted when distributed across the glacier, while relative humidity is adjusted on the basis of variations in saturation vapor pressure with altitude. It is likely, from observations, that the wind speeds are not consistent across the glacier, thus stressing the need for wind speed measurements at both the top and the bottom of the glacier. However, sensitivity tests with perturbations in the wind speed above and below the ELA shows no pronounced effect on the glacier's net balance with both the bulk method and the transfer coefficient method. Nevertheless,

these sensitivity tests suggest that the bulk method is slightly more sensitive to changes in wind speed when compared to the transfer coefficient method (Table 3.6).

As mentioned earlier, the model's use of the Monin-Obukhov (MO) theory, on which the bulk method is based off of for the calculation the turbulent heat fluxes, lends itself to some uncertainties in the presence of the wind speed maximum. Studies suggest there is evidence that the stability correction has to be limited because otherwise the turbulent fluxes are underestimated in the case of a well-developed glacier wind (Van den Broeke et al., 2005; Oerlemans, 2010). This could be one of the differences between South Cascade Glacier and Collier Glacier, where the Collier Glacier has a well-developed glacier wind system (Figure 3.24). Anslow et al. (2008) observed that the South Cascade Glacier did not demonstrate a persistent katabatic flow with a low-level jet, as opposed to the Collier Glacier, where there was a distinct diurnal wind pattern. These different wind regimes may explain the differences in the optimized values for the aerodynamic surface roughness for snow and ice between the Collier Glacier and South Cascade Glacier. Another difference that could have resulted in these different parameter values between Anslow et al. (2008) and this particular study was the location of the anemometers that record wind speed. These different locations may reflect different wind speeds locally, thus influencing the treatment of the turbulent heat fluxes and their associated parameter values. Combined with the shape and orientation of the surrounding topography and frontal systems, these representative locations may reflect wind speed in that locality, which may not be consistent over the entire glacier's area. Furthermore, these differences in

location, coupled with different valley/slope wind regimes, could contribute to different values for the aerodynamic surface roughness for snow and ice between this particular study and Anslow et al. (2008) (Table 3.3). As mentioned earlier, Oerlemans (2010) described that assumptions made with the MO similarity theory, on which the bulk method is based, are not valid in the prescience of wind speed maximum. Denby and Greuell (2000), however, found that the bulk method has been found to give good results when the measurement level is below the wind speed maximum. Multiple wind measurements at different heights and in different locations may provide some insights on the location of the wind speed maximum on the Collier Glacier and provide estimation on the most representative measurement height and location for wind speed. However, limited knowledge of the wind stratification from the surface of the glacier is not well understood on the Collier Glacier, leaving uncertainties in the usage of the bulk method for solving the turbulent fluxes. Another solution to test the validity of the bulk method could be to implement direct turbulent flux measurements via eddy correlation methods (Munro, 1989). However, the sensitive instrumentation necessary for these measurements requires constant monitoring by a field team to prevent any damage to the sonic anemometers. The complexity of using such methods to calculate turbulent fluxes only increases the logistical difficulties in the field. Furthermore, the similarities between the OSU SEBM calculating the turbulent fluxes by the Bulk Method and the Transfer Coefficient Methods suggests that both of these methods were considered practical for this particular study.

Another area of uncertainty of the implementation of the MO theory is the ability of a distant weather station to provide reasonable meteorological data to drive the OSU SEBM. This method would most likely underestimate the turbulent fluxes if wind data were collected from a distant weather station (Oerlemans, 2010). This poses an issue of the robustness of this model in simulating mass balance over larger regions where it is unlikely to have wind speed measurements on each glacier. Thus, extrapolating meteorological data to other glaciers might generate errors and thus questioning the validity of the simulated mass balance. Similar issues may arise with the use of regional climate model output to drive the OSU SEBM, due to the uncertainties associated with the representation of the wind field across a particular glacier with limited to no observations. Such small-scale features in the microclimates of these glaciers are often beyond the resolution of these regional models. Furthermore, there are limited data with how the microclimates of glaciers in the Oregon Cascade Range have changed, further exposing uncertainties with the implementation of the OSU SEBM for paleoclimatology applications. Using a temperature index model might be a better solution to ignore any bias created by the microclimates of each individual glacier of study, as many of these microclimate features are represented in the degree-day factors for snow and ice. Furthermore, temperature is also one of the most readily available data quantities, as well as being relatively easy to extrapolate and forecast.

This study did not include a tipping bucket to measure precipitation at the Moraine AWS, thus the fluxes associated with falling rain were lapsed up from the

nearest SNOTEL station using Equation 27, where linear regressions with McKenzie SNOTEL station and winter balance measurements set constraints for the precipitation lapse rates. In addition, the reliability of a tipping bucket on a glacier is questionable due to frequent freezing temperatures and debris that could hinder the tipping mechanism, jeopardizing the validity of the precipitation data. Nevertheless, the heat flux associated with falling rain was minimal in comparison to the net radiation and turbulent heat fluxes, as indicated by Figures 3.14 and 3.15. These figures suggest that the heat flux associated with falling rain are minute in comparison to the net radiation and turbulent fluxes, thus it is not as influential in the resulting mass balance. However, snowfall during the ablation season has implications on the simulated mass balance, by influencing the albedo. Thus, if a precipitation event happened and the temperature was below the prescribed threshold of 1.0 °C, then snow would fall on the glacier thus changing the albedo back to the fresh snow albedo value of 0.81. Snowfall events did occur during the 2010 ablation season in June and later in August and September. These events were noted during field observations, however these snowfall events did not contribute to the measured mass balance. These observed snowfall events did, however, coincide with the simulated snowfall events, supporting the precipitation records from the nearby SNOTEL station. Such events are evident in the model simulations, which are noted by positive spikes in the average net balance time series (Figure 3.8).

Since the net shortwave flux is one of the most influential contributors towards melt energy on an ablating glacier's surface, it is obvious that the changes in albedo

becomes an important aspect in the net radiation flux. Since there are significant feedback mechanisms associated with the changing albedo on a glacier's surface, the performance of an energy-balance model in simulating glacier mass balance depends largely on the way albedo is treated. Thus, a robust mass-balance model designed to study the response to climate change must generate albedo internally (Oerlemans, 1992). There are a lot of factors that control the changes in albedo on a melting glacier's surface. Some of these factors might include the aging and the associated grain size morphology of snow, debris from surrounding topography distributed by gravity and local wind patterns, and surface-melt water. Many of these factors, however, cannot be completely explained in the albedo submodel. As mentioned earlier, one aspect in particular is the distribution of debris across the surface of the glacier, which according to observations appears to be a major contributor to the east-west variability of ablation in the ablation area (Figure 3.23). Another factor that is uncertain with the albedo parameterization are the temporal changes in albedo over the course of the ablation season. Field observations from the 2008-2009 and 2009-2010 balance years suggest that albedo, primarily in the ablation area, changes dramatically from the beginning to the end of the ablation season. Model simulations indicate an ice albedo as low as 0.13 along the eastern margin of the glacier. However, no albedo measurements were conducted in this study, thus there are no field observations to support the albedo submodel output. Thus, the albedo of fresh snow and the albedo decay coefficient were parameterized and adjusted during the calibration process to achieve the best possible fit between the measured and modeled ablation. The

agreement between the measured and the modeled ablation indicates that there is some agreement between the modeled albedo and the real-life changes in albedo. Furthermore, the modeled albedo values also seem reasonable, considering the degree of uncertainty in parameterizing albedo variations across a melting glacier. Thus, the albedo submodel used in the OSU SEBM appeared to be a robust approach to modeling the albedo variations over the course of the ablation season. Calibrating the model to observed albedo measurements from a total radiometer may increase the precision of the model, but this would come at the expense of model robustness and increase the amount of equipment up on the glacier. Furthermore, there maybe a large degree of uncertainty associated with direct albedo measurements due to the tilting and the changing orientation of an AWS over a melting surface. Diurnal morphological changes throughout the ablation area of the Collier Glacier may also explain some of the discrepancies between the modeled and measured net balances. Field observations from this particular study, as well as Mountain (1990), noted that early in the morning the exposed ice in the ablation zone had little to no surface melt water. However, by the afternoon hours, substantial melt water flows throughout the ablation zone, resulting in the development of irregular rills, channels, and depressions. Supporting Mountain (1990), these surface features in the ablation zone result in significant surface lowering, as observed from the ablation stake measurements. Furthermore, such features formed around some of the ablation stakes, possibly altering the surface lowering readings. In addition, water and sediment also accumulated around many of the ablation stakes, possibly enhancing ablation locally

around the stakes and altering the surface lowering measurements. Mountain (1978, 1990) observed overall low values in measured albedo across the glacier. Mountain (1990) determined that virtually the entire glacier had a reflectivity of less than 50%, and the maximum measured albedo (slightly in excess of 62%) for any point on the glacier as observed high in the accumulation zone. Mountain (1990) also observed that the albedo along the eastern margin of the glacier was low due to the debris from North Sister, supporting field observations conducted during the 2009 and 2010 ablation seasons. These deposits may have influenced the eastern margin of the glacier, with low albedo magnitudes situated along this margin. Field observations during the early portions of the 2009 and 2010 ablation seasons saw a significant contribution of debris from avalanching snow off North Sister's west face. However, the danger of rock fall and avalanches from North Sister's west face prevent measurements along the eastern margin of the glacier. Further parameterization of albedo, however, could complicate the model jeopardizing its robustness and portability. However, albedo measurements from total net radiometers, such as the Kipp and Zonen CNR 4, which measures both incoming and outgoing short and long wave radiation, could be beneficial in calibrating and validating the albedo submodel. However, measurement and parameterization of albedo variations across an ablating glacier requires special care that the radiometer is level, and that the measurement times are consistent and conducted around peak daily insolation. Having such devices on an AWS equipped with self-leveling devices could eliminate the uncertainties associated with the tilting of net radiometers over an ablating surface.

Another area of uncertainty with the OSU SEBM is associated with the changes in seasonality (e.g. the transition from the end of the ablation season to the start of the accumulation season). October, often thought as the end of the ablation season, can have large degrees of variability in the regional climate of the Oregon Cascade Range. Increasing precipitation, as a result of the shift in the Aleutian Low Pressure System, brings in more precipitation. However, precipitation does not always fall as snow on the glacier, due to warmer temperatures, and as a result, rain on snow events may persist at higher elevations, strongly affecting the snowpack by enhancing the turbulent fluxes, thus contributing to melt energy (Marks et al., 1998). Marks et al. (1998) investigated on such events on multiple research sites throughout the Oregon Cascade Range, suggesting that rain on snow events can have devastating ramifications to the snowpack, due to situations where a mixture of warm temperatures, high vapor pressure, and wind result in enhanced turbulent fluxes contributing to melt energy. Averaged energy balance fluxes from this study indicated that the contribution from the turbulent heat fluxes increases towards the later half of the ablation season (Figure 3.16). As the shoulder seasons become more variable, it is conceivable that the turbulent heat flux, amplified by rain on snow events, could contribute to melt well past early October and even into the accumulation season, thus extending the ablation season.

Another area of uncertainty associated with the changes in seasonality is determining the maximum accumulation to initiate the model. Winter balance measurements on the Collier Glacier suggest that the maximum snow accumulation

happens early to mid May. Late spring storms in the Cascade Range often bring precipitation that falls as snow at the higher elevations. Early in the ablation season, around June, when temperatures are beginning to warm, precipitation may still fall as snow up high on the glacier, while rain my occur down low, further complicating the magnitude and timing of the glacier's maximum accumulation. Thus, the field constraints on the timing of maximum accumulation and ablation for a given balance year is still highly variable and uncertain, creating uncertainties in the initialization and accompanying termination of the model for a given balance year. These uncertainties associated with the timing of the maximum accumulation and ablation further stresses the need for regular mass-balance measurements, as determined through the 2010 winter balance measurements conducted on the Collier Glacier. In addition, setting up the moraine AWS to continuously collect meteorological data year-round may further alleviate these uncertainties, as well as providing any insights on the surface energy balance during the accumulation season. Further development of regression models from nearby SNOTEL stations may also aid in the uncertainty in the timing of the accumulation and ablation season, especially when coupled with routine field measurements.

Other areas of uncertainty associated with the OSU SEBM lie in modeling snow distribution in complex alpine terrain, where it is difficult to quantify modes of variability associated with snow distribution by wind and avalanches. Both processes exist on the Collier Glacier, where snow avalanches are common early in the ablation season from North Sister's west face and wind events, which both have a tendency to

transport both snow and debris, thus influencing the net shortwave radiation flux. Further parameterization may increase model accuracy, however, this would jeopardize the robustness of the model from one glacier to another, as well as increase the computation times for model runs. Furthermore, many of these processes might be insignificant in comparison to the major processes that govern the Collier Glacier's mass balance captured by the SEBM.

3.4.8 Future Work

The 2008-2010 energy balance studies on the Collier Glacier prove the robustness and portability of the OSU SEBM. However, there are some aspects to the model that could be improved to potentially increase its precision. One way to potentially increase the OSU SEBM's precision would be the addition of more meteorological sensors, thus increasing the spatial coverage of meteorological inputs for the model. Albedo measurements on the surface of the glacier may help calibrate and test the validity of the albedo submodel, and perhaps increase the model's capability to better capture the spatial and temporal variability in albedo. Sensors such as the Kipp and Zonen CNR 4 total net radiometer might be a beneficial addition, since it records both incoming and outgoing short and longwave radiation. Furthermore, albedo measurements may also provide insights as to the mechanisms that control the east-west variability in ablation across the Collier Glacier's ablation

zone as well as investigating the temporal changes in albedo over the course of the ablation season. Such instrumentation would be beneficial both above and below the ELA to not only constrain the albedo variability above and below the ELA but also provide better calibration as to how the radiation fluxes are being distributed across the glacier.

Other instrumentation that may help increase the precision of the model may include barometric pressure to help put better constraints on vapor pressure, which could be influential in the turbulent flux calculations. A barometric pressure sensor could also be important for understanding the atmospheric processes in the region and their contribution towards the microclimate of the Collier Glacier. Another set of measurements that could improve the turbulent flux calculations would be to establish a wind profile for the glacier. This could constrain the optimal measurement heights for the anemometers, minimizing the uncertainties associated with the turbulent flux calculations. Also, an additional anemometer located at the top of the glacier may also provide insights on the variability of wind speed from the top of the glacier to its terminus. These data could be beneficial in how the turbulent flux calculations are distributed across the glacier. Furthermore, the addition of directly measuring turbulence via eddy correlation methods could also prove useful to compare the performance of how the OSU SEBM calculates turbulent heat fluxes. However, the uses of sonic anemometers necessary to conduct the eddy correlation methods are quite fragile and would require constant monitoring by a field technician.

For the 2008-2010 energy balance studies on the Collier Glacier, attention was only drawn to the measurement of the meteorological data that affects net radiation and turbulent fluxes. Further investigations into the other energy fluxes may also improve the model's precision. For instance, the conduction into the snowpack may be better-constrained using soil temperature gauges to help parameterize snow temperature profiles. These data could also be beneficial for understanding the energy fluxes associated englacial processes. Improving model precision may benefit from investigations of the infrared contribution from North Sister. It is clear from field observations that the eastern margin is experiencing enhanced ablation, which is most likely due to the presence of North Sister. One way to investigate this contribution would be to implement an automated infrared (IR) temperature sensor pointing at North Sister's west face to record temperature at various times of the day to provide spatial and temporal insights on the IR contribution from surrounding topography to the glacier's energy budget. To aid in the contribution of melt water leaving the Collier Glacier, water flow sensors situated in the main outflow may be beneficial to assess the contribution this particular glacier makes to the local hydrology. These data could also be beneficial in making estimations of the contribution this glacier makes to the sea-level budget.

The addition of instrumentation to a glacier monitoring program will increase the performance and accuracy of the melt model of choice, however at the behest of model robustness. In hindsight, the consistency of the PDD model with the SEBMs suggests that perhaps simpler approaches are adequate enough to simulate mass

balance. This particular study suggests that the PDD model performs equally as well as a SEBM with fewer parameters to calibrate. Thus, for modeling mass balance on remote glaciers, the implementation of a PDD model would simplify logistics without compromising model precision.

To provide a better constraint on the volumetric inventory of ice in the Collier Glacier for estimating its contribution to local watersheds and future sea level rise, ice thickness surveys using ground-penetrating radar as a means of measuring ice thickness along the Collier Glacier is imperative. The last ice volume survey conducted in the Three Sisters Wilderness was in 1986 (Drieger and Kennard, 1986). Such surveys are also beneficial in forecasting the mass balance and volumetric contributions to local watersheds and global sea level rise of this particular glacier, as well as other glaciers throughout the Three Sisters Wilderness, with future climate scenarios.

To provide a more complete analysis of the linkages between glacier dynamics and climate change one could couple the OSU SEBM with a glacier flow model, thus providing a full, dynamic analysis of how the Collier Glacier responds to changes in climate. The precision of the models used in this particular study would be more than suitable for coupling with glacier flow models. Such coupling could provide insights of the mechanisms behind the Collier Glacier's dynamic historic response, and provide better predictions as to how this glacier will respond to future changes in its regional climate.

Another potential application for the OSU SEBM could be to couple this model to an energy and mass model for snow cover such as CROCUS (Brun et al., 1989). Models such as CROCUS could provide insights on snow metamorphism, layering, as well as fundamental characteristics of the snowpack, providing further insights on the processes associated with accumulation and how they affect ablation. However implementing such models would require continuous meteorological monitoring through the accumulation season, which may prove difficult due to heavy winter snowfall and winter road closures in the Oregon Cascade Range.

Models such as the OSU SEBM could also be coupled with regional downscaled models, where the input meteorological variables could come from these regional downscaled models. Such applications of the OSU SEBM could provide insights associated with climate change scenarios, as well as paleoclimatology applications to understand how past glaciers responded to perturbations in their regional climate. Such applications could also investigate the different parameters that govern ablation, as well as the mechanisms that controlled their response. Special care, however, must be taken to insure the meteorological inputs are representative of the glacier's microclimate and are distributed appropriately.

3.5 Conclusions

A distributed SEBM has been calibrated to the Collier Glacier, explaining approximately 78% of the variance in summer ablation. However, a simple PDD model explained approximately 82% of the variance in summer ablation, suggesting that simpler methods are just as effective at simulating the Collier Glacier's mass balance. The 2008-2010 studies on the Collier Glacier prove the robustness of the OSU SEBM, which was developed on the South Cascade Glacier, WA (Anslow et al., 2008). These results suggest the possibility of implementing this model on other glaciers providing an increased spatial coverage of glacier mass balance records. Furthermore, these methods also suggest that a minimalist approach to the methods the necessary to collect the inputs to implement the OSU SEBM, yields reasonable results and is adequate for simulating glacier mass balance.

Model comparisons between the OSU SEBM calculating turbulent fluxes with the bulk method and the transfer coefficient method; suggest no superiority in model performance between the two methods. These results suggest that simpler methods may prove more beneficial since they require less parameterization and thus less uncertainty associated with these parameterizations. Model comparisons between the OSU SEBM and a simple PDD model demonstrate the robustness and relatively high precision of simple PDD models. Furthermore, the simple PDD model explained approximately 82% of the variance in summer ablation, while the more physically comprehensive SEBM explained approximately 78% of s the variance in summer

ablation. Thus suggesting, that the more parameterizations have a tendency to overestimate ablation. These results also suggest that simpler methods may prove more beneficial in modeling mass balance on remote glaciers. Nevertheless, simple PDD models do not provide any insight into the different fluxes that control ablation, unlike the more physically comprehensive SEBM.

Sensitivity simulations of the input parameters indicate the highest sensitivities to the parameters that govern snow ablation, which could be the result of these sensitivity tests being conducted on a positive balance year for the Collier Glacier. Atmospheric transmissivity and the albedo of surrounding terrain were some of the least influential parameters for modeled net balance. Sensitivity simulations to the meteorological input variables suggest internal consistencies between the various models used in this particular study. Results from these sensitivity simulations indicate the Collier Glacier is most sensitive to changes in the incoming longwave radiation flux, since the longwave energy exchange occurs as all hours of the day. Energy balance simulations display a high contribution from the sensible heat flux due to the pronounced wind system present on the Collier Glacier, as indicated by the mean monthly energy fluxes. These studies also indicate roughly equal sensitivities to changes in temperature and precipitation, thus suggesting that the Collier Glacier's mass balance is dependent on a combination of winter accumulation and summer temperatures. Furthermore, the timing and magnitude of winter accumulation, in association with the changes in seasonality, may have a strong influence on the Collier

Glacier's mass balance, as experienced with the 2010 balance year, where late spring snowfall resulted in a positive mass balance.

Averaged monthly energy balance fluxes indicate a strong net radiation contribution throughout the first half of the ablation season, reaching a maximum around July and August. The turbulent heat fluxes, primarily through the sensible heat flux, increased their contributions towards melt energy towards the later half of the ablation season as a result of the Collier Glacier's wind regime. These turbulent fluxes begin to dominate the energy balance towards September and October, when the net radiation contributions decreased due to the lower sun angle. These results suggest a seasonal cycle in the energy balance of the Collier Glacier, with major contributions at the beginning of the ablation season coming from the net radiation flux, and major contributions at the end of the ablation season coming from the turbulent heat fluxes.

The model simulations were able to capture the seasonal mass balance, however, the majority of the discrepancies between the measured and modeled net balances were located the ablation area. Model simulations were able to capture some of the secondary fluctuations in the net balance curve, characteristic of the Collier Glacier, however, not to the magnitude observed from field measurements. SEBM simulations indicate that the net shortwave radiation flux is the main control in the variability of ablation below the ELA, however processes not captured by the model, such as debris and snow distribution by wind, avalanching, and mass wasting events on North Sister, contribute to enhance these discrepancies between the measured and

modeled net balances. Nevertheless, all models showed good representation above the ELA, showing good agreement between modeled and measured net balances in the snow-covered regions of the glacier.

This study stresses the relatively high degree of variability of the temperate mountain glaciers throughout the Cascade Range of the PNW. Furthermore, much of the glacier's mass-balance is influenced by its local microclimate, which can be highly variable from one glacier to another due to geographic location, slope, aspect, as well as surrounding topography. Contributions to the glacier's microclimate from local wind circulations can also play a large role in the variability of ablation. Thus stressing the need for increased observations on remote alpine glaciers. The variable nature of these temperate mountain glaciers are supported by the different mean energy fluxes, as well as the different parameter values used to calibrate the melt models, as determined from the Collier Glacier and the South Cascade Glacier energy balance studies. The different climate characteristics, coupled with different hypsometries, and surrounding topography results in different glacier sensitivities and subsequent responses to perturbations in their local climate. Again, questioning how representative the mass balance is for these benchmark glaciers, stressing the need for greater coverage of glacier mass-balance measurements and modeling for remote mountain glaciers. Results from this particular study suggest that even the simplest methods, requiring no more than two temperature sensors, provide an adequate representation of an individual glacier's mass balance.

3.6 References

Andreassen, L. M., M. R. Van Den Broeke, R. H. Giesen, and J. Oerlemans (2008), A 5 year record of surface energy and mass balance from the ablation zone of Storbreen, Norway, *Journal of Glaciology*, 54, 185.

Anslow, F.S. (2008), Modeling and Dating Glacier Fluctuations and Their Relation to Pacific Ocean Climate, *Unpublished PhD. Thesis*, Oregon State University, 159 pp.

Anslow, F.S., S. Hostetler, W. R. Bidlake, and P. U. Clark (2008), Distributed energy balance modeling of South Cascade Glacier, Washington and assessment of model uncertainty, *Journal of Geophysical Research*, 113, F02019.

Armstrong and Brun (2008), *Snow and Climate: Physical Processes, Surface Energy Exchange and Modeling*, Cambridge University Press, Cambridge, UK, 222 pp.

Arnold, N.S., I.C. Willis, M.J. Sharp, K.S. Richards, and W.J. Lawson (1996), A distributed surface energy-balance model for a small valley glacier. I. Development and testing for Haut Glacier d' Arolla, Valais, Switzerland, Journal of Glaciology, 42, 77-89.

Barry, R.G. (1992), *Mountain weather and climate*, Routledge, Chapman, and Hall, Inc., New York, NY, 402 pp.

Bitz, C.M., and D.S. Battisti (1999), Interannual to Decadal variability in Climate and the Mass Balance in Washington, Western Canada, and Alaska, *Journal of Climate*, 12, 3181-3196.

Braithwaite, R.J. (1977), Air temperature and glacier ablation-a parametric approach, *PhD. Thesis*, McGill University.

Braithwaite, R.J. (1985), Calculation of degree-days for glacier-climate research, *Z. Gletscherkd. Glazialgeol.*, 20, 1-8.

Braithwaite, R.J., and Y. Zhang (2000), Sensitivity of mass balance of five Swiss glaciers to temperature changes assessed by tuning a degree-day model, *Journal of Glaciology*, 46, 152.

Brock, B. W., I. C. Willis, and M. J. Sharp (2000), Measurement and parameterization of albedo variations at Haut Glacier d'Arolla, Switzerland, *Journal of Glaciology*, 46, 155.

Brock, B.W., I.C. Willis, and M.J. Sharp (2006), Measurement and parameterization of aerodynamic roughness length variations at Haut Glacier d'Arolla, Switzerland, *Journal of Glaciology*, 52, 281-297.

Brun, E, E. Martin, V. Simon, C. Gendre, and C. Coleou (1989), An energy and mass model of snow cover suitable for operational avalanche forecasting, *Journal of Glaciology*, 35, 121.

Collares-Periera, M. and A. Rabl (1979), The average distribution of solar radiation correlations between diffuse and hemispherical and between daily and hourly insolation values, *Solar Energy*, 22, 155-164.

Daly, C, R.P. Neilson, and D.L. Phillips (1994), A Statistical-Topographic Model for Mapping Climatological Precipitation over Mountainous Terrain, *Journal of Applied Meteorology*, 33, 140-158.

Denby, B. and W. Greuell (2000), The use of bulk and profile methods for determining surface heat fluxes in the presence of glacier winds, *Journal of Glaciology*, 46, 445-452.

Denby, B., W. Greuell, and J. Oerlemans (2002), Simulating the Greenland atmospheric boundary layer: Part II. Energy balance and climate sensitivity, *Tellus*, Series A, 54, 529-541.

Dozier, J. and S.G. Warren (1982), Effect of viewing angle on the infrared brightness temperature of snow, *Water Resources Research*, 18, 1424-1434.

Dozier, J., J. Frew (1990), Rapid calculation of terrain parameters for radiation modeling from digital elevation data. *IEEE Geosci. Remote*, 28, 963-969.

Driedger, C.L., and P.M. Kennard (1986), Ice Volumes on Cascade Volcanoes: Mount Rainier, Mount Hood, Three Sisters, and Mount Shasta: U.S. Geological Survay Professional Paper 1365, 28 pp.

Finsterwalder, S. and H. Schunk (1887), Der Suldenferner. Zeitschrift des Deutschen und Oesterreichischen.

Fountain, A.G., M.J. Hoffman, F. Granshaw, and J. Riedel (2009), The 'benchmark glacier' concept – does it work? Lessons from the North Cascade Range, USA, *Annals of Glaciology*, 50(50), 163-168.

Greuell, W. and J. Oerlemans (1986), Sensitivity studies with a mass balance model including temperature profile calculations inside the glacier, *Zeitschrift für Gletscherkunde un Glazialgeologie*, 22, 101-124.

Greuell, W. and W.H. Knap (1997), Elevational changes in meteorological variables along a midlatitude glacier during summer, *Journal of Geophysical Research*, 102, 25, 941-25, 954.

Hobbs, P.V. (1974), *Ice Physics*. Clarendon Press, Oxford, UK.

Hock, R (1999), A distributed temperature-index ice- and snowmelt model including potential direct solar radiation, *Journal of Glaciology*, 45, 149.

Hock, R (2003), Temperature index melt modeling in mountain areas, *Journal of Hydrology*, 282, 104-115.

Hock, R (2005), Glacier melt: a review of processes and their modeling, *Progress in Physical Geography*, 29, 362.

Hock, R. and B. Holmgren (2005), A distributed energy-balance model for complex topography and its application to Storglaciären, Sweden, *Journal of Glaciology*, 51, 25-36.

Hopson, R.E. (1960), Collier Glacier: A photographic record, *Mazama*, 42, 15-26.

Hostetler, S., and P. U. Clark (1997), Climatic controls of western U.S. glaciers at the last glacial maximum, *Quaternary Science Reviews*, 16, 505-511.

Hostetler, S., and P. U. Clark (2000), Tropical Climate at the Last Glacial Maximum Inferred from Glacier Mass-Balance Modeling, *Science*, 290, 1747-1750.

Iqbal, M. (1983), *An Introduction to Solar Radiation*, Academic Press, London, 390 pp.

Jackson, K.M., and A.G. Fountain (2007), Spatial and morphological change on Eliot Glacier, Mount Hood, Oregon, USA, *Annals of Glaciology*, 46.

Josberger, E.G., W.R. Bidlake, R.S. March, and B.W. Kennedy (2007), Glacier mass-balance fluctuations in the Pacific Northwest and Alaska, USA, *Annals of Glaciology*, 46, 291-296.

Josberger, E.G., Bidlake, W.R., March, R.S., and O'Neel, S. (2009), Fifty-Year Record of Glacier Change Reveals Shifting Climate in the Pacific Northwest and Alaska, USA: U.S. Geological Survey Fact Sheet 2009-3046, 4 p.

Klok, E. J., and J. Oerlemans (2003), Deriving historical equilibrium-line altitudes from a glacier length record by linear inverse modeling, *The Holocene*, 13 ,3, 343-351.

Kuhn, M. (2003), Redistribution of snow and glacier mass balance from a hydrometeorological model, *Journal of Hydrology*, 282, 95-103.

Lundstrom, S.C., A.E. McCafferty, and J.A. Coe (1993), Photogrammetric analysis of 1984-89 surface altitude change of the partially debris-covered Eliot Glacier, Mount Hood, Oregon, USA, *Annals of Glaciology*, 17, 167-170.

Marks, D., and J. Dozier (1992), Climate and energy exchange at the snow surface in the Alpine Region of the Sierra Nevada: 1. Meteorological measurements and monitoring, *Water Resources Research*, 28, 3029-3042.

Marks, D., and J. Dozier (1992), Climate and energy exchange at the snow surface in the Alpine Region of the Sierra Nevada: 2. Snow cover energy balance, *Water Resources Research*, 28, 3043-3054.

Marks, D., J. Kimball, D. Tingey, and T. Link (1998), The sensitivity of snowmelt processes to climate conditions and forest cover during rain-on- snow: A case study of the 1996 Pacific Northwest flood, *Hydrological Processes*, 12, 1569-1587.

McDonald, G.D. (1995), Changes in mass of Collier Glacier, Oreon, 1910-1004, Unpublished Master's Thesis, Oregon State University.

Meehl, G.A., T.F. Stocker, W.D. Collins, P. Friedlingstein, A.T. Gaye, J.M. Gregory, A. Kitoh, R. Knutti, J.M. Murphy, A. Noda, S.C.B. Raper, I.G. Watterson, A.J. Weaver and Z.-C. Zhao, 2007: Global Climate Projections. In: *Climate Change 2007: The Physical Science Basis. Contribution of Working Group I to the Fourth Assessment Report of the Intergovernmental Panel on Climate Change* [Solomon, S., D. Qin, M. Manning, Z. Chen, M. Marquis, K.B. Averyt, M. Tignor and H.L. Miller (eds.)]. Cambridge University Press, Cambridge, United Kingdom and New York, NY, USA.

Meier, M.F., W.V. Tangborn, L.R. Mayo, and A. Post (1971), Combined ice and water balances of Gulkana and Wolverine Glaciers, Alaska, and South Cascade Glacier, Washington, 1965 and 1966 Hydrologic Years: U.S. Geological Survey Professional Paper 715-A, 23 p., 4pl.

Meier, M.F. (1984), Contribution of Small Glaciers to Global Sea Level, *Science*, 226, 4681, 1418-1421.

Meier, M.F, M.B. Dyurgerov, U.K. Rick, S. O'Neel, T. Pfeffer, R.S. Anderson, S.P. Anderson, and A.F. Glazovsky. (2007), Glaciers Dominate Eustatic Sea-Level Rise in the 21st Century, *Science*, 317, 1064-1066.

Monin A.S. and A.M. Obukhov (1954), Basic laws of turbulent mixing in the surface layer of the atmosphere, *Tr. Akad. Nauk SSSR Geophiz. Inst.*, 24, 151, 163-187.

Mote, P.W., (2003), Trends in snow water equivalent in the Pacific Northwest and climatic causes, *Geophysical Research Letters*, 30, 12, 1601.

Mountain, K.R. (1978), The Chronology, Geomorphology, and Climate of Collier Glacier with Special Reference to the Ablation Process, *Unpublished M.A.* Thesis, University of Oregon, 197 pp.

Mountain, K.R. (1990), A clear sky net radiation model for the high elevation glacial environment, *Unpublished PhD. Thesis*, The Ohio State University, Dept. of Geography, 290 pp.

Munro, S.D. (1989), Surface roughness and bulk heat transfer on a glacier: comparison with eddy correlation, *Journal of Glaciology*, 35, 121.

O'Connor, J.E., J.H. Hardison III, and J.E. Costa (2001), Debris Flow from Failures of Neoglacial-Age Moraine Dams in the Three Sisters and Mount Jefferson Wilderness Areas, Oregon: U.S. Geological Survey Professional Paper 1606, 93 pp.

Oerlemans, J., and N.C. Hoogendoorn (1989), Mass balance gradients and climatic change, *Journal of Glaciology*, 35, 399-405.

Oerlemans, J., and J.P.F Fortuin (1992), Sensitivity of Glaciers and Small Ice Caps to Greenhouse Warming, *Science*, 258, 5079, 115-117.

Oerlemans, J. (1992), Climate sensitivity of glaciers in southern Norway: application of an energy-balance model to Nigardsbreen, Hellstugubreen and Alfotbreen, *Journal of Glaciology*, 38, 223-232.

Oerlemans, J., and W.H. Knap (1998), A 1 year record of global radiation and albedo in the ablation zone of Morteratschgletscher, Switzerland, *Journal of Glaciology*, 44, 231-238.

Oerlemans, J., and B.K. Reichert (2000), Relating glacier mass balance to meteorological data using a seasonal sensitivity characteristic (SSC), *Journal of Glaciology*, 46, 152, 1-6.

Oerlemans, J. (2001), *Glaciers and Climate Change*. A.A. Balkema Publishers, Lisse, 148 pp.

Oerlemans, J. (2010), *The Microclimate of Valley Glaciers*, Igitur, Utrecht Publishing and Archiving Services, Universiteitsbibliotheek, Utrecht, ND, 138 pp.

Østrem, G., and M. Brugman (1991), Glacier Mass-Balance Measurements: A manual for field and office work. *National Hydrology Research Institute Scientific Report*, 4 Environment Canada, N.H.R.I., Saskatoon and Norges Vassdrags-og Elektrisitetsvesen, Oslo.

Paterson, W. S. B. (1994), *The Physics of Glaciers*. Pergamon Press, Oxford, 480 pp.

Phillips, E.L. (1960), Climates of the States No. 60-45.: Washington, pp 1042-1049 in Climates of the States. Vol. 2, Gale Research Company, Detroit, MI.

Plüss, C. and A. Ohmura (1997), Longwave Radiation on Snow-Covered Mountainous Surfaces, *Journal of Appl. Meteorol.*, 36, 818-824.

Poellot, C.D. (2000), Ice Surface Reconstruction and Energy Balance Modeling of Alpine Glaciers, *Unpublished M.S. Thesis*, Oregon State University, 134 pp.

Rango, A., and Martinec, J. (1995), Revisiting the degree-day method for snowmelt computations, *Water Resources Bulletin*, 31, 657-669.

Rhodes, J.J, R.L. Armstrong, and S.G. Warren (1987), Mode of formation of "ablation hollows" controlled by dirt content of snow, Journal of Glaciology, 33, 114, 135-139.

Ropelwski, C.F., and M.S. Halpert (1986), North American precipitation and temperature patterns associated with El Niño/southern oscillation (ENSO), *Monthly Weather Reviews*, 114, 2352-2362.

Tangborn, W. (1980), Two models for estimating climate-glacier relationships in the North Cascades, Washington, USA, *Journal of Glaciology*, 25, 91, 3-21.

Van den Broeke, M.R., C.H. Reijmer, D. van As, R.S.W. van de Wal, and J. Oerlemans (2005), Seasonal cycles of Antarctic surface energy balance from Automatic Weather Stations, *Annals of Glaciology*, 41, 131-139.

Warren, S.G. (1982), Optical properties of snow, *Rev. Geophys.*, 20, 67-89.

Willis, I.C., N.S. Arnold, and B.W. Brock (2002), Effect of snowpack removal on energy balance, melt and runoff in a small supraglacial catchment. *Hydrological. Procesess*, 16, 2721-2749.

Wiscomb, W.J. and S.G. Warren (1980), A model for the spectral albedo of snow. I: Pure Snow, *Journal of Atmospheric Science*, 37, 2712-2733.

Chapter 4

Conclusions

Mass-balance measurements on the Collier Glacier indicate a high degree of variability, resulting in a continued areal reduction since the 1989-1994 studies. Local meteorological influences could be enhanced and/or dampened by the surrounding topography, which can have a control on shading, debris, slope, and aspect, all of which can greatly influence the surface energy exchange, and resulting energy available for melt for the glacier. The b_n curves from 1989-2010 indicate high mass loss in the lower portions of the glacier relative to the upper reaches of the glacier. Of particular interest, is the region between 2300 and 2400 m, where there is a high degree of mass loss relative to the elevations above and below this elevation band. However, these secondary fluctuations in the b_n curve seem to have risen to a higher elevation relative to the 1989-1994 measurements, likely reinforcing the continued areal loss since the 1989-1994 measurements, as well as the increasing proximity of the ELA to the icefall.

The 1989-2010 measurements demonstrate that the variability in the mass balance of Collier Glacier is likely governed by timing and magnitude of summer temperatures and precipitation that falls as snow on the glacier. Both of these variables strongly dictate the net balance of a glacier by influencing its surface energy exchange, and the associated energy available for melt. These results suggest that the

Collier Glacier is likely strongly influenced of large modes of variability from the eastern Pacific, such as El Nino-Southern Oscillation or Pacific Decadal Oscillation, which could have a pronounced influence on the timing and magnitude of the winter accumulation and summer temperatures. Nevertheless, a longer time series of mass balance data for the Collier Glacier is needed to further explore the influence of these natural modes of variability on the accumulation and/or ablation of mass.

The 1989-2010 mass-balance measurements suggest that, on average, the Collier Glacier continues to lose mass, indicating a continuation of its retreat since its Little Ice Age maximum in a step-like fashion, where there are periods of significant mass loss, accompanied by steady-state conditions. The cause of this step-like retreat remains unknown. These data suggest that any future climatic perturbation resulting in anomalously warm summers or dry winters could influence the Collier Glacier's mass budget negatively.

A distributed SEBM has been calibrated to the meteorological and mass balance measurements made on Collier Glacier during the 2009 and 2010 years, explaining approximately 78% of the variance in summer ablation. A simple PDD model explained approximately 82% of the variance in summer ablation, suggesting that simpler methods are just as effective at simulated glacier mass balance. These results suggest the possibility of implementing this model on other glaciers to provide an increased spatial coverage of glacier mass balance records. Furthermore, these methods also suggest that a minimalist approach to the methods the necessary to

collect the inputs to implement the OSU SEBM, yields reasonable results and is adequate for simulating glacier mass balance.

Comparisons between versions of the OSU SEBM that calculated turbulent fluxes with the bulk method and with the transfer coefficient method suggest no superiority in model performance between the two methods. These results suggest that simpler methods may prove just as effective since they require less parameterization and thus less uncertainty associated with these parameterizations. Model comparisons between the OSU SEBM and a simple PDD model showed that the simple PDD model explained approximately 82% of the variance in the 2010 summer ablation, while the more physically comprehensive SEBM explained approximately 78% of s the variance in the 2010 summer ablation. These results suggest that the PDD model may prove just as effective in modeling mass balance on remote glaciers as a SEBM. Nevertheless, simple PDD models do not provide any insight into the different fluxes that control ablation, unlike the more physically comprehensive SEBM.

Sensitivity experiments of the input parameters indicate the highest sensitivities to the parameters that govern snow ablation, which could be the result of these sensitivity tests being conducted on a positive balance year for the Collier Glacier. Atmospheric transmissivity and the albedo of surrounding terrain were some of the least sensitive parameters for modeled net balance. Sensitivity simulations to the meteorological input variables suggest internal consistencies between the various models used in this particular study. Results from these sensitivity simulations

indicate the Collier Glacier is most sensitive to changes in the incoming longwave radiation flux, since the longwave energy exchange occurs as all hours of the day. Energy balance simulations display a high contribution from the sensible heat flux due to the pronounced wind system present on the Collier Glacier, as indicated by the mean monthly energy fluxes. These studies also indicate roughly equal sensitivities to changes in temperature and precipitation, thus suggesting that the Collier Glacier's mass balance is dependent on a combination of winter accumulation and summer temperatures. Furthermore, the timing and magnitude of winter accumulation, in association with the changes in seasonality, may have a strong influence on the Collier Glacier's mass balance, as experienced with the 2010 balance year, where late spring snowfall resulted in a positive mass balance.

Averaged monthly energy balance fluxes indicate a strong net radiation contribution throughout the first half of the ablation season, reaching a maximum around July and August. The turbulent heat fluxes, primarily through the sensible heat flux, increased their contributions towards melt energy towards the later half of the ablation season as a result of the Collier Glacier's wind regime. These turbulent fluxes begin to dominate the energy balance towards September and October, when the net radiation contributions decreased due to the lower sun angle. These results suggest a seasonal cycle in the energy balance of the Collier Glacier, with major contributions at the beginning of the ablation season coming from the net radiation flux, and major contributions at the end of the ablation season coming from the turbulent heat fluxes.

Although the model simulations were able to capture the seasonal mass balance, the majority of the discrepancies between the measured and modeled net balances occurred in the ablation area. Model simulations were able to capture some of the secondary fluctuations in the net balance curve, characteristic of the Collier Glacier, but not to the same magnitude observed from field measurements. SEBM simulations indicate that the net shortwave radiation flux is the main control in the variability of ablation below the ELA, however processes not captured by the model, such as debris and snow distribution by wind, avalanching, and mass wasting events on North Sister, contribute to enhance these discrepancies between the measured and modeled net balances. All models showed good agreement between modeled and measured net balances above the ELA.

This study stresses the relatively high degree of variability of the temperate mountain glaciers throughout the Cascade Range of the PNW. Furthermore, much of the glacier's mass-balance is influenced by its local microclimate, which can be highly variable from one glacier to another due to geographic location, slope, aspect, as well as surrounding topography. The variable nature of these temperate mountain glaciers are supported by the different mean energy fluxes, as well as the different parameter values used to calibrate the melt models, as determined from the Collier Glacier and the South Cascade Glacier energy balance studies. These results question how representative the mass balance is for any individual glacier, stressing the need for greater coverage of glacier mass-balance measurements and modeling for remote mountain glaciers. Results from this particular study suggest that even the simplest

methods, requiring no more than two temperature sensors, provide an adequate representation of an individual glacier's mass balance. Thus, lightweight, and simplistic field approaches to glaciological monitoring are effective at measuring and simulating glacier mass balance.

Bibliography

Ahlmann, H.W. (1935), Contribution to the Physics of Glaciers, *The Geographical Journal*, 86, 97-107.

Ahlmann, H.W. (1946), Researches on Snow and Ice, 1918-40, *The Geographical Journal*, 107, 1, 11-25.

Andreassen, L. M., M. R. Van Den Broeke, R. H. Giesen, and J. Oerlemans (2008), A 5 year record of surface energy and mass balance from the ablation zone of Storbreen, Norway, *Journal of Glaciology*, 54, 185.

Andrews, J.T. (1972), Glacier power, mass balances, velocities and erosion potential, *Zeitschrift für Geomorphologie Suppl. Bd.*, 13, 1-17.

Andrews, J.T. (1975), *Glacial Systems: An Approach to Glaciers and their Environments*. Duxbury Press, North Scituate, Mass.

Anslow, F.S. (2008), Modeling and Dating Glacier Fluctuations and Their Relation to Pacific Ocean Climate, *Unpublished PhD*. Thesis, Oregon State University, 159 pp.

Anslow, F. S., S. Hostetler, W. R. Bidlake, and P. U. Clark (2008), Distributed energy balance modeling of South Cascade Glacier, Washington and assessment of model uncertainty, *Journal of Geophysical Research*, 113, F02019.

Armstrong and Brun (2008), *Snow and Climate: Physical Processes, Surface Energy Exchange and Modeling*, Cambridge University Press, Cambridge, UK, 222 pp.

Arnold, N.S., I.C. Willis, M.J. Sharp, K.S. Richards, and W.J. Lawson (1996), A distributed surface energy-balance model for a small valley glacier. I. Development and testing for Haut Glacier d' Arolla, Valais, Switzerland, *Journal of Glaciology*, 42, 77-89.

Bahr, D.B., W.T. Pfeffer, C. Sassolas, and M.F. Meier (1998), Response time of glaciers as a function of size and mass balance: 1 Theory, *Journal of Geophysical Research*, 103, B5, 9777-9782.

Bahr, D.B., M. Dyurgerov, and M.F. Meier (2009), Sea-level rise from glaciers and ice caps: A lower bound, *Geophysical Resarch Letters*, 36, L03501.

Barry, R.G. (1992), *Mountain weather and climate*, Routledge, Chapman, and Hall, Inc., New York, NY, 402 pp.

Bitz, C.M., and D.S. Battisti (1999), Interannual to Decadal variability in Climate and the Mass Balance in Washington, Western Canada, and Alaska, *Journal of Climate*, 12, 3181-3196.

Braithwaite, R.J. (1977), Air temperature and glacier ablation-a parametric approach, *PhD. Thesis*, McGill University.

Braithwaite, R.J. (1985), Calculation of degree-days for glacier-climate research, *Zeitschrift für Gletscherkunde un Glazialgeologie*, 20, 1-8.

Braithwaite, R.J., and Y. Zhang (2000), Sensitivity of mass balance of five Swiss glaciers to temperature changes assessed by tuning a degree-day model, *Journal of Glaciology*, 46, 152.

Brock, B. W., I. C. Willis, and M. J. Sharp (2000), Measurement and parameterization of albedo variations at Haut Glacier d'Arolla, Switzerland, *Journal of Glaciology*, 46, 155.

Brock, B.W., I.C. Willis, and M.J. Sharp (2006), Measurement and parameterization of aerodynamic roughness length variations at Haut Glacier d'Arolla, Switzerland, *Journal of Glaciology*, 52, 281-297.

Brun, E, E. Martin, V. Simon, C. Gendre, and C. Coleou (1989), An energy and mass model of snow cover suitable for operational avalanche forecasting, *Journal of Glaciology*, 35, 121.

Burbank, D.W. (1982), Correlations of climate, mass balance, and glacial fluctuations at Mount Rainier, Washington, USA, since 1980, *Arctic and Alpine Res.*, 14, 2, 137-148.

Collares-Periera, M. and A. Rabl (1979), The average distribution of solar radiation correlations between diffuse and hemispherical and between daily and hourly insolation values, *Solar Energy*, 22, 155-164.

Daly, C, R.P. Neilson, and D.L. Phillips (1994), A Statistical-Topographic Model for Mapping Climatological Precipitation over Mountainous Terrain, *Journal of Applied Meteorology*, 33, 140-158.

Denby, B. and W. Greuell (2000), The use of bulk and profile methods for determining surface heat fluxes in the presence of glacier winds, *Journal of Glaciology*, 46, 445-452.

Denby, B., W. Greuell, and J. Oerlemans (2002), Simulating the Greenland atmospheric boundary layer: Part II. Energy balance and climate sensitivity, *Tellus*, Series A, 54, 529-541.

Dozier, J. and S.G. Warren (1982), Effect of viewing angle on the infrared brightness temperature of snow, *Water Resources Research*, 18, 1424-1434.

Dozier, J., J. Frew (1990), Rapid calculation of terrain parameters for radiation modeling from digital elevation data. *IEEE Geosci. Remote*, 28, 963-969.

Driedger, C.L., and P.M. Kennard (1986), Ice Volumes on Cascade Volcanoes: Mount Rainier, Mount Hood, Three Sisters, and Mount Shasta: U.S. Geological Survay Professional Paper 1365, 28 pp.

Dyurgerov, M.B. (2010), *Reanalysis of Glacier Changes: From the IGY to the IPY, 1960-2008*, Data of Glaciological Studies, Publication 108, Moscow, 116 pp., ISSN 0130–3686.

Finsterwalder, S. and H. Schunk (1887), Der Suldenferner. Zeitschrift des Deutschen und Oesterreichischen.

Fountain, A.G., M.J. Hoffman, F. Granshaw, and J. Riedel (2009), The 'benchmark glacier' concept – does it work? Lessons from the North Cascade Range, USA, *Annals of Glaciology*, 50(50), 163-168.

Furbish, D.J, and J.T. Andrews (1984), The use of hypsometry to indicate long-term stability and response of valley glaciers to changes in mass transfer, *Journal of Glaciology*, 30, 105, 199-211.

Greuell, W. and J. Oerlemans (1986), Sensitivity studies with a mass balance model including temperature profile calculations inside the glacier, *Zeitschrift für Gletscherkunde un Glazialgeologie*, 22, 101-124.

Greuell, W. and W.H. Knap (1997), Elevational changes in meteorological variables along a midlatitude glacier during summer, *Journal of Geophysical Research*, 102, 25, 941-25, 954.

Hobbs, P.V. (1974), *Ice Physics*. Clarendon Press, Oxford, UK.

Hock, R (1999), A distributed temperature-index ice- and snowmelt model including potential direct solar radiation, *Journal of Glaciology*, 45, 149.

Hock, R (2003), Temperature index melt modeling in mountain areas, *Journal of Hydrology*, 282, 104-115.

Hock, R (2005), Glacier melt: a review of processes and their modeling, *Progress in Physical Geography*, 29, 362.

Hock, R. and B. Holmgren (2005), A distributed energy-balance model for complex topography and its application to Storglaciären, Sweden, *Journal of Glaciology*, 51, 25-36.

Hopson, R.E. (1960), Collier Glacier: A photographic record, *Mazama*, 42, 15-26.

Hostetler, S., and P. U. Clark (1997), Climatic controls of western U.S. glaciers at the last glacial maximum, *Quaternary Science Reviews*, 16, 505-511.

Hostetler, S., and P. U. Clark (2000), Tropical Climate at the Last Glacial Maximum Inferred from Glacier Mass-Balance Modeling, *Science*, 290, 1747-1750.

Hubley, R.C. (1956), Glaciers of the Washington Cascade and Olympic Mountains; their present activity and its relation to local climatic trends, *Journal of Glaciology*, 2, 19, 669-674.

Iqbal, M. (1983), *An Introduction to Solar Radiation*, Academic Press, London, 390 pp.

Jackson, K.M., and A.G. Fountain (2007), Spatial and morphological change on Eliot Glacier, Mount Hood, Oregon, USA, *Annals of Glaciology*, 46.

Josberger, E.G., W.R. Bidlake, R.S. March, and B.W. Kennedy (2007), Glacier mass-balance fluctuations in the Pacific Northwest and Alaska, USA, *Annals of Glaciology*, 46, 291-296.

Josberger, E.G., Bidlake, W.R., March, R.S., and O'Neel, S. (2009), Fifty-Year Record of Glacier Change Reveals Shifting Climate in the Pacific Northwest and Alaska, USA: U.S. Geological Survey Fact Sheet 2009-3046, 4 p.

Klok, E. J., and J. Oerlemans (2003), Deriving historical equilibrium-line altitudes from a glacier length record by linear inverse modeling, *The Holocene*, 13 ,3, 343-351.

Kuhn, M (1995), The mass balance of very small glaciers, *Zeitschrift für Gletscherkunde und Glazialgeologie*, 31, 171-179.

Kuhn, M. (2003), Redistribution of snow and glacier mass balance from a hydrometeorological model, *Journal of Hydrology*, 282, 95-103.

Lundstrom, S.C., A.E. McCafferty, and J.A. Coe (1993), Photogrammetric analysis of 1984-89 surface altitude change of the partially debris-covered Eliot Glacier, Mount Hood, Oregon, USA, *Annals of Glaciology*, 17, 167-170.

Marks, D., and J. Dozier (1992), Climate and energy exchange at the snow surface in the Alpine Region of the Sierra Nevada: 1. Meteorological measurements and monitoring, *Water Resources Research*, 28, 3029-3042.

Marks, D., and J. Dozier (1992), Climate and energy exchange at the snow surface in the Alpine Region of the Sierra Nevada: 2. Snow cover energy balance, *Water Resources Research*, 28, 3043-3054.

Marks, D., J. Kimball, D. Tingey, and T. Link (1998), The sensitivity of snowmelt processes to climate conditions and forest cover during rain-on- snow: A case study of the 1996 Pacific Northwest flood, *Hydrological Processes*, 12, 1569-1587.

McDonald, G.D. (1995), Changes in mass of Collier Glacier, Oreon, 1910-1004, *Unpublished M.S. Thesis*, Oregon State University.

Meehl, G.A., T.F. Stocker, W.D. Collins, P. Friedlingstein, A.T. Gaye, J.M. Gregory, A. Kitoh, R. Knutti, J.M. Murphy, A. Noda, S.C.B. Raper, I.G. Watterson, A.J. Weaver and Z.-C. Zhao (2007), *2007: Global Climate Projections. In: Climate Change 2007: The Physical Science Basis. Contribution of Working Group I to the Fourth Assessment Report of the Intergovernmental Panel on Climate Change* [Solomon, S., D. Qin, M. Manning, Z. Chen, M. Marquis, K.B. Averyt, M. Tignor and H.L. Miller (eds.)]. Cambridge University Press, Cambridge, United Kingdom and New York, NY, USA.

Meier, M.F. (1962), Proposed definitions for glacier mass budget terms, *Journal of Glaciology*, 4, 33, 252-263.

Meier, M.F. (1965). Glaciers and climate. *In* Wright, H.E. and D.G. Frey (eds.), *The Quaternary of the United States*, Princeton University Press, Princeton New Jersey, 795-805.

Meier, M.F. and W. Tangborn (1965), Net budget and flow of South Cascade Glacier, Washington, *Journal of Glaciology*, 5, 547.

Meier, M.F., W.V. Tangborn, L.R. Mayo, and A. Post (1971), Combined ice and water balances of Gulkana and Wolverine Glaciers, Alaska, and South Cascade Glacier, Washington, 1965 and 1966 Hydrologic Years: U.S. Geological Survey Professional Paper 715-A, 23 p., 4pl.

Meier, M.F. (1984), Contribution of Small Glaciers to Global Sea Level, *Science*, 226, 4681, 1418-1421.

Meier, M.F, M.B. Dyurgerov, U.K. Rick, S. O'Neel, T. Pfeffer, R.S. Anderson, S.P. Anderson, and A.F. Glazovsky. (2007), Glaciers Dominate Eustatic Sea-Level Rise in the 21st Century, *Science*, 317, 1064-1066.

Monin A.S. and A.M. Obukhov (1954), Basic laws of turbulent mixing in the surface layer of the atmosphere, *Tr. Akad. Nauk SSSR Geophiz. Inst.*, 24, 151, 163-187.

Mote, P.W., (2003), Trends in snow water equivalent in the Pacific Northwest and climatic causes, *Geophysical Research Letters*, 30, 12, 1601.

Mote, P.W., A.F. Hamlet, M.P. Clark, and D.P. Lettenmaier (2005), Declining mountain snowpack in Western North America, *Bulletin of the American Meteorological Society*, 86, 39-49.

Mountain, K.R. (1978), The Chronology, Geomorphology, and Climate of Collier Glacier with Special Reference to the Ablation Process, *Unpublished M.A. Thesis*, University of Oregon, 197 pp.

Mountain, K.R. (1990), A clear sky net radiation model for the high elevation glacial environment, *Unpublished PhD. Thesis*, The Ohio State University, Dept. of Geography, 290 pp.

Munro, S.D. (1989), Surface roughness and bulk heat transfer on a glacier: comparison with eddy correlation, *Journal of Glaciology*, 35, 121.

O'Connor, J.E., J.H. Hardison III, and J.E. Costa (2001), Debris Flow from Failures of Neoglacial-Age Moraine Dams in the Three Sisters and Mount Jefferson Wilderness Areas, Oregon: U.S. Geological Survey Professional Paper 1606, 93 pp.

Oerlemans, J., and N.C. Hoogendoorn (1989), Mass balance gradients and climatic change, *Journal of Glaciology*, 35, 399-405.

Oerlemans, J., and J.P.F Fortuin (1992), Sensitivity of Glaciers and Small Ice Caps to Greenhouse Warming, *Science*, 258, 5079, 115-117.

Oerlemans, J. (1992), Climate sensitivity of glaciers in southern Norway: application of an energy-balance model to Nigardsbreen, Hellstugubreen and Alfotbreen, *Journal of Glaciology*, 38, 223-232.

Oerlemans, J., and W.H. Knap (1998), A 1 year record of global radiation and albedo in the ablation zone of Morteratschgletscher, Switzerland, *Journal of Glaciology*, 44, 231-238.

Oerlemans, J., and B.K. Reichert (2000), Relating glacier mass balance to meteorological data using a seasonal sensitivity characteristic (SSC), *Journal of Glaciology*, 46, 152, 1-6.

Oerlemans, J. (2001), *Glaciers and Climate Change*. A.A. Balkema Publishers, Lisse, 148 pp.

Oerlemans, J. (2010), *The Microclimate of Valley Glaciers*, Igitur, Utrecht Publishing and Archiving Services, Universiteitsbibliotheek, Utrecht, ND, 138 pp.

Østrem, G., and M. Brugman (1991), Glacier Mass-Balance Measurements: A manual for field and office work. *National Hydrology Research Institute Scientific Report*, 4 Environment Canada, N.H.R.I., Saskatoon and Norges Vassdrags-og Elektrisitetsvesen, Oslo.

Paterson, W. S. B. (1994), *The Physics of Glaciers*. Pergamon Press, Oxford, 480 pp.

Pheffer, W.T., J.T. Harper, and S. O'Neel (2008), Kinematic constraints on glacier contributions to 21st century sea-level rise, *Science*, 321, 1340-1343.

Phillips, E.L. (1960), Climates of the States No. 60-45.: Washington, pp 1042-1049 in Climates of the States. Vol. 2, Gale Research Company, Detroit, MI.

Plüss, C. and A. Ohmura (1997), Longwave Radiation on Snow-Covered Mountainous Surfaces, *Journal of Appl. Meteorol.*, 36, 818-824.

Poellot, C.D. (2000), Ice Surface Reconstruction and Energy Balance Modeling of Alpine Glaciers, *Unpublished M.S. Thesis*, Oregon State University, 134 pp.

Rango, A., and Martinec, J. (1995), Revisiting the degree-day method for snowmelt computations, *Water Resources Bulletin*, 31, 657-669.

Rhodes, J.J, R.L. Armstrong, and S.G. Warren (1987), Mode of formation of "ablation hollows" controlled by dirt content of snow, *Journal of Glaciology*, 33, 114, 135-139.

Ropelwski, C.F., and M.S. Halpert (1986), North American precipitation and temperature patterns associated with El Niño/southern oscillation (ENSO), *Monthly Weather Reviews*, 114, 2352-2362.

Tangborn, W. (1980), Two models for estimating climate-glacier relationships in the North Cascades, Washington, USA, *Journal of Glaciology*, 25, 91, 3-21.

Van den Broeke, M.R., C.H. Reijmer, D. van As, R.S.W. van de Wal, and J. Oerlemans (2005), Seasonal cycles of Antarctic surface energy balance from Automatic Weather Stations, *Annals of Glaciology*, 41, 131-139.

Warren, S.G. (1982), Optical properties of snow, *Reviews of Geophysics*, 20, 67-89.

Willis, I.C., N.S. Arnold, and B.W. Brock (2002), Effect of snowpack removal on energy balance, melt and runoff in a small supraglacial catchment. *Hydrological. Procesess*, 16, 2721-2749.

Wiscomb, W.J. and S.G. Warren (1980), A model for the spectral albedo of snow. I: Pure Snow, *Journal of Atmospheric Science*, 37, 2712-2733.

APPENDIX

Appendix A Mass Balance Measurements

Snow-covered areas of the glacier were measured with probes and crevasses to measure snow depth with respect to the previous year's surface. Snow pits were dug in representative locations to measure snow density. These two quantities combined were used to estimate the water equivalent amount of snow on the glacier. Snow density was measured with a Taylor-LaChapelle snow density kit. Snow-free areas of the glacier were measured with PVC ablation stakes drilled into the ice and were measured routinely over the course of the ablation season.

Table A1 2010 Mass-Balance Measurements

Slice	Area (m^2)
1	11433.0554
2	24146.66148
3	25401.00728
4	30441.24715
5	33669.24666
6	37006.08635
7	82865.14259
8	64765.69199
9	64398.70779
10	55128.1649
11	51121.85177
12	54593.61899
13	107562.7101
	642533.1925

Winter				**Net**				**Summer**			
Elevation (m)	b_n (m.w.e)	Area (m^2)	B_n	Ave Elevation (m)	b_n Ave (m.w.e)	Area (m^2)	Bn	Elevation (m)	b_s (m.w.e)	Area (m^2)	B_s
2296	2.15	11433.0554	24552.94	2294.5	-0.78	11433.0554	-8911.50	2294.5	-2.93	11433.0554	-33464.43219
2325	2.00	24146.66148	48377.84	2332	-2.00	24146.66148	-48270.63	2332	-4.00	24146.66148	-96648.46137
2351	1.73	25401.00728	43869.41	2350.5	-2.25	25401.00728	-57067.17	2350.5	-3.97	25401.00728	-100936.5874
2382	1.90	30441.24715	57728.78	2363	-0.51	30441.24715	-15632.19	2363	-2.41	30441.24715	-73360.97033
2417	1.97	33669.24666	66217.11	2392	-1.26	33669.24666	-42298.34	2392	-3.22	33669.24666	-108515.4431
2434	1.82	37006.08635	67180.85	2434	-1.02	37006.08635	-37667.39	2434	-2.83	37006.08635	-104848.2343
2462	3.38	82865.14259	280416.51	2462	0.16	82865.14259	12990.86	2462	-3.23	82865.14259	-267425.6478
2581	2.98	129164.3998	384448.04	2581	0.70	129164.3998	89996.68	2581	-2.28	129164.3998	-294451.3659
2600	3.98	55128.1649	219572.81	2600	0.70	55128.1649	38411.14	2600	-3.29	55128.1649	-181161.6747
2626	4.17	51121.85177	213218.89	2626	0.90	51121.85177	46008.78	2626	-3.27	51121.85177	-167210.1148
2660	4.03	54593.61899	219919.13	2660	0.98	54593.61899	53571.15	2660	-3.05	54593.61899	-166347.98
2679	3.16	107562.7101	339499.24	2679	0.84	107562.7101	89934.56	2679	-2.32	107562.7101	-249564.6726
	TOTAL	642533.1925	1965001.55		TOTAL	642533.1925	121065.97		TOTAL	642533.1925	-1843935.584
		Average b_n	**3.06**			**Average b_n**	**0.19**			**Average b_s**	**-2.87**

Balance **27-Jun-10**

Location	Elevation (m)	Depth (cm)	Depth (m)	SWE	Area (m^2)	Bn
Sound 1	2296	575.5	5.75	2.83	11433.05540	32346.01923
Sound 2	2325	342	3.42	1.68	24146.66148	40632.53214
Sound 3	2351	346	3.46	1.70	25401.00728	43243.19018
Sound 4	2382	366	3.66	1.80	30441.24715	54819.39198
Sound 5	2417	368	3.68	1.81	33669.24666	60963.78262
Sound 6	2434	405	4.05	1.99	37006.08635	73742.67186
Sound 7	2462	619	6.19	3.04565942	82865.14259	252379.0021
Sound 9	2581	484	4.84	2.430363913	129164.39978	313916.4961
Pit	2600	699	6.99	3.509967717	55128.16490	193498.0791
Sound 10	2626	728	7.28	3.655588696	51121.85177	186880.4634
Sound 11	2660	706	7.06	3.545117609	54593.61899	193540.8
Sound 12	2679	502	5.02	2.520749348	107562.71013	271138.6314
				Total	642533.1925	1717101.06
				Average b_n	**2.67**	

Balance **26-Jul-10**

Location	Elevation (m)	Depth (cm)	Depth (m)	SWE	Area (m^2)	Bn
Sound 1	2296	215	2.15	1.151192982	11433.05540	13161.65314
Sound 2	2325	128	1.28	0.685361404	24146.66148	16549.1898
Sound 3	2351	102.5	1.025	0.548824561	25401.00728	13940.69668
Sound 4	2382	154	1.54	0.824575439	30441.24715	25101.10472
Sound 5	2417	172	1.72	0.920954386	33669.24666	31007.84038
Sound 6	2434	266	2.66	1.424266667	37006.08635	52706.53526
Sound 7	2462	468	4.68	2.505852632	82865.14259	207647.8356
Sound 9	2581	412	4.12	2.116821667	129164.39978	273418
Pit	2600	614	6.14	3.154680833	55128.16490	173911.7652
Sound 10	2626	701	7.01	3.601679583	51121.85177	184124.5298
Sound 11	2660	619	6.19	3.180370417	54593.61899	173627.9308
Sound 12	2679	421	4.21	2.163062917	107562.71013	232664.9095
				Total	642533.1925	1397861.991
				Average b_n	**2.18**	

Balance **28-Aug-10**

Location	Elevation (m)	Depth (cm)	Depth (m)	m.w.e	Elevation	m.w.e	Area (m^2)	Bn
ABS 1	2294	-32	-0.32	-0.29344				
ABS 4	2295	88	0.88	0.80696				
ABS 5	2329	96	0.96	0.88032	2294.5	0.25676	11433.0554	2935.551304
ABS 2	2335	-216	-2.16	-1.98072	2332	-0.5502	24146.66148	-13285.49315
ABS 3	2346	-227	-2.27	-2.08159				
ABS 6	2355	-23	-0.23	-0.21091	2350.5	-1.14625	25401.00728	-29115.9046
ABS 8	2392	-32	-0.32	-0.29344	2392	-0.29344	64110.49381	-18812.5833
Sound 6	2434	28	0.28	0.149247179	2434	0.149247179	37006.08635	5523.054012
Sound 7	2462	281	2.81	1.497802051	2462	1.497802051	82865.14259	124115.5805
Sound 9	2581	195	1.95	1.0394	2581	1.0394	129164.3998	134253.4771
Sound 10	2626	185	1.85	0.986097436	2626	0.986097436	106250.0167	104772.869
Sound 12	2679	177	1.77	0.943455385	2679	0.943455385	162156.3291	152987.2619
						Total	642533.1925	473723.7546
						Average b_n	**0.74**	

Elevation	Area
2294.5	11433.0554
2332	24146.66148
2350.5	25401.00728
2363	30441.24715
2392	33669.24666
2434	37006.08635
2462	82865.14259
2581	129164.3998
2600	55128.1649
2626	51121.85177
2660	54593.61899
2679	107562.7101

Balance **25-Sep-10**

Location	Elevation (m)	Depth (cm)	Depth (m)	m.w.e	Elevation	m.w.e	Area (m^2)	Bn
ABS 1	2294	-60	-0.6	-0.5502				
ABS 4	2295	25	0.25	0.22925				
ABS 5	2329	-12	-0.12	-0.11004	2294.5	-0.160475	11433.0554	-1834.719565
ABS 2	2335	-290	-2.9	-2.6593	2332	-1.38467	24146.66148	-33435.15775
ABS 3	2346	-313	-3.13	-2.87021				
ABS 6	2355	-126	-1.26	-1.15542	2350.5	-2.012815	25401.00728	-51127.52848
ABS 7	2363	-36	-0.36	-0.33012	2363	-0.33012	30441.24715	-10049.26451
ABS 8	2392	-100	-1	-0.917	2392	-0.917	33669.24666	-30874.69919
ABS 9	2434	-74	-0.74	-0.67858	2434	-0.67858	37006.08635	-25111.59008
Sound 7	2462	76	0.76	0.428754973	2462	0.428754973	82865.14259	35528.84197
Sound 9	2581	122	1.22	0.688264562	2581	0.688264562	129164.3998	88899.27901
Pit	2600	122	1.22	0.688264562	2600	0.688264562	55128.1649	37942.76226
Sound 10	2626	172	1.72	0.970340202	2626	0.970340202	51121.85177	49605.58796
Sound 11	2660	233	2.33	1.314472483	2660	1.314472483	54593.61899	71761.8099
Sound 12	2679	167.5	1.675	0.944953394	2679	0.944953394	107562.7101	101641.748
						Total	642533.1925	232947.0696
						Average b_n	**0.36**	

Figure A1 1910-2010 ELA Reconstructions

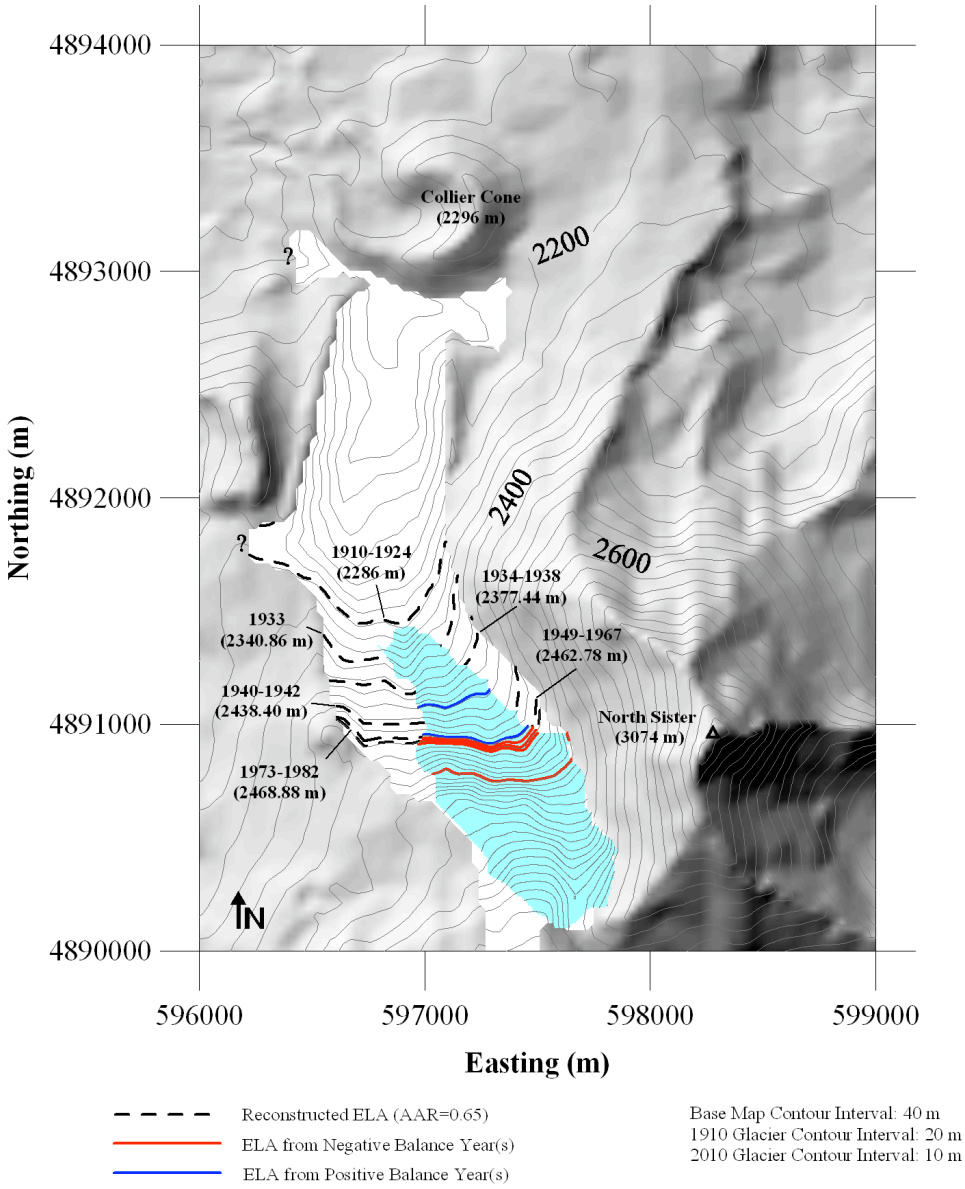

Figure A1: Shaded relief topographic map showing the reconstructed ELA positions of the Collier Glaicer, as well as ELA positions from the mass-balance measurements. *1910-1994 ELA positions from McDonald (1995).*

Appendix B Automated Weather Stations

Since the Collier Glacier is located in a protected wilderness area, all field equipment needed to be hauled in by foot. As a result, traditional approaches to automated weather stations were not possible due to the fact that no mechanized vehicles are allowed in a protected wilderness area. In response, all the towers used for the automated weather stations were hand built to minimize weight and maximize portability.

Figure B1 Moraine AWS

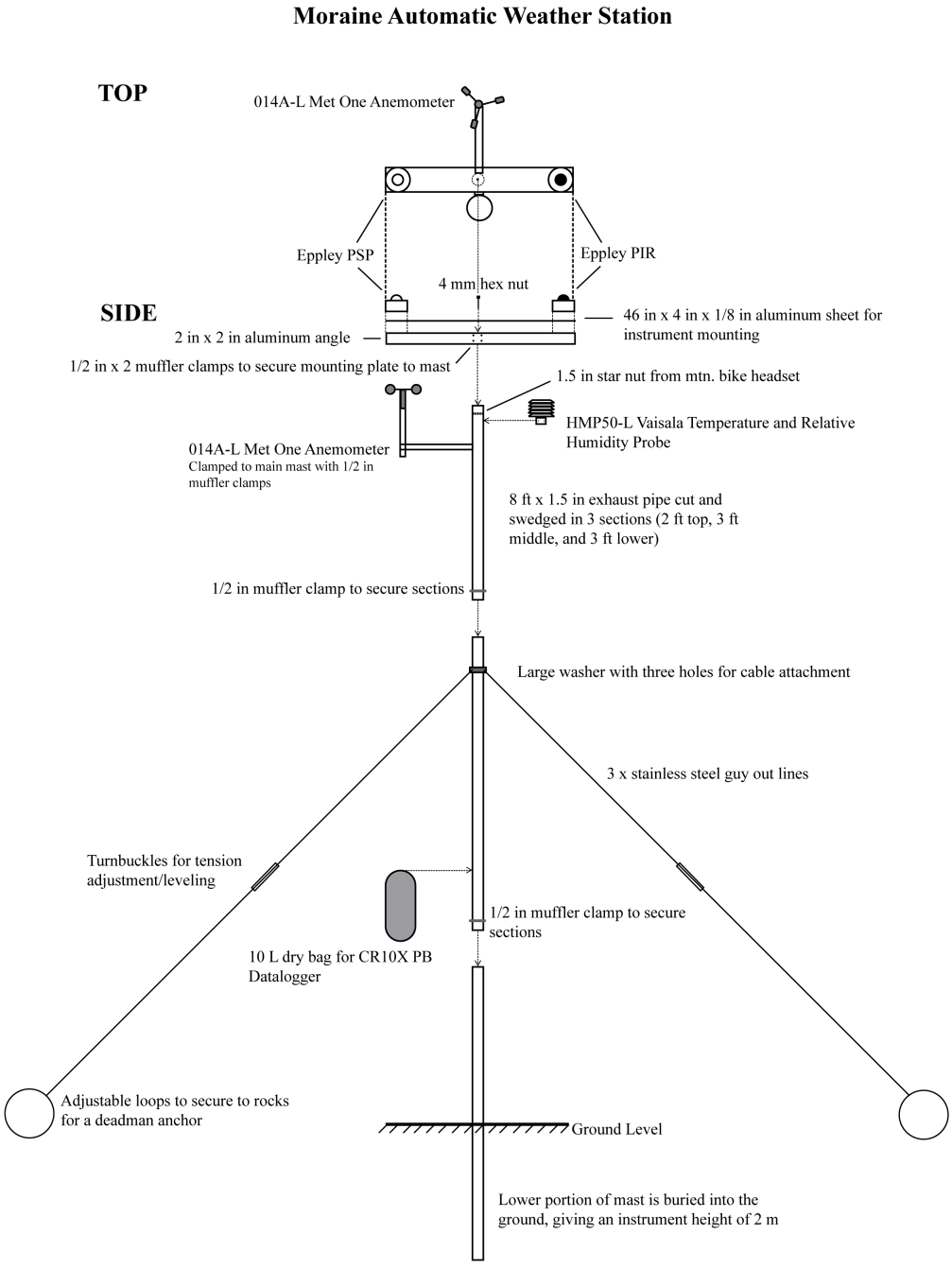

Figure B1: Schematic showing the construction of the moraine AWS.

Figure B2 On Snow AWS

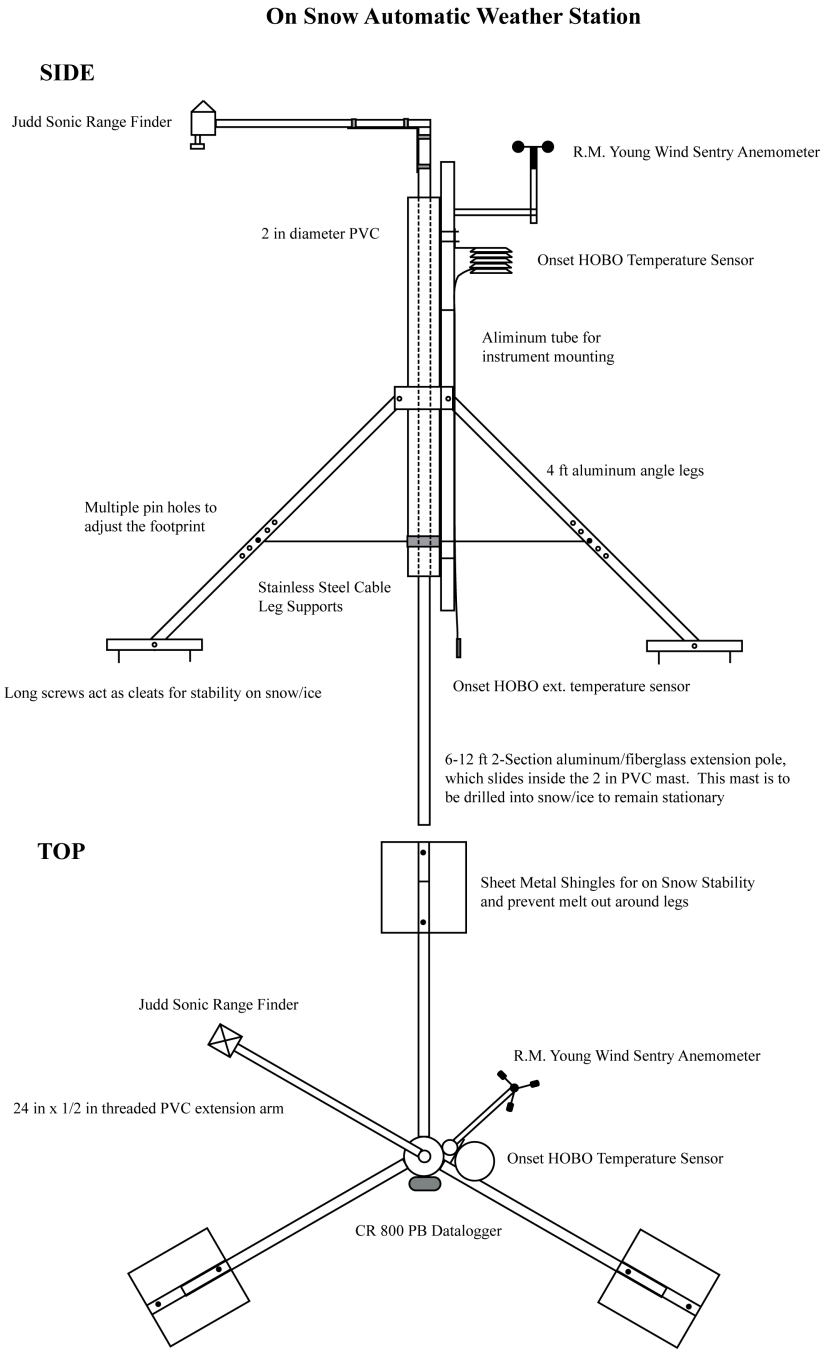

Figure B2: Schematic showing the construction of the on snow AWS.

Appendix C Model Calibration

Coarse calibration of the OSU SEBM started with secularly adjusting each input parameter independently within their respected literature ranges, while holding all other input parameters constant. This process was carried out for each parameter to achieve a best fit between the time series of modeled and measured average net balance, and net balance for each individual stake measurement. The value of the coefficient of determination was used as an indicator of the quality of fit between the measured and modeled net balances for each stake location. The order at which each parameters was calibrated depended on the model's sensitivity, thus parameters that were most sensitive were adjusted first. For finer tuning, the model's various parameters were secularly adjusted independently around a control value determined through the course calibration process to achieve an optimal least squares fit with the model and measured ablation. An optimal value was chosen as a balance between the highest R^2 value from the least squares fit of the modeled verses measured ablation, as well as achieving a least squares slope that approached the 1:1 line between the measured and modeled ablation for each individual stake. The slope of this fit was also compared to this 1:1 line as a gauge for model under/overestimation.

Table C1 Bulk method meteorological sensitivity tests

SW_in	Factor	% Change		Net Balance (m w.e)	Measured Net Balance (m w.e)	Stk R^2	Least Squares Slope	Net SW Mean	Notes
	1.5	50%	50	-1.34		0.19	0.796493	0.522980594	115.534	
	1.4	40%	40	-1.02		0.19	0.794814	0.556117589	106.568	
	1.3	30%	30	-0.72		0.19	0.794272	0.592377574	97.9217	
	1.2	20%	20	-0.42		0.19	0.793863	0.632062565	89.4447	Shiftine above the 1:1 line
	1.1	10%	10	-0.12		0.19	0.789567	0.6764201 36	81.1019	
	1	0%	0	0.18		0.19	0.781814	0.724317867	72.9036	control
	0.9	-10%	-10	0.46		0.19	0.775187	0.777883588	64.8969	
	0.8	-20%	-20	0.74		0.19	0.767723	0.833935991	57.0409	
	0.7	-30%	-30	1.01		0.19	0.755133	0.895363933	49.3309	
	0.6	-40%	-40	1.26		0.19	0.740999	0.942081545	42.2546	Least squares falls below the 1:1
	0.5	-50%	-50	1.48		0.19	0.721782	0.985588959	35.7982	

LW_in	Factor	% Change		Net Balance (m w.e)	Measured Net Balance (m w.e)	Stk R^2	Least Squares Slope	Net LW Mean	Notes
	1.5	50%	50	-4.38		0.19	0.807134	0.408928015	97.7708	
	1.4	40%	40	-3.4		0.19	0.810501	0.451233315	72.802	Least squares falls above the 1:1 line
	1.3	30%	30	-2.44		0.19	0.81293	0.501393432	47.8332	
	1.2	20%	20	-1.52		0.19	0.809631	0.561969828	22.8645	
	1.1	10%	10	-0.64		0.19	0.801134	0.636803621	-2.19423	
	1	0%	0	0.18		0.19	0.781814	0.724317867	-27.073	control
	0.9	-10%	-10	0.85		0.19	0.756703	0.825895712	-52.0416	
	0.8	-20%	-20	1.43		0.19	0.717482	0.931003934	-77.0105	Least squares falls below the 1:1 line
	0.7	-30%	-30	1.91		0.19	0.669985	1.018942281	-101.979	
	0.6	-40%	-40	2.3		0.19	0.610225	1.055247269	-126.948	
	0.5	-50%	-50	2.61		0.19	0.545891	1.065475378	-151.917	

Precip_Factor	Factor	% Change		Net Balance (m w.e)	Measured Net Balance (m w.e)	Stk R^2	Least Squares Slope	Hs Mean	Ht Mean	Notes
	1.5	50%	50	1.88		0.19	0.737644	0.670916521	40.69	-7.82091
	1.4	40%	40	1.54		0.19	0.748051	0.684173869	40.5688	-7.82722
	1.3	30%	30	1.21		0.19	0.758598	0.70087555	40.4512	-7.82649
	1.2	20%	20	0.87		0.19	0.767138	0.718454073	40.3296	-7.81483
	1.1	10%	10	0.52		0.19	0.775102	0.739279601	40.2172	-7.80412
	1	0%	0	0.18		0.19	0.781814	0.724317867	40.1288	-7.80945 control
	0.9	-10%	-10	-0.17		0.19	0.791707	0.738985369	40.0443	-7.81423
	0.8	-20%	-20	-0.53		0.19	0.794682	0.731717768	39.8521	-7.80596
	0.7	-30%	-30	-0.88		0.19	0.797994	0.731215126	39.5251	-7.84464 Least squares above 1:1
	0.6	-40%	-40	-1.26		0.19	0.798899	0.727062393	39.0548	-7.81837
	0.5	-50%	-50	-1.65		0.19	0.803158	0.724292445	38.4154	-7.7669

RH	Factor	% Change		Net Balance (m w.e)	Measured Net Balance (m w.e)	Stk R^2	Least Squares Slope	Hs Mean	Ht Mean	Notes
	1.5	50%	50	-0.57		0.19	0.804991	0.644152253	39.8681	16.7839
	1.4	40%	40	-0.45		0.19	0.803018	0.656606262	39.9461	12.8872
	1.3	30%	30	-0.31		0.19	0.799745	0.670862599	40.0137	8.4988
	1.2	20%	20	-0.16		0.19	0.795886	0.686885821	40.0591	3.58804
	1.1	10%	10	0.01		0.19	0.789972	0.704403075	40.0927	-1.79826
	1	0%	0	0.18		0.19	0.781814	0.724317867	40.1288	-7.80945 control
	0.9	-10%	-10	0.4		0.19	0.774582	0.743248314	40.1955	-15.742
	0.8	-20%	-20	0.69		0.19	0.766744	0.802363159	40.2985	-26.1576
	0.7	-30%	-30	0.95		0.19	0.751763	0.842890647	40.4206	-36.9879
	0.6	-40%	-40	1.2		0.19	0.737943	0.882595302	40.5652	-48.018 Least squares below 1:1
	0.5	-50%	-50	1.42		0.19	0.717588	0.919374046	40.7343	-59.1941

Wind	Factor	% Change		Net Balance (m w.e)	Measured Net Balance (m w.e)	Stk R^2	Least Squares Slope	Hs Mean	Ht Mean	Notes
	1.5	50%	50	-1.09		0.19	0.815954	0.562152322	73.2448	-11.9666
	1.4	40%	40	-0.84		0.19	0.809236	0.606125315	66.8072	-11.1413
	1.3	30%	30	-0.59		0.19	0.806627	0.631579792	60.3113	-10.1267
	1.2	20%	20	-0.34		0.19	0.803956	0.65913597	53.6051	-9.32911
	1.1	10%	10	-0.08		0.19	0.793073	0.692027056	46.9308	-8.68988
	1	0%	0	0.18		0.19	0.781814	0.724317867	40.1288	-7.80945 control
	0.9	-10%	-10	0.43		0.19	0.771334	0.762760879	33.3785	-6.89104
	0.8	-20%	-20	0.66		0.19	0.761746	0.80456644	26.7646	-5.93326
	0.7	-30%	-30	0.89		0.19	0.748411	0.844951932	20.3924	-4.95639
	0.6	-40%	-40	1.09		0.19	0.734298	0.888306466	14.4191	-3.85495
	0.5	-50%	-50	1.26		0.19	0.717831	0.919259507	9.09944	-2.7646

Wind_Above_ELA	Factor	% Change		Net Balance (m w.e)	Measured Net Balance (m w.e)	Stk R^2	Least Squares Slope	Hs Mean	Ht Mean	Notes
	1.5	50%	50	-0.52		0.19	0.8059	0.758862325	60.0425	-10.8183
	1.4	40%	40	-0.38		0.19	0.803795	0.75433664	56.1024	-10.2173
	1.3	30%	30	-0.24		0.19	0.800228	0.748317039	52.3024	-9.63994
	1.2	20%	20	-0.1		0.19	0.795275	0.741471611	48.3068	-9.05988
	1.1	10%	10	0.04		0.19	0.789067	0.731828393	44.2224	-8.4405
	1	0%	0	0.18		0.19	0.781814	0.724317867	40.1288	-7.80945 control
	0.9	-10%	-10	0.31		0.19	0.773807	0.714823668	36.0674	-7.14753
	0.8	-20%	-20	0.43		0.19	0.765573	0.705182165	32.0828	-6.45586
	0.7	-30%	-30	0.55		0.19	0.757354	0.69581881	28.2399	-5.72154
	0.6	-40%	-40	0.65		0.19	0.749724	0.687276685	24.635	-4.9666
	0.5	-50%	-50	0.73		0.19	0.742518	0.679501094	21.4146	-4.20255

Wind_Below_ELA	Factor	% Change		Net Balance (m w.e)	Measured Net Balance (m w.e)	Stk R^2	Least Squares Slope	Hs Mean	Ht Mean	Notes
	1.5	50%	50	-0.4		0.19	0.786609	0.55278 3943	53.331	-8.95782
	1.4	40%	40	-0.29		0.19	0.783004	0.580463595	50.7436	-8.73349
	1.3	30%	30	-0.18		0.19	0.785991	0.610304497	48.1377	-8.4963
	1.2	20%	20	-0.06		0.19	0.787577	0.643727905	45.5169	-8.27866
	1.1	10%	10	0.06		0.19	0.785617	0.68177601	42.8371	-8.05287
	1	0%	0	0.18		0.19	0.781814	0.724317867	40.1288	-7.80945 control
	0.9	-10%	-10	0.3		0.19	0.77917	0.772978281	37.4398	-7.55309
	0.8	-20%	-20	0.41		0.19	0.777731	0.826913484	34.8107	-7.28692
	0.7	-30%	-30	0.52		0.19	0.77237	0.88312936	32.2812	-7.00946
	0.6	-40%	-40	0.62		0.19	0.765591	0.938093922	29.9128	-6.69764
	0.5	-50%	-50	0.7		0.19	0.755969	0.984928471	27.8135	-6.39163 Least squares below 1:1

Air_Temp	Factor	% Change		Net Balance (m w.e)	Measured Net Balance (m w.e)	Stk R^2	Least Squares Slope	Net LW Mean	Hs Mean	Ht Mean	Notes
	1.5	50%	50	-1.17		0.19	0.810701	0.592361494	-27.2522	50.1013	12.536
	1.4	40%	40	-0.93		0.19	0.806483	0.613123899	-27.228	48.4786	8.64275
	1.3	30%	30	-0.68		0.19	0.801807	0.638881855	-27.1979	46.724	4.68685
	1.2	20%	20	-0.41		0.19	0.800333	0.665908203	-27.1621	44.7707	0.618709
	1.1	10%	10	-0.12		0.19	0.79577	0.683665424	-27.1205	42.5571	-3.55801
	1	0%	0	0.18		0.19	0.781814	0.724317867	-27.073	40.1288	-7.80945 control
	0.9	-10%	-10	0.48		0.19	0.769303	0.758005578	-27.0195	37.5248	-12.1796
	0.8	-20%	-20	0.8		0.19	0.762182	0.802521834	-26.9602	34.7191	-16.7054
	0.7	-30%	-30	1.13		0.19	0.750934	0.852754928	-26.895	31.757	-21.4241 Least squares below 1:1
	0.6	-40%	-40	1.47		0.19	0.720668	0.952095862	-26.8238	28.5102	-26.3043
	0.5	-50%	-50	1.86		0.19	0.686175	1.028859387	-26.7465	24.9311	-31.402

Air_Temp_Degrees	Air Temp (°C)			Net Balance (m w.e)	Measured Net Balance (m w.e)	Stk R^2	Least Squares Slope	Net LW Mean	Hs Mean	Ht Mean	Notes
	2			-1.1		0.19	0.816326	0.632097096	-27.6032	48.7211	5.8866
	1.5			-0.81		0.19	0.815444	0.648790432	-27.5468	46.6593	0.90726
	1			-0.5		0.19	0.801614	0.667856693	-27.4406	44.5964	-2.05625
	0.5			-0.16		0.19	0.796074	0.691274946	-27.2832	42.3085	-4.98812
	0			0.18		0.19	0.781814	0.724317867	-27.073	40.1288	-7.80945 control
	-0.5			0.51		0.19	0.767981	0.773853058	-26.8094	37.9447	-10.5471
	-1			0.8		0.19	0.758295	0.834518459	-26.4922	35.8071	-13.1781
	-1.5			1.05		0.19	0.764866	0.875376878	-26.121	33.7346	-15.6875
	-2			1.27		0.19	0.754811	0.936583442	-25.6959	31.7369	-18.078 Least squares below 1:1

Air_Temp_Night	Air Temp (°C)			Net Balance (m w.e)	Measured Net Balance (m w.e)	Stk R^2	Least Squares Slope	Net LW Mean	Hs Mean	Ht Mean	Notes
	2			-0.47		0.19	0.800756	0.65458 7011	-27.5129	43.9235	-9.744899
	1.5			-0.3		0.19	0.798005	0.668145079	-27.4441	44.4967	-2.57585
	1			-0.13		0.19	0.78537	0.684500436	-27.3473	43.0406	-4.35896
	0.5			0.03		0.19	0.804598	0.7140252 8	-27.2234	41.5886	-6.11979
	0			0.18		0.19	0.781814	0.724317867	-27.073	40.1288	-7.80945 control
	-0.5			0.38		0.19	0.792297	0.764237078	-26.9618	39.17	-9.16762
	-1			0.55		0.19	0.777452	0.786393133	-26.8288	38.2168	-10.4635
	-1.5			0.69		0.19	0.779329	0.816234489	-26.6495	37.2874	-11.7084
	-2			0.81		0.19	0.75452	0.844843954	-26.4511	36.3772	-12.9066

Air_Temp_Day	Air Temp (°C)			Net Balance (m w.e)	Measured Net Balance (m w.e)	Stk R^2	Least Squares Slope	Net LW Mean	Hs Mean	Ht Mean	Notes
	2			-0.57		0.19	0.80772	0.667056957	-27.2107	44.2431	-2.61122
	1.5			-0.4		0.19	0.799029	0.676687465	-27.2183	43.244	-3.50789
	1			-0.22		0.19	0.795652	0.68957394	-27.1995	42.2152	-4.98153
	0.5			-0.03		0.19	0.803111	0.704433893	-27.1521	41.1607	-6.42006
	0			0.18		0.19	0.781814	0.724317867	-27.073	40.1288	-7.80945 control
	-0.5			0.38		0.19	0.792297	0.764237078	-26.9618	39.17	-9.16762
	-1			0.55		0.19	0.777452	0.786393133	-26.8288	38.2168	-10.4635
	-1.5			0.69		0.19	0.779329	0.816234489	-26.6495	37.2874	-11.7084
	-2			0.81		0.19	0.75452	0.844843954	-26.4511	36.3772	-12.9066

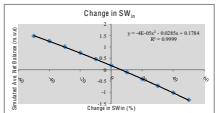

SW Sensitivity
y=-0.0008x-0.0285
Slope= -0.0285 x=0

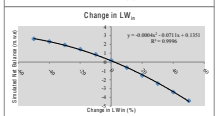

LW Sensitivity
y=-0.0008x-0.0711
Slope= -0.0711 x=0

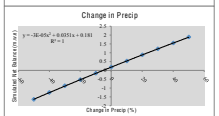

Precip Sensitivity
y=-0.0351+0.0008x
Slope= 0.0351 x=0

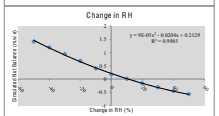

RH Sensitivity
y=-0.0008x-0.0204
Slope= -0.0204 x=0

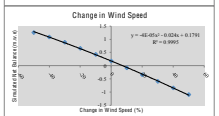

Wind Speed Sensitivity
y=-0.0008x-0.024
Slope= -0.024 x=0

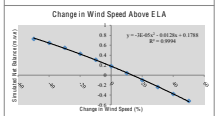

Wind Above Sensitivity
y=-0.0008x-0.0128
Slope= -0.0128 x=0

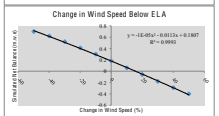

Wind Below Sensitivity
y=-0.0008x-0.0113
Slope= -0.0113 x=0

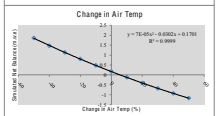

Air Temp Sensitivity
y=-0.0001x-0.0302
Slope= -0.0302 x=0

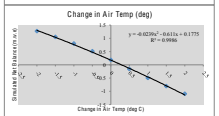

Air Temp (deg C) Sensitivity
y=-0.0239x^2-0.611x+0.1775
y=-0.0478x-0.611 x=0
Slope= -0.611

Linear
y=-0.611x+0.1378
Slope= -0.611

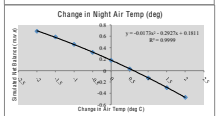

Night Air Temp (deg C) Sensitivity
y=-0.0173x^2-0.2927x+0.1811
y=-0.0346x-0.2927 x=0
Slope= -0.2927

Linear
y=-0.2927x+0.1522
Slope= -0.2927

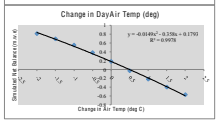

Day Air Temp (deg C) Sensitivity
y=-0.0149x^2-0.358x+0.1793
y=-0.0298x-0.358 x=0
Slope= -0.358

Linear
y=-0.358x+0.1544
Slope= -0.358

Table C2 Transfer coefficient method meteorological sensitivity tests

SW_in	Factor	% Change		Net Balance (m.w.e)	Measured Net Balance (m.w.e)	Stk R^2	Least Squares Slope	Net SW Mean	Notes
	1.5	50%	50	-1.34		0.19	0.795118	0.509934448	115.107
	1.4	40%	40	-1.03		0.19	0.793898	0.5414628	106.257
	1.3	30%	30	-0.71		0.19	0.793819	0.574669684	97.4404 Least squares fit falls above 1:1
	1.2	20%	20	-0.41		0.19	0.792995	0.613809874	89.3174
	1.1	10%	10	-0.11		0.19	0.789195	0.654726315	81.1267
	1	0%	0	0.19		0.19	0.782488	0.699085205	72.8504 control
	0.9	-10%	-10	0.48		0.19	0.77423	0.749049834	65.0513
	0.8	-20%	-20	0.77		0.19	0.766273	0.804248569	57.2134 Least squares fit falls below 1:1
	0.7	-30%	-30	1.04		0.19	0.753841	0.861540359	49.4826
	0.6	-40%	-40	1.3		0.19	0.737731	0.915687253	42.3142
	0.5	-50%	-50	1.54		0.19	0.71865	0.96712958	35.7504

LW_in	Factor	% Change		Net Balance (m.w.e)	Measured Net Balance (m.w.e)	Stk R^2	Least Squares Slope	Net LW Mean	Notes
	1.5	50%	50	-4.55		0.19	0.808203	0.356804685	97.7708
	1.4	40%	40	-3.54		0.19	0.810957	0.437105288	72.802
	1.3	30%	30	-2.54		0.19	0.813297	0.445247018	47.8332
	1.2	20%	20	-1.56		0.19	0.808505	0.542902349	22.8645 Least squares fit falls above 1:1
	1.1	10%	10	-0.64		0.19	0.800692	0.61617249	-2.19423
	1	0%	0	0.19		0.19	0.782488	0.699085205	-27.073 control
	0.9	-10%	-10	0.87		0.19	0.755916	0.796049463	-52.0416
	0.8	-20%	-20	1.47		0.19	0.711254	0.90705765	-77.0105
	0.7	-30%	-30	1.97		0.19	0.663602	1.013550635	-101.979
	0.6	-40%	-40	2.33		0.19	0.60814	1.052319943	-126.948
	0.5	-50%	-50	2.62		0.19	0.546996	1.059381823	-151.917

Precip_Factor	Factor	% Change		Net Balance (m.w.e)	Measured Net Balance (m.w.e)	Stk R^2	Least Squares Slope	Hs Mean	HI Mean	Notes
	1.5	50%	50			1.92	0.754675	0.6750705	38.3809	-4.6016
	1.4	40%	40			1.58	0.746606	0.669595539	38.4264	-4.67616
	1.3	30%	30			1.23	0.757296	0.686676044	38.4737	-4.67418 Least squares line below 1:1
	1.2	20%	20			0.88	0.787293	0.688418678	38.5195	-4.67442
	1.1	10%	10			0.54	0.774064	0.694623055	38.5636	-4.67248
	1	0%	0			0.19	0.782466	0.699696205	38.6006	-4.66652 control
	0.9	-10%	-10			-0.16	0.796993	0.704506769	38.636	-4.65951
	0.8	-20%	-20			-0.52	0.793859	0.707853916	38.7014	-4.65382 Least squares line above 1:1
	0.7	-30%	-30			-0.89	0.795566	0.70585094	38.825	-4.63564
	0.6	-40%	-40			-1.29	0.797358	0.70894078	38.9921	-4.63239
	0.5	-50%	-50			-1.71	0.799646	0.695396726	39.2182	-4.63089

RH	Factor	% Change		Net Balance (m.w.e)	Measured Net Balance (m.w.e)	Stk R^2	Least Squares Slope	Hs Mean	HI Mean	Notes
	1.5	50%	50	-0.53		0.19	0.802536	0.615516603	38.4832	18.3584
	1.4	40%	40	-0.41		0.19	0.800578	0.628640536	38.6614	14.6433
	1.3	30%	30	-0.28		0.19	0.797507	0.643498376	38.6431	10.4935 Least squares line above 1:1
	1.2	20%	20	-0.13		0.19	0.79342	0.659665521	38.6285	5.88499
	1.1	10%	10	0.02		0.19	0.788161	0.678268051	38.6155	0.9621199
	1	0%	0	0.19		0.19	0.782466	0.699696205	38.6006	-4.66652 control
	0.9	-10%	-10	0.39		0.19	0.775133	0.73256948	38.5764	-11.516
	0.8	-20%	-20	0.63		0.19	0.767406	0.784488071	38.5438	-19.9417
	0.7	-30%	-30	0.85		0.19	0.75879	0.803768109	38.5055	-28.6319
	0.6	-40%	-40	1.08		0.19	0.744822	0.84024287	38.4641	-37.435
	0.5	-50%	-50	1.29		0.19	0.72881	0.8800794	38.415	-46.2944

Wind	Factor	% Change		Net Balance (m.w.e)	Measured Net Balance (m.w.e)	Stk R^2	Least Squares Slope	Hs Mean	HI Mean	Notes
	1.5	50%	50	-0.55		0.19	0.803005	0.607503191	58.028	-6.96881
	1.4	40%	40	-0.4		0.19	0.800727	0.623902171	54.1225	-6.52271
	1.3	30%	30	-0.25		0.19	0.79372	0.640977745	50.2321	-6.08783
	1.2	20%	20	-0.1		0.19	0.792794	0.659132481	46.3514	-5.59426 Least squares line above 1:1
	1.1	10%	10	0.04		0.19	0.787849	0.678955917	42.4751	-5.10807
	1	0%	0	0.19		0.19	0.782466	0.699696205	38.6006	-4.66652 control
	0.9	-10%	-10	0.33		0.19	0.776373	0.721549551	34.7273	-4.20218
	0.8	-20%	-20	0.48		0.19	0.770158	0.745441779	30.8553	-3.73725
	0.7	-30%	-30	0.62		0.19	0.76462	0.77207721	26.9849	-3.27696
	0.6	-40%	-40	0.76		0.19	0.757863	0.799246614	23.1161	-2.804
	0.5	-50%	-50	0.9		0.19	0.748769	0.826313168	19.2501	-2.3368

Wind_Above_ELA	Factor	% Change		Net Balance (m.w.e)	Measured Net Balance (m.w.e)	Stk R^2	Least Squares Slope	Hs Mean	HI Mean	Notes
	1.5	50%	50	-0.19		0.19	0.800196	0.732296693	69.6877	-6.4043
	1.4	40%	40	-0.11		0.19	0.797262	0.717476322	67.4621	-6.05552
	1.3	30%	30	-0.03		0.19	0.793997	0.713364712	65.2444	-5.70787
	1.2	20%	20	0.04		0.19	0.789628	0.709031698	63.0292	-5.36055
	1.1	10%	10	0.11		0.19	0.784052	0.704473367	60.8149	-5.01339
	1	0%	0	0.19		0.19	0.782466	0.699696205	38.6006	-4.66652 control
	0.9	-10%	-10	0.26		0.19	0.778145	0.694702622	56.3865	-4.31922
	0.8	-20%	-20	0.33		0.19	0.773611	0.689703871	34.1723	-3.97217
	0.7	-30%	-30	0.4		0.19	0.768932	0.68452421	31.9582	-3.62498
	0.6	-40%	-40	0.47		0.19	0.764112	0.679266622	29.7439	-3.27862
	0.5	-50%	-50	0.54		0.19	0.758094	0.673863984	27.5299	-2.93089

Wind_Below_ELA	Factor	% Change		Net Balance (m.w.e)	Measured Net Balance (m.w.e)	Stk R^2	Least Squares Slope	Hs Mean	HI Mean	Notes
	1.5	50%	50	-0.17		0.19	0.784275	0.589454092	66.9812	-5.35066
	1.4	40%	40	-0.1		0.19	0.785352	0.608559881	45.2611	-5.13338
	1.3	30%	30	-0.03		0.19	0.785389	0.628819784	43.5083	-5.01627
	1.2	20%	20	0.04		0.19	0.784718	0.650536427	41.9228	-4.9001
	1.1	10%	10	0.12		0.19	0.783714	0.674279907	40.2699	-4.78297
	1	0%	0	0.19		0.19	0.782466	0.699696205	38.6006	-4.66652 control
	0.9	-10%	-10	0.26		0.19	0.780801	0.726693149	36.9415	-4.54929
	0.8	-20%	-20	0.33		0.19	0.778994	0.756446521	35.2837	-4.43147
	0.7	-30%	-30	0.4		0.19	0.776172	0.788759711	33.6275	-4.31229
	0.6	-40%	-40	0.48		0.19	0.776324	0.82463449	31.9728	-4.19255
	0.5	-50%	-50	0.55		0.19	0.77231	0.866861322		

Air_Temp	Factor	% Change		Net Balance (m.w.e)	Measured Net Balance (m.w.e)	Stk R^2	Least Squares Slope	Net LW Mean	Hs Mean	HI Mean	Notes
	1.5	50%	50	-1.67		0.19	0.813182	0.523071872	-27.2522	58.4505	19.0156
	1.4	40%	40	-1.27		0.19	0.809059	0.550426775	-27.228	54.4263	13.7107
	1.3	30%	30	-0.89		0.19	0.803717	0.578236688	-27.1979	50.4147	8.70489
	1.2	20%	20	-0.52		0.19	0.800816	0.614391077	-27.1621	46.4256	3.99609
	1.1	10%	10	-0.17		0.19	0.794724	0.650769062	-27.1205	42.5065	-0.45089
	1	0%	0	0.19		0.19	0.782466	0.699696205	-27.073	38.6006	-4.66632 control
	0.9	-10%	-10	0.53		0.19	0.767938	0.743539199	-27.0195	34.7013	-8.65589
	0.8	-20%	-20	0.87		0.19	0.758076	0.796777289	-26.9602	30.7955	-12.4355
	0.7	-30%	-30	1.22		0.19	0.74435	0.877526576	-26.895	26.8852	-16.0271
	0.6	-40%	-40	1.57		0.19	0.738747	0.964943338	-26.8238	22.9798	-19.4325
	0.5	-50%	-50	1.93		0.19	0.677717	1.045081608	-26.7465	19.1099	-22.6658

Air_Temp_Degrees	Air Temp (°C)			Net Balance (m.w.e)	Measured Net Balance (m.w.e)	Stk R^2	Least Squares Slope	Net LW Mean	Hs Mean	HI Mean	Notes
	2			-1.15		0.19	0.815941	0.60526283	-27.6032	58.2476	5.63614
	1.5			-0.83		0.19	0.804314	0.626828284	-27.5468	47.1956	2.8522
	1			-0.5		0.19	0.801306	0.645317429	-27.4406	44.2187	0.201705
	0.5			-0.15		0.19	0.79608	0.66590624	-27.2832	41.3578	-2.30032
	0			0.19		0.19	0.782466	0.699696205	-27.073	38.6006	-4.66632 control
	-0.5			0.52		0.19	0.787377	0.74917061	-26.8094	35.9154	-6.88039
	-1			0.82		0.19	0.767707	0.795978232	-26.4922	33.3234	-8.94846
	-1.5			1.07		0.19	0.761999	0.852881505	-26.121	30.8253	-10.8729
	-2			1.3		0.19	0.751616	0.919182902	-25.6939	28.4228	-12.6513

Air_Temp_Night	Air Temp (°C)			Net Balance (m.w.e)	Measured Net Balance (m.w.e)	Stk R^2	Least Squares Slope	Net LW Mean	Hs Mean	HI Mean	Notes
	2			-0.42		0.19	0.799559	0.633096648	-27.5129	45.1569	0.630617
	1.5			-0.26		0.19	0.79647	0.64613923	-27.4441	43.4524	-0.86516
	1			-0.1		0.19	0.794318	0.661749982	-27.3473	41.7924	-2.16835
	0.5			0.05		0.19	0.802789	0.683774075	-27.2234	40.1725	-3.4535
	0			0.19		0.19	0.782466	0.699696205	-27.073	38.6006	-4.66632 control
	-0.5			0.32		0.19	0.779343	0.712892971	-26.8971	37.0724	-5.80562
	-1			0.45		0.19	0.775114	0.726875168	-26.6941	35.5901	-6.86901
	-1.5			0.57		0.19	0.775239	0.747898411	-26.4617	34.15	-7.84963
	-2			0.66		0.19	0.772539	0.772290908	-26.1991	32.7711	-8.74625

Air_Temp_Day	Air Temp (°C)			Net Balance (m.w.e)	Measured Net Balance (m.w.e)	Stk R^2	Least Squares Slope	Net LW Mean	Hs Mean	HI Mean	Notes
	2			-0.63		0.19	0.808956	0.63600958	-27.2189	44.3378	1.17193
	1.5			-0.43		0.19	0.799669	0.647782147	-27.2244	42.9952	-0.39827
	1			-0.24		0.19	0.786596	0.662189673	-27.2036	41.4803	-1.89405
	0.5			-0.03		0.19	0.802429	0.688882222	-27.1542	40.0203	-3.31778
	0			0.19		0.19	0.782466	0.699696205	-27.073	38.6006	-4.66632 control
	-0.5			0.41		0.19	0.791539	0.739833057	-26.9598	37.2125	-5.92623
	-1			0.58		0.19	0.774718	0.765981501	-26.8162	35.8823	-7.11089
	-1.5			0.74		0.19	0.771517	0.797788382	-26.6435	34.6075	-8.21714
	-2			0.86		0.19	0.770915	0.827885893	-26.4433	33.3859	-9.24593

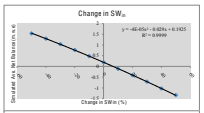

SW Sensitivity
y=-0.0000lx-0.029
Slope= -0.029 x=0

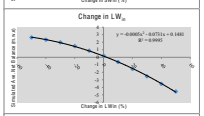

LW Sensitivity
y=-0.001x-0.0731
Slope= -0.0731 x=0

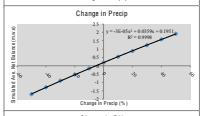

Precip Sensitivity
y=0.0559+0.0000lx
Slope= 0.0559 x=0

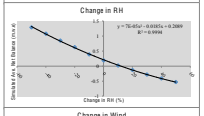

RH Sensitivity
y=0.0001lx-0.0185
Slope= -0.0185 x=0

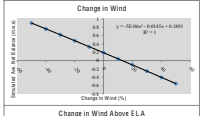

Wind Sensitivity
y=-0.0000lx-0.0145
Slope= -0.0145 x=0

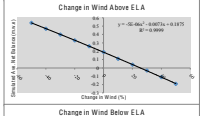

Wind Above E.L.A Sensitivity
y=-0.0000lx-0.0073
Slope= -0.0073 x=0

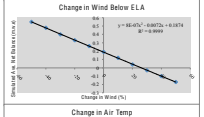

Wind Below E.L.A Sensitivity
y=0.0000lx-0.0072
Slope= -0.0072 x=0

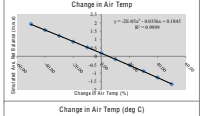

Air Temp Sensitivity
y=-0.0000lx-0.0356
Slope= -0.0356 x=0

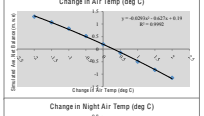

Air Temp (deg C) Sensitivity
y=-0.0291x²-0.627x+0.19
y'=-0.0586x-0.627 x=0
Slope= -0.627

Linear
y=-0.627x-0.1411
Slope= -0.627

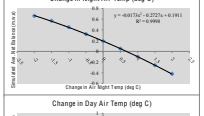

Night Air Temp (deg C) Sensitivity
y=-0.0173x²-0.2727x+0.1911
y'=-0.0346x-0.2727 x=0
Slope= -0.2727

Linear
y=-0.2727x+0.1622
Slope= -0.2727

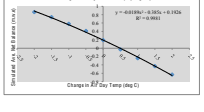

Day Air Temp (deg C) Sensitivity
y=-0.0189x²-0.385x+0.1926
y'=-0.0378x-0.385 x=0
Slope= -0.385

Linear
y=-0.385x+0.1611
Slope= -0.385

Table C3 PDD meteorological sensitivity tests

Precip_Factor	Factor	% Change		Net Balance (m.w.e)	Measured Net Balance (m.w.e)	Stk R^2	Least Squares Slope	Notes
	1.5	50%	50	1.79	0.19	0.767802	0.695692676	
	1.4	40%	40	1.47	0.19	0.778771	0.719448822	
	1.3	30%	30	1.15	0.19	0.78952	0.743378965	
	1.2	20%	20	0.83	0.19	0.799726	0.767426958	
	1.1	10%	10	0.51	0.19	0.809123	0.791641644	
control	1	0%	0	0.19	0.19	0.817491	0.815743674	
	0.9	-10%	-10	-0.13	0.19	0.824591	0.839527439	
	0.8	-20%	-20	-0.47	0.19	0.830057	0.86246372	
	0.7	-30%	-30	-0.8	0.19	0.83361	0.884198723	
	0.6	-40%	-40	-1.15	0.19	0.834609	0.904223836	
	0.5	-50%	-50	-1.5	0.19	0.833025	0.922403715	

Air_Temp	Factor	% Change		Net Balance (m.w.e)	Measured Net Balance (m.w.e)	Stk R^2	Least Squares Slope	Notes
	1.5	50%	50	-1.7	0.19	0.836383	0.592128023	
	1.4	40%	40	-1.32	0.19	0.836173	0.628950668	
	1.3	30%	30	-0.94	0.19	0.834432	0.668592528	
	1.2	20%	20	-0.56	0.19	0.831718	0.714631507	
	1.1	10%	10	-0.18	0.19	0.826172	0.762740165	
control	1	0%	0	0.19	0.19	0.817491	0.815743674	
	0.9	-10%	-10	0.56	0.19	0.803523	0.874114775	
	0.8	-20%	-20	0.94	0.19	0.787135	0.94262851	
	0.7	-30%	-30	1.32	0.19	0.762362	1.023640129	
	0.6	-40%	-40	1.7	0.19	0.72006	1.09160213	
	0.5	-50%	-50	2.1	0.19	0.661132	1.140300983	

Air_Temp_Degrees	Air Temp (°C)		Net Balance (m.w.e)	Measured Net Balance (m.w.e)	Stk R^2	Least Squares Slope	Notes
	2		-1.08	0.19	0.838823	0.697510973	
	1.5		-0.76	0.19	0.833181	0.725442044	
	1		-0.44	0.19	0.830362	0.755299995	
	0.5		-0.12	0.19	0.825258	0.785999733	
control	0		0.19	0.19	0.817491	0.815743674	
	-0.5		0.49	0.19	0.815059	0.859762657	
	-1		0.77	0.19	0.79872	0.900772093	
	-1.5		1.03	0.19	0.788219	0.945583712	
	-2		1.26	0.19	0.773808	0.995278993	

Air_Temp_Night	Air Temp (°C)		Net Balance (m.w.e)	Measured Net Balance (m.w.e)	Stk R^2	Least Squares Slope	Notes
	2		-0.44	0.19	0.831737	0.748048738	
	1.5		-0.28	0.19	0.828825	0.765010162	
	1		-0.12	0.19	0.825428	0.781062989	
	0.5		0.04	0.19	0.822598	0.798942863	
control	0		0.19	0.19	0.817491	0.815743674	
	-0.5		0.33	0.19	0.813526	0.832980521	
	-1		0.48	0.19	0.809127	0.852212978	
	-1.5		0.61	0.19	0.805648	0.874487416	
	-2		0.74	0.19	0.799861	0.898775152	

Air_Temp_Day	Air Temp (°C)		Net Balance (m.w.e)	Measured Net Balance (m.w.e)	Stk R^2	Least Squares Slope	Notes
	2		-0.52	0.19	0.83484	0.752894266	
	1.5		-0.34	0.19	0.828155	0.767378197	
	1		-0.17	0.19	0.825905	0.784589106	
	0.5		0.01	0.19	0.821218	0.806125903	
control	0		0.19	0.19	0.817491	0.815743674	
	-0.5		0.36	0.19	0.819114	0.844671283	
	-1		0.51	0.19	0.808473	0.867625463	
	-1.5		0.65	0.19	0.804241	0.89046165	
	-2		0.78	0.19	0.800377	0.915402822	

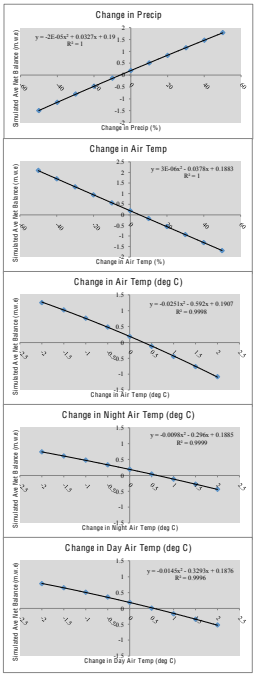

Precip Sensitivity
y=0.0327-0.00004x
Slope= 0.0327 x=0

Air Temp Sensitivity
y=0.000006x-0.0378
Slope= -0.0378 x=0

Air Temp (deg C) Sensitivity
y=-0.0251x^2-0.592x+0.1907
y'=-0.0502x-0.592 x=0
Slope= -0.592

Linear
y=-0.592x+0.1489
Slope= -0.592

Night Air Temp (deg C) Sensitivity
y=-0.0098x^2-0.296x+0.1885
y'=-0.0196x-0.296 x=0
Slope= -0.296

Linear
y=-0.296x+0.1722
Slope= -0.296

Day Air Temp (deg C) Sensitivity
y=-0.0145x^2-0.3293x+0.1876
y'=-0.029x-0.3293 x=0
Slope= -0.3293

Linear
y=-0.3293x+0.1633
Slope= -0.3293

Table C4 SEBM precipitation lapse rate sensitivity test

Precip Lapse Rate	Factor	% Change	Net Balance (m.w.e)	Measured Net Balance (m.w.e)	Stk R^2	Least Squares Slope	Notes
MO							
0.0026			0.36	0.19	0.77099	0.70634306	
0.0025			0.33	0.19	0.772266	0.706210962	
0.0024			0.31	0.19	0.773542	0.706048933	
0.0023			0.28	0.19	0.774721	0.705855106	
0.0022			0.25	0.19	0.775928	0.705632736	
0.0021			0.23	0.19	0.777098	0.705420129	
0.002			0.2	0.19	0.778212	0.705175391	MO
0.0019			0.17	0.19	0.779354	0.704937448	
0.0018			0.14	0.19	0.780483	0.704601802	Intersect
0.0017			0.12	0.19	0.781578	0.704380959	
0.0016			0.09	0.19	0.78266	0.703949476	
0.0015			0.06	0.19	0.783747	0.703590365	
0.0014			0.03	0.19	0.784803	0.703289711	
0.0013			0.01	0.19	0.785833	0.702838023	
0.0012			-0.02	0.19	0.78678	0.702321356	
0.0011			-0.05	0.19	0.787672	0.701798101	
0.001			-0.08	0.19	0.788389	0.701250945	
Paterson							
0.0026			0.37	0.19	0.771408	0.683328953	
0.0025			0.34	0.19	0.772649	0.683171137	
0.0024			0.31	0.19	0.773883	0.682945675	
0.0023			0.28	0.19	0.774951	0.682525092	Net Balance curve shifts up
0.0022			0.26	0.19	0.77608	0.682264481	
0.0021			0.23	0.19	0.777316	0.682016621	
0.002			0.2	0.19	0.778552	0.681761019	Paterson
0.0019			0.17	0.19	0.779654	0.681471472	
0.0018			0.14	0.19	0.780649	0.681033957	Intersect
0.0017			0.12	0.19	0.78167	0.680603118	
0.0016			0.09	0.19	0.782819	0.680282083	
0.0015			0.06	0.19	0.783851	0.679875266	
0.0014			0.03	0.19	0.784842	0.679477987	
0.0013			0.01	0.19	0.785788	0.678999377	
0.0012			-0.02	0.19	0.786723	0.678454774	
0.0011			-0.05	0.19	0.787548	0.677824616	
0.001			-0.08	0.19	0.788424	0.677256233	

MO Opt. Value	Factor	% Change	Net Balance (m.w.e)	Measured Net Balance (m.w.e)	Stk R^2	Least Squares Slope	Notes
0.0020	1.1	10%	10	0.23	0.779353	0.724463238	
0.0019	1.05	5%	5	0.2	0.780524	0.724404689	
0.0018	1	0	0	0.18	0.781814	0.724317867	control
0.0017	0.95	-5%	-5	0.15	0.783003	0.724152007	
0.0016	0.9	-10%	-10	0.12	0.784047	0.723906427	
Paterson Opt. Value							
0.0020	1.1	10%	10	0.24	0.780102	0.699978469	
0.0019	1.05	5%	5	0.22	0.781266	0.699829407	
0.0018	1	0	0	0.19	0.782466	0.699696205	control
0.0017	0.95	-5%	-5	0.16	0.78358	0.699463518	
0.0016	0.9	-10%	-10	0.13	0.784649	0.699213591	

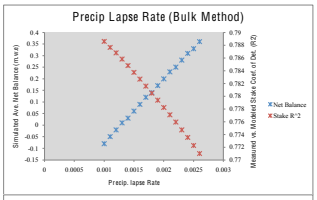

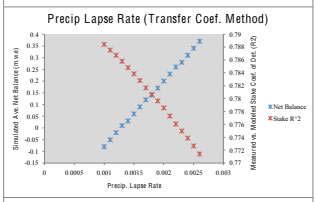

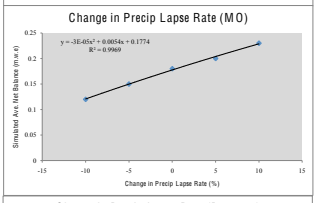

Precip Lapse Rate Sensitivity (MO)
y=0.0054-0.00006x
Slope= 0.0054 x=0

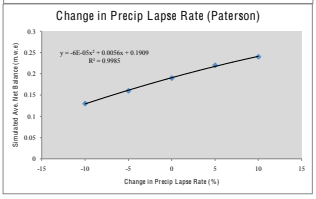

Precip Lapse Rate Sensitivity (Paterson)
y=0.0056-0.00012x
Slope= 0.0056 x=0

Table C5 PDD model precipitation lapse rate

Precip Lapse Rate	Factor	% Change	Net Balance (m.w.e)	Measured Net Balance (m.w.e)	Stk R^2	Least Squares Slope	Notes	
PDD								
0.0026			0.56	0.19	0.774056	0.689551071		
0.0025			0.53	0.19	0.775288	0.689016749		
0.0024			0.51	0.19	0.776563	0.688551232		
0.0023			0.48	0.19	0.777915	0.688061664		
0.0022			0.45	0.19	0.779107	0.687510151		
0.0021			0.43	0.19	0.780199	0.686801517		
0.002			0.4	0.19	0.78137	0.686246636		
0.0019			0.37	0.19	0.782562	0.685645787		
0.0018			0.35	0.19	0.783606	0.684986045	Intersect	Opti
0.0017			0.32	0.19	0.784636	0.684281697		
0.0016			0.29	0.19	0.78567	0.683586751		
0.0015			0.27	0.19	0.786558	0.682849698		
0.0014			0.24	0.19	0.787688	0.682116129		
0.0013			0.21	0.19	0.78847	0.68134555		
0.0012			0.19	0.19	0.789316	0.680447273	Control	
0.0011			0.16	0.19	0.790238	0.679616863	Opti	
0.001			0.13	0.19	0.791045	0.678807149		

Opt. Value	Factor	% Change	Net Balance (m.w.e)	Measured Net Balance (m.w.e)	Stk R^2	Least Squares Slope	Notes
0.00121	1.1	10%	10	0.21	0.816413	0.814945816	
0.00116	1.05	5%	5	0.2	0.816892	0.81529614	
0.0011	1	0	0	0.19	0.817491	0.815743674	
0.00105	0.95	-5%	-5	0.18	0.818007	0.816142996	
0.00099	0.9	-10%	-10	0.16	0.818595	0.816535138	

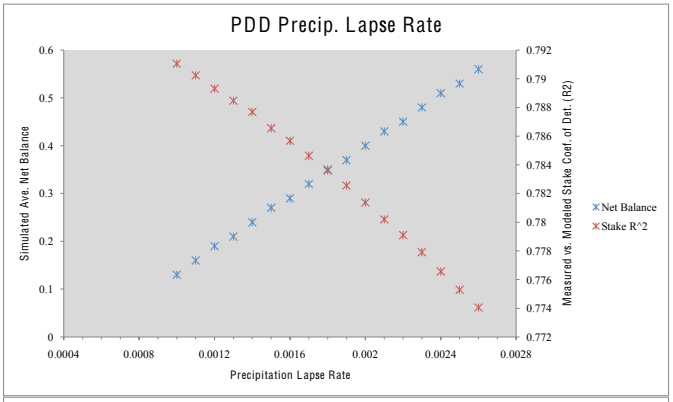

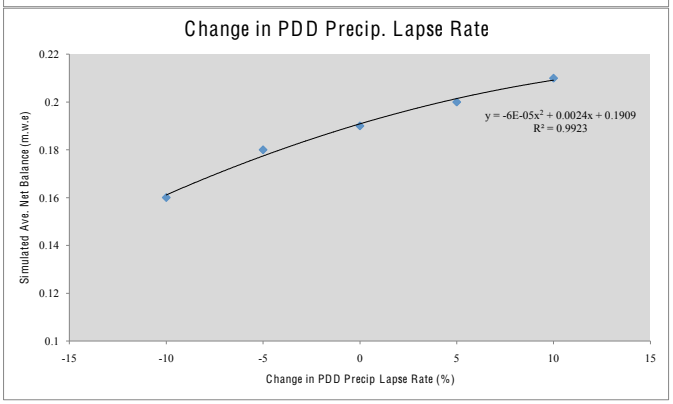

PDD Precip. Lapse Rate Sensitivity
y'=0.0024-0.00012x
Slope= 0.0024 x=0

Table C6 Surface roughness of ice

Zo Ice (m)	Factor	% Change	Net Balance (m.w.e)	Measured Net Balance (m.w.e)	Stk R^2	Least Squares Slope	Mean H_s (W m^{-2})	Mean H_l (W m^{-2})	Notes
0.0015			0.16	0.19	0.777771	0.689218152	40.1203	-7.36196	
0.0014			0.17	0.19	0.77785	0.691548216	39.9651	-7.35657	
0.0013			0.17	0.19	0.777898	0.693976894	39.8032	-7.35101	
0.0012			0.18	0.19	0.777998	0.696540094	39.6336	-7.34512	
0.0011			0.18	0.19	0.778082	0.699259085	39.4556	-7.33896	
0.001			0.19	0.19	0.778124	0.702113635	39.2673	-7.33248	
0.0009			0.2	0.19	0.778212	0.705175391	39.0636	-7.32562	Control (MO)
0.0008			0.21	0.19	0.778277	0.708454082	38.8535	-7.31826	
0.0007			0.21	0.19	0.778343	0.712037664	38.6224	-7.31016	
0.0006			0.22	0.19	0.778366	0.715952805	38.3696	-7.30145	
0.0005			0.23	0.19	0.77841	0.720341216	38.0886	-7.29181	
0.0004			0.25	0.19	0.778431	0.725376008	37.769	-7.28078	opti
0.0003		ERROR		0.19	ERROR	ERROR	ERROR	ERROR	Lower Limit

Opt. Value	Factor	% Change	% Change	Net Balance (m.w.e)	Stk R^2	Least Squares Slope	Mean H_s (W m^{-2})	Mean H_l (W m^{-2})	Notes
0.00048	1.2	20%	20	0.17	0.781748	0.720173623	40.3914	-7.81898	
0.00046	1.15	15%	15	0.17	0.781802	0.72117948	40.3287	-7.81666	
0.00044	1.1	10%	10	0.17	0.781784	0.722180861	40.264	-7.81437	
0.00042	1.05	5%	5	0.18	0.7818	0.723228161	40.1974	-7.81191	
0.0004	1	0	0	0.18	0.781814	0.724317867	40.1288	-7.80945	MO
0.00038	0.95	-5%	-5	0.18	0.781796	0.725440421	40.0579	-7.80689	
0.00036	0.9	-10%	-10	0.18	0.78182	0.726589679	39.9846	-7.80418	
0.00034	0.85	-15%	-15	0.19	0.781827	0.727793251	39.9085	-7.80143	
0.00032	0.8	-20%	ERROR	ERROR	ERROR	ERROR	ERROR	ERROR	

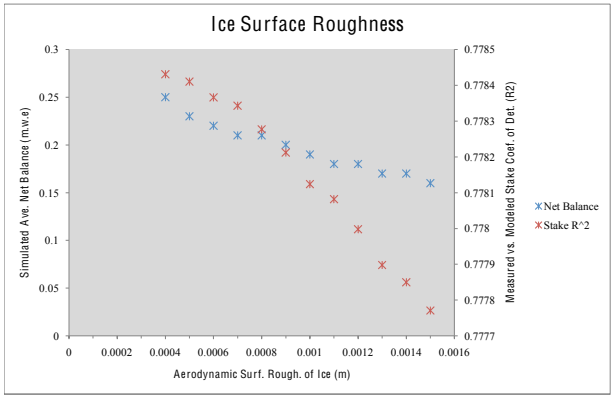

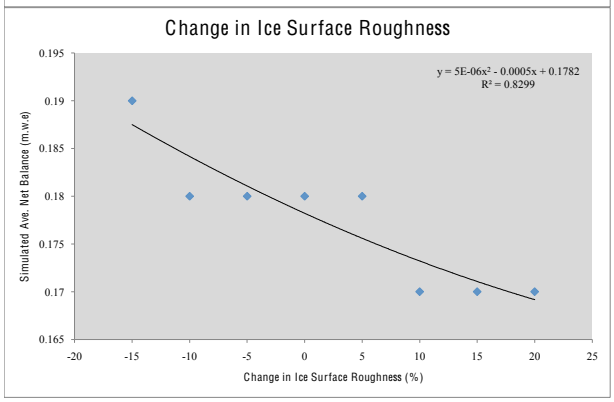

Ice Surface Roughness Sensitivity
y=0.00001x-0.0005
Slope= -0.0005 x=0

Table C7 Surface roughness of snow

Zo Snow (m)	Factor	% Change	Net Balance (m.w.e)	Measured Net Balance (m.w.e)	Stk R^2	Least Squares Slope	Mean H_s (W m^{-2})	Mean H_l (W m^{-2})	Notes
0.0015			-0.12	0.19	0.793554	0.681367757	47.5812	-9.25063	
0.0014			-0.09	0.19	0.792279	0.683407178	46.8357	-9.07941	
0.0013			-0.06	0.19	0.790986	0.685580364	46.0568	-8.90122	
0.0012			-0.03	0.19	0.789472	0.687784864	45.2386	-8.71453	
0.0011			0	0.19	0.787853	0.690054694	44.377	-8.51841	
0.001			0.04	0.19	0.786227	0.692617094	43.4639	-8.31124	
0.0009			0.07	0.19	0.784559	0.6953883	42.4909	-8.09145	
0.0008			0.11	0.19	0.7826	0.698228554	41.4457	-7.8563	Intersect
0.0007			0.15	0.19	0.780534	0.701476863	40.3122	-7.60247	
0.0006			0.2	0.19	0.778212	0.705175391	39.0636	-7.32562	Control (MO)
0.0005			0.25	0.19	0.775757	0.709506855	37.6773	-7.01836	
0.0004			0.31	0.19	0.772793	0.714808171	36.0871	-6.66898	
0.0003		ERROR		0.19	ERROR	ERROR	ERROR	ERROR	Lower Limit

Opt. Value	Factor	% Change	% Change	Net Balance (m.w.e)	Stk R^2	Least Squares Slope	Mean H_s (W m^{-2})	Mean H_l (W m^{-2})	Notes
0.00088	1.1	10%	10	0.15	0.78331	0.721786202	40.9636	-7.99884	
0.00084	1.05	5%	5	0.16	0.782652	0.72303139	40.5526	-7.90552	
0.0008	1	0	0	0.18	0.781814	0.724317867	40.1288	-7.80945	MO
0.00076	0.95	-5%	-5	0.19	0.780887	0.72560502	39.6909	-7.71007	
0.00072	0.9	-10%	-10	0.21	0.780054	0.726972065	39.2385	-7.60746	

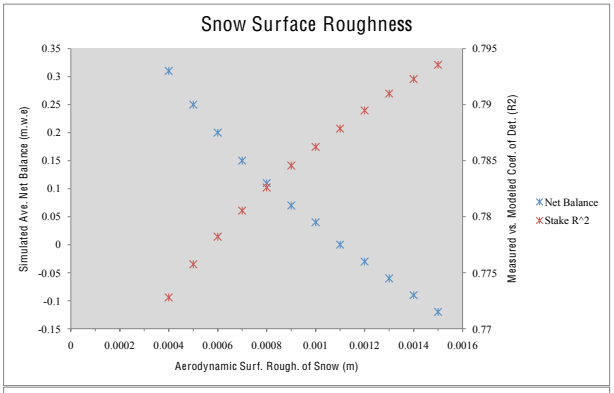

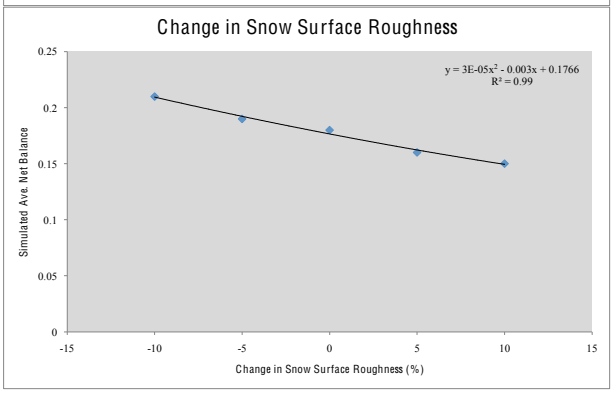

Snow Surface Roughness Sensitivity
y=0.00006x-0.003
Slope= -0.003 x=0

Table C8 Sky transmissivity

Sky Transmissivity	Factor	Change (%)	% Change	Net Balance (m.w.e)	Measured Net Balance (m.w.e)	Stk R^2	Least Squares Slope	mean Net SW (W m^{-2})	Notes
MO									
0.68	1.1	10%	10	0.17	0.19	0.782383	0.723663789	73.1233	
0.65	1.05	5%	5	0.17	0.19	0.782047	0.724022954	73.0064	
0.62	1	0	0	0.18	0.19	0.781814	0.724317867	72.9036	MO
0.59	0.95	-5%	-5	0.18	0.19	0.781519	0.724579012	72.804	
0.56	0.9	-10%	-10	0.18	0.19	0.781271	0.724829492	72.7076	
Paterson									
0.68	1.1	10%	10	0.18	0.19	0.782994	0.699075296	73.2393	
0.65	1.05	5%	5	0.18	0.19	0.782678	0.699389115	73.1228	
0.62	1	0	0	0.19	0.19	0.782466	0.699696205	73.0204	Paterson
0.59	0.95	-5%	-5	0.19	0.19	0.782204	0.699949635	72.9212	
0.56	0.9	-10%	-10	0.19	0.19	0.781946	0.700181582		

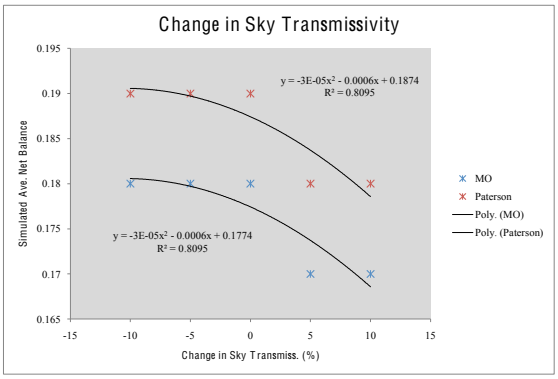

Sky Transmissivity Sensitivity

MO

y'=-0.00006x-0.0006

Slope= -0.0006

x=0

Paterson

y'=-0.00006x-0.0006

Slope= -0.0006

x=0

Table C9 Albedo of surrounding terrain

Terrain Albedo	Factor	% Change	% Change	Net Balance (m.w.e)	Measured Net Balance (m.w.e)	Stk R^2	Least Squares Slope	mean Net SW (W m^{-2})	Notes
MO									
0.22	1.1	10%	10	0.17	0.19	0.781956	0.723476408	73.0529	
0.21	1.05	5%	5	0.18	0.19	0.781886	0.723902081	72.9783	
0.2	1	0	0	0.18	0.19	0.781814	0.724317867	72.9036	MO
0.19	0.95	-5%	-5	0.18	0.19	0.781719	0.724732295	72.8289	
0.18	0.9	-10%	-10	0.18	0.19	0.781629	0.725156721	72.7543	
Paterson									
0.22	1.1	10%	10	0.18	0.19	0.782585	0.698889333	73.1687	
0.21	1.05	5%	5	0.19	0.19	0.782514	0.699262364	73.0946	
0.2	1	0	0	0.19	0.19	0.782466	0.699696205	73.0204	Paterson
0.19	0.95	-5%	-5	0.19	0.19	0.782382	0.700066628	72.9462	
0.18	0.9	-10%	-10	0.19	0.19	0.782325	0.70050762	72.8721	

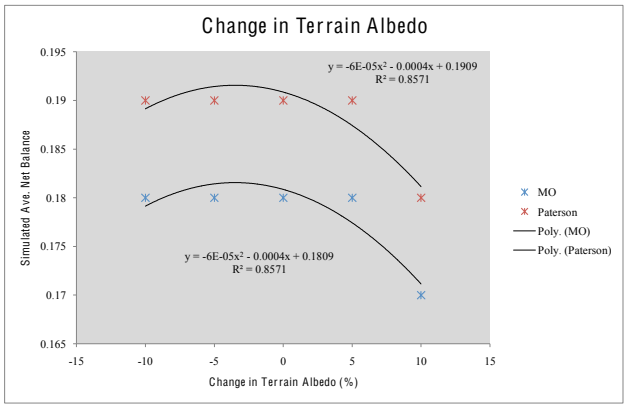

Terrain Albedo Sensitivity

MO

y=-0.00012x-0.0004

Slope= -0.0004

x=0

Paterson

y=-0.00012x-0.0004

Slope= -0.0004

x=0

Table C10 Albedo decay coefficient

Albedo Decay Coef.	Factor	% Change	Net Balance (m.w.e)	Measured Net Balance (m.w.e)	Stk R^2	Least Squares Slope	mean Net SW (W m^{-2})	Notes
MO								
-0.045			0.06	0.19	0.785319	0.693305388	78.0569	
-0.044			0.09	0.19	0.784078	0.695642486	77.332	
-0.043			0.12	0.19	0.782665	0.697932323	76.6048	
-0.042			0.14	0.19	0.781183	0.70025167	75.8743	
-0.041			0.17	0.19	0.779722	0.702691639	75.1391	
-0.04			0.2	0.19	0.778212	0.705175391	74.4013	Control (MO)/Intersect
-0.039			0.23	0.19	0.776739	0.707756065	73.6607	
-0.038			0.25	0.19	0.775189	0.710482375	72.9165	
-0.037			0.28	0.19	0.773536	0.713331459	72.1676	
-0.036			0.31	0.19	0.772025	0.716365825	71.4145	
-0.035			0.34	0.19	0.770661	0.719531226	70.6591	
Paterson								
-0.045			0.07	0.19	0.784789	0.670259777	78.1304	
-0.044			0.09	0.19	0.783706	0.672553077	77.4168	
-0.043			0.12	0.19	0.782398	0.674737142	76.7001	
-0.042			0.15	0.19	0.781146	0.676986305	75.9802	
-0.041			0.17	0.19	0.77979	0.679326953	75.2653	
-0.04			0.2	0.19	0.778582	0.681781019	74.5297	Control (Paterson)/Intersect
-0.039			0.23	0.19	0.777012	0.684113758	73.7988	
-0.038			0.25	0.19	0.775729	0.686767418	73.0648	
-0.037			0.28	0.19	0.774213	0.689304653	72.3277	STDEV going down
-0.036			0.31	0.19	0.772674	0.691939362	71.5871	
-0.035			0.34	0.19	0.771255	0.694805619	70.8433	

MO	Factor	% Change	Net Balance (m.w.e)	Measured Net Balance (m.w.e)	Stk R^2	Least Squares Slope	mean Net SW (W m^{-2})	Notes
-0.044	1.1	10%	10	0.07	0.787629	0.714917333	75.8514	
-0.042	1.05	5%	5	0.12	0.784834	0.719432931	74.3836	
-0.04	1	0	0	0.18	0.781814	0.724317867	72.9036	MO
-0.038	0.95	-5%	-5	0.23	0.778635	0.729475925	71.4099	
-0.036	0.9	-10%	-10	0.29	0.775428	0.73527153	69.9035	
Paterson								
-0.044	1.1	10%	10	0.08	0.787607	0.690787963	75.9215	
-0.042	1.05	5%	5	0.13	0.785066	0.69598804	74.4778	
-0.04	1	0	0	0.19	0.782466	0.699696205	73.0204	Paterson
-0.038	0.95	-5%	-5	0.24	0.779643	0.704466262	71.5493	
-0.036	0.9	-10%	-10	0.3	0.776645	0.709520666	70.0645	

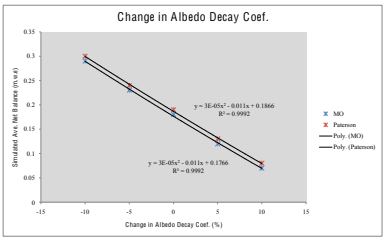

Albedo Decay Coef. Sensitivity

MO

y=0.00006x-0.011

Slope= -0.011
x=0

Paterson

y=0.00006x-0.011

Slope= -0.011
x=0

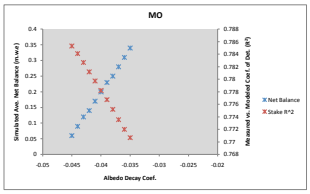

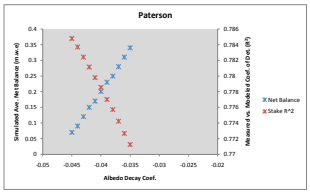

Table C11 Albedo of fresh snow

Fresh Snow Albedo	Factor	% Change	Net Balance (m.w.e)	Measured Net Balance (m.w.e)	Stk R^2	Least Squares Slope	mean Net SW ($W m^{-2}$)	Notes
MO								
0.9			0.96	0.19	0.745583	0.802885519	52.8836	
0.89			0.88	0.19	0.749966	0.791683226	55.1437	
0.88			0.8	0.19	0.753753	0.77936291	57.3627	
0.87			0.73	0.19	0.757658	0.767707229	59.564	
0.86			0.65	0.19	0.761401	0.756814155	61.7445	
0.85			0.58	0.19	0.76458	0.747283785	63.8878	
0.84			0.5	0.19	0.767328	0.738144847	66.0308	
0.83			0.42	0.19	0.769504	0.728631927	68.1654	
0.82			0.35	0.19	0.771705	0.719687566	70.2682	
0.81			0.27	0.19	0.774777	0.71195727	72.3435	Intersect
0.8			0.2	0.19	0.778212	0.705175391	74.4013	Control (MO)
0.79			0.12	0.19	0.781656	0.698975423	76.4461	
0.78			0.05	0.19	0.784787	0.692878893	78.4783	
0.77			-0.02	0.19	0.787707	0.686869307	80.4996	
0.76			-0.09	0.19	0.790291	0.68097354	82.5022	
0.75			-0.17	0.19	0.792492	0.675359159	84.4851	
0.74			-0.24	0.19	0.794681	0.670158907	86.4482	
0.73			-0.31	0.19	0.796566	0.665787893	88.3898	
0.72			-0.38	0.19	0.798088	0.661329991	90.3167	
0.71			-0.45	0.19	0.799262	0.656875843	92.211	
0.7			-0.51	0.19	0.8003	0.652620303	93.9788	
Paterson								
0.9			0.97	0.19	0.744421	0.773954601		
0.89			0.89	0.19	0.749181	0.762120207	55.4207	
0.88			0.82	0.19	0.753308	0.750896072	57.6361	
0.87			0.74	0.19	0.7572	0.740557639	59.826	
0.86			0.66	0.19	0.760224	0.73090364	61.9817	
0.85			0.58	0.19	0.763183	0.721222734	64.1256	
0.84			0.5	0.19	0.765792	0.711738428	66.252	
0.83			0.43	0.19	0.768594	0.702762129	68.3541	
0.82			0.35	0.19	0.771957	0.694950629	70.4321	
0.81			0.28	0.19	0.775287	0.688154805	72.4884	Intersect
0.8			0.2	0.19	0.778552	0.681761019	74.5287	Control (Paterson)
0.79			0.13	0.19	0.781538	0.675672858	76.5552	
0.78			0.05	0.19	0.784321	0.6697055	78.5659	
0.77			-0.02	0.19	0.787054	0.66399519	80.556	
0.76			-0.09	0.19	0.78957	0.658803808	82.5196	
0.75			-0.17	0.19	0.791706	0.653678844	84.4681	
0.74			-0.24	0.19	0.793687	0.648732713	86.4038	
0.73			-0.31	0.19	0.79533	0.644210042	88.3216	
0.72			-0.38	0.19	0.796884	0.639857265	90.2247	
0.71			-0.45	0.19	0.798192	0.635506668	92.0966	
0.7			-0.52	0.19	0.799421	0.631229951	93.8482	

MO_Opt_Value	Factor	% Change	Net Balance (m.w.e)	Measured Net Balance (m.w.e)	Stk R^2	Least Squares Slope	mean Net SW ($W m^{-2}$)	Notes
0.89	1.1	10%	10	0.77	0.759661	0.796928214	55.8953	
0.85	1.05	5%	5	0.47	0.771605	0.756972166	64.5415	
0.81	1	0	0	0.18	0.78184	0.724317867	72.9036	
0.77	0.95	-5%	-5	-0.11	0.793963	0.700285591	81.0276	
0.73	0.9	-10%	-10	-0.39	0.801187	0.680978345	88.8604	
Paterson_Opt_Value								
0.89	1.1	10%	10	0.78	0.759109	0.765607195	56.1788	
0.85	1.05	5%	5	0.48	0.769996	0.728576017	64.7503	
0.81	1	0	0	0.19	0.782466	0.699696205	73.0204	
0.77	0.95	-5%	-5	-0.1	0.793666	0.677858011	81.0125	
0.73	0.9	-10%	-10	-0.38	0.800412	0.659716825	88.7301	

Fresh Snow Albedo Sensitivity
MO/Paterson
y=0.0002x+0.058

Slope= 0.058
x=0

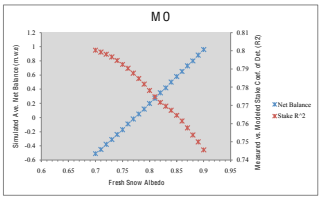

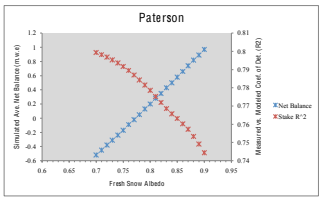

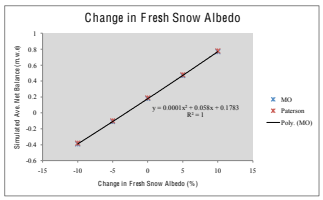

Table C12 Transfer coefficient for ice

Paterson Khi	Factor	% Change	Net Balance (m.w.e)	Measured Net Balance (m.w.e)	Stk R^2	Least Squares Slope	Mean H_s (W m^{-2})	Mean H_l (W m^{-2})	Notes
0.0025			0.13	0.19	0.77644	0.651538534	39.764	-4.39229	
0.0024			0.14	0.19	0.776917	0.657457629	39.3688	-4.39034	
0.0023			0.16	0.19	0.777347	0.663440052	38.9735	-4.38829	
0.0022			0.17	0.19	0.777771	0.669485893	38.5782	-4.38632	
0.0021			0.19	0.19	0.778187	0.675605764	38.183	-4.3843	
0.002			0.2	0.19	0.778552	0.681761019	37.7877	-4.38229	Control
0.0019			0.21	0.19	0.778883	0.68799884	37.3925	-4.38033	
0.0018			0.23	0.19	0.779187	0.69428537	36.9973	-4.37832	
0.0017			0.24	0.19	0.779461	0.70061861	36.602	-4.37627	opti
0.0016			0.26	0.19	0.779674	0.70699523	36.2067	-4.37433	
0.0015			0.27	0.19	0.779905	0.713440539	35.8115	-4.37227	
0.0014			0.27	0.19	0.780087	0.719923745	35.4163	-4.37023	

Opt. Value	Factor	% Change	Net Balance (m.w.e)	Measured Net Balance (m.w.e)	Stk R^2	Least Squares Slope	Mean H_s (W m^{-2})	Mean H_l (W m^{-2})	Notes
0.0019	1.1	10%	10	0.16	0.781777	0.68690659	39.4039	-4.67298	
0.0018	1.05	5%	5	0.17	0.782134	0.693274053	39.0023	-4.66971	
0.0017	1	0	0	0.19	0.782466	0.699696205	38.6006	-4.66632	control
0.0016	0.95	-5%	-5	0.2	0.782729	0.706123064	38.1989	-4.66298	
0.0015	0.9	-10%	-10	0.22	0.78296	0.712623816	37.7972	-4.65966	

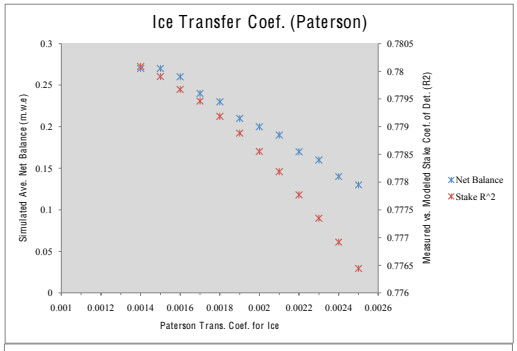

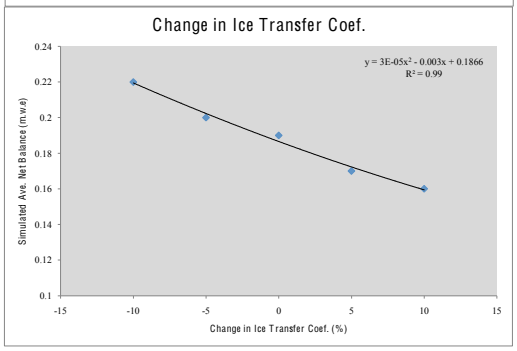

Paterson Transfer Coefficients for melting snow and ice (Table 4.3)

Surface	Heat	Vapor	Reference
Snow	0.00166	0.002	Holmgren, 1971
Snow/ice	0.002	0.002	Hogg et al., 1982
Snow	0.0013	0.0015	Ambach and Kirchlechner, 1986
Ice	0.0019	0.0022	Ambach and Kirchlechner, 1986
Ice	0.0039	0.0039	Hay and Fitzharris, 1988

Accept Value Range (Paterson, 1994)
0.0015-0.002

Ice Transfer Coef. Sensitivity
y'=0.00006x-0.003
Slope= -0.003
x=0

Table C13 Transfer coefficient for snow

Paterson Khs	Factor	% Change	Net Balance (m.w.e)	Measured Net Balance (m.w.e)	% Change	Stk R^2	Least Squares Slope	Mean H_s (W m^{-2})	Mean H_l (W m^{-2})	Notes
0.002			-0.17	0.19		0.796231	0.653748468	47.7488	-5.82714	
0.0019			-0.1	0.19		0.792988	0.65836987	45.7897	-5.53505	
0.0018			-0.03	0.19		0.789472	0.663414144	43.8148	-5.24426	STDEV going up
0.0017			0.05	0.19		0.785891	0.669154902	41.8248	-4.9544	
0.0016			0.12	0.19		0.782254	0.675237421	39.8169	-4.66813	Opti
0.0015			0.2	0.19		0.778552	0.681761019	37.7877	-4.38229	Control/Intersect
0.0014			0.28	0.19		0.774582	0.688747507	35.7394	-4.10091	STDEV going down
0.0013			0.35	0.19		0.770695	0.69634287	33.6678	-3.82223	
0.0012			0.43	0.19		0.766228	0.704636555	31.5655	-3.5426	
0.0011			0.51	0.19		0.762056	0.713948109	29.4308	-3.25606	
0.001			0.59	0.19		0.757789	0.724043044	27.2683	-2.97049	

Opt. Value	Factor	% Change	Net Balance (m.w.e)	Measured Net Balance (m.w.e)	% Change	Stk R^2	Least Squares Slope	Mean H_s (W m^{-2})	Mean H_l (W m^{-2})	Notes
0.0018	1.1	10%	10	0.04	0.19	0.789921	0.687541704	42.556	-5.24445	
0.0017	1.05	5%	5	0.11	0.19	0.786187	0.69341154	40.5866	-4.95425	
0.0016	1	0	0	0.19	0.19	0.782466	0.699696205	38.6006	-4.66632	control
0.0015	0.95	-5%	-5	0.26	0.19	0.778533	0.706411236	36.5968	-4.38106	
0.0014	0.9	-10%	-10	0.34	0.19	0.774508	0.713719314	34.5738	-4.09948	

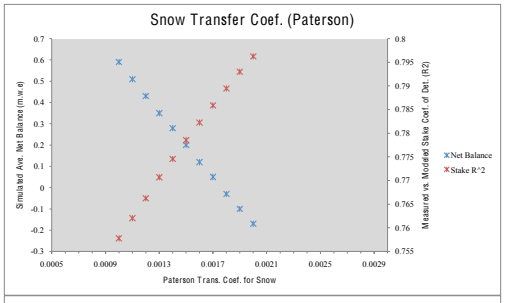

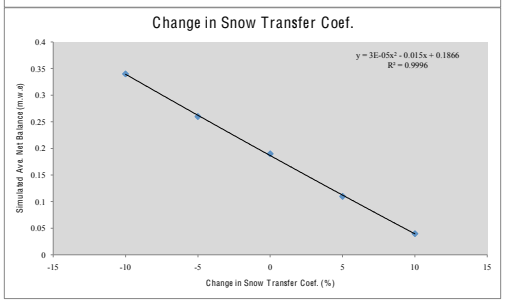

Surface	Heat	Vapor	Reference
Snow	0.0013	0.0015	Ambach and Kirchlechner, 1986
Ice	0.0019	0.0022	Ambach and Kirchlechner, 1986
Ice	0.0039	0.0039	Hay and Fitzharris, 1988

Accept Value Range (Paterson, 1994)
0.0015-0.002

Snow Transfer Coef. Sensitivity
y'=0.00006x-0.015
Slope= -0.015
x=0

Table C14 Degree-day factor for snow

DDF_{snow} ($m^{o}C^{-1}d^{-1}$)	Factor	% Change	Net Balance (m.w.e)	Measured Net Balance (m.w.e)	Stk R^2	Least Squares Slope	Notes
0.005			-1.06	0.19	0.821124	0.574158259	
0.0049			-0.97	0.19	0.819504	0.578623138	
0.0048			-0.88	0.19	0.81783	0.583367227	
0.0047			-0.79	0.19	0.816138	0.58853338	
0.0046			-0.69	0.19	0.814283	0.593984207	
0.0045			-0.6	0.19	0.812193	0.599781031	
0.0044			-0.51	0.19	0.810194	0.606076284	
0.0043			-0.43	0.19	0.807803	0.612743556	
0.0042			-0.34	0.19	0.805753	0.620122352	
0.0041			-0.26	0.19	0.803512	0.628122839	
0.004			-0.17	0.19	0.800981	0.636742603	opti
0.0039			-0.09	0.19	0.798453	0.646274325	
0.0038			0	0.19	0.795622	0.656562075	Opti
0.0037			0.09	0.19	0.79268	0.66808763	
0.0036			0.19	0.19	0.789316	0.680447273	Control
0.0035			0.28	0.19	0.785772	0.694269269	
0.0034			0.38	0.19	0.781904	0.709726274	
0.0033			0.48	0.19	0.777494	0.726699994	
0.0032			0.58	0.19	0.772348	0.745760599	
0.0031			0.69	0.19	0.766449	0.766944748	
0.003			0.8	0.19	0.760237	0.790654912	
0.0029			0.91	0.19	0.754677	0.817014642	
0.0028			1.03	0.19	0.749469	0.847127003	
0.0027			1.15	0.19	0.742724	0.881240219	Drops below 1:1
0.0026			1.27	0.19	0.734114	0.918538623	
0.0025			1.4	0.19	0.72457	0.956262138	
0.0024			1.53	0.19	0.716279	0.996848513	
0.0023			1.65	0.19	0.7048	1.03858504	Intersect
0.0022			1.75	0.19	0.697172	1.069617464	
0.0021			1.84	0.19	0.690324	1.097859546	
0.002			1.93	0.19	0.67962	1.119085915	

Opt. Value	Factor	% Change	Net Balance (m.w.e)	Measured Net Balance (m.w.e)	Stk R^2	Least Squares Slope	Notes
0.0044	1.1	10%	10	-0.1	0.826289	0.791590826	
0.0042	1.05	5%	5	0.04	0.82228	0.802881149	
0.004	1	0	0	0.19	0.817491	0.815743674	
0.0038	0.95	-5%	-5	0.34	0.811861	0.830598523	
0.0036	0.9	-10%	-10	0.49	0.805147	0.847961367	

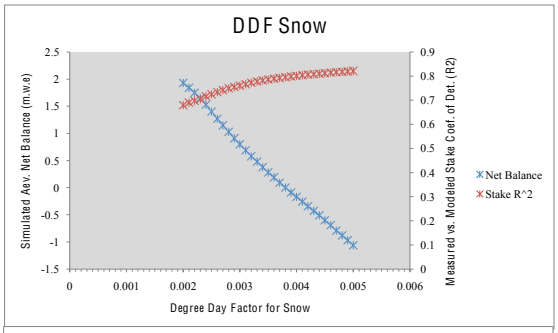

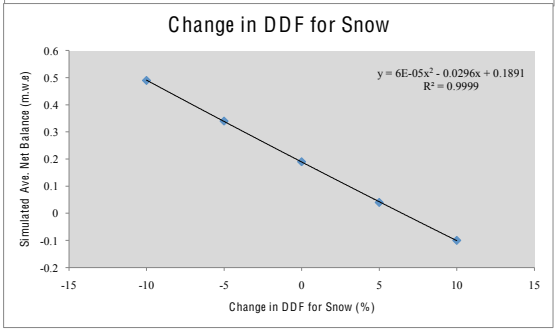

Cascade DDF

Mt. Rainier	*from Rasmussen and Wenger (2009)*
Snow:	0.00146-0.00085
Ice:	0.00644-0.00435
Mt. Shasta	*from Howat et al. (2007)*
Snow:	0.0014-0.0016
Ice:	0.0069-0.0055
SCG	*from Anslow et al. (2008)*
Snow:	0.003
Ice:	0.008

DDF Snow Sensitivity

y'=0.00012x-0.0296

Slope= -0.0296

x=0

Table C15 Degree-day factor for ice

DDF_{ice} ($m^0C^{-1}d^{-1}$)	Factor	% Change	Net Balance (m.w.e)	Measured Net Balance (m.w.e)	Stk R^2	Least Squares Slope	Notes
0.01			0	0.19	0.777305	0.605269426	
0.0099			0.01	0.19	0.777913	0.608690657	
0.0098			0.02	0.19	0.778533	0.612140402	
0.0097			0.03	0.19	0.779141	0.615615354	
0.0096			0.04	0.19	0.779766	0.619143244	
0.0095			0.04	0.19	0.78038	0.622710521	
0.0094			0.05	0.19	0.781001	0.626321387	
0.0093			0.06	0.19	0.781593	0.6299222	
0.0092			0.07	0.19	0.782217	0.633582358	
0.0091			0.08	0.19	0.782829	0.637310386	
0.009			0.09	0.19	0.783421	0.641028831	
0.0089			0.1	0.19	0.78402	0.644791287	
0.0088			0.11	0.19	0.784623	0.648595686	
0.0087			0.12	0.19	0.785238	0.65246239	
0.0086			0.13	0.19	0.785827	0.656321601	
0.0085			0.14	0.19	0.786432	0.660265589	
0.0084			0.15	0.19	0.787013	0.664217715	
0.0083			0.16	0.19	0.787603	0.66822867	
0.0082			0.17	0.19	0.78819	0.672261096	
0.0081			0.18	0.19	0.788764	0.676353697	
0.008			0.19	0.19	0.789316	0.680447273	Control
0.0079			0.2	0.19	0.789901	0.684612228	
0.0078			0.21	0.19	0.790476	0.6888081	
0.0077			0.22	0.19	0.791048	0.693062087	Opti
0.0076			0.23	0.19	0.7916	0.69733378	
0.0075			0.24	0.19	0.792164	0.701671606	
0.0074			0.25	0.19	0.792727	0.706041658	
0.0073			0.25	0.19	0.793267	0.710457791	
0.0072			0.26	0.19	0.793813	0.714936326	
0.0071			0.27	0.19	0.794296	0.719400742	
0.007			0.28	0.19	0.794832	0.723949161	
0.0069			0.29	0.19	0.795357	0.72854961	
0.0068			0.3	0.19	0.795863	0.733172231	
0.0067			0.31	0.19	0.796345	0.737863594	
0.0066			0.32	0.19	0.796852	0.742594777	
0.0065			0.33	0.19	0.797327	0.747357962	
0.0064			0.34	0.19	0.797798	0.752181998	
0.0063			0.35	0.19	0.79827	0.757061261	
0.0062			0.36	0.19	0.798681	0.761951712	
0.0061			0.37	0.19	0.799112	0.766915008	
0.006			0.38	0.19	0.799542	0.771916461	
0.0059			0.39	0.19	0.799957	0.776979619	
0.0058			0.4	0.19	0.800365	0.782099976	
0.0057			0.41	0.19	0.800746	0.787244016	
0.0056			0.42	0.19	0.80113	0.792446942	
0.0055			0.43	0.19	0.801505	0.797722414	
0.0054			0.44	0.19	0.801834	0.803017115	
0.0053			0.45	0.19	0.802128	0.808354261	Intersect
0.0052			0.46	0.19	0.802445	0.813749505	
0.0051			0.46	0.19	0.802725	0.819193254	
0.005			0.47	0.19	0.80299	0.824707662	
0.0049			0.48	0.19	0.803249	0.830288347	
0.0048			0.49	0.19	0.803462	0.83584082	
0.0047			0.5	0.19	0.803691	0.841518506	
0.0046			0.51	0.19	0.803879	0.847221628	opti
0.0045			0.52	0.19	0.804037	0.852976797	
0.0044			0.53	0.19	0.804144	0.858736127	
0.0043			0.54	0.19	0.804273	0.864604669	
0.0042			0.55	0.19	0.804355	0.870505935	
0.0041			0.56	0.19	0.80442	0.876462373	
0.004			0.57	0.19	0.804402	0.882463072	

Opt. Value	Factor	% Change	Net Balance (m.w.e)	Measured Net Balance (m.w.e)	Stk R^2	Least Squares Slope	Notes
0.0051	1.1	10%	10	0.13	0.816332	0.784857496	
0.0048	1.05	5%	5	0.16	0.817115	0.803210946	
0.0046	1	0	0	0.19	0.817491	0.815743674	
0.0044	0.95	-5%	-5	0.21	0.817778	0.828552896	
0.0041	0.9	-10%	-10	0.24	0.817951	0.848300983	

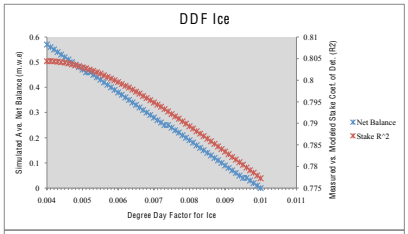

Cascade DDF

Mt. Rainier	*from Rasmussen and Wenger (2009)*
Snow:	0.00146-0.00085
Ice:	0.00644-0.00435
Mt. Shasta	*from Howat et al. (2007)*
Snow:	0.0014-0.0016
Ice:	0.0069-0.0055
SCG	*from Anslow et al. (2008)*
Snow:	0.003
Ice:	0.008

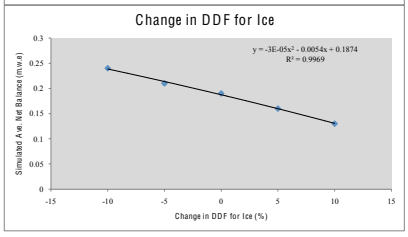

DDF Ice Sensitivity
y=-0.00006x-0.0054
Slope= -0.0054
x=0

Figure C1 Model Flowchart

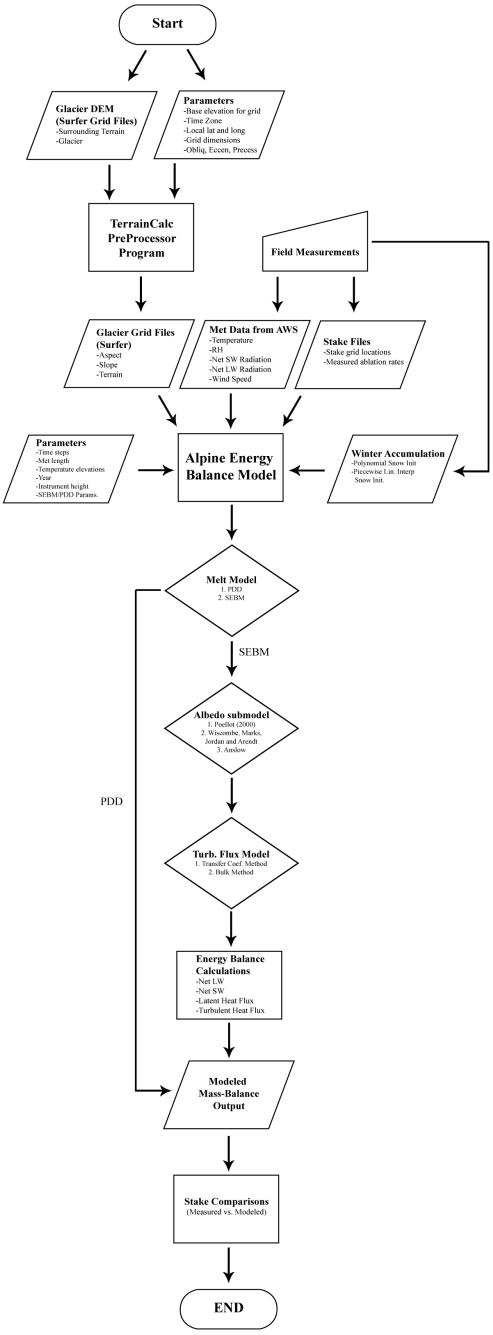

Figure C1: Flowchart of the OSU SEBM.

Appendix D McKenzie Snow Melt

Accumulation measurements were conducted on 10 May 2009, however, the moraine AWS was not erected until 12 July 2009, resulting in a significant gap in the datasets. In response to this gap, the winter balance measurements recorded on 10 May 2009 were adjusted to 12 July 2009 by estimating the snowpack by a linear snowpack model from the 1982-2009 average snow water equivalent (SWE) recorded at the McKenzie SNOTEL station. The output from this snowpack model served as the snow initialization for the 2009 SEBM and PDD simulations, since the meteorological record did not start until 13 July 2009.

Table D1 Linear Snowmelt

Ave Lin Model (y = -0.0151x + 0.8253)																																
Coeff 1 =	-0.0151	SWE Diff	1.13	1.13	0.99	0.84	0.99	0.35	0.69	0.16	0.33	0.26	0.24	0.46	0.46		2.29	3.16	3.30	3.11	*2.11*	2.51	0.95	1.10	1.03	0.86	1.13	1.28				
Coeff 2 =	0.8253	10 May Collier	2.00	2.00	1.86	1.71	1.86	1.22	1.56	1.03	1.20	1.13	1.11	1.33	1.33		3.16	4.03	4.17	3.98	*2.98*	3.38	1.82	1.97	1.90	1.73	2.00	2.15				
Day ID Number	SWE_AVE		S12	S11	S10	S9	S8	S7	S6	S5	S4	S3	S2	S1	Term		S12	S11	S10	S9	*S8*	S7	S6	S5	S4	S3	S2	S1				
1	0.87	1.33	1.94	1.94	1.80	1.65	1.80	1.16	1.50	0.97	1.14	1.07	1.05	1.27	1.27		3.10	3.97	4.11	3.92	*2.92*	3.32	1.76	1.91	1.84	1.67	1.94	2.09				
2	0.86	1.32	1.92	1.92	1.78	1.63	1.78	1.14	1.48	0.95	1.12	1.05	1.03	1.25	1.25		3.08	3.95	4.09	3.90	*2.90*	3.30	1.74	1.89	1.82	1.65	1.92	2.07				
3	0.85	1.32	1.91	1.91	1.77	1.62	1.77	1.13	1.47	0.94	1.11	1.04	1.02	1.24	1.24		3.07	3.94	4.08	3.89	*2.89*	3.29	1.73	1.88	1.81	1.64	1.91	2.06				
4	0.84	1.30	1.89	1.89	1.75	1.60	1.75	1.11	1.45	0.92	1.09	1.02	1.00	1.22	1.22		3.05	3.92	4.06	3.87	*2.87*	3.27	1.71	1.86	1.79	1.62	1.89	2.04				
5	0.82	1.29	1.88	1.88	1.74	1.59	1.74	1.10	1.44	0.91	1.08	1.01	0.99	1.21	1.21		3.04	3.91	4.05	3.86	*2.86*	3.26	1.70	1.85	1.78	1.61	1.88	2.03				
6	0.80	1.26	1.86	1.86	1.72	1.57	1.72	1.08	1.42	0.89	1.06	0.99	0.97	1.19	1.19		3.02	3.89	4.03	3.84	*2.84*	3.24	1.68	1.83	1.76	1.59	1.86	2.01				
7	0.79	1.24	1.84	1.84	1.70	1.55	1.70	1.06	1.40	0.87	1.04	0.97	0.95	1.17	1.17		3.00	3.87	4.01	3.82	*2.82*	3.22	1.66	1.81	1.74	1.57	1.84	1.99				
8	0.76	1.22	1.83	1.83	1.69	1.54	1.69	1.05	1.39	0.86	1.03	0.96	0.94	1.16	1.16		2.99	3.86	4.00	3.81	*2.81*	3.21	1.65	1.80	1.73	1.56	1.83	1.98				
9	0.75	1.23	1.81	1.81	1.67	1.52	1.67	1.03	1.37	0.84	1.01	0.94	0.92	1.14	1.14		2.97	3.84	3.98	3.79	*2.79*	3.19	1.63	1.78	1.71	1.54	1.81	1.96				
10	0.73	1.18	1.80	1.80	1.66	1.51	1.66	1.02	1.36	0.83	1.00	0.93	0.91	1.13	1.13		2.96	3.83	3.97	3.78	*2.78*	3.18	1.62	1.77	1.70	1.53	1.80	1.95				
11	0.71	1.16	1.78	1.78	1.64	1.49	1.64	1.00	1.34	0.81	0.98	0.91	0.89	1.11	1.11		2.94	3.81	3.95	3.76	*2.76*	3.16	1.60	1.75	1.68	1.51	1.78	1.93				
12	0.69	1.13	1.77	1.77	1.63	1.48	1.63	0.99	1.33	0.80	0.97	0.90	0.88	1.10	1.1		2.93	3.80	3.94	3.75	*2.75*	3.15	1.59	1.74	1.67	1.50	1.77	1.92				
13	0.67	1.11	1.75	1.75	1.61	1.46	1.61	0.97	1.31	0.78	0.95	0.88	0.86	1.08	1.08		2.91	3.78	3.92	3.73	*2.73*	3.13	1.57	1.72	1.65	1.48	1.75	1.90				
14	0.65	1.09	1.74	1.74	1.60	1.45	1.60	0.96	1.30	0.77	0.94	0.87	0.85	1.07	1.07		2.90	3.77	3.91	3.72	*2.72*	3.12	1.56	1.71	1.64	1.47	1.74	1.89				
15	0.63	1.07	1.72	1.72	1.58	1.43	1.58	0.94	1.28	0.75	0.92	0.85	0.83	1.05	1.05		2.88	3.75	3.89	3.70	*2.70*	3.10	1.54	1.69	1.62	1.45	1.72	1.87				
16	0.61	1.05	1.71	1.71	1.57	1.42	1.57	0.93	1.27	0.74	0.91	0.84	0.82	1.04	1.04		2.87	3.74	3.88	3.69	*2.69*	3.09	1.53	1.68	1.61	1.44	1.71	1.86				
17	0.59	1.02	1.69	1.69	1.55	1.40	1.55	0.91	1.25	0.72	0.89	0.82	0.80	1.02	1.02		2.85	3.72	3.86	3.67	*2.67*	3.07	1.51	1.66	1.59	1.42	1.69	1.84				
18	0.56	0.99	1.68	1.68	1.54	1.39	1.54	0.90	1.24	0.71	0.88	0.81	0.79	1.01	1.01		2.84	3.71	3.85	3.66	*2.66*	3.06	1.50	1.65	1.58	1.41	1.68	1.83				
19	0.54	0.96	1.66	1.66	1.52	1.37	1.52	0.88	1.22	0.69	0.86	0.79	0.77	0.99	0.99		2.82	3.69	3.83	3.64	*2.64*	3.04	1.48	1.63	1.56	1.39	1.66	1.81				
20	0.52	0.93	1.65	1.65	1.51	1.36	1.51	0.87	1.21	0.68	0.85	0.78	0.76	0.98	0.98		2.81	3.68	3.82	3.63	*2.63*	3.03	1.47	1.62	1.55	1.38	1.65	1.80				
21	0.49	0.91	1.63	1.63	1.49	1.34	1.49	0.85	1.19	0.66	0.83	0.76	0.74	0.96	0.96		2.79	3.66	3.80	3.61	*2.61*	3.01	1.45	1.60	1.53	1.36	1.63	1.78				
22	0.47	0.88	1.62	1.62	1.48	1.33	1.48	0.84	1.18	0.65	0.82	0.75	0.73	0.95	0.95		2.78	3.65	3.79	3.60	*2.60*	3.00	1.44	1.59	1.52	1.35	1.62	1.77				
23	0.45	0.85	1.60	1.60	1.46	1.31	1.46	0.82	1.16	0.63	0.80	0.73	0.71	0.93	0.93		2.76	3.63	3.77	3.58	*2.58*	2.98	1.42	1.57	1.50	1.33	1.60	1.75				
24	0.43	0.82	1.59	1.59	1.45	1.30	1.45	0.81	1.15	0.62	0.79	0.72	0.70	0.92	0.92		2.75	3.62	3.76	3.57	*2.57*	2.97	1.41	1.56	1.49	1.32	1.59	1.74				
25	0.40	0.79	1.57	1.57	1.43	1.28	1.43	0.79	1.13	0.60	0.77	0.70	0.68	0.90	0.9		2.73	3.60	3.74	3.55	*2.55*	2.95	1.39	1.54	1.47	1.30	1.57	1.72				
26	0.38	0.77	1.56	1.56	1.42	1.27	1.42	0.78	1.12	0.59	0.76	0.69	0.67	0.89	0.89		2.72	3.59	3.73	3.54	*2.54*	2.94	1.38	1.53	1.46	1.29	1.56	1.71				
27	0.35	0.74	1.54	1.54	1.40	1.25	1.40	0.76	1.10	0.57	0.74	0.67	0.65	0.87	0.87		2.70	3.57	3.71	3.52	*2.52*	2.92	1.36	1.51	1.44	1.27	1.54	1.69				
28	0.33	0.71	1.53	1.53	1.39	1.24	1.39	0.75	1.09	0.56	0.73	0.66	0.64	0.86	0.86		2.69	3.56	3.70	3.51	*2.51*	2.91	1.35	1.50	1.43	1.26	1.53	1.68				
29	0.31	0.69	1.51	1.51	1.37	1.22	1.37	0.73	1.07	0.54	0.71	0.64	0.62	0.84	0.84		2.67	3.54	3.68	3.49	*2.49*	2.89	1.33	1.48	1.41	1.24	1.51	1.66				
30	0.30	0.68	1.50	1.50	1.36	1.21	1.36	0.72	1.06	0.53	0.70	0.63	0.61	0.83	0.83		2.66	3.53	3.67	3.48	*2.48*	2.88	1.32	1.47	1.40	1.23	1.50	1.65				
31	0.27	0.66	1.48	1.48	1.34	1.19	1.34	0.70	1.04	0.51	0.68	0.61	0.59	0.81	0.81		2.64	3.51	3.65	3.46	*2.46*	2.86	1.30	1.45	1.38	1.21	1.48	1.63				
32	0.25	0.64	1.47	1.47	1.33	1.18	1.33	0.69	1.03	0.50	0.67	0.60	0.58	0.80	0.8		2.63	3.50	3.64	3.45	*2.45*	2.85	1.29	1.44	1.37	1.20	1.47	1.62				
33	0.24	0.61	1.45	1.45	1.31	1.16	1.31	0.67	1.01	0.48	0.65	0.58	0.56	0.78	0.78		2.61	3.48	3.62	3.43	*2.43*	2.83	1.27	1.42	1.35	1.18	1.45	1.60				
34	0.22	0.60	1.44	1.44	1.30	1.15	1.30	0.66	1.00	0.47	0.64	0.57	0.55	0.77	0.77		2.60	3.47	3.61	3.42	*2.42*	2.82	1.26	1.41	1.34	1.17	1.44	1.59				
35	0.21	0.57	1.42	1.42	1.28	1.13	1.28	0.64	0.98	0.45	0.62	0.55	0.53	0.75	0.75		2.58	3.45	3.59	3.40	*2.40*	2.80	1.24	1.39	1.32	1.15	1.42	1.57				
36	0.19	0.55	1.41	1.41	1.27	1.12	1.27	0.63	0.97	0.44	0.61	0.54	0.52	0.74	0.74		2.57	3.44	3.58	3.39	*2.39*	2.79	1.23	1.38	1.31	1.14	1.41	1.56				
37	0.17	0.52	1.39	1.39	1.25	1.10	1.25	0.61	0.95	0.42	0.59	0.52	0.50	0.72	0.72		2.55	3.42	3.56	3.37	*2.37*	2.77	1.21	1.36	1.29	1.12	1.39	1.54				
38	0.16	0.49	1.38	1.38	1.24	1.09	1.24	0.60	0.94	0.41	0.58	0.51	0.49	0.71	0.71		2.54	3.41	3.55	3.36	*2.36*	2.76	1.20	1.35	1.28	1.11	1.38	1.53				
39	0.14	0.46	1.36	1.36	1.22	1.07	1.22	0.58	0.92	0.39	0.56	0.49	0.47	0.69	0.69		2.52	3.39	3.53	3.34	*2.34*	2.74	1.18	1.33	1.26	1.09	1.36	1.51				
40	0.13	0.44	1.35	1.35	1.21	1.06	1.21	0.57	0.91	0.38	0.55	0.48	0.46	0.68	0.68		2.51	3.38	3.52	3.33	*2.33*	2.73	1.17	1.32	1.25	1.08	1.35	1.50				
41	0.12	0.41	1.33	1.33	1.19	1.04	1.19	0.55	0.89	0.36	0.53	0.46	0.44	0.66	0.66		2.49	3.36	3.50	3.31	*2.31*	2.71	1.15	1.30	1.23	1.06	1.33	1.48				
42	0.11	0.40	1.32	1.32	1.18	1.03	1.18	0.54	0.88	0.35	0.52	0.45	0.43	0.65	0.65		2.48	3.35	3.49	3.30	*2.30*	2.70	1.14	1.29	1.22	1.05	1.32	1.47				
43	0.10	0.38	1.30	1.30	1.16	1.01	1.16	0.52	0.86	0.33	0.50	0.43	0.41	0.63	0.63		2.46	3.33	3.47	3.28	*2.28*	2.68	1.12	1.27	1.20	1.03	1.30	1.45				
44	0.10	0.37	1.29	1.29	1.15	1.00	1.15	0.51	0.85	0.32	0.49	0.42	0.40	0.62	0.62		2.45	3.32	3.46	3.27	*2.27*	2.67	1.11	1.26	1.19	1.02	1.29	1.44				
45	0.10	0.35	1.27	1.27	1.13	0.98	1.13	0.49	0.83	0.30	0.47	0.40	0.38	0.60	0.6		2.43	3.30	3.44	3.25	*2.25*	2.65	1.09	1.24	1.17	1.00	1.27	1.42				
46	0.09	0.33	1.26	1.26	1.12	0.97	1.12	0.48	0.82	0.29	0.46	0.39	0.37	0.59	0.59		2.42	3.29	3.43	3.24	*2.24*	2.64	1.08	1.23	1.16	0.99	1.26	1.41				
47	0.08	0.32	1.24	1.24	1.10	0.95	1.10	0.46	0.80	0.27	0.44	0.37	0.35	0.57	0.57		2.40	3.27	3.41	3.22	*2.22*	2.62	1.06	1.21	1.14	0.97	1.24	1.39				
48	0.08	0.30	1.23	1.23	1.09	0.94	1.09	0.45	0.79	0.26	0.43	0.36	0.34	0.56	0.56		2.39	3.26	3.40	3.21	*2.21*	2.61	1.05	1.20	1.13	0.96	1.23	1.38		27-Jun-10		
49	0.07	0.29	1.21	1.21	1.07	0.92	1.07	0.43	0.77	0.24	0.41	0.34	0.32	0.54	0.54		2.37	3.24	3.38	3.19	*2.19*	2.59	1.03	1.18	1.11	0.94	1.21	1.36				
50	0.07	0.27	1.20	1.20	1.06	0.91	1.06	0.42	0.76	0.23	0.40	0.33	0.31	0.53	0.53		2.36	3.23	3.37	3.18	*2.18*	2.58	1.02	1.17	1.10	0.93	1.20	1.35				
51	0.06	0.25	1.18	1.18	1.04	0.89	1.04	0.40	0.74	0.21	0.38	0.31	0.29	0.51	0.51		2.34	3.21	3.35	3.16	*2.16*	2.56	1.00	1.15	1.08	0.91	1.18	1.33				
52	0.05	0.23	1.17	1.17	1.03	0.88	1.03	0.39	0.73	0.20	0.37	0.30	0.28	0.50	0.5		2.33	3.20	3.34	3.15	*2.15*	2.55	0.99	1.14	1.07	0.90	1.17	1.32				
53	0.05	0.21	1.15	1.15	1.01	0.86	1.01	0.37	0.71	0.18	0.35	0.28	0.26	0.48	0.48		2.31	3.18	3.32	3.13	*2.13*	2.53	0.97	1.12	1.05	0.88	1.15	1.30				
54	0.04	0.19	1.14	1.14	1.00	0.85	1.00	0.36	0.70	0.17	0.34	0.27	0.25	0.47	0.47		2.30	3.17	3.31	3.12	*2.12*	2.52	0.96	1.11	1.04	0.87	1.14	1.29				
55	0.04	0.18	1.12	1.12	0.98	0.83	0.98	0.34	0.68	0.15	0.32	0.25	0.23	0.45	0.45		2.28	3.15	3.29	3.10	*2.10*	2.50	0.94	1.09	1.02	0.85	1.12	1.27				
56	0.04	0.16	1.11	1.11	0.97	0.82	0.97	0.33	0.67	0.14	0.31	0.24	0.22	0.44	0.44		2.27	3.14	3.28	3.09	*2.09*	2.49	0.93	1.08	1.01	0.84	1.11	1.26				
57	0.03	0.15	1.09	1.09	0.95	0.80	0.95	0.31	0.65	0.12	0.29	0.22	0.20	0.42	0.42		2.25	3.12	3.26	3.07	*2.07*	2.47	0.91	1.06	0.99	0.82	1.09	1.24				
58	0.03	0.14	1.07	1.07	0.93	0.78	0.93	0.29	0.63	0.10	0.27	0.20	0.18	0.40	0.4		2.23	3.10	3.24	3.05	*2.05*	2.45	0.89	1.04	0.97	0.80	1.07	1.22				
59	0.03	0.12	1.06	1.06	0.92	0.77	0.92	0.28	0.62	0.09	0.26	0.19	0.17	0.39	0.39		2.22	3.09	3.23	3.04	*2.04*	2.44	0.88	1.03	0.96	0.79	1.06	1.21				
60	0.02	0.10	1.04	1.04	0.90	0.75	0.90	0.26	0.60	0.07	0.24	0.17	0.15	0.37	0.37		2.20	3.07	3.21	3.02	*2.02*	2.42	0.86	1.01	0.94	0.77	1.04	1.19				
61	0.02	0.09	1.03	1.03	0.89	0.74	0.89	0.25	0.59	0.06	0.23	0.16	0.14	0.36	0.36		2.19	3.06	3.20	3.01	*2.01*	2.41	0.85	1.00	0.93	0.76	1.03	1.18				
62	0.01	0.07	1.01	1.01	0.87	0.72	0.87	0.23	0.57	0.04	0.21	0.14	0.12	0.34	0.34		2.17	3.04	3.18	2.99	*1.99*	2.39	0.83	0.98	0.91	0.74	1.01	1.16				
63	0.01	0.04	1.00	1.00	0.86	0.71	0.86	0.22	0.56	0.03	0.20	0.13	0.11	0.33	0.33		2.16	3.03	3.17	2.98	*1.98*	2.38	0.82	0.97	0.90	0.73	1.00	1.15				
64	0.00	0.02	0.98	0.98	0.84	0.69	0.84	0.20	0.54	0.01	0.18	0.11	0.09	0.31	0.31		2.14	3.01	3.15	2.96	*1.96*	2.36	0.80	0.95	0.88	0.71	0.98	1.13				
		Init. Correct.	0.06	0.06	0.06	0.06	0.06	0.06	0.06	0.06	0.06	0.06	0.06	0.06	0.06																	
		Corrected_1 (0.06)	1.05	1.05	0.91	0.76	0.91	0.27	0.61	0.08	0.25	0.18	0.16	0.38	0.38	Meas 27 Jun	2.52	3.54	3.65	2.43		3.05	1.99	1.81	1.80	1.70	1.68	2.83				
			1.05	1.05	0.91	0.76	0.91	0.27	0.61	0.08	0.25	0.18	0.16	0.38	0.38	Mod 27 Jun	2.39	3.26	3.40	3.21	*2.21*	2.61	1.05	1.20	1.13	0.96	1.23	1.38	Average		Stdev	
		Corrected_2 (+ 0.1)	1.08	1.08	0.94	0.79	0.94	0.30	0.64	0.11	0.28	0.21	0.19	0.41	0.41	Diff	0.13	0.28	0.25	-0.78		0.44	0.94	0.61	0.67	0.74	0.45	1.45		**0.48**		**0.55**
			1.1	1.1	0.9	0.8	0.9	0.3	0.6	0.1	0.3	0.2	0.2	0.4	0.4	% Diff	0.05	0.08	0.07	-0.32		0.15	0.47	0.34	0.37	0.44	0.27	0.51		**0.38**		**0.47**
		Corrected_3 (+1 STDEV)	1.46	1.46	1.32	1.17	1.32	0.68	1.02	0.49	0.66	0.59	0.57	0.79	0.79		0.03	0.03	0.03	0.04		0.05	0.04	0.06	0.05	0.06	0.06	0.05		0.22	% Difference	
																Corrected (+0.06)	2.45	3.32	3.46	3.27		2.67	1.11	1.26	1.19	1.02	1.29	1.44				
																Corrected (+0.1)	2.5	3.4	3.5	3.3	2.3	2.7	1.1	1.3	1.2	1.1	1.3	1.5				
																	0.03	0.18	0.15	-0.88		0.34	0.84	0.51	0.57	0.64	0.35	1.35		0.38		0.55

Table D2 Polynomial Snowmelt

Ave Poly Model (y = 0.0002x^2 - 0.0287x + 0.9751)

Day ID Number	SWE_AVE		S12	S11	S10	S9	S8	S7	S6	S5	S4	S3	S2	S1	Term
Coeff 1 =	0.0002														
Coeff 2 =	-0.0287	SWE Diff	1.13	1.13	0.99	0.84	0.99	0.35	0.69	0.16	0.33	0.26	0.24	0.46	0.46
Coeff 3 =	0.9751	10 May Collier	2.00	2.00	1.86	1.71	1.86	1.22	1.56	1.03	1.20	1.13	1.11	1.33	1.33
1	0.87		2.07	2.07	1.93	1.78	1.93	1.29	1.63	1.10	1.27	1.20	1.18	1.40	1.40
2	0.86		2.04	2.04	1.90	1.75	1.90	1.26	1.60	1.07	1.24	1.17	1.15	1.37	1.37
3	0.85		2.02	2.02	1.88	1.73	1.88	1.24	1.58	1.05	1.22	1.15	1.13	1.35	1.35
4	0.84		1.99	1.99	1.85	1.70	1.85	1.21	1.55	1.02	1.19	1.12	1.10	1.32	1.32
5	0.82		1.96	1.96	1.82	1.67	1.82	1.18	1.52	0.99	1.16	1.09	1.07	1.29	1.29
6	0.80		1.94	1.94	1.80	1.65	1.80	1.16	1.50	0.97	1.14	1.07	1.05	1.27	1.27
7	0.79		1.91	1.91	1.77	1.62	1.77	1.13	1.47	0.94	1.11	1.04	1.02	1.24	1.24
8	0.76		1.88	1.88	1.74	1.59	1.74	1.10	1.44	0.91	1.08	1.01	0.99	1.21	1.21
9	0.75		1.86	1.86	1.72	1.57	1.72	1.08	1.42	0.89	1.06	0.99	0.97	1.19	1.19
10	0.73		1.83	1.83	1.69	1.54	1.69	1.05	1.39	0.86	1.03	0.96	0.94	1.16	1.16
11	0.71		1.81	1.81	1.67	1.52	1.67	1.03	1.37	0.84	1.01	0.94	0.92	1.14	1.14
12	0.69		1.78	1.78	1.64	1.49	1.64	1.00	1.34	0.81	0.98	0.91	0.89	1.11	1.11
13	0.67		1.76	1.76	1.62	1.47	1.62	0.98	1.32	0.79	0.96	0.89	0.87	1.09	1.09
14	0.65		1.74	1.74	1.60	1.45	1.60	0.96	1.30	0.77	0.94	0.87	0.85	1.07	1.07
15	0.63		1.71	1.71	1.57	1.42	1.57	0.93	1.27	0.74	0.91	0.84	0.82	1.04	1.04
16	0.61		1.69	1.69	1.55	1.40	1.55	0.91	1.25	0.72	0.89	0.82	0.80	1.02	1.02
17	0.59		1.67	1.67	1.53	1.38	1.53	0.89	1.23	0.70	0.87	0.80	0.78	1.00	1.00
18	0.56		1.65	1.65	1.51	1.36	1.51	0.87	1.21	0.68	0.85	0.78	0.76	0.98	0.98
19	0.54		1.63	1.63	1.49	1.34	1.49	0.85	1.19	0.66	0.83	0.76	0.74	0.96	0.96
20	0.52		1.61	1.61	1.47	1.32	1.47	0.83	1.17	0.64	0.81	0.74	0.72	0.94	0.94
21	0.49		1.59	1.59	1.45	1.30	1.45	0.81	1.15	0.62	0.79	0.72	0.70	0.92	0.92
22	0.47		1.57	1.57	1.43	1.28	1.43	0.79	1.13	0.60	0.77	0.70	0.68	0.90	0.90
23	0.45		1.55	1.55	1.41	1.26	1.41	0.77	1.11	0.58	0.75	0.68	0.66	0.88	0.88
24	0.43		1.53	1.53	1.39	1.24	1.39	0.75	1.09	0.56	0.73	0.66	0.64	0.86	0.86
25	0.40		1.51	1.51	1.37	1.22	1.37	0.73	1.07	0.54	0.71	0.64	0.62	0.84	0.84
26	0.38		1.49	1.49	1.35	1.20	1.35	0.71	1.05	0.52	0.69	0.62	0.60	0.82	0.82
27	0.35		1.47	1.47	1.33	1.18	1.33	0.69	1.03	0.50	0.67	0.60	0.58	0.80	0.80
28	0.33		1.45	1.45	1.31	1.16	1.31	0.67	1.01	0.48	0.65	0.58	0.56	0.78	0.78
29	0.31		1.44	1.44	1.30	1.15	1.30	0.66	1.00	0.47	0.64	0.57	0.55	0.77	0.77
30	0.30		1.42	1.42	1.28	1.13	1.28	0.64	0.98	0.45	0.62	0.55	0.53	0.75	0.75
31	0.27		1.40	1.40	1.26	1.11	1.26	0.62	0.96	0.43	0.60	0.53	0.51	0.73	0.73
32	0.25		1.39	1.39	1.25	1.10	1.25	0.61	0.95	0.42	0.59	0.52	0.50	0.72	0.72
33	0.24		1.37	1.37	1.23	1.08	1.23	0.59	0.93	0.40	0.57	0.50	0.48	0.70	0.70
34	0.22		1.36	1.36	1.22	1.07	1.22	0.58	0.92	0.39	0.56	0.49	0.47	0.69	0.69
35	0.21		1.34	1.34	1.20	1.05	1.20	0.56	0.90	0.37	0.54	0.47	0.45	0.67	0.67
36	0.19		1.33	1.33	1.19	1.04	1.19	0.55	0.89	0.36	0.53	0.46	0.44	0.66	0.66
37	0.17		1.31	1.31	1.17	1.02	1.17	0.53	0.87	0.34	0.51	0.44	0.42	0.64	0.64
38	0.16		1.30	1.30	1.16	1.01	1.16	0.52	0.86	0.33	0.50	0.43	0.41	0.63	0.63
39	0.14		1.29	1.29	1.15	1.00	1.15	0.51	0.85	0.32	0.49	0.42	0.40	0.62	0.62
40	0.13		1.27	1.27	1.13	0.98	1.13	0.49	0.83	0.30	0.47	0.40	0.38	0.60	0.60
41	0.12		1.26	1.26	1.12	0.97	1.12	0.48	0.82	0.29	0.46	0.39	0.37	0.59	0.59
42	0.11		1.25	1.25	1.11	0.96	1.11	0.47	0.81	0.28	0.45	0.38	0.36	0.58	0.58
43	0.10		1.24	1.24	1.10	0.95	1.10	0.46	0.80	0.27	0.44	0.37	0.35	0.57	0.57
44	0.10		1.22	1.22	1.08	0.93	1.08	0.44	0.78	0.25	0.42	0.35	0.33	0.55	0.55
45	0.10		1.21	1.21	1.07	0.92	1.07	0.43	0.77	0.24	0.41	0.34	0.32	0.54	0.54
46	0.09		1.20	1.20	1.06	0.91	1.06	0.42	0.76	0.23	0.40	0.33	0.31	0.53	0.53
47	0.08		1.19	1.19	1.05	0.90	1.05	0.41	0.75	0.22	0.39	0.32	0.30	0.52	0.52
48	0.08		1.18	1.18	1.04	0.89	1.04	0.40	0.74	0.21	0.38	0.31	0.29	0.51	0.51
49	0.07		1.17	1.17	1.03	0.88	1.03	0.39	0.73	0.20	0.37	0.30	0.28	0.50	0.50
50	0.07		1.17	1.17	1.03	0.88	1.03	0.39	0.73	0.20	0.37	0.30	0.28	0.50	0.50
51	0.06		1.16	1.16	1.02	0.87	1.02	0.38	0.72	0.19	0.36	0.29	0.27	0.49	0.49
52	0.05		1.15	1.15	1.01	0.86	1.01	0.37	0.71	0.18	0.35	0.28	0.26	0.48	0.48
53	0.05		1.14	1.14	1.00	0.85	1.00	0.36	0.70	0.17	0.34	0.27	0.25	0.47	0.47
54	0.04		1.13	1.13	0.99	0.84	0.99	0.35	0.69	0.16	0.33	0.26	0.24	0.46	0.46
55	0.04		1.13	1.13	0.99	0.84	0.99	0.35	0.69	0.16	0.33	0.26	0.24	0.46	0.46
56	0.04		1.12	1.12	0.98	0.83	0.98	0.34	0.68	0.15	0.32	0.25	0.23	0.45	0.45
57	0.03		1.11	1.11	0.97	0.82	0.97	0.33	0.67	0.14	0.31	0.24	0.22	0.44	0.44
58	0.03		1.11	1.11	0.97	0.82	0.97	0.33	0.67	0.14	0.31	0.24	0.22	0.44	0.44
59	0.03		1.10	1.10	0.96	0.81	0.96	0.32	0.66	0.13	0.30	0.23	0.21	0.43	0.43
60	0.02		1.10	1.10	0.96	0.81	0.96	0.32	0.66	0.13	0.30	0.23	0.21	0.43	0.43
61	0.02		1.09	1.09	0.95	0.80	0.95	0.31	0.65	0.12	0.29	0.22	0.20	0.42	0.42
62	0.01		1.09	1.09	0.95	0.80	0.95	0.31	0.65	0.12	0.29	0.22	0.20	0.42	0.42
63	0.01		1.09	1.09	0.95	0.80	0.95	0.31	0.65	0.12	0.29	0.22	0.20	0.42	0.42
64	0.00		1.08	1.08	0.94	0.79	0.94	0.30	0.64	0.11	0.28	0.21	0.19	0.41	0.41

Day ID Number	S12	S11	S10	S9	S8	S7	S6	S5	S4	S3	S2	S1	Term	
SWE Diff	2.29	3.16	3.30	3.11	2.11	2.51	0.95	1.10	1.03	0.86	1.13	1.28		
10 May Collier	3.16	4.03	4.17	3.98	2.98	3.38	1.82	1.97	1.90	1.73	2.00	2.15		
1	3.23	4.10	4.24	4.05	3.05	3.45	1.89	2.04	1.97	1.80	2.07	2.22		
2	3.20	4.07	4.21	4.02	3.02	3.42	1.86	2.01	1.94	1.77	2.04	2.19		
3	3.18	4.05	4.19	4.00	3.00	3.40	1.84	1.99	1.92	1.75	2.02	2.17		
4	3.15	4.02	4.16	3.97	2.97	3.37	1.81	1.96	1.89	1.72	1.99	2.14		
5	3.12	3.99	4.13	3.94	2.94	3.34	1.78	1.93	1.86	1.69	1.96	2.11		
6	3.10	3.97	4.11	3.92	2.92	3.32	1.76	1.91	1.84	1.67	1.94	2.09		
7	3.07	3.94	4.08	3.89	2.89	3.29	1.73	1.88	1.81	1.64	1.91	2.06		
8	3.04	3.91	4.05	3.86	2.86	3.26	1.70	1.85	1.78	1.61	1.88	2.03		
9	3.02	3.89	4.03	3.84	2.84	3.24	1.68	1.83	1.76	1.59	1.86	2.01		
10	2.99	3.86	4.00	3.81	2.81	3.21	1.65	1.80	1.73	1.56	1.83	1.98		
11	2.97	3.84	3.98	3.79	2.79	3.19	1.63	1.78	1.71	1.54	1.81	1.96		
12	2.94	3.81	3.95	3.76	2.76	3.16	1.60	1.75	1.68	1.51	1.78	1.93		
13	2.92	3.79	3.93	3.74	2.74	3.14	1.58	1.73	1.66	1.49	1.76	1.91		
14	2.90	3.77	3.91	3.72	2.72	3.12	1.56	1.71	1.64	1.47	1.74	1.89		
15	2.87	3.74	3.88	3.69	2.69	3.09	1.53	1.68	1.61	1.44	1.71	1.86		
16	2.85	3.72	3.86	3.67	2.67	3.07	1.51	1.66	1.59	1.42	1.69	1.84		
17	2.83	3.70	3.84	3.65	2.65	3.05	1.49	1.64	1.57	1.40	1.67	1.82		
18	2.81	3.68	3.82	3.63	2.63	3.03	1.47	1.62	1.55	1.38	1.65	1.80		
19	2.79	3.66	3.80	3.61	2.61	3.01	1.45	1.60	1.53	1.36	1.63	1.78		
20	2.77	3.64	3.78	3.59	2.59	2.99	1.43	1.58	1.51	1.34	1.61	1.76		
21	2.75	3.62	3.76	3.57	2.57	2.97	1.41	1.56	1.49	1.32	1.59	1.74		
22	2.73	3.60	3.74	3.55	2.55	2.95	1.39	1.54	1.47	1.30	1.57	1.72		
23	2.71	3.58	3.72	3.53	2.53	2.93	1.37	1.52	1.45	1.28	1.55	1.70		
24	2.69	3.56	3.70	3.51	2.51	2.91	1.35	1.50	1.43	1.26	1.53	1.68		
25	2.67	3.54	3.68	3.49	2.49	2.89	1.33	1.48	1.41	1.24	1.51	1.66		
26	2.65	3.52	3.66	3.47	2.47	2.87	1.31	1.46	1.39	1.22	1.49	1.64		
27	2.63	3.50	3.64	3.45	2.45	2.85	1.29	1.44	1.37	1.20	1.47	1.62		
28	2.61	3.48	3.62	3.43	2.43	2.83	1.27	1.42	1.35	1.18	1.45	1.60		
29	2.60	3.47	3.61	3.42	2.42	2.82	1.26	1.41	1.34	1.17	1.44	1.59		
30	2.58	3.45	3.59	3.40	2.40	2.80	1.24	1.39	1.32	1.15	1.42	1.57		
31	2.56	3.43	3.57	3.38	2.38	2.78	1.22	1.37	1.30	1.13	1.40	1.55		
32	2.55	3.42	3.56	3.37	2.37	2.77	1.21	1.36	1.29	1.12	1.39	1.54		
33	2.53	3.40	3.54	3.35	2.35	2.75	1.19	1.34	1.27	1.10	1.37	1.52		
34	2.52	3.39	3.53	3.34	2.34	2.74	1.18	1.33	1.26	1.09	1.36	1.51		
35	2.50	3.37	3.51	3.32	2.32	2.72	1.16	1.31	1.24	1.07	1.34	1.49		
36	2.49	3.36	3.50	3.31	2.31	2.71	1.15	1.30	1.23	1.06	1.33	1.48		
37	2.47	3.34	3.48	3.29	2.29	2.69	1.13	1.28	1.21	1.04	1.31	1.46		
38	2.46	3.33	3.47	3.28	2.28	2.68	1.12	1.27	1.20	1.03	1.30	1.45		
39	2.45	3.32	3.46	3.27	2.27	2.67	1.11	1.26	1.19	1.02	1.29	1.44		
40	2.43	3.30	3.44	3.25	2.25	2.65	1.09	1.24	1.17	1.00	1.27	1.42		
41	2.42	3.29	3.43	3.24	2.24	2.64	1.08	1.23	1.16	0.99	1.26	1.41		
42	2.41	3.28	3.42	3.23	2.23	2.63	1.07	1.22	1.15	0.98	1.25	1.40		
43	2.40	3.27	3.41	3.22	2.22	2.62	1.06	1.21	1.14	0.97	1.24	1.39		
44	2.38	3.25	3.39	3.20	2.20	2.60	1.04	1.19	1.12	0.95	1.22	1.37		
45	2.37	3.24	3.38	3.19	2.19	2.59	1.03	1.18	1.11	0.94	1.21	1.36		
46	2.36	3.23	3.37	3.18	2.18	2.58	1.02	1.17	1.10	0.93	1.20	1.35		
47	2.35	3.22	3.36	3.17	2.17	2.57	1.01	1.16	1.09	0.92	1.19	1.34		
48	2.34	3.21	3.35	3.16	2.16	2.56	1.00	1.15	1.08	0.91	1.18	1.33		27-Jun-10
49	2.33	3.20	3.34	3.15	2.15	2.55	0.99	1.14	1.07	0.90	1.17	1.32		
50	2.33	3.20	3.34	3.15	2.15	2.55	0.99	1.14	1.07	0.90	1.17	1.32		
51	2.32	3.19	3.33	3.14	2.14	2.54	0.98	1.13	1.06	0.89	1.16	1.31		
52	2.31	3.18	3.32	3.13	2.13	2.53	0.97	1.12	1.05	0.88	1.15	1.30		
53	2.30	3.17	3.31	3.12	2.12	2.52	0.96	1.11	1.04	0.87	1.14	1.29		
54	2.29	3.16	3.30	3.11	2.11	2.51	0.95	1.10	1.03	0.86	1.13	1.28		
55	2.29	3.16	3.30	3.11	2.11	2.51	0.95	1.10	1.03	0.86	1.13	1.28		
56	2.28	3.15	3.29	3.10	2.10	2.50	0.94	1.09	1.02	0.85	1.12	1.27		
57	2.27	3.14	3.28	3.09	2.09	2.49	0.93	1.08	1.01	0.84	1.11	1.26		
58	2.27	3.14	3.28	3.09	2.09	2.49	0.93	1.08	1.01	0.84	1.11	1.26		
59	2.26	3.13	3.27	3.08	2.08	2.48	0.92	1.07	1.00	0.83	1.10	1.25		
60	2.26	3.13	3.27	3.08	2.08	2.48	0.92	1.07	1.00	0.83	1.10	1.25		
61	2.25	3.12	3.26	3.07	2.07	2.47	0.91	1.06	0.99	0.82	1.09	1.24		
62	2.25	3.12	3.26	3.07	2.07	2.47	0.91	1.06	0.99	0.82	1.09	1.24		
63	2.25	3.12	3.26	3.07	2.07	2.47	0.91	1.06	0.99	0.82	1.09	1.24		
64	2.24	3.11	3.25	3.06	2.06	2.46	0.90	1.05	0.98	0.81	1.08	1.23		
Meas 27 Jun	2.52	3.54	3.65	2.43		3.05	1.99	1.81	1.80	1.70	1.68	2.83		
Mod 27 Jun	2.34	3.21	3.35	3.16		2.56	1.00	1.15	1.08	0.91	1.18	1.33		
	0.18	0.33	0.30	-0.73		0.49	0.99	0.66	0.72	0.79	0.50	1.50		

Figure D1 McKenzie snowmelt

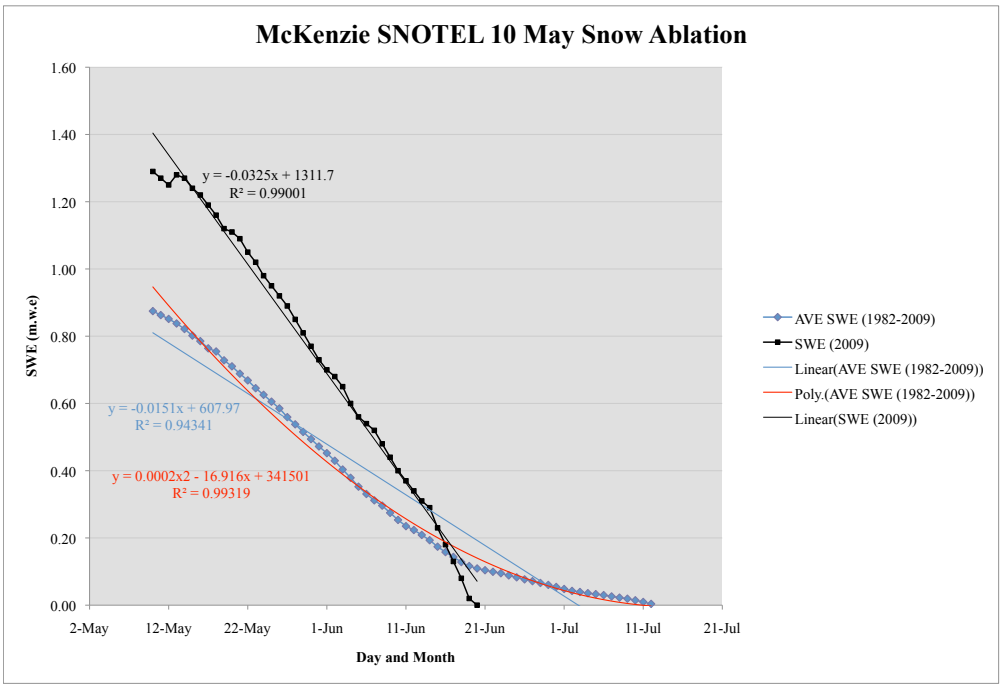

Figure D1: 1982-2009 McKenzie SNOTEL May to July snow melt.